PETROTECTONIC AND LITHOSTRUCTURAL STUDIES OF OKEMESI-IWARAJA AREA, SOUTHWESTERN NIGERIA

BY

JOHN OWOICHO, OGBOLE,

B.Tech. Geology, Minna (1998), M.Sc. Mineral Exploration and Mining Geology, Jos (2007)

(Matriculation Number: 181517)

A thesis in the Department of GEOLOGY

Submitted to the Faculty of Science in partial fulfillment of

the requirements for the Degree of

DOCTOR OF PHILOSOPHY

of the

UNIVERSITY OF IBADAN

September, 2021

CERTIFICATION

I certify that this work was carried out by John Owoicho Ogbole, in the department of Geology, University of Ibadan.

……

Supervisor

Dr. A. A. Omitogun

B.Sc. (Ilorin), M.Sc. (Ilorin), Ph.D. (Toulouse)

Senior Lecturer, Department of Geology, University of Ibadan, Nigeria.

DEDICATION

I dedicate this thesis to the Lord God almighty the most gracious, merciful, and praise worthy, the Lord of heaven and the universe, the provider of all things, for his mercies and unfailing love, without whom, all these wouldn’t have been possible.

ACKNOWLEDGEMENTS

I express sincere gratitude to Dr. A. A. Omitogun, my supervisor, who devoted his time from the beginning to the end of this research in guiding me, he left no stone unturned, critically perusing my manuscript. His invaluable suggestions and support from his loving wife Prof. Mrs. Omitogun have contributed to the quality of this dissertation.

My appreciation in a special way goes to my late father, Justice Emanuel O. Ogbole and my mother Mrs. Angelina. O. Ogbole for their unfailing love, concern and un-quantifiable support, their encouragement and prayers have brought me this far. May God continue to be with you always.

My heartfelt gratitude goes to my elder brother Paul Harris Ogbole (SAN) and his wife for their understanding and untiring support in the pursuit of my PhD program. They have continuously inspired me with their selfless and generous nature, with an ever ready, open and welcoming arms.

I express sincere gratitude to the Director of Advanced Unmanned Aerial Vehicle (AUAVL) Uburu, Engr. Chebe Akachukwu for his understanding, patience, and granting me permission and logistics support which enabled me conclude this higher level of education, improving the confidence level in my profession.

I acknowledge the rest of my brothers and sisters; Sister Ada, Grace, Prof. Friday, Engr. Dan, Franki, Engr. Eddy, Hon. Bar. Josh, Angela, Dr. Christy, Rose, Rev. Sister Julie, Dr. Edwina, Mercy, Engr. Austine, Ray, Tessy, Tina, Mary and Alex and all those I am not able to mention here. I appreciate their support, concern and prayers; they have continued to be source of inspiration to me, God bless you all abundantly.

Sincere thanks to Dr. O. O. Ocan, for accommodating me in his Petrography Laboratory at Osun State University, during my entire period of petrographic analysis teaching me the rudiments of petrography. I will also not forget all those times he took me in his vehicle for field visits to my study area to unravel some of the field structural mysteries and also guide me through geochemical analysis. I will always continue to be indebted to him.

Particular acknowledgement is also given to Dr. A.T. Bolarinwa who put in so many hours helping me with corrections on my abstract, and the entire members of staff of Geology Department, University of Ibadan: Prof. A. I Olayinka, Prof. G. O. Adeyemi, Prof. O. A. Okunola, Prof. O. A. Ehinola, Dr. I. A. Oyediran, Prof. M. N. Tijani, Prof. M. E. Nton, Dr. O. A. Boboye, Dr. O. O. Osinowo, Dr. O. C. Adeigbe, Dr. M. A. Oladunjoye, Dr. J. A. Aladejana, and Dr. F. F. Ajayi. Their guidance and criticisms during the periodic departmental seminars have kept me on the right path, and I also appreciate the non-academic staff: Mr. Adelaku, Mrs. Badamuse, Wale, Iyabeji, and all others not mentioned here. I will always remember them for their love and care.

I would also like to use this opportunity to specially aknowledge my dear friend Remi, for all the continous encouragement, all the help with the seceteriate work when ever there were urgent tables to deal with and documents to print. Your faith in my ability to carry out this research is amazing, your contrbutions will always be remembered.

Finally, I express my profound appreciation to my beautiful, kind, understanding and loving wife, Dr. Alex and my wonderful kids: Aeron, Derick and Jayden, for their moral support and putting up with my long absence from home.

Above all, I thank the Lord God Almighty the most gracious, merciful, and praise worthy, the Lord of the heaven and the universe, the provider of all things, without His will, all this would not have been possible.

ABSTRACT

Okemesi-Iwaraja area lies within the Ilesha Schist belt, and has been described as a polydeformational high strain transcurrent shear belt in the Basement Complex of Southwestern Nigeria. In addition, the structures, important for mineral exploration, associated with this major transcurrent shear zone has not been fully investigated. The aim of this study was to classify the rocks, characterise the structures, and determine their petrotectonic evolution.

Remote sensing and Aeromagnetic data were procured and analysed. Band ratios prepared from Landsat-8 were used to delineate structures. Digital Elevation Model and RADAR data were used for identification of surface lineaments. The Aeromagnetic data were processed for subsurface structural features. Geological mapping was undertaken to delineate lithologic units and structures. Trend and plunge of fold axis were determined using stereographic analysis. Rock texture and mineralogical composition was by petrographic studies of thin sections prepared from eighty-four fresh rock samples. Major, trace and Rare Earth Elements (REE), of twenty-four samples were determined using Inductively Coupled Plasma Mass-Spectroscopy technique.

Lineament orientation dominantly trend NE-SW (56.9%). Other orientations were NNE-SSW (17.1%), NW-SE (22.3%), E-W (3.8%) and N–S (1.3%). Subsurface structures were also dominantly NE-SW, strongly corresponding to the surface lineaments. Rock types identified in the area were migmatites, amphibole schists, quartz schists, biotite schists, amphibolites, quartzites and the granitoids (grey gneiss, granite gneiss, two-mica granite, medium-grained biotite granite, porphyritic biotite granite). Rock structures were lineations, foliations, folds, joints, shear zones, and faults. Two major deformational phases (D1 and D2) were identified**,** D1 event recorded mainly on quartz schist were associated with the development of S1 schistosity and a recumbent F1 folding, D2 was well developed in some granite gneisses, with the development of an S2 and tight to isoclinal F2 folds. Fold and foliation axial plane trend in the NNE-SSW and NE-SW directions, while the trend and plunge of the fold axis were dominantly NE, suggesting an E-W compression, which is expressed in the surface lineaments and the subsurface structures. Mineral alteration of perthite to sericite in the granitoids and the calculated Chemical Index of Alteration (49.71 – 62.11) for granites, indicated onset of weathering. The granitoids were relatively potassic K_2O (3.34 – 6.23), and classified as high-K calc-alkaline, with high SiO_2 composition of 64.83–86.63wt% and molar A/CNK (1.18-2.75) suggesting strong peraluminous, S-type granite. The grey gneisses were however metaluminous. The light REE enrichment and depleted heavy REE with negative Eu anomaly in the granitoids, as revealed by spider plots, confirmed a felsic crustal origin. Plots of Rb/Y+N and Rb/Ta+Yb revealed, the tectonic environments were mainly post collision and within plate granite settings.

Okemesi-Iwaraja area is underlain by migmatites and schists intruded by the granites. The rocks have suffered polyphase deformation and are of crustal origin emplaced in a post-collision and within plate tectonic settings.

Keywords: Aeromagnetics, Geochemistry, Landsat-8, Petrotectonic structures, Remote sensing, Shear zones.

Word counts: 458.

TABLE OF CONTENTS

LIST OF TABLES

LIST OF FIGURES

LIST OF ABBREVIATIONS

A/CNK:	$Al_2O_3/CaO + Na_2O + K_2O$
A/NK:	$Al_2O_3/Na_2O + K_2O$
AS:	Analytical signal
BIF:	Banded Iron Formation
CIA:	Chemical Index of Alteration
DEM:	Digital elevation model
HFSE:	High Field Strength Element
HRAM:	High Resolution Aeromagnetic Map
ICP-AES:	Inductively Coupled Plasma-Atomic Emission Spectroscopy
IGRF:	International Geomagnetic Reference Field
LATEA:	Laouni, Azrou-n-Fad, Tefedest, Egéré-Aleksod
LILE:	Large Ion Lithofil Element
NGSA:	Nigerian Geological Survey Agency
OLI:	Operational Land Imager
PCA:	Principal Component Analysis
OSGF:	Office of Surveyor General of the Federation
RADAR:	Radio Detection and Raging
REE:	Rear Earth element
RTE:	Reduction to Equator
TAS:	Total Aluminum Saturation
TDR	Tilt Derivative
THDR	Total Horizontal derivative
TMI:	Total Magnetic Intensity
TTG:	Tonalite-Trondhjemite Granodiorite

LIST OF EQUATIONS

LIST OF APPENDICES

CHAPTER ONE

INTRODUCTION

1.1 Background of Study

Many extensive studies on the pre-Mesozoic region of the Nigerian Shield have been conducted over the years, Rahaman (1976), Fitches et al., (1985) sugested the inclusion of a polycyclic basement and remnants of metamorphic shield series well-preserved in large synforms and schist belts with variable mineral assemblages varying from greenschist to amphibolite facies. According to studies, basement/cover relationships have been formed in different regions through areas where they are expossed (Caby, 1989), suggesting large portion of the shield represents an earlier ensialic environment that was submerged under pericratonic sediments and then extensively reworked during the multistage Pan-African orogeny. Ajibade and Wright (1989), on the other hand, proposed a more multifaceted approach involving the collection of many terranes. Within the basement rocks of southwestern, northcentral and northeastern Nigeria, rocks of Archean age have been recognized (Rahaman, 198; Dada, 1998; Kroner et al., 2001). In the Okene axis, a typical Archean greenstone association consisting of Banded Iron Formations (BlFs) with intermediate temperature metamorphism is also commonly exposed (Annor, 1995), other researchers (Caby and Boesse 2001) believe that the Palaeoproterozoic orthogneisses found in the northern portion of the shield is part of a suture region.

Major shear zones have been discovered (Black et al 1984) in a variety of tectonic settings and have been linked to tectonic transpositions in various orogenies. Steep, north-south trending shear zones have been discovered in the western portion of the Nigerian basement complex (Ajibade, 1982; Caby, 1989). To the north, these shear zones have been established and linked to the Central Hoggar shear zones (Caby, 1989, 2003). These areas are characterized by mylonites and cataclasites as a result of shearing and grinding of these rocks under differing crustal conditions (confining pressures and temperatures) and fluid phase operations.

The Nigerian Shield, as defined by Black et al (1994), may represent a southern extension of central/eastern Tuareg terranes on a Gondwana scale (Caby, 1989). Existing geochronological evidence in northeastern Nigeria indicates that two distinct tectonic and magmatic events occurred in the Jos and Bauchi region (Dada and Respaut, 1989; Ferre et al., 1998), with the older tectonic event dated at around 640-620 Ma and the younger event dated at around 585 Ma. The ages of Pan-African granites in southwestern Nigeria range from 620 to 580 Ma (Tubosun et al., 1984; Rahaman et al., 1991). The 730 Ma early Pan-African domain identified in the Tuareg Shield's eastern part (Caby and Boesse 2001) is not reflected in the Nigerian Basement, according to both of these ages reported in the Nigerian shield. If this is the case, the Nigerian Shield (Fig. 2.1) might be the southern extension of the LATEA (Laouni-Tefedest-Azrou-n-fad) terrane, which is separated by Liegeois et al., (2000), Latouche et al., (2000), and Liegeois et al., (2000). (2000). The LATEA terrane, according to these authors, is the remnant of a thrust oceanic basin affected by eclogitic metamorphism over 686 Ma. Though regional kyanite-sillimanite metamorphism has been verified in central Nigeria (Onyeagocha and Ekwueme, 1990), a study of metamorphic-facies by these authors reveals that high-pressure rocks similar to those found in central Hoggar are not present in the Nigerian Shield.

Fault detection in field geological mapping is a vital factor in structural and environmental geology; tradional methods are generally the most common method used in fault detection. Fieldwork can be demanding and time-consuming in most cases and can take a lot of time to accomplish; this will usually depend largely on the nature of the region, extent and

mostly the accessibility of the area under study. The geologist's experience is very important in identifying important physical elements such as vegetation overgrowth, topography, erosion, and other factors controlling fault detection in the field.

Remote sensing technique is an important tool and have the advantage of providing a synoptic and bird's eye view of the expanse, making it much easier to identify geological structures covering regional scale. In contrast to field geological surveys, remote sensing and image processing method account for the least laborious and a more economical approach to detecting faults. However, such techniques do not in any way replace field mapping, but, only complement the other techniques.

Satellite images often reveal faults and fractures as linear or curvilinear traces. The contrasting lines from the image are often denoted as lineaments and can stretch from a few meters to several kilometres. It is worthy of note that not all image lineaments are faults; they could also be related to roads, lithological borders, drainage lines, or even boundaries between different land uses. As a result, interpreting the likely structural origins of lineaments based solely on satellite imagery is difficult. Streams, in fact, have a proclivity for meandering. As a result, certain typical stream irregularities, such as abrupt twists in stream channels, straight segments, displacement, or even local drainage system disappearance into sinkhole lines, could suggest a fault line on the photographs. Furthermore, groundwater transported via faults raises the moistness of the soil in comparison to the adjoining environment, promoting enhanced vegetation arrangements or dramatic shifts in the canopy of vegetation, as well as the disapearance of certain plant species.

In this project Landsat-8 OLI images and Radio Detection and Ranging (RADAR) data were processed alongside the Digital Elevation Model (DEM); different processing approaches (such as Principal Component Analysis, the display of False Color Composite images, and the transformation of intensity-hue-saturation and band ratio) aided in geology and fault mapping by enhancing lineaments that are possible fractures, faults, geological structures. The applicability of the Landsat-8 OLI and ASTER DEM remote sensing data

sets for the automated derivation of geological lineaments, surface lithology, and geomorphology information was investigated.

Aeromagnetic test is a geophysical method that tests the strength of the Earth's magnetic field; this is achieved from the air to the ground covering a wide area, this can penetrate deep into the subsurface. It can map subsurface structures including faults, grabben, horst, and lithology. The presence of faults and fractures generates magnetic variability, and in magnetic measurements can cause anomaly. Abiye and Tigitsu (2008) emphasized the importance of hydrothermally altered zones, because in this zone, most magnetic rocks are altered and converted from magnetite to pyrite, resulting in generally lower magnetic anomaly than areas that are unaltered. Fluid position within the faults and fractures will usually result in decreased or no magnetic reaction. Thus, the subsurface structure can be constructed using various inversion processes from magnetic profiles.

1.2 Justification

The tectonic setting and evolution of the structures related to the main transcurrent shear zone in southwestern Nigeria are yet to be investigated in detail and therefore, not well understood. Whereas, only regional studies at small scales (e.g. Caby, 2003; Caby and Boesse, 2001) related to the study area's structural evolution and references (e.g. Arthaud *et al*., 2008; Viegas et al., 2010) that record the Nigeria shield's continent-scale relationship with the other Neoproterozoic shear zones in North Africa and NE Brazil are available.

Several explanations have been given since the discovery of the shear zones of the Tuareg shield (Caby and Boesse 2001), on the structural evolution and nature of displacement in this shear zone. Some researchers inferred an entirely transcurrent motion, while others proposed a displacement of the thrust. Such results have primarily centered on geophysical and remote sensing measurements with minimal petrostructural data. In addition, previous investigations suggested deformation around Okemesi-Iwaraja area but the area's subsurface portion was not investigated. Also, the structures associated with the Okemesi-Iwaraja area have not been characterized to date and the lithostructures have not been configured.

Therefore, the focus of this study is on analysis of geological field data, geochemical, remote sensing and geophysical data, to understand the configuration of the lithostructures and the influence of these active lineaments (fractures), and also map the geometry of some of the structures, define the folds, fractures, and characterized the fold and faults associated with the Okemesi-Iwaraja area. This research is with a view of establishing a relationship between the surface tectonic lineaments and the subsurface structures. The analysis of geochemical and petrographic data, is expected to enable the chemical charerization of the rocks as well classification of the structures of Okemesi-Iwaraja of the shear zone and to further define the tectonic environment of the rocks, so as to position it within the context of the overall structural evolution.

1.3 Aim

The aim of this study is to investigate the rocks around Okemesi folds and Iwaraja areas, using field geological data, petrography, remote sensing, geophysical and geochemical techniques, in order to classify the rocks, define the lithostructures and their tectonic settings.

1.4 Objectives

The objectives of this research were to:

1. map and classify the rocks of Okemesi-Iwaraja area,
2. map the geometry of some of the structures, define the folds, fractures, and characterize the fold and faults of the Okemesi folds and Iwaraja area,
3. define the lithostructural configuration of the Okemesi-Iwaraja folds,
4. determine the relationships between the regional thrust and the mesoscopic, brittle ductile faults in some of the high fracture-density structural corridor, and
5. define the tectonics of the rocks of Okemesi-Iwaraja area.

1.5 Scope of Work

The scope of the work entailed interpreting ASTER L1A, LANDSAT8 OLI, RADAR images also interpret ASTER DEM and Aeromagnetic data sets covering the entire area for geologic structures, followed by ground thruthing and comprehensive field work. Petrographic and geochemical analysis of the rocks were also carried out to define the microfabrics of the rocks of Okemesi-Iwaraja area with a view to investigate the relationship between regional and microstructures. Geochemical analysis was used to classify the rocks and determine their source and tectonic settings.

1.6 Study Area

1.6.1 Location, Accessibility and Human Settlement

Okemesi-Iwaraja region lies within Latitudes $07^0$27'1.24"N and $07^0$54'18.67''N and Longitudes $004^0$43'41.96"E and $05^0$08'47.14''E. Topographic map sheets that cover the Okemesi-Iwaraja area are (Ilesha N.W, N.E, S.W, S.E, Ado Ekiti N.W, S.W, Akure NW, Ondo NE, NW all at 1: 50,000). The research area spans parts of Ekiti and Osun States in southwestern Nigeria and has a total surface area of 1665.5 km^2. Ilesa, Ibokun, Ikogosi, Igbara odo, Oke-Ila, Okemesi, Ilupeju, Soso, Oba-Sinkin, Ayegunle, Kajola, Ijero, and Ajindo are just a few of the key towns in the area (Fig. 1.1).

Due to road interconnectivity, parts of the study area in Osun State can be classified as moderate, whereas areas in Ekiti State may be classified as poor because it has only minor roads and footpaths that are not motorable. The field mapping was carried out during the dry season, which made it easier to locate outcrops. Minor linear settlements predominate in Ekiti State, while towns with nucleated settlements predominate in Osun State. Majority of the rocks in the area are mildly to heavily weathered, with only minor exposures near/along stream channels and road cuts. Because of human activities such as deforestation and seasonal bush burning, much of the area's vegetation is derived from savannah, whereas other areas are characterized by thick vegetation and soil cover.

The area of study (Fig. 1.2) lies between llesha, Ayetoro and Iganga to the southwest and Ijero and Ayegunle to the north. These towns which are important educational,

administrative and commercial centres are well linked by roads, with other parts of the country. There is a well-developed network of roads, paved and laterite, linkin these towns and traversing the study area. Villages and farm settlements are fairly well distributed throughout the area, interconnected by footpaths. Throughout the field investigation period, traverse was primarily along these roads and footpaths.

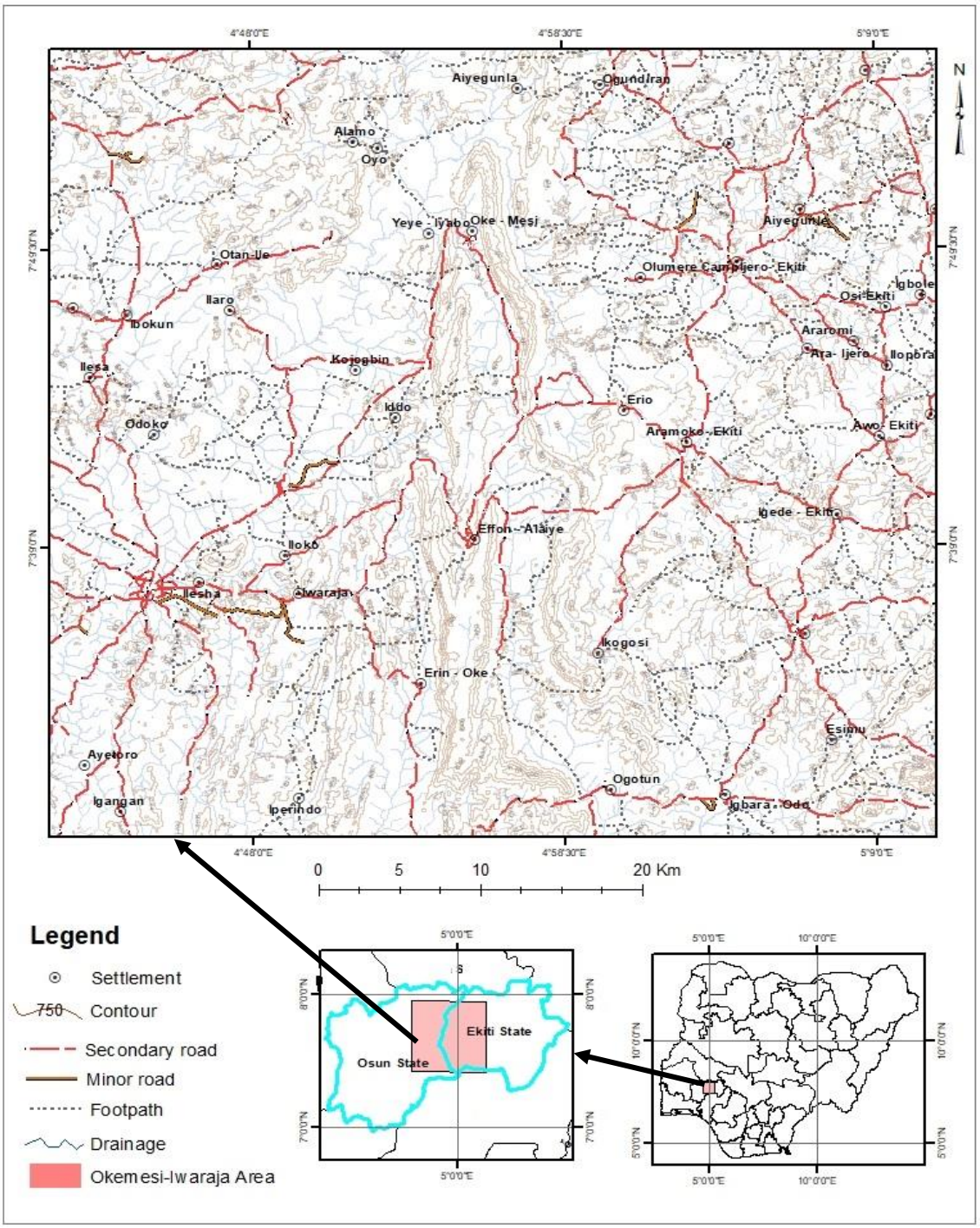

Fig. 1. 1 Location map of Okemesi-Iwaraja area

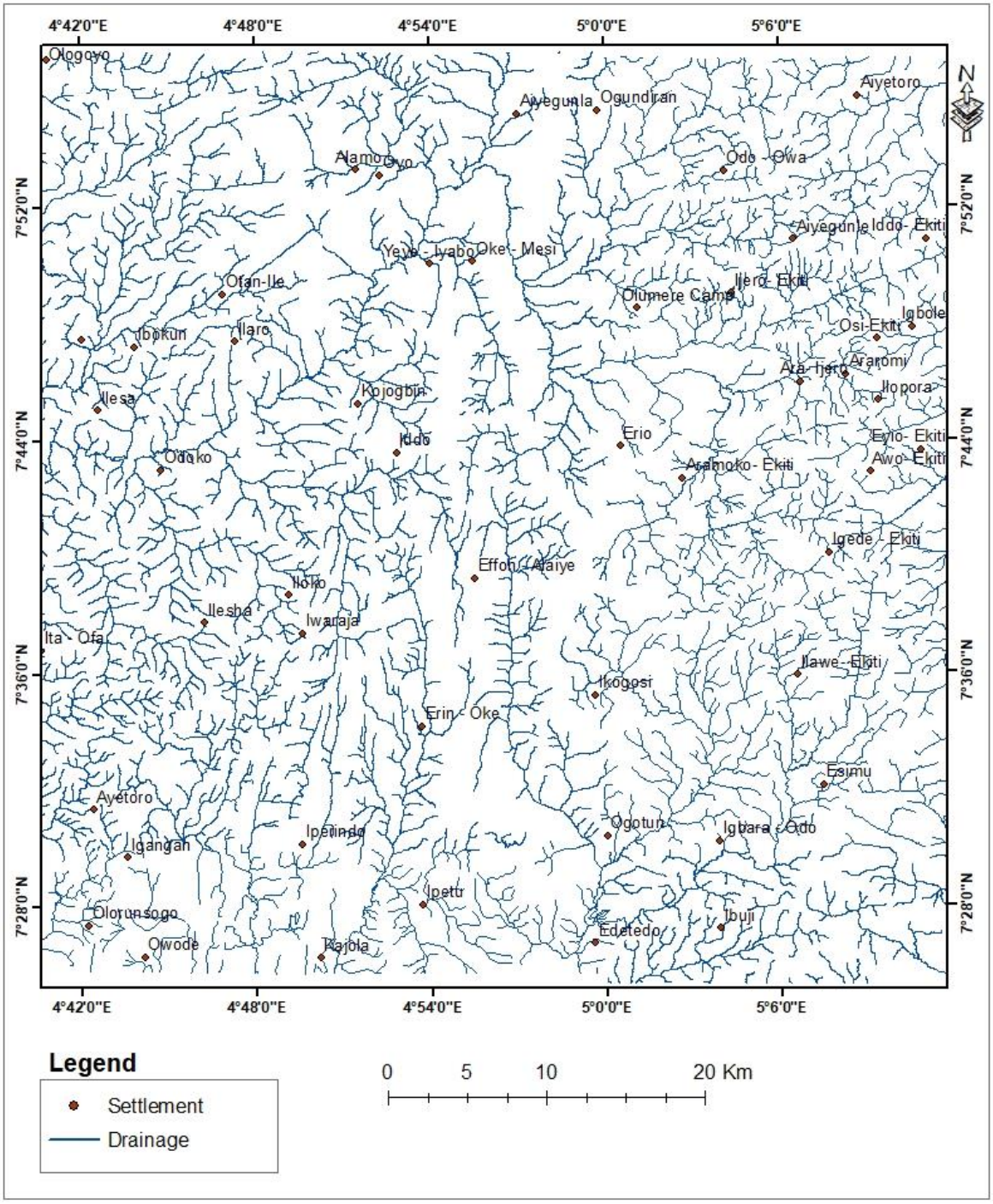

Fig. 1. 2 Drainage map of Okemesi-Iwaraja area

1.6.2 Drainage

The drainage system in the Okemesi-Iwaraja region and its surroundings is well established (Fig. 1.2). The main rivers, such as the Mokuro, Shasha, and Obabu, flow through the topographic lows. The tributaries of these rivers drain the northwest and southwest regions of the study area. The tributaries of the Rivers Osun and Ora drain the northeast and southeast regions. The mudflats are enriched in organic matter originating from shrubs, palm trees, and bamboo that grow in the stream valleys make up the majority of the vegetation aolong these waterways, which are largely sandy. Within the Okemesi-Iwaraja area, the drainage pattern is mostly dendritic, the drainages are structurally controlled; this can be seen along the River Oyi, a famous drainage that flows southwards.

1.6.3 Topography

Okemesi-Iwaraja area is hilly, with altitudes varying from 221 meters in the west (muscovite-quartz schist and pegmatites) to 799 meters in the centre (amphibolites and undifferentiated migmatite gneiss complex and schist). The Effon Psammite Formation stretches from Oke-Ila, Ilupeju, Oba-Sinkin, and Ayegunle to the eastern sections of Okemesi, with a ravine near Ayikunnugba (Oke-Ila), as well as low-lying outcrops and distant hills rising to an estimated height of 799 meters above sea level (Fig. 1.3).

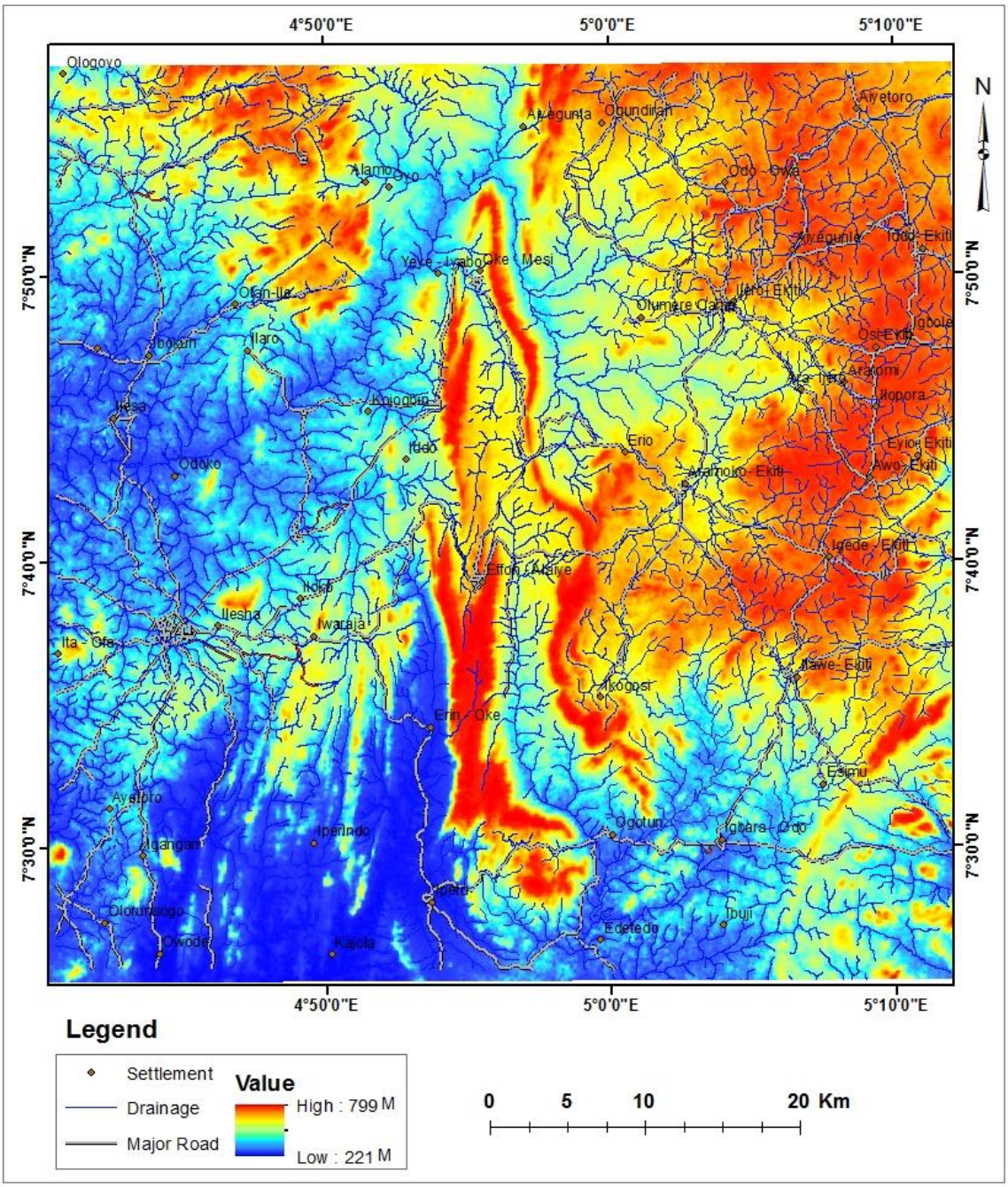

Fig. 1.3: Topographic map of Okemesi-Iwaraja area generated from DEM

1.6.4 Climate and Vegetation

In the Okemesi-Iwaraja area, a humid tropical climate is predominant, marked by alternating dry and wet seasons. The rainy season generally runs from April through October. During this time much of the rainfall, which amounts to about 1400 mm annually, is discharged. A dry season follows this wet season from November till March. During the dry season harmattan period, cool, hazy conditions usually prevail during the period November-February. Hot and powdery conditions are experienced for the rest of the season. During the dry season sporadic light showers can occur at any time. The average temperature ranges from 25^{o}C to 28^{o}C in the dry season (Adepitan, et al., 2017).

Rain forest conditions generally prevail throughout the district as typified by the occurrence of tall trees with foliage canopy, dense vegetation particularly along river valleys, and clustered grasses. However, these conditions have been modified in several places, due to cultivation, housing, and bush burning. The vegetation is therefore now primarily secondary forest and bush re-growth (Elueze, 1977).

CHAPTER TWO

LITERATURE REVIEW

2.1 Regional Geological Setting of West African Precambrian

The West African craton with the adjacent mobile belts largely constitutes the Precambrian subcontinent west of the Congo craton. It is believed to have evolved through three major orogenies, namely, the Leonian (ca. 3200 Ma), Liberian (ca. 2700 Ma) and Eburnean (ca. 2000 Ma). Footprints of the late Proterozoic Kibaran (ca. 1200 Ma) and Pan-African (ca. 600 Ma) events were confined to the mobile belt (Ajibade et al., 1987).

The Pan-African province or mobile zone east of the craton, embraces the Nigerian domain and the adjacent Dahomeyan basement (Fig.2.1). To the west, is the Dahomeyide fold belt, comprising the Buem formation and Atacora units wich separate the province from the West African craton. Northwards the province extends to the Tuareg or Hoggar shield. Bertrand and Caby (1978) distinguished three main structural zones which include the Pharusian belt composed essentially of late Pan-African calc-alkaline volcanics, in the west. Within the eastern zone occurs the N-S trending Tiririne fold belt consisting mainly of supracrustals. The Nigerian basement complex is essentially a part of the Pan-African province which is usually refered to as the mobile belt.

2.2 Nigerian Basement Complex

The Basement Complex of Nigeria is thought to have probably evolved by plate tectonic processes, which continued across the whole of Africa, linking Ghana-Benin-Togo sectors in West Africa; Mozambique belt of east Africa to the north, the Hogger massif in

central Sahara; and in North Africa, the Alpine fold belt. At least four (4) orogenic processes are thought to have occurred during the evolution of the Nigerian Basement Complex: Liberian (2800 ± 200ma), Eburnian (2200 ± 200ma), Kibaran (1100 ± 200ma), and Pan-African (600 ± 150ma) (Wright et al.,1985).

The Precambrian basement complex of Nigeria (Fig. 2.2) may be differentiated into three major units, the early gneiss-migmatite, the schist belts and the Pan African intrusive series. A variety of' migmatitic gneiss and minor meta-sedimentary bodies make up the gneiss-migmatite complex. These rocks commonly show complex structural patterns and include in places such as in the Okene-Kabba district, ferruginous quartzites or banded iron ore bodies. The schist belt occupies essentially north-south trending troughs within the gneiss-migmatite complex. They are thought to be Middle and or Late Proterozoic in age, and comprise mostly low to medium grade metasediments. Assemblages include metamorphosed pelites, semi-pelites, psammites, iron formations carbonate rocks and mafic to ultramafic bodies. However, the Ilesha schist belt is generally lacking in carbonate bodies and ferruginous units.

It is generally considered that the evolution of' the schist belts involved openings of crustal segments, either by rifting or plate motion with creation of rift or backarc basins and island arcs (Olade and Elueze, 1979; Ajayi, 1980). Consequently, depth variations tend to reflect the nature of sediments and basaltic volcanics emplaced in the troughs (Elueze, 1985). In addition, metamorphic-deformational cycles are other components of the development of the schist belts. Arising from these environmental and geological features, various mineral deposits originated within the schist belts. These notably include talc, magnesite and asbestos that are associated with mafic and ultramafic units; gold and sulfide mineralizations, possibly products of metamorphic-hydrothermal mobilization and the iron formations which are probably of volcano-sedimentary association. In the shallower troughs, carbonate bodies now represented as economic deposits of marble and dolomite are found as examplified in the Igarra-Jakura- Lokoja schist belts.

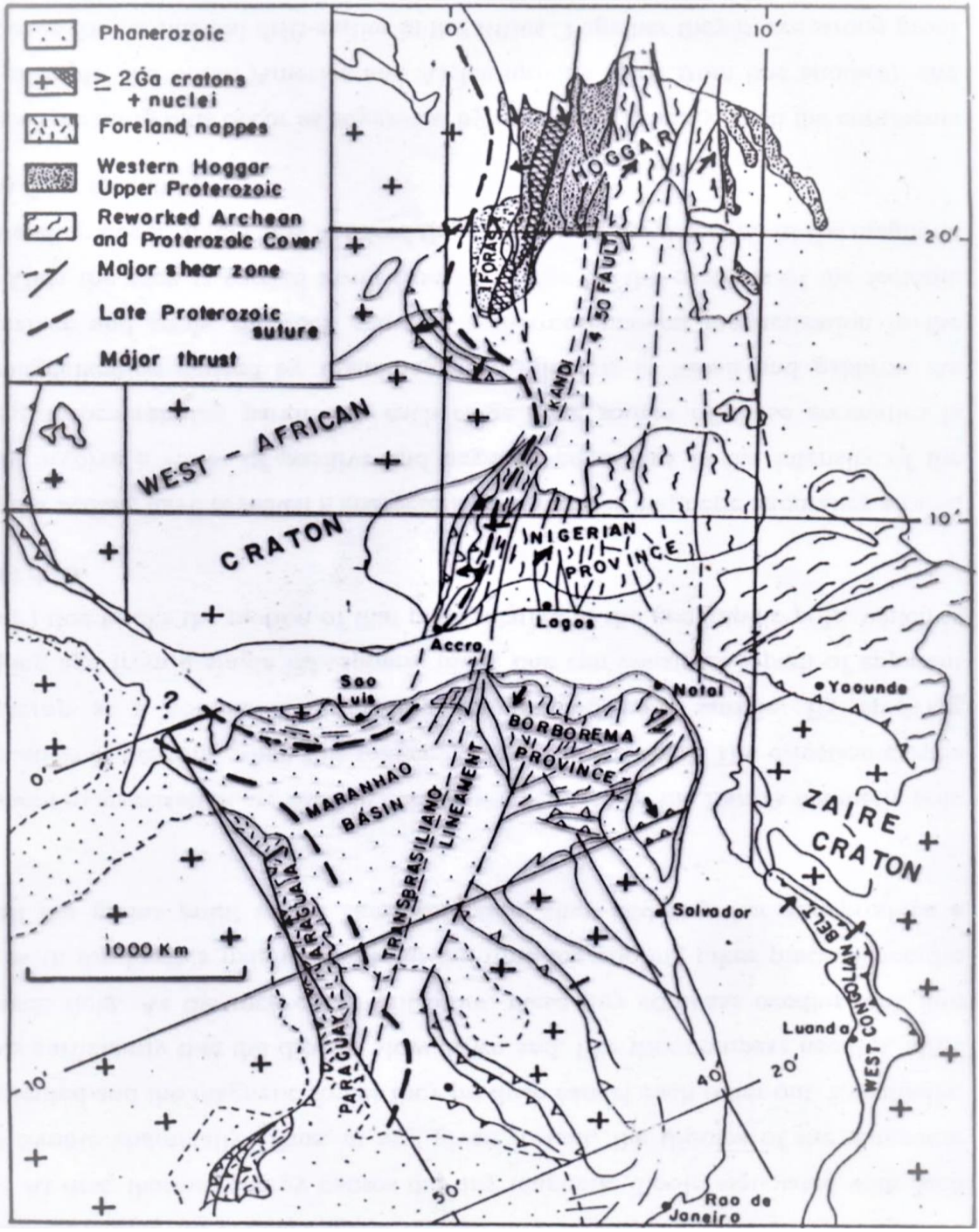

Fig. 2. 1 Geological Map of the Region East of West African Craton Showing the Pan-African Mobile Belt in the Hogger and Benin Nigeria Region and their Correlation with N.E Brazil (Modified after Caby et al., 1989)

The Pan-African orogeny is the most significant orogeny in Nigeria, which climaxed in the emplacement of the Pan-African Granites and also accountable for the wide spread amphibolite facies metamorphism of the rocks of the Basement.

Obini and Omietimi (2020), carried out study on Eiyenkorin area of Kwara state within the Precambrian Basement Complex of Southwestern Nigeria. The aim of the investigation was to map the area and evaluate the different rock types in order to understand their structural relationships and identify their geologic boundaries. They were able to establish that the fold axis is primarily E-W, with few trends in the NNW-SSE direction and an average plunge angle of 27°, and that the joints are mostly NE-SW, with small trends in the NW-SE directions, based on their structural interpretations. The foliation dipped SW and the overall orientation was NNW-SSE. There were few trends in the NE-SW direction. These structural patterns are consistent with Pan-African structural trends in the NE-SW directions. The structural orientation of rocks from the Eiyenkorin area of Kwara State follows the orientations associated with various tectonic events showing polycyclic deformation processes and metamorphism in the area, according to their research.

Pegmatites in southern Akwanga, which are found inside Nigeria's reactivated belt of the basement complex, have recently been studied. According to Chukwu and Obiora (2021), the pegmatites intruded a gneiss-migmatitic complex made up of metasedimentary rocks such as granitic gneisses and biotite gneisses, as well as meta-igneous amphibolites. Pegmatites and their host rocks exhibit similar geochemical signatures, typically corundum and hypersthene normative, and are highly peraluminous; however, rare metal pegmatites are more fractionated than host rocks and biotite microcline pegmatites. Rare metal pegmatites contain higher concentrations of Rb, Li, Cs, B, Be, Nb, and Ta and lower K/Rb and Al/Ga ratios than biotite–microcline–pegmatites and their host rocks. They went on to infer that the pegmatites are the result of sedimentary crustal anatexis. This suggests that rather than fractional crystallization, the rare metal pegmatites are regulated by the parent rock (as a result of post-collision processes).

2.2.1 Geochronology of the Basement Rocks

Evidence from geochronological data indicates that the Basement Complex bears an exceedingly long history due to the thermotectonic events; they have experienced greater or less amounts of alteration by higher temperature and stress in the earth crust; they have been folded and crushed, elevated into mountain ranges and worn down by agents of denudation to a gentle topography with differing intensities from Archean to late Proterozoic (Ajibade et al., 1988). The most apparent indicator of these events is the widespread occurrences of gneisses and migmatites spanning all ages mentioned above with the syntectonic to late emplacement of abundant amount of granitoids and rearranging of mineral ages in nearly all the Basement rocks.

Kroner et al. (2001) used zircons recovered from a migmatitic orthogneiss of granodioritic composition from Kabala, Kaduna district of northern Nigerian basement complex to undertake a geochronological age study. They found a SHRIMP 207Pb/206Pb zircon age of 35713, indicating that the Nigerian basement complex comprises Early Archean crust. Although the Kabala gneisses are the oldest rocks known from the West African shield, evidence for rocks of comparable age has recently been identified in the Reguibat and Kenema-Man shields of West Africa, indicating a probable Early Archean link between these terrains. The ramifications of the new age discovered by their study are far-reaching, not just in terms of understanding the crustal history of the Nigerian basement, but also of the entire West African shield.

In the Iwo area of the Nigerian basement complex, Adetunji et al. (2018) examined the petrography, whole rock geochemistry, and in-situ U-Pb zircon geochronology of quartz potassic syenite. The data show that the syenite was syn-tectonically emplaced throughout the Pan-African orogeny and that it is deformed heterogeneously. Based on geochemical data, the rock is categorized as a high potassic calc-alkaline that originated from metasomatized mantle with little crustal contamination. Using in-situ laser ablation inductively coupled plasma mass spectrometry, U-Pb zircon dating revealed a Concordia age of 642 Ma, which may be used as an emplacement and deformation age. The Iwo quartz

potassic syenite's position in relation to other undeformed syenite bodies in southwestern Nigeria and the major Pan-African suture zone indicates that during the Neoproterozoic, at least four terranes or microblocks were integrated in southern Nigeria. They concluded that the emplacement and deformation of the Iwo quartz potassic syenite coincided with basin closure around Ilesha-Ife and the resulting collision of two terranes/microblocks, and that the collision was caused by a west-dipping subduction-related tectonics distinct from the major Pan-African subduction zone at the West African craton's margin.

Table 2. 1 Generalized Geochronology for the Metamorphic Rocks of Nigeria, after McCurry (1976)

Approximate Date (Ma)	Orogenic Event	Effect of Orogenic events	Rock Type
540±40ma	Mid-Cambrian	Uplift, cooling, fracturing, faulting, high level magmatic activity.	
650±58ma	Late-Cambrian	Granitic intrusion, pegmatite and aplite development.	Older Granite.
600±150ma	Pan-African	Orogenesis: deformation, metamorphism, migmatisation and reactivation of pre-existing rocks.	
800±100ma	Katanga	Geo-synclinal deposition, intrusion of hypersthene bearing rocks.	Katanga Metasediments.
2000±200ma	Eburnean	Granite intrusion orogenesis: Folding, metamorphism, and reactivation of pre-existing rocks.	Eburnean Granites
2500ma	Birrimian	Geosynclinal deposition	Birrimian Metasediments
2800±200ma	Liberian cycle	Possible formation of banded gneiss complex near Ibadan (Grant, 1970)	
2800ma	Dahomeyan	Crystalline Basement	

2.2.2 Structural Relationship

The long history of the Basement Complex has resulted in complex structural pattern (Oluyide, 1988). Oluyide, (1988), also noted that the most prominent structure is the N-S planar structures, but relics of E-W, NE-SW and NW-SE structures are preserved. The basement rocks have over time been buckled into a sequence of open to close folds (antiforms and synforms), with the majority of them plunging to the north or south.

Several sets of fractures with N-S NNE-SSW, NE-SW, NNW-SSE and NW-SE trends are characteristics of the Basement Complex. The least E-W structures are presumably the oldest. The NE-SW dextral and NW-SE sinistral conjugate sets of strike-slip faults which resulted from the transcurrent movements are well developed within the Basement Complex. Field evidence include zones of mylonites, cataclastic and silicified rocks often expressed as dykes. These fractures control mineralization in the basement complex particularly gold mineralization associated with quartzfilled veins in both the migmatite-gneiss complex and the schist belts.

Ominigbo et al., (2021) noted that there has been very little study and reporting on Irruan granitoids, so they decided to map the region, conduct laboratory studies, and determine the petrological, geochemical, and structural characteristics of the Irruan Basement Rocks in the southern Obudu Plateau, southeastern Nigeria. They discovered the area contains five petrological units: granite gneiss, banded gneiss, migmatite gneiss, granodiorite, and biotite granite. The common consensus is that the rocks are siliceous and quartzo-feldspathic. Peraluminous metamorphosed rocks are the most common. In general, the granitoids were formed by partial melting of the crust with potential contributions from mantle-derived, crust-contaminated magma, as revealed by the marked variations in trace element distribution. They also discovered that fractures occur in the NW-SE, NE-SW, NNE-SSW, E-W, and N-S orientations on the outcrop scale. They found primary and secondary structure evidence. And they came to the conclusion that the dominant NE-SW fractures formed at the same time as the foliations and lineaments. Later episodes gave rise to the N-S and fairly poor E-W fracture sets.

2.3 Major Rocks of the Basement Complex

Oyawoye (1964), categorised the Basement rocks as: older metasediments which include; the gneiss-migmatites, the Older Granites and the Younger metasediments. In reviewing the basement geology, Mc Curry (1989), recognized four major groups:

i. An underlying high grade amphibolite facies complex of quartzo-feldspatic biotite and hornblende-gneiss-migmatites and high grade metasedimentry relics comprising Older metasediments.
ii. A supracrustal cover of low to medium grade metasediments.
iii. A suit of potassic syntectonic to late syntectonic granitoids, the Older Granite intrusives into the crystalline complex and the belts of the Younger metasediments.
iv. Volcanic rocks belonging to the post Pan-African (Older) Granite episode of high level magmatic activity.

Rahaman (1988) also classified the Basement rocks as follows: migmatite-gneiss-quartz complex; slightly migmatised to non - migmatised - metasedimentary and metaigneous rock, newer metasediments; and charnockitic, gabbroic and dioritic rock.

In general, Oyawoye, (1970) classified the rocks of the basement complex into four main groups, which are as follows:

i. The gneiss-migmatite complex
ii. The metasedimentary/schist belt
iii. The Pan-African (Older) Granites
iv. The Mafic-Ultramafic Complex

In their review of the Basement Geology and Mineral Belts of Nigeria, Haruna (2017), noted that crystalline basement rocks and Cretaceous to Quaternary sediments and volcanics are almost evenly distributed across Nigeria. Three lithologic classes are widely used to classify the basement complex: The migmatite gneiss complexes, schist belts, and Older Granites suites. The Migmatite gneiss complexes are said to be the Nigeria Basement

The earliest rocks in the complex are considered to be reworked older crust (most likely Liberian in age) that was further reworked by later orogenies along with the Eburnean (2000 + 200 Ma) and Pan African (600+150 Ma) orogenies, which included granitoids and schist belts. The Kibaran was preceded by lithologic units produced as a result of the Pan African event, including migmatites, gneisses, Older Granite intrusives, and other lithologic units, with dates ranging from 900 to 450 Ma. The Mesozoic is marked by the uplift and intrusion of the Younger Granites, a series of anorogenic, alkaline, shallow subvolcanic intrusives that occur along a narrow N-S strip in the western portion of the Eastern Province and extend north into Niger Republic.

2.3.1 The Gneiss-Migmatite Complex

The oldest rocks in the Basement Complex are gneisses and migmatites. They make up about half of the Basement (Rahaman, 1976). High-grade migmatites and gneisses, as well as relics of metasedimentary and metavolcanic rocks known as "Older Metasediments," make up the migmatite gneiss complex. Two generations of migmatites can be distinguished (Ajibade et al 1987); they include early migmatites which are complexly folded high grade migmatites and Pan - African injection type migmatites which are considered as altered pre-Pan-African Granite bodies. Gneisses also have lithologic varieties that include augen gneiss, sheared gneiss and mylonites. Other members include calcareous schists, marbles and quartzites, biotite-hornblende schists and amphibolites. The pegmatites of central Nigeria are almost entirely hosted by the migmatite gneiss complex.

Balogun (2019) updated current information on the geology of the Ilorin area using aeromagnetic data to get a better understanding of the geologic settings and structural disposition of Nigerian basement rocks. He discovered some NE-SW trending irregularities aligned diagonally and running from the SW to the NE, which correlated with the Banded Gneiss zone in the area; the regional study led him to the conclusion that the presence of major fractures interfering with metamorphic processes in regional settings may affect the grades of metamorphism that may result; that the schist region in the study area may be

overlying a region of downthrown bedrock; coupled with stress pattern that defined the crustal deformation style previously at the upper crust that had changed.

2.3.2 The Younger Metasediments (Schist Belts)

The younger metasediments are strictly speaking the schist belts which are N-S, NE-SW trending supracrustal belts. They are low-medium grade metamorphosed sedimentary and volcanic rocks, they form prominent NNE-SSW trending belts within the migmatite gneiss complex especially in northwestern Nigeria (Truswell and Cope, 1963; Rahaman, 1989). Although the northwestern Nigerian schist belts appear to be continuous with the Younger Metasediments of the southwestern Nigeria, ten main belts have been classified, (Ajibade et al, 1987); these are Birnin Gwari, Wonaka, Zuru, Anka, Maru, Ushama, Malumfashi, Kazaure and Toto schist belts. In southwestern Nigeria, occurrences include those of Ife - Ilesha, Egbe-Isanlu, Kabba-Lokoja-Igarra and Iseyin-Oyan. These belts have undergone different episodes of deformation, Ajibade, 1980; Grant, 1978; Other lithologies of the Younger Metasediments consist of quartzites, quartz schists, mica schists and granulites, metamorphosed clastic sediments containing little volcanics.

Osinowo et al., (2021) used airborne Time-domain electromagnetic data to characterize the subsurface in terms of rock distribution, structural arrangement, and gold and base metal mineralisation potential in the Ilesha Schist Belt in southwestern Nigeria. The findings show that amphibole schist and pegmatite terrain in the west has comparatively high subsurface conductivity, whereas granitic rocks in the east have mild to poor conductivity values. Their findings revealed anomalous response, especially along fractures and veins, implying the presence of structurally controlled gold and base metal mineralisation.

2.3.4 The Pan-African (Older Granites)

The distinction between the Older Granites which are of Precambrian to Lower Paleozoic age from the Jurassic Younger Granites was first differentiated by Falconer (1911); they vary greatly in age, structure, composition, rock association and mode of origin. The batholiths and plutons that intrude the migmatite-gneiss complex and schist belts are believed to represent the Older Granites. According to Jacobson and Webb (1946) and

Kuster (1947), the pegmatite belts in central and southwestern Nigeria are all connected to the Older Granite (1990). The Older Granite intrusions occurred at various periods during the tectonic development of the collision zones between the West African and Congo Craton (Kinnaired 1984). The granites, granodirites, adamelites, quartz-feldspathic granodiorites, monzonites, charnockites, and syenites are all part of the Older Granites.

Ibe and Obiora (2019) compared granitic rocks from Katchuan Irruan and surrounding areas in southeastern Nigeria to granitic rocks in Nigeria's Precambrian era, through a petrographic and geochemical study, the goal of geochemically characterizing the Granitic rocks in the Katchuan Irruan area and providing evidence for peraluminous and shoshonitic compositions as well as post-collisional setting. Garnetiferous biotite granite, aplitic granite, porphyritic hornblende biotite granite, porphyritic muscovite biotite granite, weakly foliated leuco-granodiorite, and simple pegmatite are among the Older Granite rocks found in this area. According to their findings, these rocks are closely related to the Precambrian Basement Complex rocks into which they intruded. The rocks are shoshonitic, alkali-calcic to calcic, ferroan, and peraluminous, according to geochemical data. They are rich in lithophile elements with large ion lithophil elements as well as high field-strength elements (Hf, Ta, Yb, Sm, Zr and Y). They have identical trace element and REE profiles, suggesting that they are co-genetic. They were most likely formed by partial melting of crustal materials in an orogenic (post-collisional) tectonic system, based on their overall geochemical characteristics.

2.3.5 Volcanic Rocks

Volcanic and hypabyssal rocks are unmetamorphosed alkaline and calc-alkaline rocks which intruded the migmatite-gneiss complex, the younger metasediments and the Older Granites during epirogenic uplift and fracturing in the closing stages of the Pan-African orogeny, (McCurry, 1989).

141

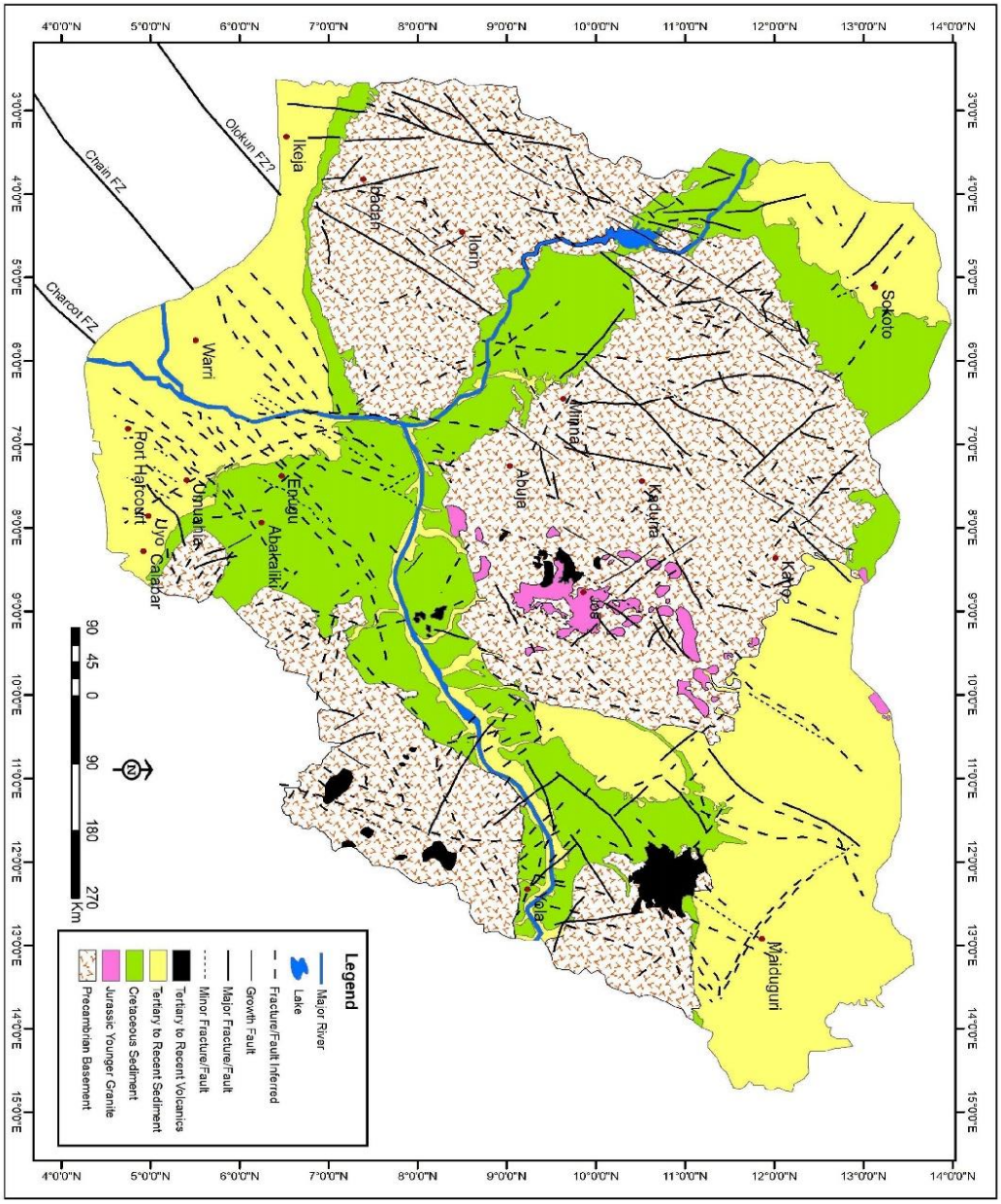

Fig. 2. 2 Geological map of Nigeria showing the lineaments and the major fault zones (after NGSA, 2006; Campbell et al., 2018)

2.3.6 Mafic-Ultramafic Complex

Several mafic-ultramafic complexes occur in both high-grade gneiss-migmatite environments as well as lower-grade metasedimentary schist belts, particularly in the northwestern and central regions of Nigeria. They consist generally of highly depleted serpentinised dunites with subordinate harzburgite and amphibolites. The geotectonic and economic importance of these bodies, possibly represent depleted upper mantle rocks and a complex of partly dismembered ophiolites (Ogezi, 1988).

Amphibolite is a lithologic unit found in the Nigerian basement complex, where it is frequently intercalated with metasedimentary phases. Aside from the Iseyin-Oyan schist belt, scattered grains of sulphide minerals and base metal deposits have been discovered in amphibolites and other lithologies in other Nigerian schist belts, although petrotectonic data for this region is lacking. Abdus-Salam et al., (2020) investigated the petrography and geochemical properties of amphibolites in the Iseyin-Oyan schist region around Itasa, with the aim of delineating them. The amphibolites were discovered to be mostly basalt to quartz mica schist in the form of lenses of tiny to large rocky boulders running NNE-SSW. The amphibolites are composed of tholeiitic basaltic to basaltic-andesite protolith that has been contaminated by the crust, according to geochemical studies. According to their results, t he rocks were emplaced in the Mid Ocean Ridge, but were affected by collision owing to the tectonic occurrence of Pan African Orogeny.

2.4 Younger Granites

Nigeria's Younger Granite Ring Complex forms part of a 200 km long ring complex region stretching 1600 km from Niger's Air area to central Nigeria (MacLeod, 1971). In Nigeria, there are more than 50 ring complexes, with localized intrusions varying in size from 2 to 25 kilometers across, Kinnaird (1984). In comparison to the Older Granites, the origin of the Younger Granites Complex is believed to be unrelated to any orogenic episode; hence they are called anorogenic granites.

Ibeneme et al., (2018) carried out surface and subsurface structural interpretation, using aeromagnetic data over a portion of the Younger Granite provinces of Northern Nigeria, Results indicated that the area's distinct magnetic anomalies are spatially associated with outcropping ring complexes. In addition to outcropping ring complexes, some ring complexes with no surface exposure (unexposed ring complexes) were identified. The Ririwai, Tibchi, Banke, Amo, Kudaru, and Zuku ring complexes, according to their findings, have outcrops of approximately 1300 m, 950 m, 920 m, 1400 m, 1150 m, and 1220 m above mean sea level, respectively. Numerous lineaments were identified as structural features with a significant pattern in the NE-SW direction. It was also discovered that the ring complexes of Northern Nigeria have a variety of surface concentric, as well as structural orientations that dip inward and outward with depth.

2.5 General Geological Setting of Southwestern Nigeria Basement Complex

The southwestern part of Nigeria lies between latitudes $7^0$00N and $10^0$00N, and longitudes $2^0$00E and $7^0$00E, and is underlain dominantly by Precambrian rocks. Okemesi-Iwaraja area is part of the Precambrian Basement complex in southwestern Nigeria, which lies west of the West African Craton in the late Precambrian to early Paleozoic orogenesis zone. The Nigerian basement complex stretches westward, linking to the Dahomeyan of the Dahomey – Togo – Ghana area to the east, as well as the recent south Mesozoic sediments of the Dahomey and Niger coastal basins. The West African Craton and the Pan African event, which locates West Africa within Africa's entire igneous/metamorphic structural system, are made up of Precambrian rocks that have been exposed to substantial supracrustal tectonic activities, such as the Liberian (3,000–200 million years ago), Eburnean (1,850 ± 250my), Kibaran (1,150 ± 100my) and Pan African (600my).

Around half of Nigeria's land area is covered by the crystalline rocks that make up the country's basement complex rocks. The remainder is made up of sedimentary rocks from the Sokoto, Chad, or Bornu Basin, the Niger Valley, the Benue Trough, and the Anambra Basin. In the southeastern, southwestern northcentral region of the country, the Basement rocks are still exposed and are isolated by sedimentary rocks except in the northcentral

where they are entwined. Nonetheless, according to Dada (2006), the rocks of Nigeria's Precambrian basement complex can be divided into four lithologic units: The amphibolite, hornblende gneiss, and granite gneisses found in southwestern Nigeria's Ilesha district are all duplicates of rocks found in southwestern Nigeria. The order in which these rocks are classified are seen below:

- The massive melanocratic amphibolites
- The hornblende gneiss
- The biotite granite gneiss complex
- The pink granite gneisses
- The grey granite gneiss

The structural, mineralogical, and petrochemical diversity of migmatite-gneiss in Southwestern Nigeria's Basement complex was re-evaluated by Obasi and Akinola (2020). They were able to demonstrate that the country rocks had structural heterogeneities that divided them into migmatite, banded gneiss, and granite gneiss sub-groups in their research. The units are usually hypidiomorphic to porphyroblastic in structure, with differing degrees of complexity. The foliations and lineaments of the variably deformed rocks are dominated by N-S and NNE-SSW trends. This leucocratic to melanocratic rocks are usually low-lying and contain differing proportions of felsic-mafic elements. Quartz, feldspars, biotite, hornblende, and muscovite dominate the mineral composition, with opaque minerals and pyroxene appearing in minor quantities. The rocks exhibit cryptic yet systematic variation in major element distribution, according to analytical findings. Geochemical research revealed that the rocks were igneous in origin, and that these gneisses are the product of igneous protolith anatexis.

2.6 Geology of Ilesha Area

The Precambrian Basement Complex of southwestern Nigeria, which are also part of Nigeria's Basement Complex rocks, underlie Okemesi-Iwaraja, which is located within the

Ilesha schist belt. Okemesi-Iwaraja area is also part of the regional Dahomeyide fold belt identified by Affaton et al. (1991), therefore it is not exempted from the structural and deformation events that affected Nigeria's Precambrian Basement Complex.

The Precambrian basement complex in southwestern Nigeria's Ilesha district (Fig.2.3), has remained recognized for its significant gold production for many years (De Swardt, 1953; Elueze, 1982). There are gold mines strewn around two main geologic regions. The district, which covers a large portion of Ilesha's western and northern regions and is noted for eluvial and alluvial deposits. The mafic-ultramafic units and metasediment, also known as the oolitic belt, are the underlying and potential source rocks (Elueze, 1986), (Osinowo et al., 2021). Primary gold mineralization occurs in felsic veins hosted in granite gneisses in another area to the southeast of the Ilesa.

In the Ilesha district, the largest rock associations are typically found in Nigeria's Proterozoic schist belts, which are mostly found within the country's western region. Nickel, chrome ores, talc, magnesite, asbestos, and iron ores are among the other mineral resources present in the schist belts. Nigerian schist belts are remarkably similar to Archaean greenstone belts within the context of structural features, lithology, and mineralization. Elueze (1986), pointed out that the Nigeria schist belts constitutes of high concentrations of mafic and ultramafic bodies, as well as lower metamorphic grade assemblages.

A major fracture zone known as the lwaraja fault system structurally divides the rocks of the Ilesha schist belts into two main segments (Fig. 2.3). (Elueze, 1986). Amphibolites, oolitic schists, meta-utramafites, and metape1ites dominate the region west of the fault. The eastern segments are made up of extensive psammitic units with minor metapelites, quartzites and quartz schists are examples. Many of these assemblages are intruded by a number of granitic bodies and are aligned with migmatitic gneisses.

The rocks of the Ilesha district can be classified as gneiss-migmatite complex, mafic-ultramafic suite or oolitic complex, metasedimentary assemblages, and intrusive suite of granitic rocks based on field association and petrological characteristics. These groups are

often related to a number of small rock types. Gneisses, calcareous and granulitic minerals, and migmatitic and granitic gneisses make up the gneiss-migmatite complex. Amphibolites and oolitic schists, as well as minor meta-ultramafites, make up the mafic-ultramafic suite. Quartzites and quartz schists are the most common metasedimentary assemblages with mainly metapelites and psammitic classes. The invasive suite is mostly made up of Pan-African Granitic Units (approx. 600 Ma). Minor rocks include garnet-quartz-chlorite bodies, biotite-garnet soil, syenitic bodies, diorites, and dolerites.

The schist belt of Ilesha area is divided into two sections of distinct lithologies, separated by the "Ifewara fault" main fault zone (Hubbard, 1975), the eastern and western parts, respectively. "Amphibolites, amphibole schist, quartz schist, associated pegmatites and gneisses underlie the western segment, while the eastern segment, in which Okemesi-Iwraja area is located, is denoted to as the "Effon Psammite Formation". The Effon Psammite Formation is made up of quartzite, quartz schists, and quartzo-feldsparthic gneisses of thin iron-rich schists and granulites that stretch for around 180 kilometers in the general direction of NNE-SSW, with quartzite thickness due to overthrusting of the Effon Psammite.

Furthermore, equally the eastern and western portions of the research area contain undifferentiated schists. The lithologies described include amphibolites, oolitic schist, and talcose rocks, all of which may be volcanic in nature. The eu-geosynclinal deposition environment is shown by the relationship of volcanic and clastic rocks (Hubbard et al, 1966; Dempster, 1967). The quartzites in this region, on the other hand, are oolitic, having metamorphosed from sandstone, and they appear to have good terain characteristics, with long-hogback ridge bands stretching from Okemesi to Itawure and streatching to Aramoko, at topographic heights of about 100 m above the surrounding terrain.

The rocks of the Ilesha schist belt are divided into two lithological and structural groups by the Ifewara fracture zone (Hubbard, 1975; Odeyemi, 1993). Other scientists (Wright et al., 1985; Anifowose, 2004) agreed that the structure existed and played a role in tectonic movements (Ayodele, 2013).

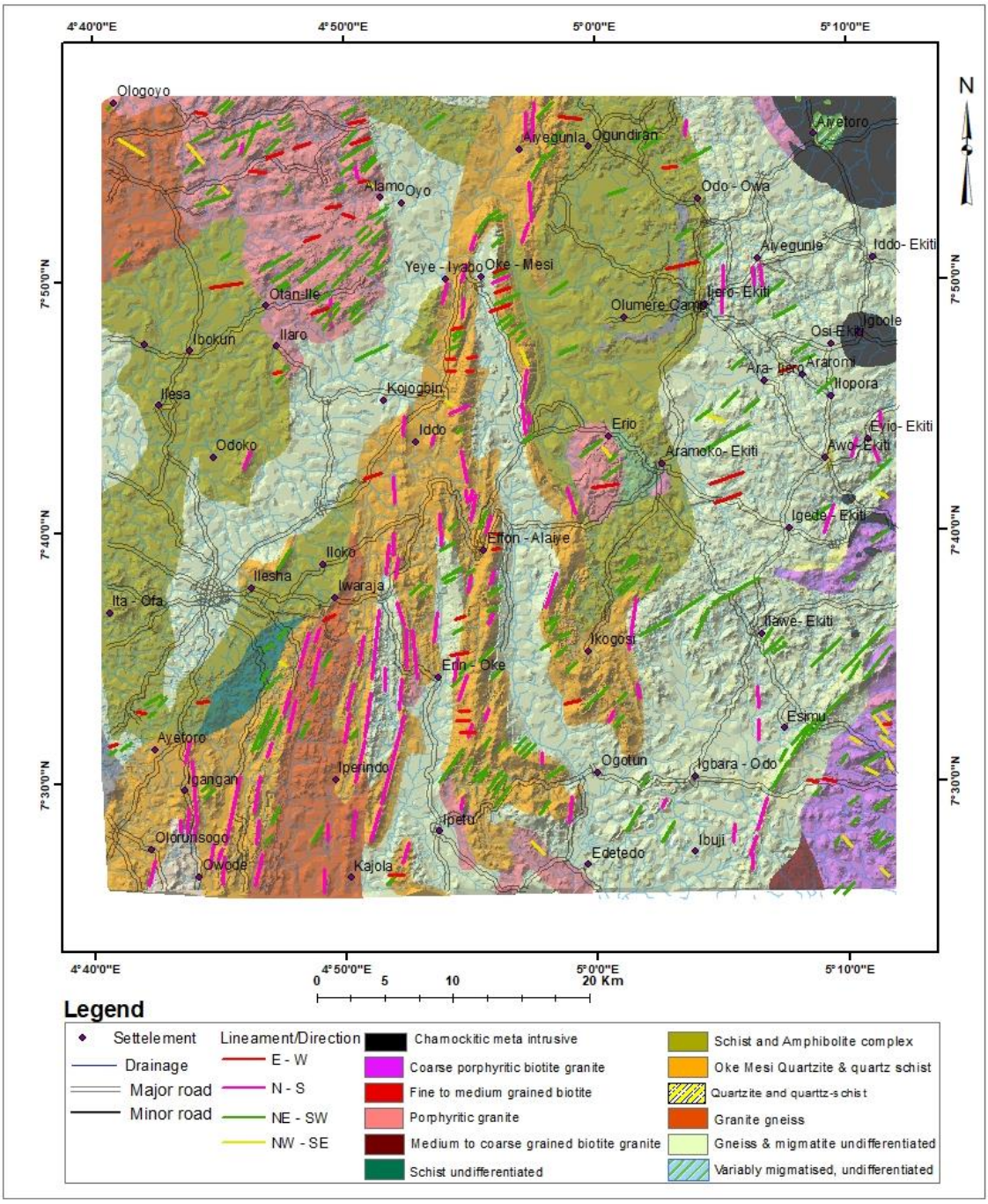

Fig. 2. 3 Geology and lineament map of parts of Iwo and Akure Sheets, showing the general study area, modified after De Swardt & Van Coppenhegan 1946-48; Dempster 1958 -1963.

2.7 Review of Previous Work

Early studies of the rocks of Ilesha area tended to concentrate on their petrological and structural relationships (e.g Oyawoye, 1964; and Hubbard 1975). De Swardt (1953) recognised the occurrence of the following major rock groups; the gneiss complex, the amphibolites complex, the granite gneiss, the quartz-sericite schists, quartz veins, dolerites, coarse porphyritic granite and muscovite pegmatite complex. Oyawoye (1964) observed that the metasedimentary rocks could be distinguished into an older and younger series, based on lithology, tectonic setting, structure, degree of metamorphism level of metasomatism or relation to granites. However, Hubbard (1975), recognized a three-stage tectonic evolution for the region, namely, the Eburnean, the Kibaran and lastly the Pan African. Two main descriptive subdivisions for rocks of Okemesi-Iwaraja area were proposed and include a migmatite gneiss-granite complex and metasupracrustal schist. In addition to researching the metallogeny of these rocks, Elueze (1977 and 1986), and Ajayi (1980), provided invaluable data on their geochemistry, petrogenesis and tectonic affinity that were used to develop models for their evolution.

These workers have differentiated three major rocks units in the area, which include the early migmatite-gneiss complex, the schist belt and the Pan-African intrusive series. The schist belts are thought to be middle and/or late Proterozoic age and comprise mainly low medium grade metasediments (Turner, 1983). The evolution of the schist belts is generally believed to include the opening of crustal segments, either by rifting or plate motion with the formation of rift or back-arc basins and island arcs (Olade and Elueze 1979; Ajayi, 1980). Matheis (1983), used soil survey as a tool for geochemical mapping of parts of the area under study. Variations in Co, Cu, Cr, Ni, Mn, and Zn were effectively applied to calculate ultramafic composition of rock units in the area. In comparison, it has been found that Cs, Be, Li, Rb, plus Mg / Li and K / Rb ratios adequately dermarcate the pegmatic host rocks of the usually felsic Sn-Nb-Ta mineral group. Tietz (1983) studying the dispersion of elements in two profiles along the Ife-Ilesha Akure road showed that laterites formed over amphibolites and mica schist display characteristic patterns of dispersion, with Al, Fe, Mn, Ti, Ni, and Cr increasing while Ca, Na, Mg and K, decrease.

Onuogu and Ferrante (1986) conducted an orientation survey to determine the feasibility of geochemical exploration for nickeliferous pyrhotite zones within the Ife-Ilesha area amphibolite complex. They also attempted to assess the possibility of employing arsenic as pathfinder element for gold. Their result suggests that routine sampling and analysis of soils may assist in location of zones of nickel mineralization. Earlier studies from Oyawoye, (1972) to Elueze, (1977), explained the geology and geochemistry of the Ilesa gold belt as part of Southwest basement complex rock and Klemm, et. al, (1979) worked on the chemistry of the mylonite complex and the metasedimentary order in the Ife- Ilesa region. Similarly, Ajayi, (1981) also worked on chemistry and mylonite sources in the Ife-Ilesha area while Rahaman and Ajayi, (1988), reported on the trace element geochemistry and geotectonic setting of the Ile-Ife schist belt as part of the Precambrian Geology of Nigeria. Rahaman, (1989) went on to classify the gneisses of the region into the early gneisses also known as grey gneisses and granite gneisses or pink gneisses in his study of the geology of southwest Nigeria.

A school of thought argues that the Ifewara fault is a transcurrent fault (Odeyemi, 1992), while others say it has a thrusted relationship (Boesse and Ocan, 1988). Hubbard (1975) and Odeyemi (1993) proposed an overthrust relationship with associated quartzo-feldspathic gneisses between the amphibolites and the rocks of Effon Psammite Formation. Odeyemi (1993), using Landsat MSS, SLAR and Aerial photos in his comparative study of lineaments of megascopic structures in the Okemesi fold belt, was able to show the advantage of using multi-source remote sensing to study geological structures. Although Turner (1983) suggested the fault may be a collisional suture.

Part of more recent research in the area include works by Oyinloye, (1992), where he investigated the geology, geochemistry, and genesis of the Iperindo primary gold deposit, Ilesha schist, southwestern Nigeria. and went further to clarify the geology and geochemistry of Iperindo primary gold deposit, Ilesha schist belt, southwestern Nigeria, interpretations from stable carbon isotope studies, in Oyinloye and Steed, (1996). In 1998, the same author talked and wrote about the geology, chemistry, and sources of banded

gneisses in the basement complex of southwestern Nigeria's Ilesha region, as well as Oyinloye, Odeyemi (2001), published on the Ilesha Schist Belt, Southwest Nigeria, about the geochemistry, tectonic setting, and source of major melanocratic amphibolites; Oyinloye (2002b, 2004a, 2006b, 2007), report on the evolution of the Ilesha schist belt, systemic and geotectonic environment, metallogenesis of the area's lode gold deposit, and provenance research, among others.

Other recent research in the area include work by Caby and Boesse (2001), who wrote about the Pan African Nappe System in southwestern Nigeria, in his work he noted that the Ife-Ilesha schist belt, presented new petro-structural data which revealed a detailed geology of the Ife-llesha region, showing that the general syn-metamorphic flat-lying structures, the overturned folding and the related strong boudinage of the mafic and ultramafic rocks are due to the Pan-African syn-metamorphic piling of thrust units above the Archean basement. Anifowose and Borode (2007), used aerialphotos to study the fold structures in Okemesi region. Kolawole and Anifowose (2011), applied remote sensing analysis to the study of a dextral discontinuity along Ifewara-Zungeru area, Nigeria, West Africa, and went on to relate the structures to those of the Zungeru area.

Anifowose et al. (2006), observed that all the rock forms had joints ranging in size from small to large, with some of these joints packed with quartz, feldspar, or a mixture of the two. They seem to mostly trend in a NE-SW direction. Since the pre-existing primary structures have been wipe out by successive deformations, Odeyemi (1999) stated that almost all foliations exposed by rocks of south western Nigeria, except intrusives, are tectonic in nature. Deformation is responsible for the general north-south trend of major fractures and foliations within the basement complex. A few number of workers have carried out analysis of remote sensing data of parts of the area. Ayodele (2006) carried out a remote sensing evaluation and geological studies of the area.

Anifowose (2004), carried out an integrated remote sensing study using remotely sensed images (Landsat, SLAR, Airphotos) of the Ifewara-Zungeru Megalinear structures. The outcomes presented, revealed two general sets of fractures, NNE-SSW set and the E-W set,

which is perpendicular to the bearing of the quartzite bands related to gold mineralization in the Ilesha region, and advocated that the continuity of the Ifewara-Zungeru fracture system points to a probable alignment through the Okitipupa Ridge submarine ridge with an oceanic fracture zone. Odeyemi (1993) also performed a comparative study of some aerial photographs of the Okemesi Fold system in southwestern Nigeria and inferred that SLAR is very useful for regional structural studies due to its dual (i.e. north and south) look direction in terms of lineaments detection. Odeyemi (1992) carried out remote sensing study of the area around Ifewara fault using imageries, and came to a conclusion that combinations of transcurrent and dip slip movements may have occurred at various times along the fault. Boesse et al (1989), Caby and Boesse (2001) deduced and identified the shallow dips of foliations and shear zones' low angle thrusts, and related recumbent folds in the Ife/Ilesha area.

Adebayo and Bello, (2012) went on to do a critical study of gold recovery in order to propose a flow sheet for the Igun gold field; their results were published in the Journal of analysis in pure and applied sciences, June 2012 Ademoso and colleagues (2013) found further proof of cataclasis in the schist belt of Ife-Ilesha area. According to the research of Adeoti and Okonkwo (2017), Fagbohun et al., (2017), The Iwaraja shear zone was formed through the later phase of structural deformation in the Iwaraja region, and it was related with retrograde mineralogical evolution from protolith of amphibolite facies to greenschist facies ultramylonites in the shear zone. They also used structural styles derived from remote sensing research to characterize tectonic events. They were able to recognize three distinct deformation events, however. The first episode (D1), which is mainly a ductile deformation, produced NNE-SSW axial plane foliations and folds. The second deformation case is a systematic reactivation of the D1 occurrence, with the prevalence of E-W compression which led to folding of the F1 folds axis and the S1 foliation. The development of brittle-ductile structures during the third deformation episode is said to have fractured and displaced the limbs of the F1 folds, resulting in sigmoidal twisting of the limbs. Ayodele carried out geological mapping of a landslide-affected region near Okemesi in (2020), to assess the nature of the rocks, the geological and environmental causes that may have

triggered the landslides, with a particular focus on rock types, fractures, and anthropogenic activities along the slope toe of the hill, as well as the types and sizes of the materials transported. The impacted area, according to the geological report, reveals that the rocks in the analyzed area have been heavily fractured.

CHAPTER THREE

MATERIALS AND METHOD

3.1 Datasets

Landsat-8 OLI (Operational Land Imager) image has a spatial resolution of 30 meters in eight out of its' nine spectral bands which are Bands 1 – 7 and 9. The spatial resolution for Band 8 which is a panchromatic band is 15 meters. Because of its spectral capabilities, and the wide range and variety of features that are required for analysis, LandSat 8 (OLI) was selected for this study. One LandSat scene corresponding row and path P190R55 of 15/01/2015 with ID LC81900552015015LGN00 covering Okemesi-Iwaraja area was acquired. Shortwave infrared Band 7 (2.11 - 2.29μ) is known to be appropriate for extracting geological data and rock features. TM, ETM, and ETM+ sensors were used in previous studies involving extraction of lineaments using Landsat. While carrying out this research, the band of short wave infrared in OLI, which ceresponds to that of the other Landsat images was used.

ASTER (Advanced Spaceborne Thermal Emission and Reflection Radiometer) is a NASA and METI (Japan Ministry of Economic Trade and Industry) advanced multi-spectral satellite imaging system that was deployed on board the TERRA spacecraft in December 1999. It also has a DEM component, which was used in this research.

The Nigerian Geological Survey Agency (NGSA), supplied the high resolution aeromagnetic (HRAM) data for Okemesi-Iwaraja. The data were collected at an altitude of 80 meters, along 500-meter-spaced NE-SW flight lines, at a scale of 1: 100,000 covering a half-degree sheet. The effect of the regional geomagnetic field (IGRF; 2004) has been removed, resulting in HRAM anomaly or residual field. During the processing by FUGRO, noise was eliminated by continuing the aeromagnetic anomaly field upwards thus creating the region's upward continued aeromagnetic anomaly map. On the upward continued aeromagnetic anomaly results, various processing inversions were also performed, but only the enhancement with optimum details for the intended purpose of this analysis was considered for interpretation.

Topographic maps for the area at the scale of 1:50,000 covering Okemesi-Iwaraja were acquired from the Office of the Surveyor General of the Federation (OSGOF), this scale is expected to give high resolution. The sheets acquired include Ilesa NE, NW, SE, SW, Ado-Ekiti NW, SW, Ondo NE, NW and Akure NW. Existing Geological maps covering the area under study on scale of 1: 250,000 (Akure and Iwo heets) were also acquired from Nigerian Geological Survey Agency. SAR RADAR data covering the area under study was acquired from The European Space Agency (ESA), this SAR data specification belongs to a series of RADAR data acquired by sensors abored the sentinel series launched by ESA. The data has 10m resolution.

List of Datasets

1. ASTER DEM 30m
2. RADAR (SAR) 10m
3. LandSat8 Image of Okemesi-Iwaraja with a resolution of 30m
4. Aeromagnetic map of Okemesi-Iwaraja at the scale of 1: 100
5. Topographic map of Okemesi-Iwaraja at the scale of 1:50,000
6. Existing geology map of Okemesi-Iwaraja at the scale of 1:100,000

3.2 Software

Listed below are the software used for this research

- ArcGIS 10.6
- Erdas Imagine 2014
- Envi 5.3
- Geosoft Oasis Montage 4.4
- Euler Deconvolution.
- Georient
- Geomatica
- SNAP

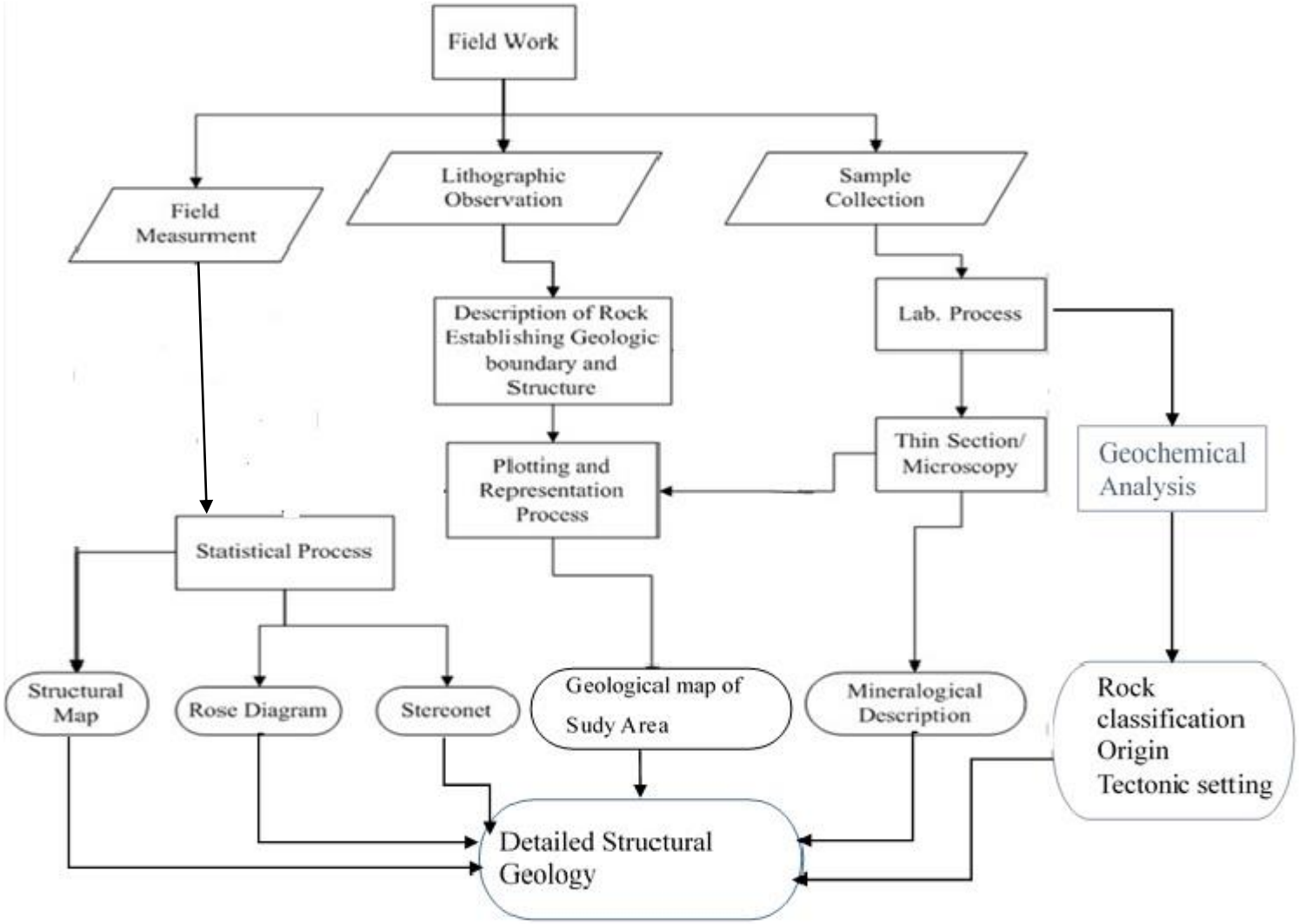

Fig. 3. 1 Flow Chart of Field Work process for the study

3.3 Remote Sensing

Remote sensing offers extensive aerial coverage of spatial, temporal, and spectral details, permitting for mapping of lineament covering large areas (Jensen, 2005). The process of mapping lineaments from an image involves detecting changes in the surface reflectivity as a result of changes in topography and vegetation coverage (Jensen, 2005; Abrams, 2000). For the detection of lineaments that can be viewed in topographic terms, DEM shaded relief depictions were used. Remote sensing was used to isolate lineaments that were likely to be associated with geological structures such as faults and fractures in areas where there are no outcrops (Rahiman and Pettinga, 2008).

A hillshade image from Digital Elevation Model (DEM) improves the expression of lineaments for identification and digitizing by producing shadows dependent on the bearing of artificial sun illumination. All image processing were performed using ENVI and ERDAS IMAGIN software (Figure 3.2).

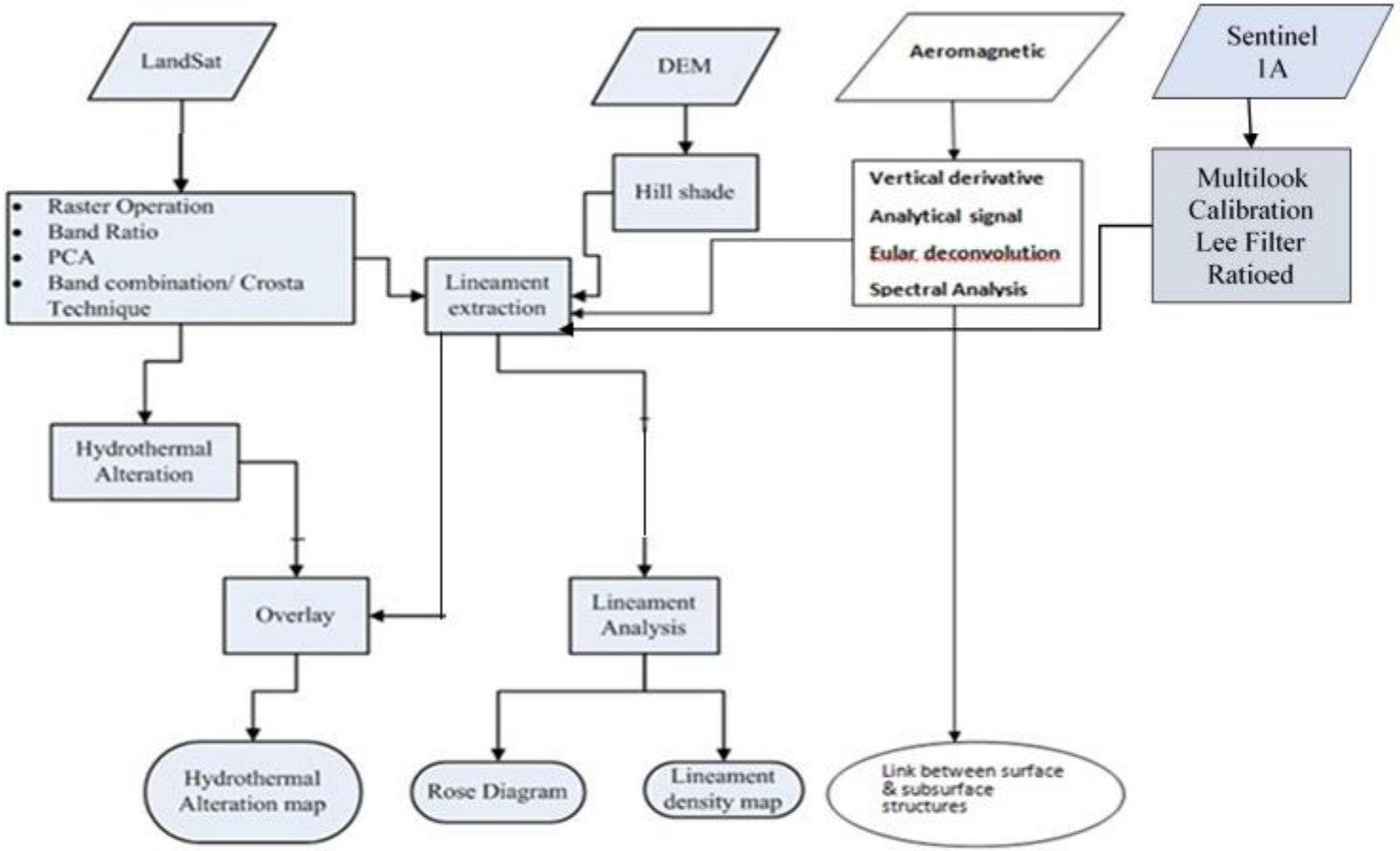

Fig. 3. 2 : Flow Chart of Raster and Spatial Operations

3.3.1 Image Processing

The FLAASH tool in ENVI was used to transform the Landsat-8 image from Digital Numbers (DN) and radiance to surface reflectance. The radiance and DN data were rescaled to reflectance data during atmospheric correction. As a consequence, the albedo of both spectra were adjusted to roughly the same. The spectral generated can then be directly compared to reflectance spectra in the lab or in the field. The panchromatic and cirrus cloud bands were excluded in this study (band 9). The study area was selected from a larger scene that covered most of Southwestern Nigeria, useful information was extracted from the OLI image of the area. Atmospheric, geometric, and radiometric effects were all corrected across the scene. Lineaments in the images that would not have been apparent otherwise were identified using image processing. Since the lineaments were digitized, the rose diagram was used to display the lengths and orientations of the lineaments. The Shear Zones were also digitized.

On the Landsat-8 OLI image of the region, digital spatial operations were performed, as well as contrast and edge enhancement filters applied to the image to improve visual clarity, as well as principal component analysis (PCA) and band ratio operations. The lineaments in the image were digitized to produce a lineament map, which was then used to calculate the density of the lineament.

3.3.2 Automated Lineament and Manual Lineament Extraction

Six distinct sets of factors were employed in the procedure, and the derived lineaments were physically compared to one another. These lineaments were visually modified by overlaying highways identified in the region and immediately removing any straight edges that matched with the subset image's boundary. The manual extraction approach consisted of digitizing lineaments from the research area's established Geological map as well as observable lineaments and faults in the image composite, Sobel filtered Band 6 and ASTER

DEM in the four primary directions. The second stage was by applying four directional filters to the Band 6 of Landsat8 image that covered the area.

3.4 Digitizing

To collect digital dataset that were available in hardcopies of topographical or geological maps, the datasets were scanned and saved as raster data, which is usually organized in rows and columns. The resulting scanned raster formats were georeferenced using tiepoints and compared to real-world coordinates by establishing a coordinate system. After georeferencing, a value domain was created for the maps separately. This was to assign ID values to the data base being created since the values of the contours to be digitized represent elevations and total intensity of the respective maps. When creating domain for datasets that do not use values, they are created either as image, unique or class domain, as applicable.

The relationship between rows and columns of a raster map (row, col) and real-world coordinates (X, Y) can be stored using a georeferencing method (X, Y, Z). For raster maps, a georeference is needed. A georeference uses the database's coordinate system. It is important that raster maps of the same area use the same georeference, as raster operations that merge raster maps would only make sense if the pixels in the maps correspond to the same location on the earth. A coordinate system specifies the types of coordinates that can be used in maps; for example, you can use user-defined coordinates, defined national standard coordinates, or UTM (universal traverse macator) zone coordinates. The potential XY- or LatLon coordinates that can be used in a map are described by a coordinate system.

A domain determines, i.e. stores, the details that a map, a column, etc. can have. A domain is a set of class names or IDs, a sequence of values, colors, etc. All elements in a map or column must use one of the domain groups, IDs, or values that the map or column uses; otherwise, these elements would appear as undefined. After these procedures as described above, the maps were ready for digitizing. The maps were digitized by creating a segment map that allows one to use the segment editor to trace each contour line, the contour values were entered at the end of each trace. The purpose of digitizing was to convert the analog

maps or objects to their digital formats acceptable by GIS software for processing and manipulation.

3.5 Contour Interpolation

The digitized maps were stored in digital formats for further processing and manipulation depending on the information been sort. Contour interpolation exercise was carried out on the data. Contour interpolation is a method that begins by rasterizing contour lines of a segment map with a value domain, and then uses a linear interpolation to compute values for pixels that are not covered by segments. This technique also uses a raster map as an input raster map on the command line. A value map can be used to represent the input section. Contour interpolation creates an intermediate map of rasterized segments as a result of the operation. For all pixel values with unknown values, an output value is computed in this intermediate map. It is the output value created from the interpolation that can be manipulated, by applying other statistical operations.

3.5.1 Hill Shading

Hill shading procedure was also applied to the aeromagnetic and topographic data, this operation was done in Oasis Montage ArcGIS respectively, using a standard linear filters. This technique is often used in cartography to create the appearance of a three dimensional view from a digital terrain model. The dimensions of the filter are given

As follows: [-3] [-2] [-1]

[-2] [1] [2]

[-1] [2] [4]

Structural analysis using DEM technique is centered on shaded relief images with varying elevations. Subsequently, this was combined with enhancement methods such as vertical amplification of multiple sun azimuths and angles, which enhanced the perception of elevation images. The following steps were taken toward achieving the goals of interpreting structures from the DEM: (1) The DEM image was first subjected to image enhancement filters such as vertical augmentation and shading; (2) To create a lineament map, the

enhanced image data was viewed using visual rationalization; (3) The results from the lineaments that were interpreted, were then plotted in a rose diagram; (4) The geological structural analysis of the area was defined, based on the major trends observed from the stereo net. Most of the linear features seen in the DEM image were interpreted as faults, fractures, and, in some cases, foliations.

3.6 RADAR Processing

Sentinel-1B is one of the range of products of the Sentinel Mission by ESA for monitoring of the earth's surface, among which are multispectral images and Synthetic Aperture Radar (SAR) such as Sentinel-1B. SNAP is software developed by Sentinel European Space Agency (ESA) for processing of Sentinel products and other Images. Sentinel-1B IW GRDH 1SDV was acquired from the Sentinel Website and was processed using SNAP and ENVI software.

The data was opened in SNAP software; Okemesi-Iwaraja area was subset from a lager scene covering the area. The Sentinel-1B SAR data is made up of two image bands, the VH and VV bands; V and H are the Vertical and Horizontal amplitudes respectively. It is captured in the microwave region of the electromagnetic spectrum by the sensor unlike the optical images that are captured within the visible to near infrared region of the electromagnetic spectrum. These bands were calibrated, and converted to decibels in logarithmic scale and afterwards converted to bands from the virtual state and saved.

Various inversion techniques were used on the pre-processed SAR data, to enhance features interpretable for structural analysis. Speckle Filtering LEE and Frost filters were used on the SAR data, Geocoding and Terrain Correction was also carried out. Contrast stretch and colour manipulations were applied, the VV and VH band subtracted, multiplied or divided by each and output in RGB to give the desired results. Structures were extracted from the final outputs. All these processes are represented in the flow chart in Figure 3.2.

3.7 Aeromagnetics

This is a method in geophysics that measures the magnetic field strength of the Earth, this process of measurement is carried out from the air over an extensive area, and has the capability of measuring magnetic field strengths deep into the subsurface. It is able to effectively map lithology and subsurface structures such as faults, graben, horst. Presence of fractures and faults, creates magnetic difference in geologic units which can cause magnetic anomaly. In most cases, magnetic rocks that have undergone alteration and conversion from magnetite to pyrite show results in lower magnetic anomaly than the rocks of unaltered zones. In light of the magnetic property of alteration zones, Abiye and Tigistu (2008) highlight the significance of hydrothermal alteration zones, this is because the presence of fluid within the faults and fractures would reduce or have no magnetic response, causing low magnetic anomaly. The subsurface structure can therefore be modeled from magnetic profiles using several inversion processes. Magnetic method was used in this study for mapping of the subsurface structures in the study area.

3.7.1 Processing TMI Data

Processing of airborne dataset involved the use of enhancement method involving the subtraction of the earth's background magnetic field as well as gridding routine. Background correction (aircraft, radon, and cosmic), stripping, and microleveling are some of the corrections employed. Microleveling was used to correct minor differences and spatially homogenize the data, allowing for the creation of a better image for evaluation. FUGRO (the contractors) removed diurnal changes in the earth's magnetic field, aircraft heading, instrument deviation, lag error between aircraft and sensor, and differences between flight lines and tie lines. The datasets spaced equally in a 100-meter square grid cells, using a minimum curvature interpolation algorithm (Briggs 1974). This technique allowed for direct use of the proposed filtering and enhancement techniques. The aeromagnetic data covering Okemesi-Iwaraja area and its environs was georeferenced using the Universal Transverse Mercator (UTM) Coordinate System, zone 31 within the northern hemisphere. Mainly, Geosoft® (Oasis Montaj) software was utilised for processing and enhancement of

the airborne geophysical data. Whereas ArcGIS was used for integration of results that were interpreted in a GIS environment.

Advanced enhancement filters such as reduction to the pole, analytic signal, first vertical derivative, and tilt angle derivative were used to process the magnetic dataset. Magnetic intensity generated from the profile to grid data was then rendered as an image in natural colour (magenta for high intensity, blue for low intensity) using histogram equalization to maximize the colour ranges. Since there was a substantial change in magnetic intensities from the inclination and declination at low latitudes, it was vital to define the magnetic anomalies at the place where they sit over the source. To position the magnetic anomaly to simulate sitting over the magnetic source, mathematical transformation or filtering techniques such as reduction to the pole (RTP) or equator (RTE) and analytic signal were used. The majority of linear anomalies in the study area were not visible on gridded residual intensity magnetic imagery. After the high amplitude, long wavelength anomalies were eliminated using vertical derivative and automated gain control filters, the linear anomalies were revealed. Upward continuation filtering was also used to aid in defining the depth ranges of deeper magnetic sources. Edge detection filters are typically used to demarcate linear characteristics while reducing long wavelength anomalies (Oruc and Selim, 2011). As a result, the Tilt derivative (TDR) filter was applied to produce short wavelengths that showed the presence of magnetic lineaments.

Total horizontal derivative (THDR) was applied to the HRM data of Okemesi-Iwaraja area because this approach can reveal faults and contact features, making it appropriate for this study. The total horizontal gradient technique calculates the rate of change in magnetic susceptibility in both the x and y directions, yielding a grid. The TMI's frequency content and total gradient remain unchanged, but the gradient's spectral phase shifts as presented in equation 1(Cordell and Grauch, 1985).

Equation 1. Full (or Total) Horizontal derivative (THDR)

$$THDR = \sqrt{\left(\left(\frac{\partial T}{\partial x}\right)^2 + \left(\frac{\partial T}{\partial y}\right)^2\right)}$$

Analytical signal (AS) when used, the methods to be applied should be selected cautiously when working in equatorial regions, because of the difficulties related with analyses of magnetic anomalies at low latitudes. At all magnetic latitudes, the analytical signal works well because it is not distorted by the orientation of the ambient field, and the peak determines the edges of magnetic bodies. The analytical approach has been shown to be an efficient method for identifying contacts and sheet-like structures, independent of their dip angle or magnetic latitude as expressed in the equation below (Phillips, 2000).

Equation 2. Analytical signal (AS)

$$A=A(X,Y) = \sqrt{\left(\left(\frac{\partial T}{\partial x}\right)^2 + \left(\frac{\partial T}{\partial y}\right)^2 + \left(\frac{\partial T}{\partial z}\right)2\right)} +$$

The $\tan^{-1}$ expression variable that is between +1.57 and -1.57 provides an automatic gain control (AGC) that amplifies the amplitude of low signals, making the Tilt derivative very efficient for RTE and RTP data (Verduzco et al., 2004), tilt derivative is expressed in equation 3 below. The tilt method was applied to the RTE data.

Equation 3. Tilt Derivative (TDR)

$$TDR = \tan^{-1}\left[\frac{VDR}{THDR}\right]$$

3.8 Geologic Field Mapping

Reconnaissance field mapping of Okemesi-Iwaraja area was conducted by traversing along footpaths, roads and stream channels. The field equipment used included Global Positioning Systems (GPS), this was used in accurately pinpointing the spatial location of outcrops and observed features. Compass, geologic hammer, hand lens, measuring tape, field note book, marker pens were also employed in the field; sampling bags were used to carry rock samples. A camera was used to take photographs of observed geological structures and their relationships with the rocks.

Field mapping operations were used to produce the required geological and structural data. The technique necessitates in-situ inspection and analysis of outcrops and their structures, as well as detailed examination of rock structural features such as folds, joints, dykes, foliation, and so on, as well as the compilation of necessary field data during the geological

field mapping. This exercise included careful examination, identification, and systematic description of the rocks, as well as the subsequent compilation of structural details, which included recording the nature, shapes, styles, size, symmetry, axis, plunge, orientation, types of folds and other structural features. Rose diagrams were generated for the various structural parameters. Thin sections of focused specimens were prepared to allow the identification of constituent mineralogy, using transmitted and reflected light microscopy for microstructural analysis of deformation textures and fabric components. Results from the field were combined with the results of some systematic digital analysis performed on the satellite image and topographic data digitized to produce the area's structural geological map with rock boundaries, drainage, lineaments and relief. During interpretation and analysis of the structural distribution, map compilation and cross-section construction were also used to establish cross-cutting relationships that represent regional deformation events (see Figure 3.1).

3.9 Geochemical Analysis

ICP-AES (inductively coupled plasma atomic emission spectroscopy), also known as ICP-OES (inductively coupled plasma optical emission spectrometry), is a chemical element detection technique. It is a form of emission spectroscopy that uses an inductively coupled plasma to produce excited atoms and ions that emit electromagnetic radiation at wavelengths specific to a specific element. This method employs flames with temperatures ranging from 6,000 to 10,000 K. The strength of this emission is a good indicator of the element's concentration in the sample.

From the field samples collected during the mapping, 24 fresh samples were selected, the selected samples were pulverized to 70µ mesh size. 20 grams of the different samples the pulverized rocks were carefully measured and bagged in separate cellophane sample bags for the respective samples. Afterwards, the samples were sent to M.I. Analytical in Canada for analysis. Induced Coupled Plasma – Atomic Emission Spectrometer (ICP-AES) method was used, Major, Minor and trace elements were determined. The results were plotted as spider graphs, variation diagrams, ternary diagrams, normalized chondrite plots, etc.

CHAPTER FOUR

RESULTS AND DISCUSSION

4.1 Preamble

Geological maps which contain lineaments, rock types, and landform were generated using image processing algorithms applied to Landsat OLI images, ASTER DEM, RADAR, and Aeromagnetic data.

4.2 Remote Sensing Image Processing and Analysis

Standard techniques used in processing image such as image composite of selected bands, ratioing techniques, decorrelation stretch alongside principal component analysis were applied to Landsat OLI to get morphological, structural and lithological information of Okemesi-Iwaraja area.

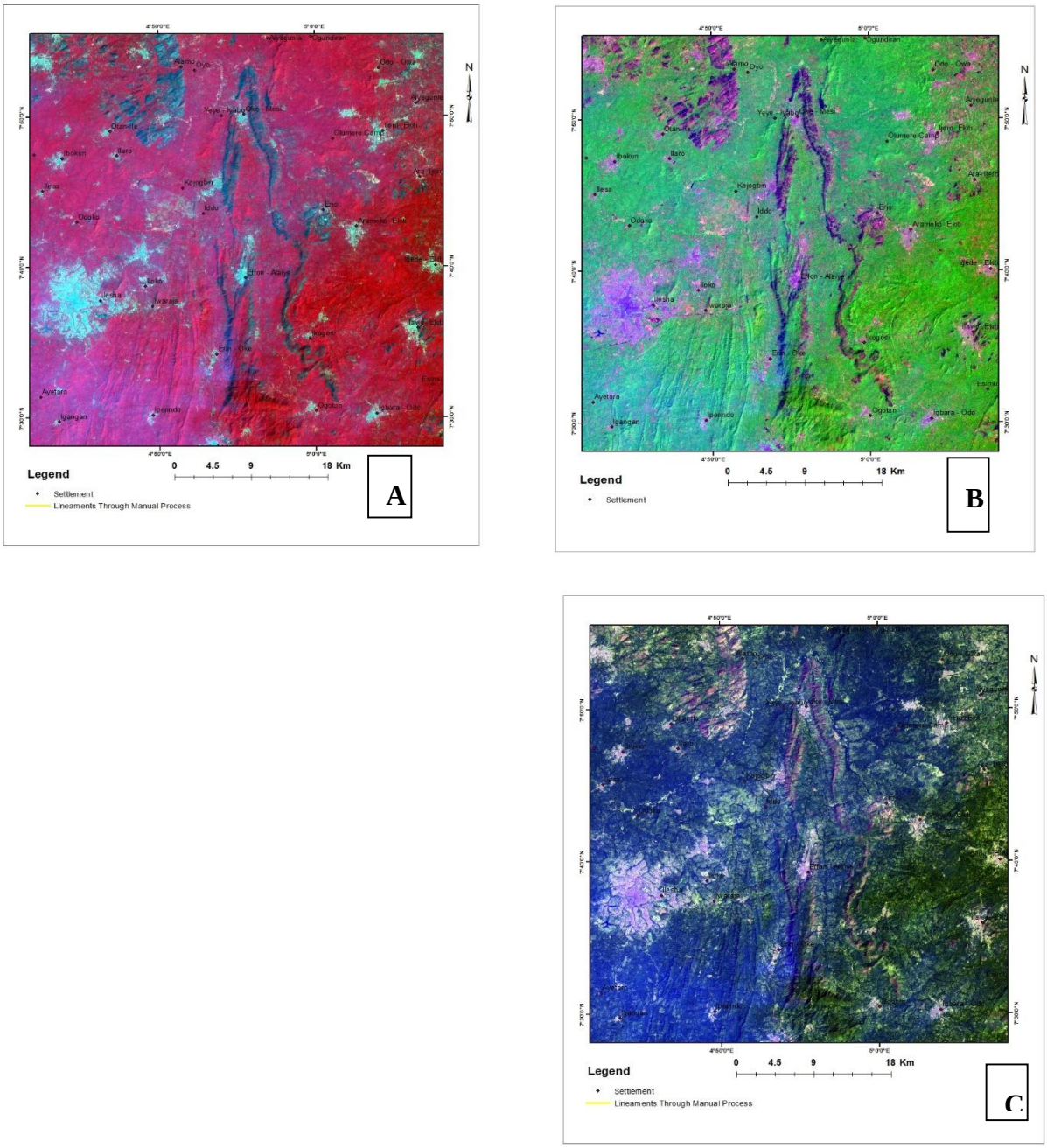

Fig. 4. 1 Landsat-8 OLI RGB Band Composites; (A) Band 5,4,2, (B) Band 6,5,2, (C) Band 7,6,2

4.2.1 Colour Composite

New raster data comprising subset of the initial raster dataset bands were generated through spectral approach. This process was achieved with a definite band arrangement and order. The unique arrangement of the bands specified in the Multi-Value Input control box determines the arrangement of bands in the output data raster set. The extent of the output raster data is usually determined by the spatial reference of the first raster band with a spatial reference in the array. Different models for false colour composite were suggested in this project for Landsat-8 OLI covering Okemesi-Iwaraja area (Fig. 4.1). The most uncorrelated bands are combined in RGB based on the models that were considered due to their correlation coefficient.

The colour composite for Landsat OLI (Fig. 4.1 A, B & C) showed different levels of information, their interpretation requires some level of experience and background knowledge in some cases. Texture, tone, pattern, association, size e.t.c of the image elements were considered in the understanding and proper interpretation process. Figure 4.1(B) is also an OLI composite of Band combinations 6 5 2 in RGB which is similar in wavelength to ASTER 731 combination.

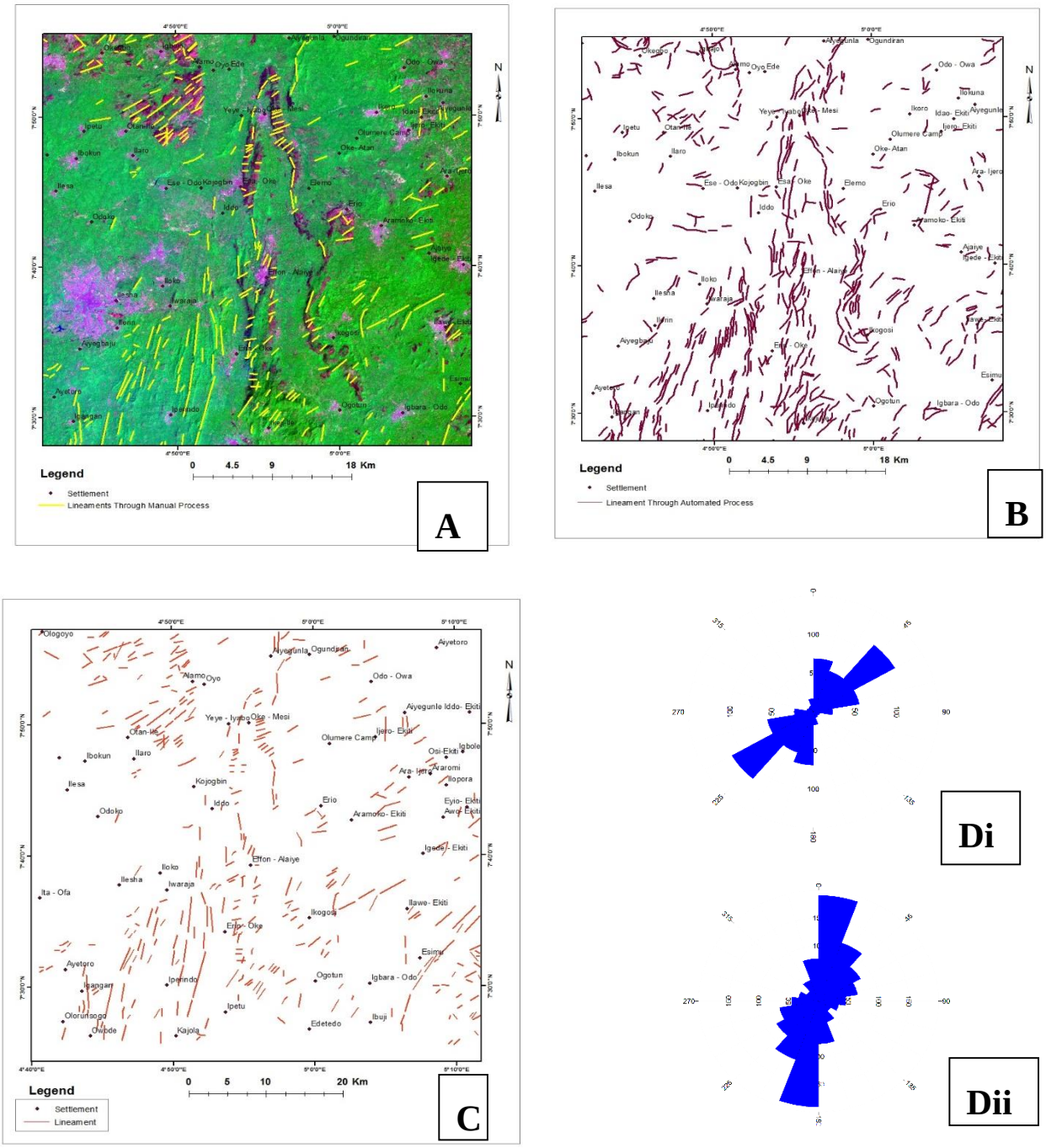

Fig. 4. 2 (A) Landsat (8) Composite 6, 5, 2 overlain with manually extracted lineament, (B) Lineament extracted through automated process, (C) Lineament extracted through manual process, (Di) Orientation diagram for lineament derived manually, (Dii) Orientation diagram for lineaments from automated process.

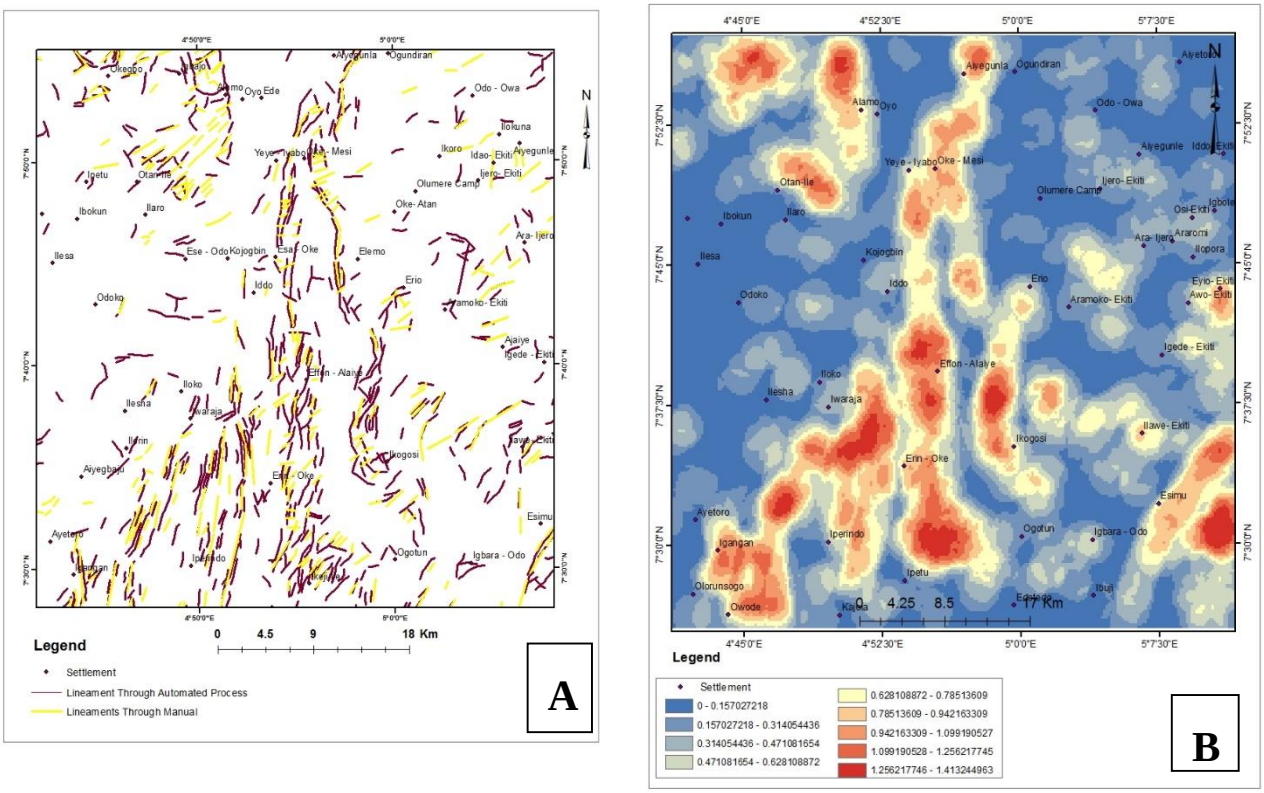

Fig. 4. 3 (A) Combination of lineaments derived by automated and manual process, (B) Lineament density map of the combination of manual and automated lineament

Lineaments were automatically extracted from the Band 6 5 2 Landsat-8 composite (Fig. 4.2 A & B) using Geomatica software. The lineaments were scrutinised and modified, context artefacts were removed, and the final lineament was plotted in a rose diagram. The most common patterns discovered were NE – SW, with a few NNE – SSW and NNW – SSE (Fig. 4.2 Dii). Lines were manually extracted from the Band 6 5 2 Landsat-8 composite by outlining the interpreted linear components. The manually derived lineament (Figure 4.2 C) were plotted into a rose plot (Fig. 4.2 Di), and both the automated and manually extracted lineaments were combined (Fig. 4.3 A).

The main linear structures in the OLI Band 762 composite (Fig. 4.1 C) were clearly distinguishable, and lineaments were derived from this mixture (Fig. 4.2 C). These structures were then plotted on an orientation rose diagram, with the most prominent trend being NEE – SWW and a few NE – SW and E – W trending structures (4.2 Di). The structures were then interpolated into a lineament density map (Fig. 4.3 B). A specialised procedure of spatial statistical analysis that calculates the intensity per unit area of lineament features within a radius of each pixel, is refered to as a lineament density analysis.

Table 4. 1 Table showing the number of lineaments and their directions

S/N	Direction	Number of Lineament
1	NE – SW	197
2	NNE - SSW	66
3	ENE - WSW	25
4	NNW - SSE	13
5	N – S	17
6	E – W	15
7	WNW - ESE	5
8	NW – SE	19

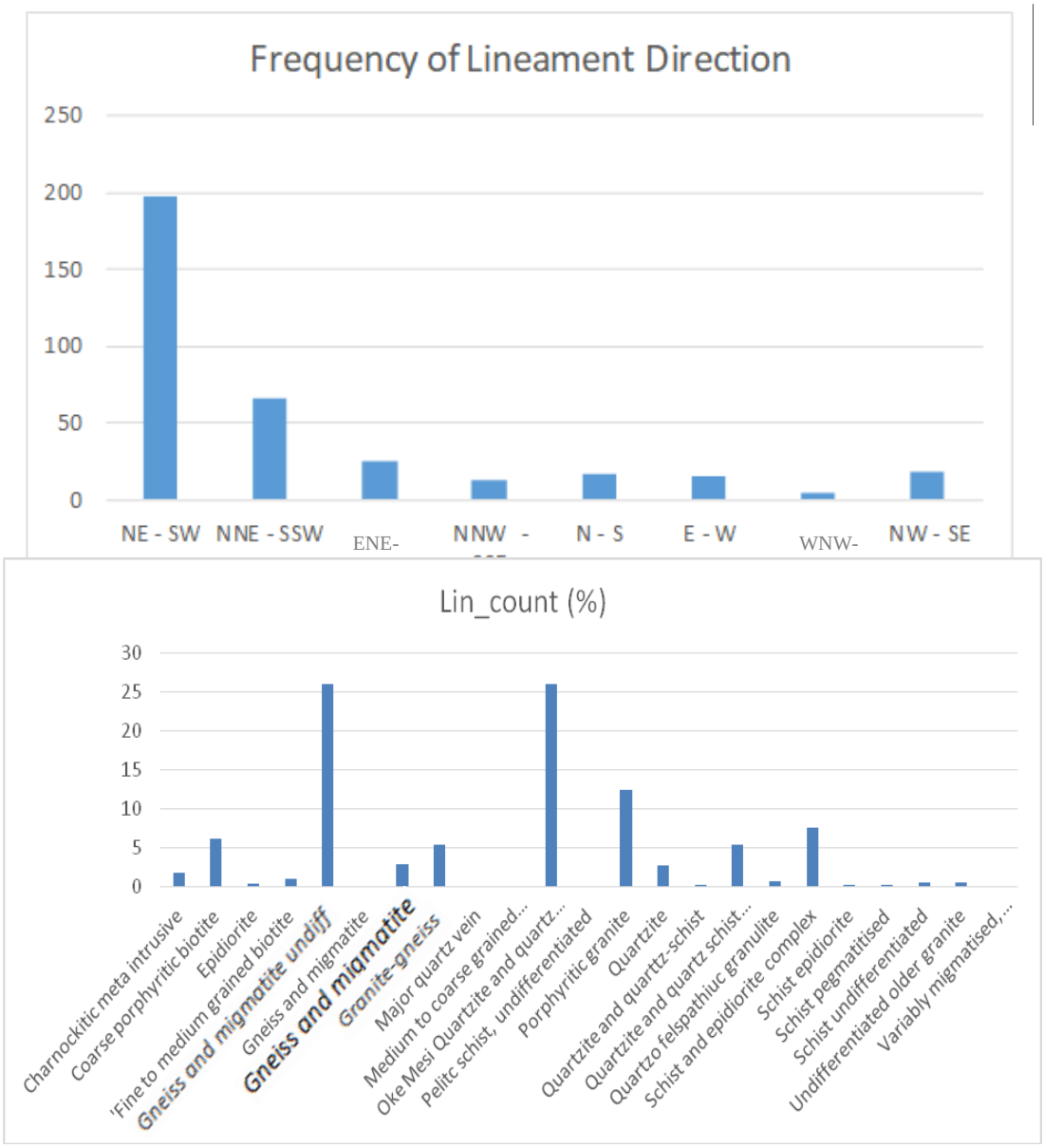

Fig. 4. 4 (A) Histogram of predominant Lineament directions, (B) Histogram of Percentage of Lineament in Lithology

4.2.2 Band Ratio

Ratioing of bands is a technique for exposing valuable information by combining various wavelengths in different representative bands at the same time. Ratio images were created for the research area to aid in the detection and classification of structures and lithology. The ratio images were created by the divion of Digital Number (DN) in one band by the DN in another band, keeping the value of the result constant, and plotting the new values as an image for each pixel. The RGB band ratios of the Landsat-8 b4/b3, b6/b2, and b7/b4 bands (Figure 4.5 A) were computed to futher expose the lithology and structures. The texture and tone of the Landsat-8 b4/b3, b6/b2, and b7/b4 Band ratios in RGB and the Landsat-8 762 composite were comparable, they both seemed to have comparable ability to improve structures. Figure 4.5 A-D shows major trending structures derived from these sets of images, as well as rose diagrams and lineament density maps were also produced.

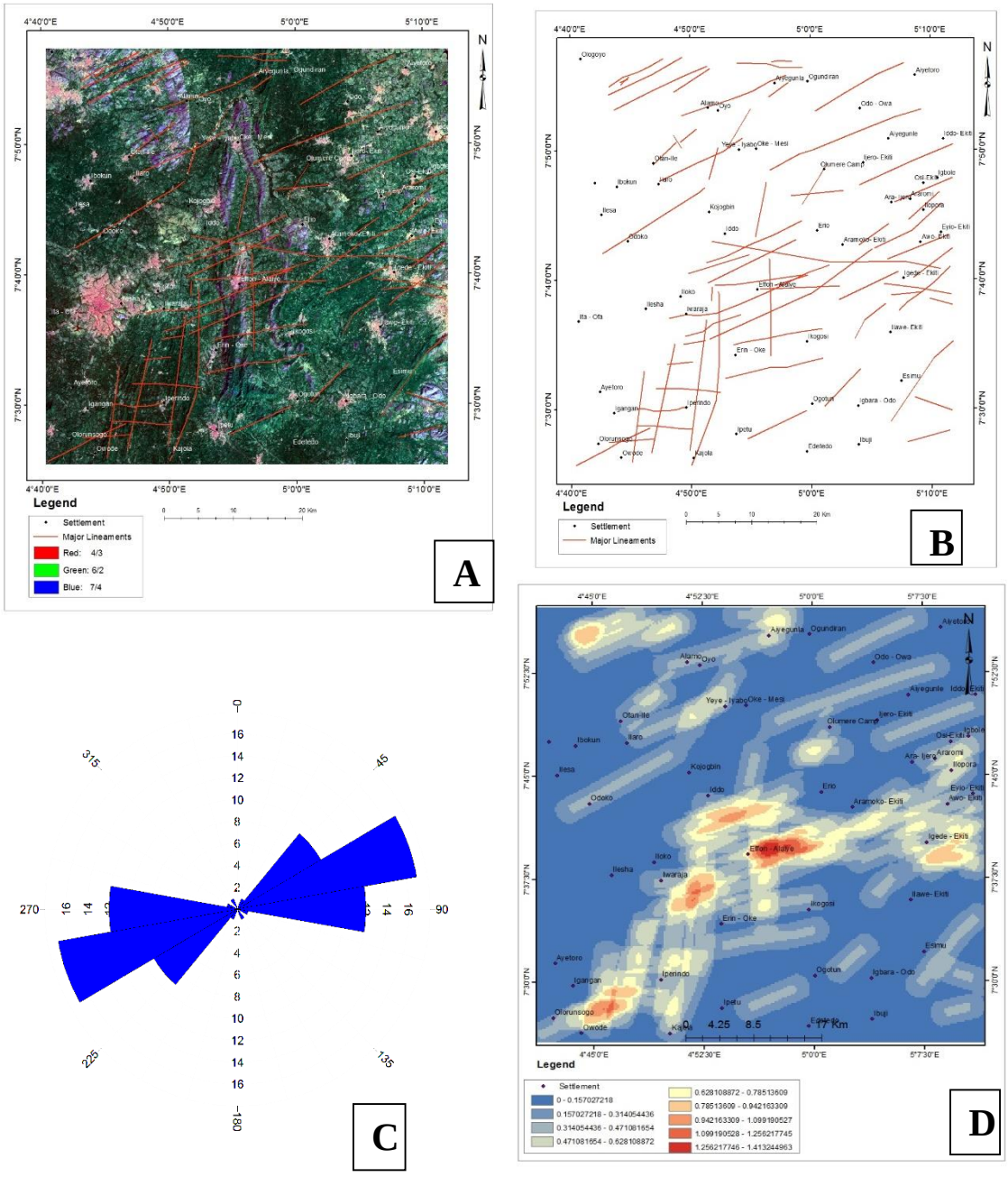

Fig. 4. 5 (A) Landsat-8 OLI Band ration 4/3, 6/2, 7/4 overlain with major lineaments, (B) Lineaments derived from OLI Band ratio showing major trends, (C) Rose plot for trends of major lineaments, (D) Lineament density for orientation of major lineaments derived from Landsat-8 Band ratio 4/3, 6/2, 7/4

4.2.3 Principal Component Analysis

Prinsipa Component Analysis (PCA) is a mathematical process for converting multivariate data sets of intercorrelated variables into new uncorrelated data sets (Benomar & Fuling, 2005). This technique was also applied in this research, where the first principal component is responsible for the majority of the variance in the new results, and residual components account for the rest. PCA is a broadly used procedure whereby the information content of the variouse bands are streamlined and limited to the first few bands. Landsat-8 OLI's corresponding Bands are calibrated to remove inaccuracies that can occur during image acquisition. Examples are sensor accuracy and dynamic range differences (Yesou et al., 1993).

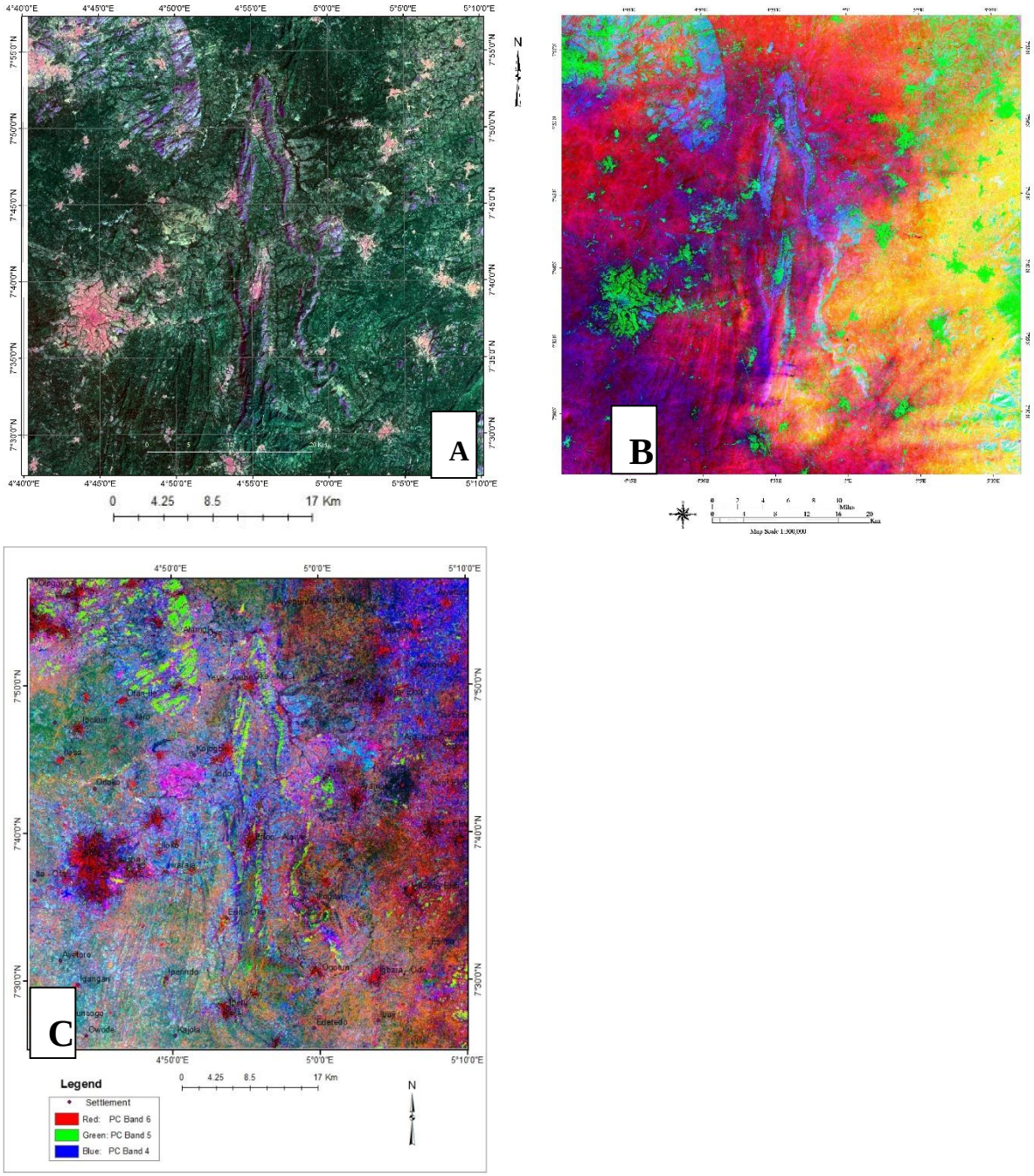

Fig. 4. 6 (A) Landsat-8 Band ratio 4/3, 6/2, 7/4, (B) Landsat-8 PCA 4,3,2, (C) Landsat-8 PCA 6, 5, 4

Table 4. 2 LandSat 8 OLI PCA Covariance Matrix

PCA	Band 1	Band 2	Band 3	Band 4	Band 5	Band 6	Band 7	Eigenvalue
Band 1	**0.000036**	**0.000040**	**0.000039**	**0.000048**	**0.000003**	**0.000052**	**0.000060**	**0.002325**
Band 2	**0.000040**	**0.000045**	**0.000047**	**0.000062**	**-0.000009**	**0.000084**	**0.000096**	**0.000560**
Band 3	**0.000039**	**0.000047**	**0.000054**	**0.000083**	**-0.000015**	**0.000144**	**0.000158**	**0.000129**
Band 4	**0.000048**	**0.000062**	**0.000083**	**0.000155**	**-.000106**	**0.000325**	**0.000366**	**0.000035**
Band 5	**0.000003**	**-.000009**	**-0.000015**	**-0.000106**	**0.000630**	**-0.000190**	**-0.000378**	**0.000007**
Band 6	**0.000052**	**0.000084**	**0.000144**	**0.000325**	**-.000190**	**0.001023**	**0.000997**	**0.000000**
Band 7	**0.000060**	**0.000096**	**0.000158**	**0.000366**	**-0.000378**	**0.000997**	**0.001112**	**0.000000**

The PCs were determined for the seven OLI bands that were callibrated. Statistics were obtained for each image, and percentages of data variation were calculated, as well as covariance matrices for the variable PCs (Table 4. 3). Landsat-8 PCAs for PC bands 432 and 654 were also produced. In Figures 4.6 (B) and (C), the Landsat-8 PCs 432 and 654 were matched, and although they equally differentiated rock types, the rock cartigorization in Landsat-8 PC 432 produced a broader class of lithologic classification, whereas the lithologic variation and structural enhancement in Landsat-8 PC 654 produced a more comprehensive rock type variation and structural enhancement (Fig. 4.6 C).

4.3 DEM and RADAR Interpretation

Elevation data carries values representing terrain information of a place, many researchers in the past have used it in structural analysis (Owusu et al., 2006; Soulakellis et al., 2006). Height data can be viewed in a variety of ways, but DEMs (grid types) are best at reading linear geologic formations with topographic expressions amplified by surface offset. DEM is favored over aerial photographs for producing shaded relief images because it allows you to choose lighting from any angle (Henderson et al., 1996; Soulakellis et al., 2010). Solar elevation and azimuth are crucial factors to consider when evaluating topographically linked and dependent characteristics, according to the authors. DEMs may also be used in conjunction with other multispectral images to improve interpretability and give more detail than a single image (Soulakellis et al., 2006). Various image improvement methods, such as directional, edge, and Sobel filters, can be applied to DEM to improve various linear architectures (Henderson et al., 1996). The main aim here was to enhance and trace out surface lineament, establish their general pattern and density, and infer the region's structural texture.

The 30m resolution ASTER DEM covering Okemesi-Iwaraja and its environs provided important terrain and structural details for lineament study in the field. The three phases in extracting lineaments from the ASTER DEM of the research region were to create hillshade images, fuse them with multispectral data, and extract linear vector features from the processed images. Hillshade images were created using four azimuth directions (NE, SE, SW, and NW) (Fig. 4.7–4.9). These relief images helped to improve the size, height, and slope variations of the morphology. Some sun angles, such as 15^0, 30^0, and 45^0, were tried to obtain more details, with 30^0 being selected as the best because of its interpretability. Figures 4.7 A, B, and C show the images generated by combining different hillshade images that face the similar direction. Hillshade images of illumination directions N, NE, and E were combined and stretched to enhance the E-W, N-S, and NW-SE lineaments (Fig. 4.8 A, B, C, D).

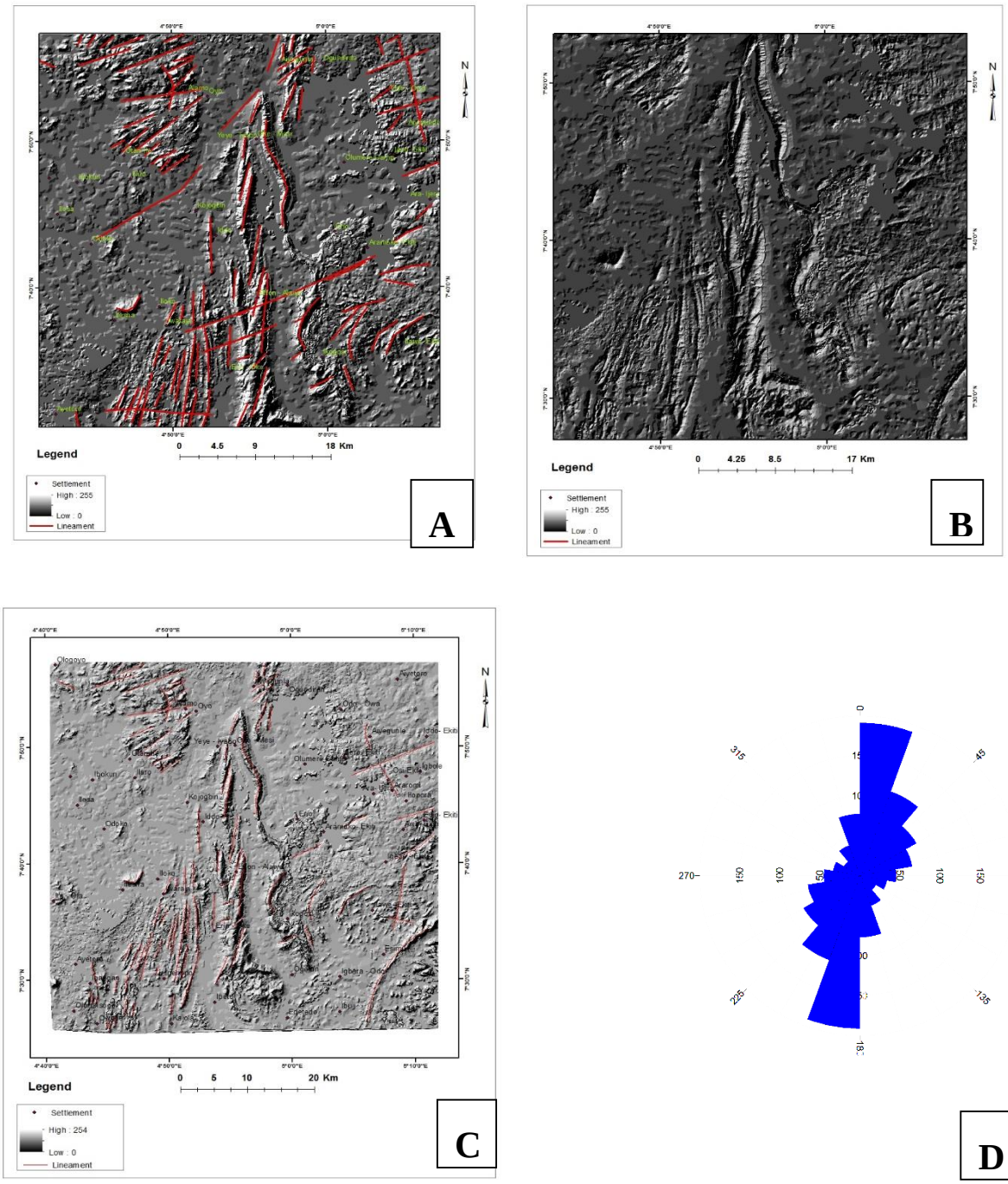

Fig. 4. 7 (A) Hillshade image with azimuth angle of 315 and sun angle of 15^0, (B) hillshade image with azimuth angle of 135 and sun angle of 30^0, (C) hillshade image with azimuth angle of 315 and sun angle of 45^0 (D) orientation diagrame of lineaments derived from these stached DEMs

Fig. 4. 8 (A) Image display for stack of hillshade images of 315 sun azimuth, (B) Image display for stack of shaded relief images of 225 sun azimuth, (C) Image display for stack of shaded relief images of 135 sun azimuth, (D) Image display for stack of shaded relief images of 45 sun azimuth

Combining relief images from the N, NW, and W directions yielded the other shaded relief images (Fig. 4.8 A-D). By superimposing the features present in the different single shaded relief images, these hillshade composite images contributed to a greater understanding of lineaments in general. The eight hillshade images were multiplied by the Landsat-8 OLI Band 6 images to create fused images, while 6 was favored over the others because it contained more details on topographic and boundary delineation (Fig. 4.9 A).

A total of 248 lineaments originating from the ASTER DEM were used to create the final modeled lineament map (Fig. 4.9 B). The azimuthal distribution (Fig. 4.9 C) with NE-SW and NW-SE trends, as presented in Table 4.1, Figures 4.4 (A) and (B), revealed that most of the lineaments in the Okemesi-Iwaraja area were scattered around the Okemesi fold axis and most of the rock complexes.

Structure were also delineated from the sentinel 1A imagery over the area. These structures trended mostly NNE-SSW directions as seen in Figure 4.10: A, B and C, and were digitized.

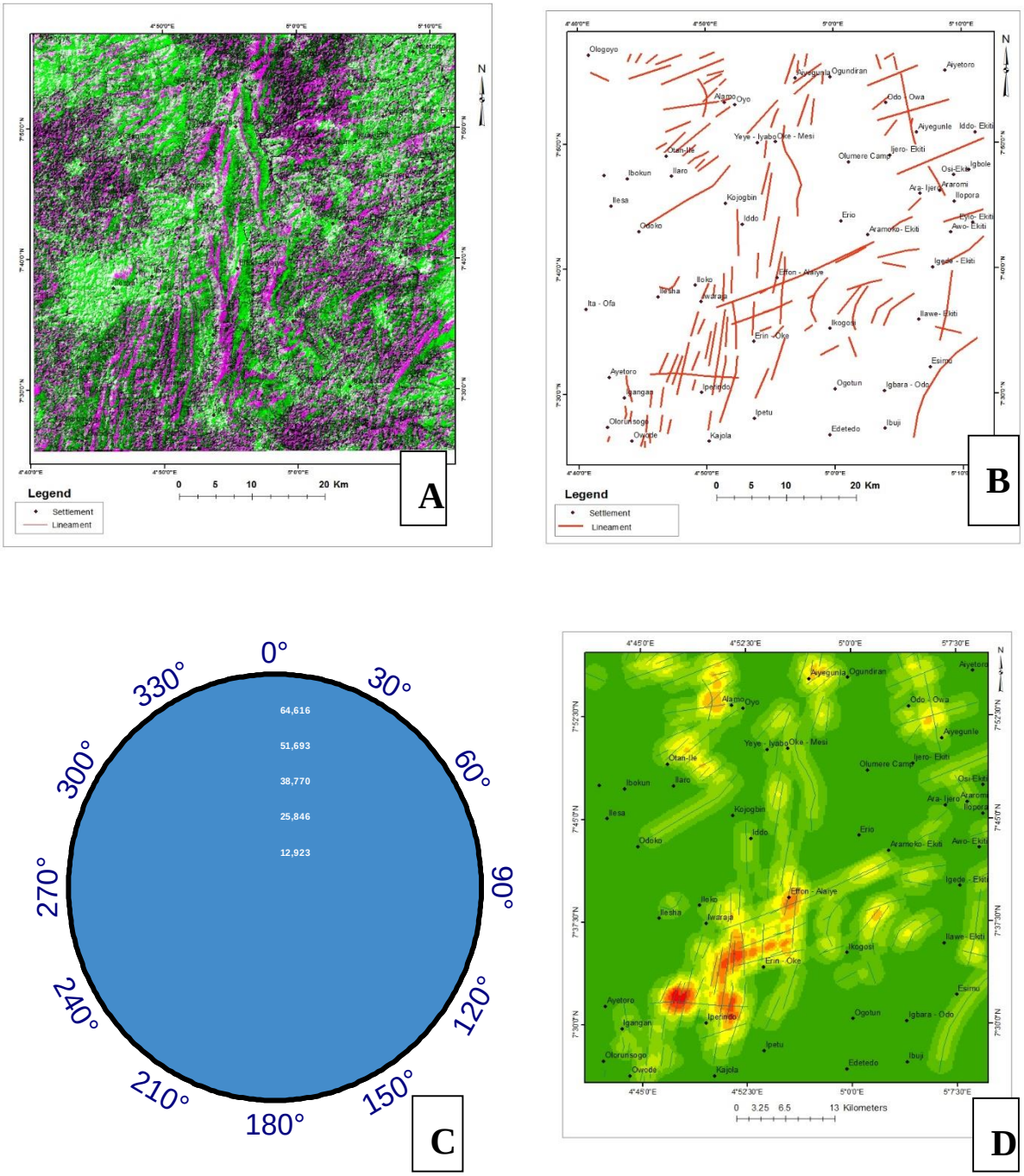

Fig. 4. 9 (A) Image composite of corresponding hillshade images multiplied by Band 6 Landsat-8, (B) total lineaments derived from ASTER DEM, (C) lineament density map of lineament extracted from DEM

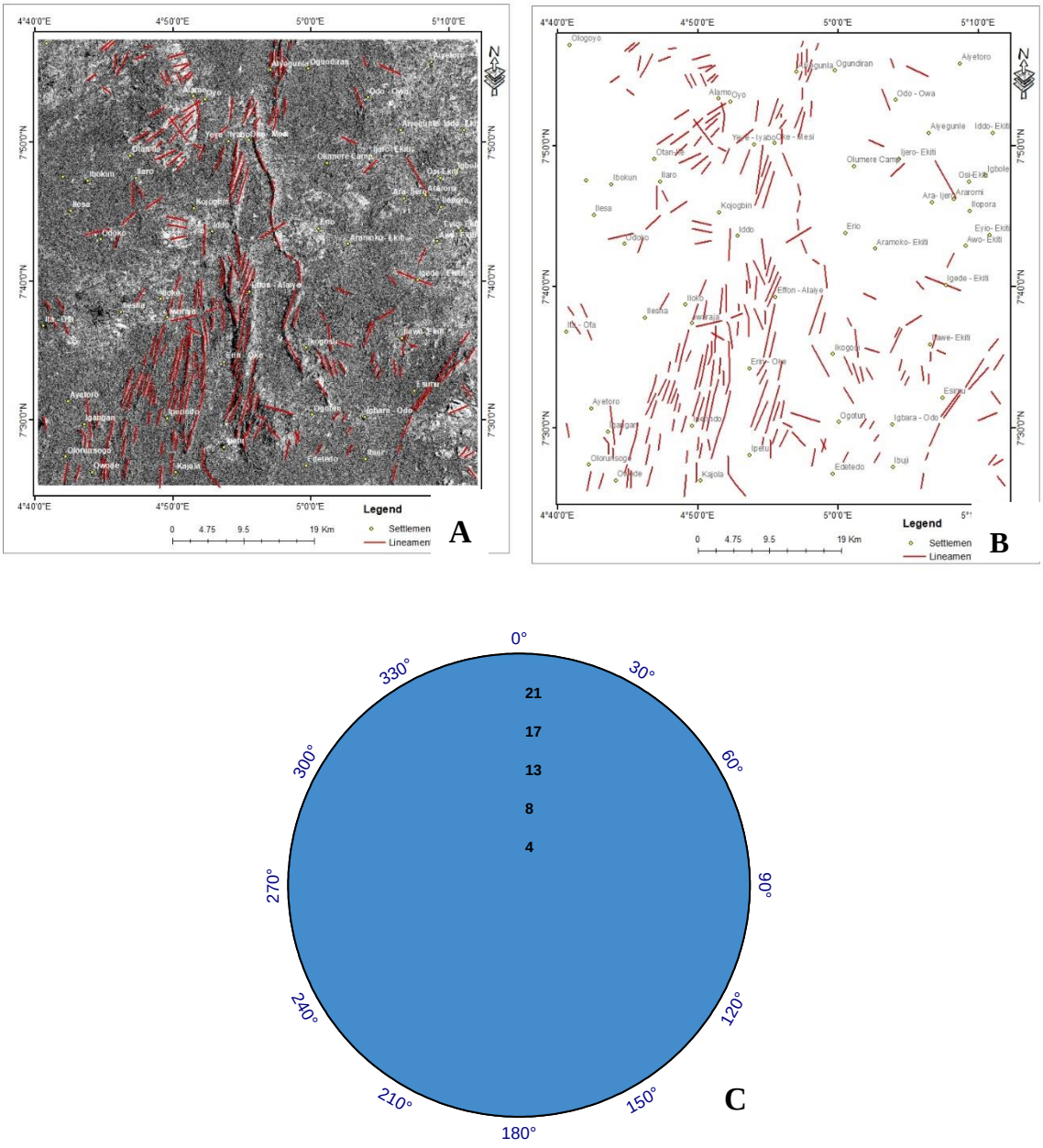

Fig. 4. 10 A) Sentinel 1A Radar Image of Okemesi-Iwaraja area overlain with lineaments extracted, B) Lineament derived from Sentinel 1A Radar data of study area, C) orientation diagram of the lineaments derived from the Radar image, showing the predominant NNE – SSW direction

Lineaments extracted from Bands 6 5 2 of OLI composite (Fig. 4.2 A & B) through the automated process plotted into rose diagram showed NE – SW and a few NNE – SSW, ENE – WSW trends (Fig. 4.2 Dii). While Lineaments derived through manual process from the same OLI 652 composite, plotted into a rose diagram, revealed NE – SW as the major trend, while a few NNE – SSE and sub E – W trends as recorded (Fig. 4.3 Di). Both automated and manualy derived lineaments were combined together (Fig. 4.4 A) and a subsequent lineament density map was produced (Fig. 4.4 B). These structures were not extended and were likely to represent brittle structures.

The OLI band 762 composite, revealed the major trending structures which were strongly differentiated in this composite (Fig. 4.1 C). The texture and tone of the OLI 762 composite and the b4/b3, b6/b2, b7/b4 Band ratio in RGB were identical (Fig. 4.5 A & 4.1 C), they seem to have similar ability to improve structures. This ratio produces structures that are longer in length (Fig. 4.5 B) and the main pattern observed for these structures were ENE – WSW, with a few NE – SW and E – W trending structures. This ratioed image was used to generate these trending structures as well as rose diagrams and lineament density maps (Fig. 4.5 C&D).

Both OLI PCAs of PC bands 432 and 654 were produced (Fig. 4.2 (B) and (C)), and the OLI PCs 432 and 654, which were compared afterwards; they equally differentiated rock types, but OLI PC 432's lithologic discrimination gave a broader category of lithology division, whereas OLI PC 654's lithologic differentiation presented a more comprehensive lithology variance and structural enhancement (Fig. 4.6 C). Table 4.2 contains the OLI covariance and eigenvector matrix.

The Okemesi-Iwaraja ASTER DEM provided valuable structural and topographic details for lineament analysis in the field. The shaded relief images (Fig. 4.7-4.8) generated from four different azimuthal directions, NE, SE, SW, and NW, were valuable in enhancing the size, elevation, and slope differences of the morphology and structures within the study area. The sun angle of 30^0 was discovered to be more interpretable and revealed structures more

effectively than the other sun angles suggested. Stretching hillshade images with lighting directions N, NE, and E (Fig. 4.8 A, B, C) improved the E-W, N-S, and NW-SE lineaments, while stacking hillshade images with lighting directions N, NW, and W improved the E-W, N-S, and NE-SW lineaments. These hillshade composite images led to a better understanding of lineaments in general because they superimposed the details present in several single hillshade images.

From the results derived from geometric, radiometric and terrain alongside multi-looking processing carried out on the sentinel 1A Radar image of the study area, lineaments were extracted and rose diagram plotted. The structures are predominantly NE – SW trending, this agrees with the results obtained from the other respective Remote sensing techniques (RADAR) (Fig. 4.10).

Most of the lineaments in the Iwaraja - Okemesi fold areas and most of the rock complexes trended NE-SW and NW-SE, according to the azimuthal distribution (Fig. 4.9 C) (see Table 4.1 and Figures 4.4 A&B). This was evident in the map generated from a total of 248 lineaments extracted from the ASTER DEM to create the overall translated lineament map (Fig. 4.9 B).

4.4 Aeromagnetic Analysis and Interpretation

4.4.1 Data Processing

Figure 4.11 (A) and (B) shows the high resolution aeromagnetic data in grid and data base format (*gdb), which has variouse data layers such as IGRF removed TMI and processed derivatives (B). OASIS Montaj data processing and visualization software was used to perform further image enhancement. Magnetic anomalies have basic characteristics that signify the relative inclination of magnetic sources, lateral extent, and relative magnetic anomalies, such as wavelength, relative amplitudes, geometry, and directions (Porwal et al., 2006). Wide amplitude shallow depth anomalies frequently dominate magnetic maps, masking subtle and deep-seated anomalies (Alsaud, 2008). A number of techniques for normalizing magnetic image signatures have been suggested over

the years in order to amplify minor variations in addition to greater and larger amplitude anomalies. Reduced to Equator (RTE) with Total Magnetic Intensity (TMI), Total Horizontal Derivative (THD), Analytical Signal (AS), and Tilt Derivative (TDR). were the normalized derivatives used in this analysis.

Analysis of aeromagnetic data necessitates a thorough review of the various levels of detail obtained from the key data profiles. The analytical signal (AS), total magnetic intensity (TMI) reduced to the equator (RTE), tilt derivative, and horizontal derivative are all examples of this. Magnetic anomalies are normally complex in nature due to differences in the magnetic field of the Earth at the time of measurement. Reduction of the overall magnetic field to the pole or equator, depending on where you are on Earth in relation to the pole or equator, is method to overcome this complex phenomenon. RTE specifically positions the anomaly over the source, making interpretation simpler. As a result, the RTE of the total magnetic intensity (TMI) grid is used to extract additional data strata. The magnetic field intensity was around -93.2 - 148.0 nT in the enhanced RTE image of the region (Fig. 4.12 B), meaning that the magnetic strength was varying due to lithological or topographical differences. An analytical signal for the region was generated by integrating both vertical and horizontal derivatives (Fig. 4.13 A), which places the anomaly in the middle of the causative body. Analytical signal amplification is preferred because dipolar properties are lacking and the peaks converge even for small bodies, resulting in an anomaly centered above the causative body (Alsaud, 2008). It is also worth noting that after being exposed to vertical derivative, the analytical signal sharpened and located the phenomenon more precisely than the initial AS image. The tilt derivative (Fig. 4.14) added to RTE data also provided improved information by positioning the anomalies above the causative body. A horizontal gradient image was computed from the RTE to reflect deep seated anomalies and magnetic contacts, and upward continuations were performed at different depths. Short wave length anomalies were enhanced by the tilt derivative, which has been shown to be useful in tracing anomalies along their strike path (Alsaud, 2008). The use of first vertical derivative images made the demarcation of near surface magnetic structures simpler.

different angles of illumination were added to AS, RTE, and tilt derivatives to generate hillshade images that highlighted various sets of structures.

4.4.2 Interpretation of Litho-Magnetic Domains

According to Porwal et al., 2006, the first step in analyzing crustal domains from aeromagnetic studies is to comprehend the properties of magnetic anomalies such as direction, relative amplitude, and wave length. Three distinct litho-magnetic domains were identified with the aid of the RTE map, which represent areas of differing magnetic signature as seen at locations A, B, and C. (Fig. 4.12 B). These litho-magnetic domains that have been interpreted showed close correlation and were a good complement to the regional geology groups that Rahaman, 1976 investigated previously. As seen in the map Figure 4.12 (B), Domain A comprised porphyritic granites in the northwest and undifferentiated gneiss and migmatite in the west of the study area, which were marked by high amplitude and shorter wavelength regional magnetic highs. Lower magnetic anomalies with smoother, wider, and longer wave lengths in the quartzite, quartz schist and undifferentiated schist in the southwest region indicated deeper basement and western sections, which were grouped as Domain B. and C. The RTE image. As compared to other data layers, Figure 4.12 (B) generally revealed deep source magnetic anomalies by attenuating shallow surface anomalies. Magnetic sources were used in both deep and shallow depths. The map of analytical signal in Figure 4.13 (A) clealy showed regions of shallow and deep source magnetic anomaly. Furthermore, the examination of the analytical signal indicated the presence of many bounding bodies (anomaly peaks) which were identified as contacts in certain places. Amphibolite, schist amhphibole, and schist pegmatised anomalies of high amplitude, closely spaced, and shorter wavelength were also found in the south west portion of the general study area. Undifferentiated gneiss and granite, as well as charnockite meta intrusive, cover the north east corner. Due to a variation in the nature of magnetic field, contact between the granites, the schists and gneissic terrain was detected (Fig. 4.15A).

Total Horizontal Derivative enhanced predominantly near surface structures, where basement structures are most likely to be identified, and anomalies in the region could be traced along their strike. The prevailing magnetic nature and orientation of the magnetic anomaly underneath the Okemesi-Iwaraja area and environs was shown by the THD image of the area (Fig. 4.13 B). The alignment of magnetic anomalies, determined by magnetic sources which could be tectonically controlled, determined the directions of anomalies. The tilt derivative, analytical signal, and upward continued total horizontal gradients were found to be especially helpful in amplifying the orientations of magnetic anomalies. To decode the region's tectonic grain, these anomaly orientations were isolated and studied separately. As a result, a statistical analysis was performed to establish the azimuthal distribution, and the results indicated that the main magnetic anomalies mainly trended in ENE-WSW directions, as seen in Figure 4.16 B&C.

In the reduced to equator image, four main magnetic zones were delineated: high magnetic anomalous zone (A), mid to high magnetic anomaly (B), moderate magnetic anomalous zone (D), and low magnetic anomalous zone (C) (Fig. 4.12 B). Lithological contacts portrayed by sharp magnetic contrast were delineated (Fig. 4.15 A); By enhancing weak and strong magnetic anomalies, the TDR filter was applied to the RTE grid to determine structures (faults and folds), contacts and edges or boundaries of magnetic sources, and to see near-surface source magnetic features that were associated with geological structures in the field. Tilt angle derivative (TDR) of RTE (Fig. 4.14), which uses the principle that zero contours are formation edges, assisted in locating edges of structures, particularly at shallow depths (Salem et al., 2007).

4.4.3 Interpretation of Magnetic Lineaments

In their study, Gunn et al. (1997) provided an overview of the different requirements for recognizing magnetic lineaments. Offset of seemingly identical magnetic units, sudden change in linear gradient, and linear narrow magnetic highs and lows were some of the criteria used in this analysis. The hillshade image of the Tilt derivative image revealed a significant number of lineaments; lineament interpretation was performed on different layers of enhanced images. The magnetic faults caused by the offset of equivalent magnetic

gradients were classified using Tilt Derivative, RTE, and Total Horizontal Gradient (THD) images. All of the data layers revealed very prominent faults with a strong magnetic signature, as shown in Figure 4.15 B. Different illumination directions were used in the tilt derivative image to distinguish very discernible magnetic lineaments (Fig. 4.16 A). Other magnetic lineaments were also extracted by closely examining different layers of enhanced images.

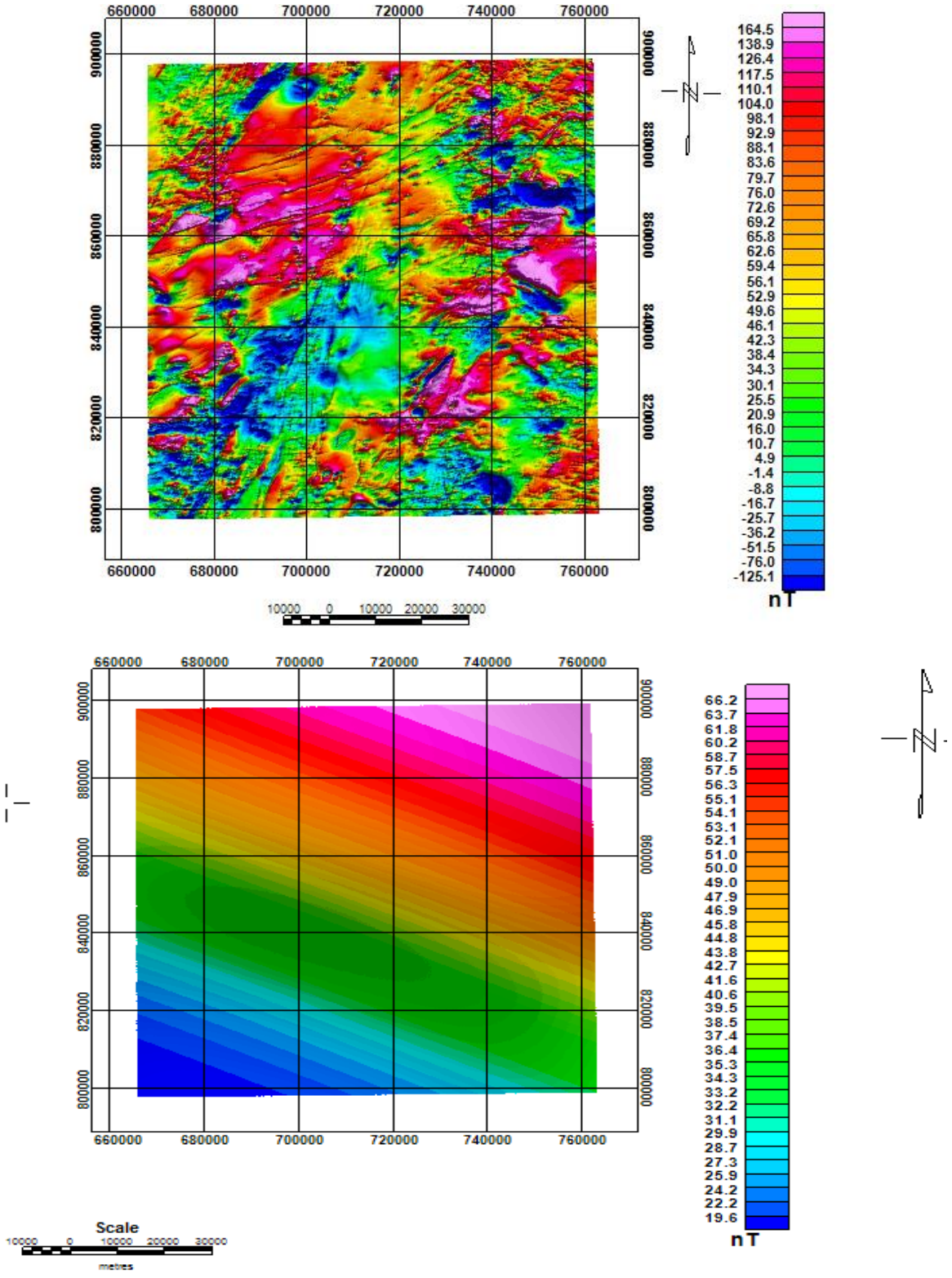

Fig. 4. 11 (A) Total Magnetic Intensity Image, (B) Regional Magnetic Field

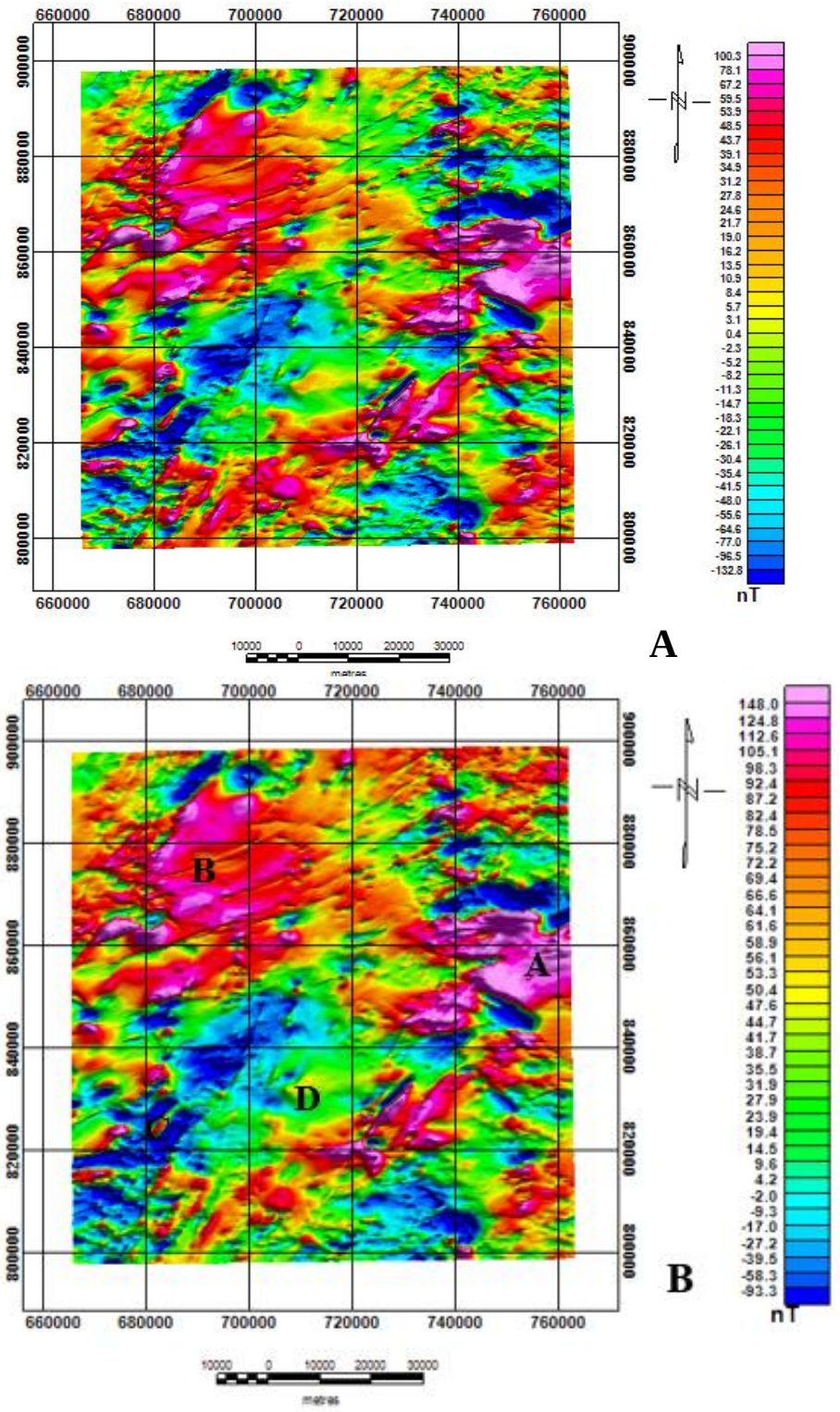

Fig. 4. 12 (A) Residual Magnetic Intensity Map, (B) Reduction to the Equator

Short wavelength curvilinear magnetic anomalies are visible on tilt, total horizontal derivative, and analytical signal images in the northern portion of the field, where schist amphibolite, porphyritic granitic, and undifferentiated migmatite gneiss dominated (Fig. 4.15 A and B & 4.16 A). In certain cases, these magnetic anomalies defined rock foliation styles, and they were digitized. The diagram in Figure 4.16(B) depicts the area's structural framework as viewed from magnetic results. Based on their azimuthal frequency, this analysis identified three main classes of lineaments. A group of lineaments trending N0-60E, which correlated to basement systems, were the most prominent in terms of lineament frequency. These magnetic anomalies were digitized since they may have defined rock foliation patterns in some cases. The fundamental structure of the region as presented from magnetic findings is depicted in Figure 4.16(B). The other big magnetic lineament group had a pattern of $N0^0$-60^0W and were found beneath almost all the lithological units in Okemesi-Iwaraja area. The prevailing magnetic anomaly in the area (Fig. 4.16 C) appeared to favor those structures. In terms of frequency and length, magnetic lineaments with the $N60^0$-120^0E pattern were also widespread. These lineaments had largely influenced the undifferentiated units identified in the northern portion of the area, as seen in the lineament density map (Fig. 4.16 B). The general research area's lineament density map also exposed a high concentration of lineaments in the central portion of Okemesi quartzite.

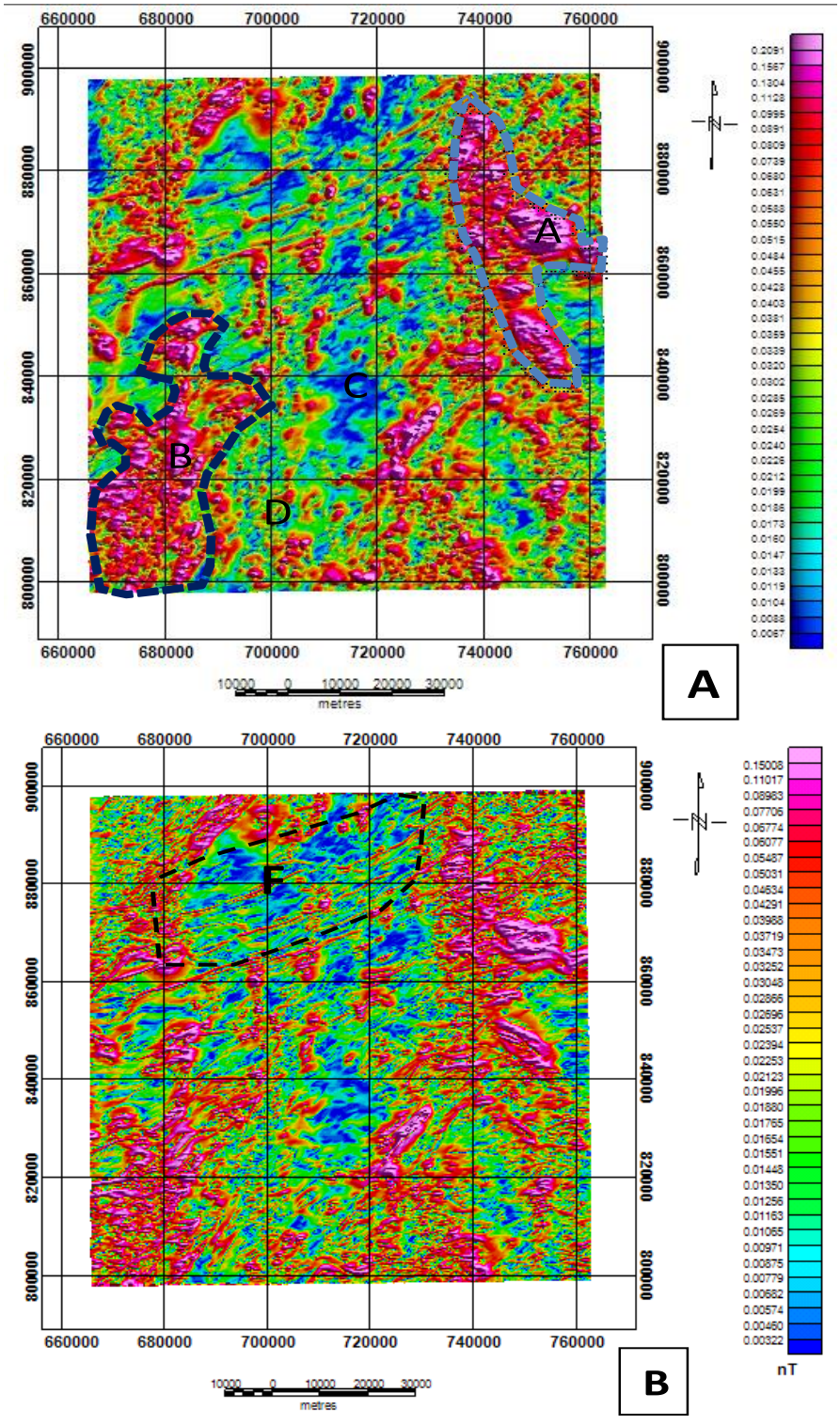

Fig. 4. 13 (A) Analytical Signal, (B) Total Horizontal Derivative

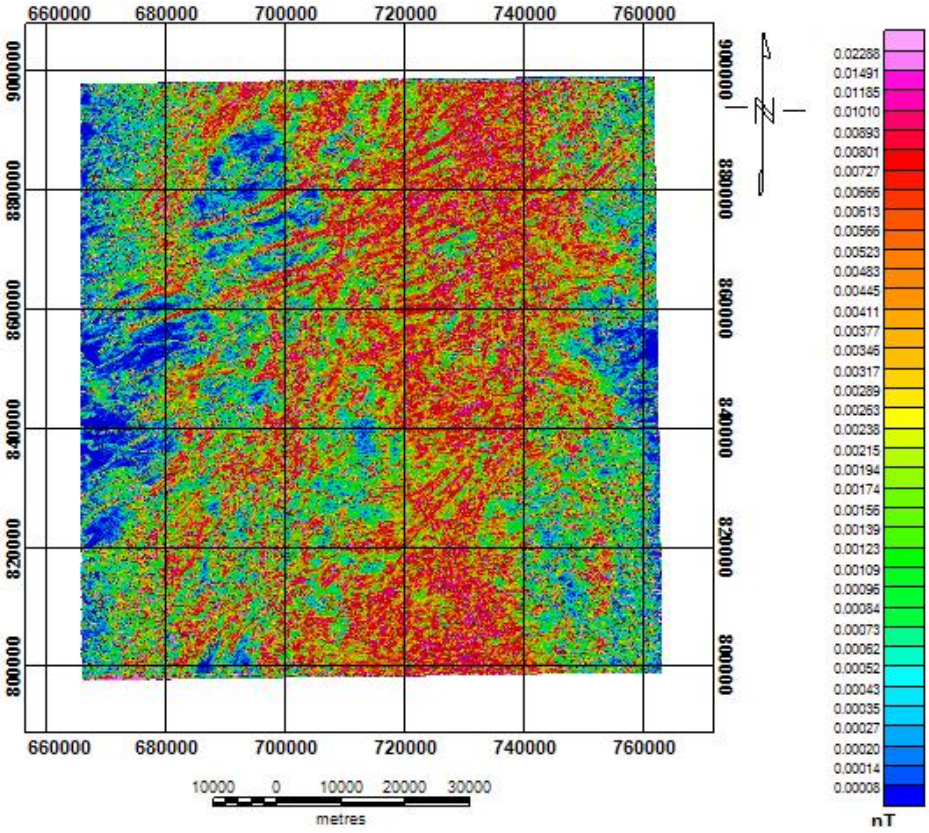

Fig. 4. 14 Tilt Derivative Image

The RTE grid (Fig. 4.12 B), analytical signal grid (Fig. 4.13 A), and TDR grid (Fig. 4.14) maps provided an overview of the geological structural influence and lithologic deformation in the region. It depicted the Okemesi fold axis and environment's strong structural deformation (folding and shearing) (Fig. 4.15A). In addition, a map of the interpreted fault, folds, and contacts was overlaid on the TDR image, as well as a rose diagram (Fig. 4.16 C) displaying the orientation of lineaments around Okemesi-Iwaraja area was generated. The rose diagram indicated the distribution of lineaments, this knowledge aided in the comprehension of the research area's structures. The rose diagram (azimuth-frequency), Figure 4.16 B, showed trends in (E-W), (NE-SW) directions. The area was dominated by a series of NS and EW trending structures and were interpreted as higher degree of shearing and faulting which may have been formed during thermo-tectonic activity.

The comparison between these studies and lineament analysis of remote sensing data of this study area were in agreement

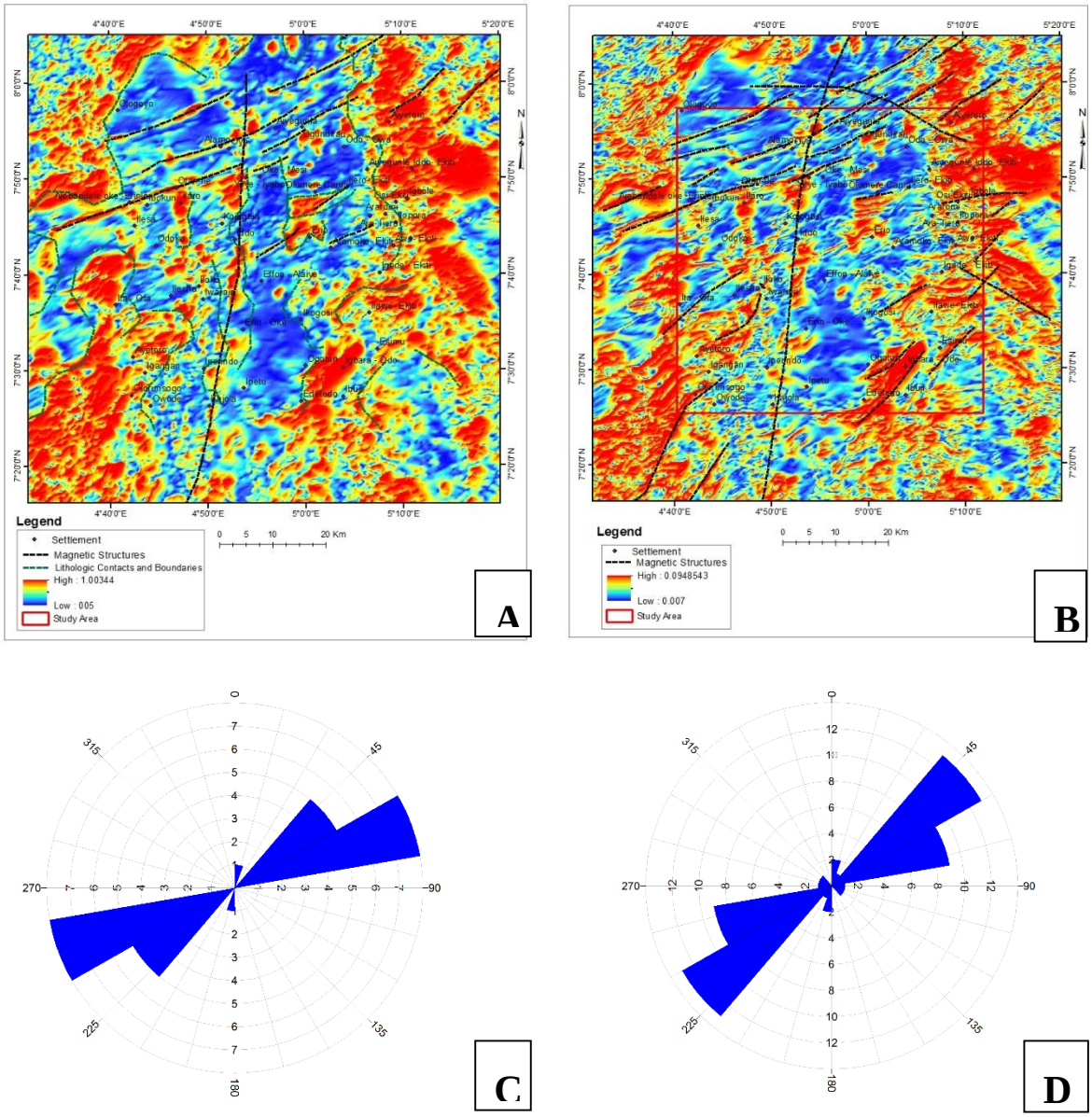

Fig. 4. 15 (A) Analytical signal showing inferred lithology boundary magnetic lineaments, (B) Total horizontal derivative image showing magnetic lineaments, (C) Rose plot showing the trend of magnetic lineament in AS image, (D) Rose plot showing the trend of magnetic lineament in THD

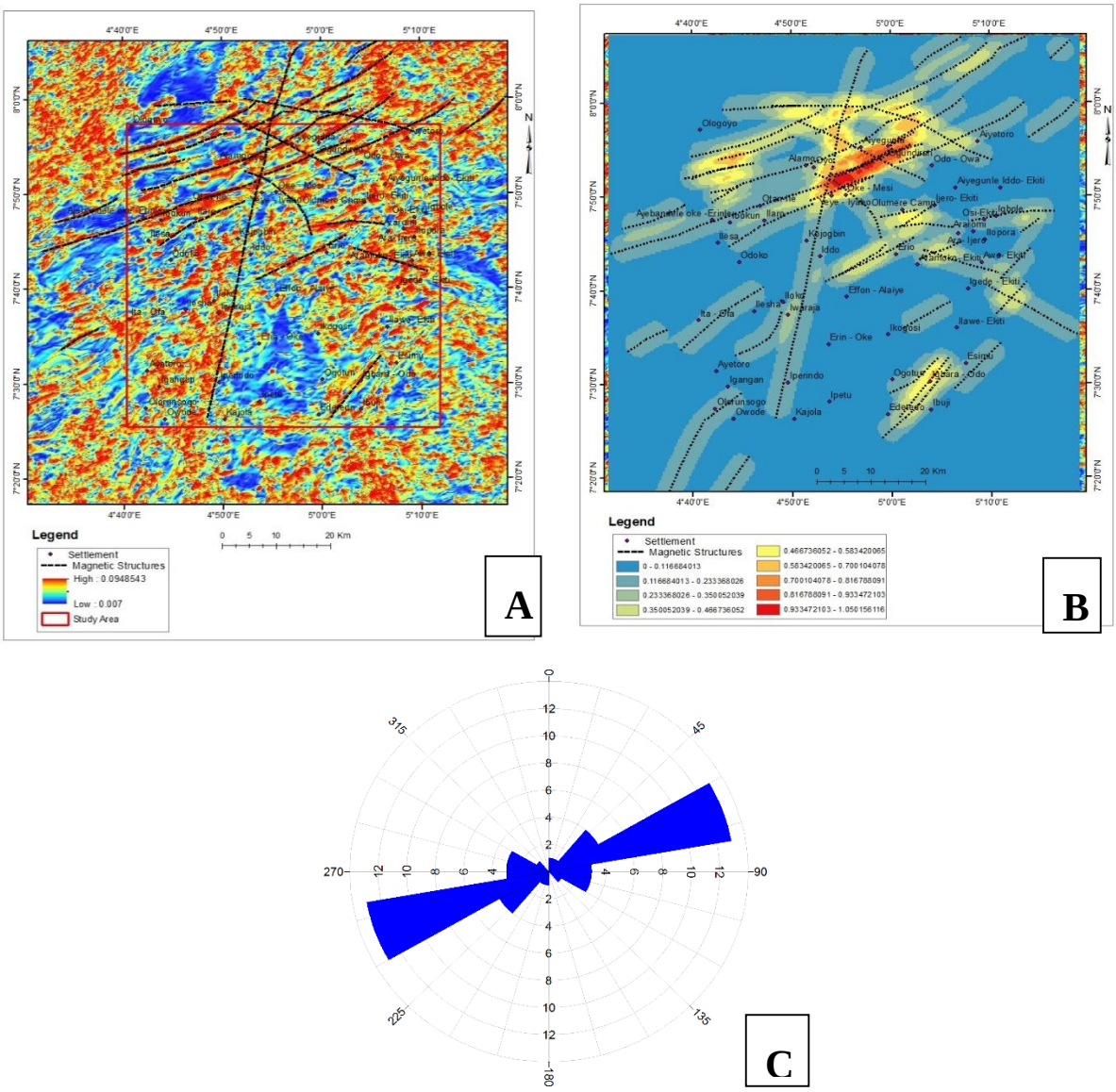

Fig. 4. 16 (A) Tilt derivative image showing magnetic lineaments, (B) magnetic lineament density of the total magnetic lineaments extracted, (C) Rose plot showing the trend of magnetic lineament in TDR

The output maps resulting from Euler's solutions in Figures 4.17 A and 4.17 B made possible the evaluation of the depth of the geological structures observed from the other filters applied. This map also showed new faults with depths ranging from <300m to > 500m, where the solution of SI = 0.5 delineates the trend of the Ifewara-Zungeru faultline better that SI = 0. (Fig. 4.17 A and 4.17 B).

The established lineaments may be related to the Pan-African orogeny and appears to correlate to deep-seated basement formations, indicating the tectonic boundary between the Congo Craton and the Pan-African orogeny belt. The trending of the structural features observed was presented on the structural map of the study area, which was NE-SW, NW-SE, ENE-WSW, and WNW-ESE, respectively, while the E-W and N-S were secondary bearings of the detected tectonic evidence.

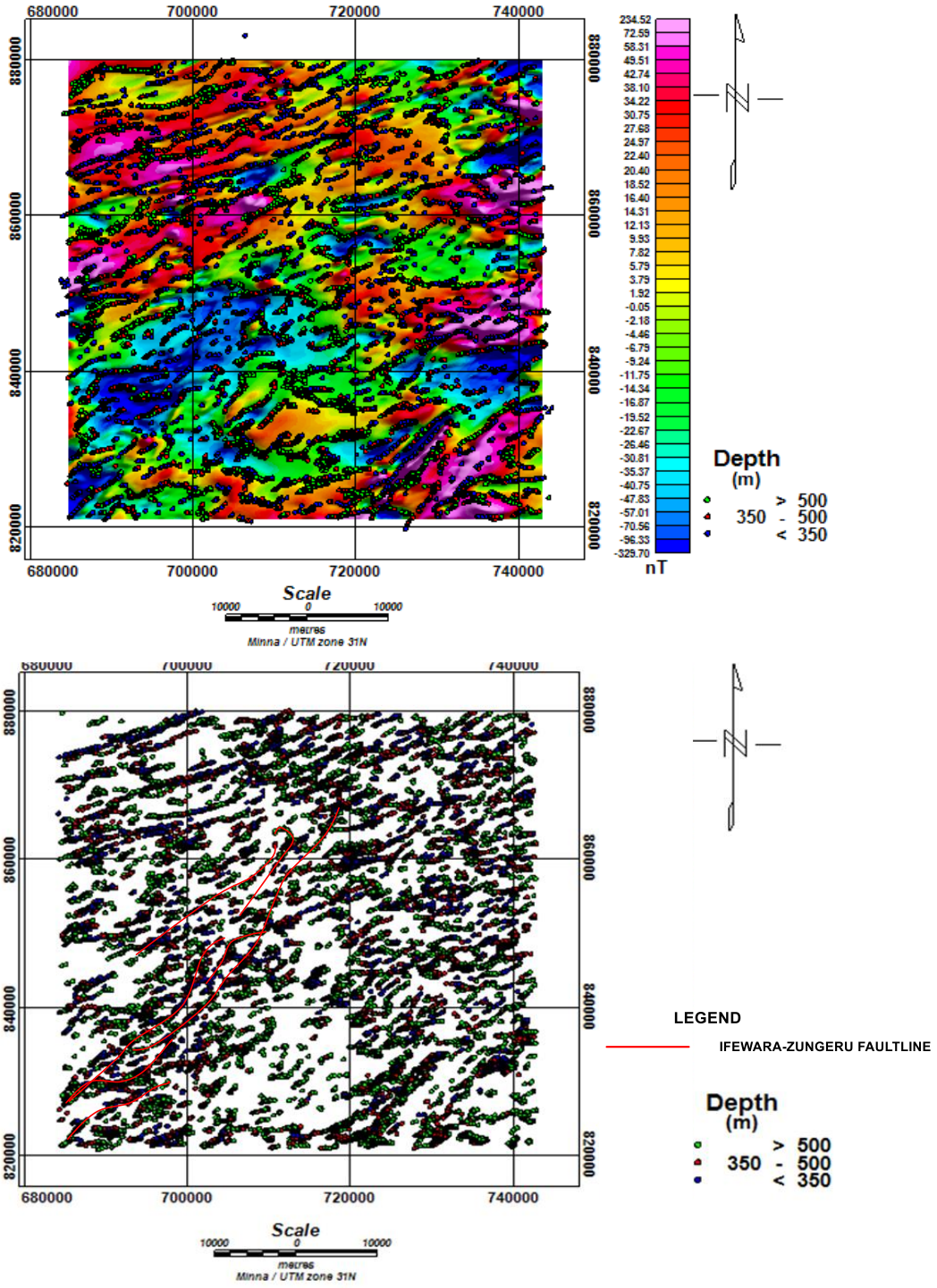

Fig. 4. 17 A & B: Euler solution with SI of 0 superimposed on the Residual TMI map and Euler solution with SI of 0.5 depicting a model between a horizontal cylinder and sill/Dykes (i.e. faults/contacts and sill/dyke).

The geological and surface structural map of the Okemesi Iwaraja region, derived from Landsat OLI data, was combined with the subsurface structural map derived from magnetic anomaly data. The complex existence of magnetic anomalies over the Okemesi - Iwaraja region was studied in order to establish their relationship to surface geology, surface structure, and their tectonic environment. There was a close relationship between magnetic and many of the region's main geological features. Magnetic data analysis and interpretations have revealed a better picture of the research area's tectonic pattern. Using an aggregation of all the results of the aeromagnetic analyses, the regional tectonic framework of the studied area was established. The location of two main sets of faults NNE–SSW to N–S, which were dissected by an E–W to WNW–ESE fault system, was revealed by the analysis of the area's basement tectonic map. These two sets of fault systems, as deduced from aeromagnetic evidence, were found to match the structures from Landsat OLI image and geological map quite well (Khamies etal 2010).

From the overall structures extracted using the various techniques, we were able to produce a structural density map. The density map revealed areas with high fracture densities. These revelations led to the selection of two regions/areas within the general study area, for detailed ground sampling, measurement of structural elements, rock sample collection for petrography, geochemical analysis and hand specimen description, and ultimately produce detailed structural geological maps of the sampling areas, (see Figure 4.18).

4.5 Structural Setting and Geology of Study Area

Structures, such as joints, dykes, and folds, are signs of deformation left as imprints on rocks. Such structural features show varying patterns that agree with the overall trends seen in Nigeria's Basement complex. These structures are thought to have formed due to extreme regional tectonic activity that preceeded the emplacement of Older Granites during the Pan–African orogeny, which created a large N–S pattern in Nigeria, including the study area (Fig. 2.2). These structures aren't entirely attributable to tectonics and related deformations; they may also be the result of tensional forces generated as a result of cooling.

The geological environment, relief, drainage, and lithological borders in Okemesi-Iwaraja area have all been affected by the structural setting. The magnitude and extent of structures are generally determined by the duration and degree of deformation. N-S, NE-SW, NW-SE, NNW-SSE, and WNW-ESE were the main structural patterns in the study area. They were relatively younger than the E W Pan-African structures. As a result, the structures were mostly the result of Pan-African orogeny. Weathering and flooding, on the other hand, have obliterated these structures. They were observed as relics in some parts. While in a few exposures they were still well preserved.

4.5.1 Method of Study

The geological field mapping operations were used to produce the necessary geological and structural details. From the results derived from lineaments and lineament density generated from Landsat OLI, ASTER DEM, RADAR and Aeromagnetic Data, two areas with the highest fracture density were selected for detailed mapping, these were Sampling Areas A and B (Figure 4.18).

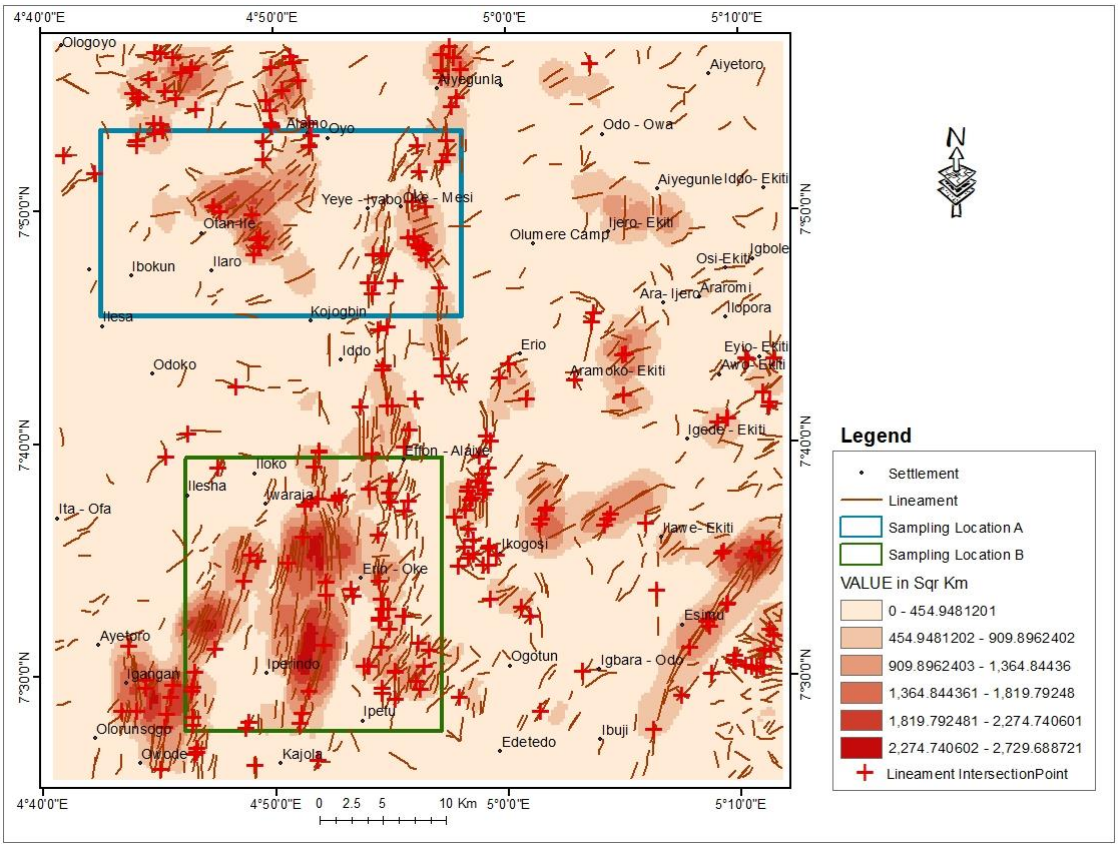

Fig. 4. 18 Lineament Intersection and Lineament Density Map of Okemesi-Iwaraja Area Showing the Selected Sampling Areas A and B.

The grid sampling method was used in the field work exercise, which was divided into two stages: observation and interpretation of outcrops and their locations in situ, as well as a detailed examination of structural characteristics in the rocks such as folds, joints, dykes, and foliation, and so on, accompanied by collection of required field data during geologic field mapping. This approach involved careful inspection, recognition, and systematic description of the rocks, as well as the subsequent compilation of structural details, including folds and other structural elements' inclination, shapes, styles, size, symmetry, patterns, axis, plunge, orientation, and groups. The basemap which is on a scale of 1: 50,000 was divided into segments and rock samples were taken from each portion of the sampling areas. The exact location of outcrops was determined using the Global Positioning System (GPS). A total of 130 fresh rock samples were taken from different locations within the research area (Appendix 8).

4.6 Geology of Okemesi-Iwaraja Area

Okemesi-Iwaraja area was underlain by eight major rock types namely: migmatitic grey gneiss, amphibolites, quartzite, quartz schist, biotite schist, and granitoids (granite gneiss, two-mica granite, medium-grained biotite granite, porphyritic biotite granite). (Fig. 4.80 and 4.81)

4.6.1 Quartzite

Other areas where Quartzites were observed in the study area included Ore Egba where they occured as a ridge, along Ilesa - Akure Road, Erinmo Ijesha where they were exposed as highly weathered out crops at the top of a ridge showing strong presence of quartz vein and joints. Samples were also obtained at Erin Ijesa from a hand dug well under construction at about 6m, they were highly weathered Quartzite. Further down at the Erin Ijesa (water fall) the outcrop was a massive quartzite ridge located at the Olumerin water fall, Erin Ijesa. It was a steep high rise quartzite ridge. There was presence of quartzo feldspathic vein intrusion made up dominantly of quartz and muscovite flakes. Black tourmaline was also seen within vein composition. Quartzite was also encountered at Okemesi, where it occurred as an extensive high rising ridge, covered by moderate to thick vegetation, with scattered

boulders of weathered rocks. The scattered boulders were observed to be highly weathered at the bottom of the main Quartzite ridge, covered with thick vegetation. Presence of low lying outcrop at the basal part of the ridge, occurred as displaced boulders from the original/parent outcrop.

Quartz Schist

The Quartz Schists in the study area occured in most cases as extensive ridges defining the topography of the area, this was notably observed within the Okemesi fold also known as Effon Psammite. Around Okemesi, the Quartz schist was seen as steep ridge, covered by moderate to thick vegetation, with scattered boulders of weathered rocks. Pegmatitic intrusions were seen cutting the Quartz Schist these intrusions were coarse grained, mostly of quartz and feldspar, trending NNE – SSW. Towards the north around the tip of the fold closure of the ridge, the rocks were highly weathered with presence of fractures, joint and quartz veins. They were also observed in other areas as pockets of small outcrops and or low-lying weathered exposures. At Okemesi, near Saint Michael Nursery and Primary School, Quartz schist occured as low lying outcrop. A road cut exposure, also extending inside the school showed that the rocks were highly weathered with presence of pegmatitic intrusion, and quartz vein showing mild jointing trending NE-SW and some NW-SE.

Quartz schist were also observed as exposures along road cuts along Ijero road they were seen to be gently sloping, and weathered in most parts, the rocks appeared as low lying outcrop. Close to Kajola farm settlement, they were also exposed as highly weathered outcrops.

Along Esa Oke road, Quartz schist were observed as road cut and outcrop, they were also highly weathered with the presence of quartz vein along the schistose plane.

At Oke Adun Community, Efon Alaye, Quartz schists appeared as high rising steep outcrop, accessible via a minor road at through the Community. Also at Iwaji Ekiti and Iloro Ekiti, high rise quartzite outcropped as ridges, with the top covered by vegetation with a stream running down the hill. Whereas at Ikeji-Ile, the Quartz schist were low lying outcrop near St. Jude Anglican Church, with quartz vein intrusion and multiple joints.

Along Ipetu - Ajegunle Road quartz schist outcrop was seen exposed along a road under construction (Ipetu - Ajegunle Road). It was a high rise ridge generally trending 32^0NW. It is weathered and folded, some of the folds extends up to 20m. The outcrop itself extend up to about 700m. It was covered by fairly thick vegetation. There was presence of pegmatite intrusion cross cutting the main outcrop. While at Ayeni Temidire, a quartz schist outcrop occurred as a ridge trending 84°, rising high above the background covered by vegetation and cocoa farm, there was the presence of multiple joints. The Quartz schist at Ipole Ijesa occured as flat lying, fairly extensive quartz schist outcrop, highly weathered and exposed in front of the Chiefs Palace Ipole, Osun State.

4.6.2 Porphyritic Granite

The Porphyritic granites occured mostly around Imesi-Ile, the outcrops were intruded as mostly dome shaped batholiths, they were seen as high rising outcrops in most cases they occured as extensive massive outcrops, and some cases could be seen as low lying out crops to boulders. They were mostly fresh and unweathered. In some cases, exfoliations were observed on the rocks in the field. They were non-foliated and not deformed. At about 2.5km from the boundary between Imesi-Ile and Esa Oke, and about 2km from the Ila Orangun junction (about 2km), was an extensive Porphyritic Granite outcrop, some exfoliated layers were weathered. The major mineral composition was quartz, feldspar, biotite, and other accessory minerals. The rock was coarse grained with quartzo-feldspathic (Q, F, M) pegmatitic vein, with individual minerals grain sizes ranging from 2 - 10 cm the phenocryst was mostly feldspar. Some Porphyritic granites were observed as low lying outcrops close to the main road south of the area described above. It was fairly extensive, the rock was similar to the previous outcrop described above, there was presence of open joint of about 1.2m width, and about 100m in length. There were xenoliths inclusion (darker than the host rock). There was presence of pegmatitic vein composed of quartz, feldspar and biotite.

At Ibokun, after the police station along Ada road, via a foot path; Coarse grained granitic rock occurs as low lying out crops with quartzo-feldspathic intrusions. At Ada, adjacent to the Golf course It was a high rise outcrop located about 40m away from the road. There was

presence of xenoliths (older rock, finer and darker, about 5cm by 15cm). It was a coarse grained granitic rock which extends up to 100m by 60m.

In some cases, they were observed as coarse grained, weakly porphyritic granite, occurring as high rise outcrop having very steep slope, accessible via footpath, at about 200m from the main road. It was very extensive, the access path was covered with thick vegetation, with farming activities (cocoa, kolanut, orange, etc) going on at the base of the exposed outcrop. Along Iree Road Ada by a church, medium to coarse grained Porphyritic granite occured. The outcrop was accessible via a foot path along Iree Road. There was presence of quartzo-feldspathic pegmatitic intrusion (also contains black tourmaline), with individual grains up to 6cm, the veins attained up to 36cm width trending 32°. There was also a quartzo-feldspathic vein (about 4cm by 3.2m) trending 6º on this outcrop.

4.6.3 Medium Grained Biotite-Granite

Medium grained granitic rocks were fairly extensive outcrop, exposed on both sides of the Ada - Igbajo Road rich in quartz, feldspar, and biotite, the once around Aagba Methodist High School, Ada, the rock occurs as high rise outcrop, with evidence of ex-foliation, it covers about 500m^2, some of the rocks were seen as high rise, extensive, fine grained granitic outcrop, along the road, quartzo-feldspathic pegmatitic intrusion were observed on them. The outcrop shows some evidence of exfoliation.

Along Effon Alaye Road Fine grained granite, was observed poorly exposed along Erinmo - Effon Alaye Road, about 80m from the main road. It was covered with extensive pegmatite (about 150 by 220m) Quartz, feldspar, biotite. Medium grained granite was also encountered at Ipetu- Ijesa at quarry site. Mineralogy was mainly quartz, feldspar, and biotite. The Medium grained granite outcrop at an abandoned quarry site in Erin- Ijesa. The abandoned quarry pit contained pool of water. It was partly covered by vegetation, It was located at about 800m - 1km from Erin-Ijesa Ilesa Road, adjacent to the junction to the water fall.

Ikeji-Ile- Ipetu axis, a high rise granitic outcrop stands out notably along the road. Some other smaller outcrops also occur around this out crop. It was leucocratic in colour,

Porphyritic and of medium to coarse grains. It was partly covered by vegetation, with farming activities going on around. These rocks were also found at Iperindo, within the Community Middle School. They were medium to fine grained. Mineralogy Quartz, feldspar, biotite, with little muscovite. While along Iperindo - Odo Road, Atakumosa East Local Government, Osun State, the rocks occur as a low lying granitic outcrop by the road side inside a cocoa farm. The rock was a fine grained granite, with quartz, feldspar, biotite and other accessory minerals.

4.6.4 Granite Gneiss

Okemesi and its environs are underlain predominantly by gneisses, although with poor exposure, at Okemesi relics of Gneiss were exposed along the river channel beside General Hospital, Okemesi. It was fairly weathered, flat lying outcrop with presence of joints, pegmatitic intrusion and quartz veins. They were also exposed along a road and the drainage beside Deeper Life Bible Church, Odoba/Itio Okemesi. It extends down to the police station. It was highly weathered. There was presence of pegmatitic intrusion. The outcrop grades from schistose to gneissic fabric, the zone was likely a contact between the schist and gneiss.

Granite gneisses of medium to fine grained size were also exposed along Osogbo - Ibokun Road, opposite Chief Magistrate Court, Ibokun. It occurs as road cuts. Also observed at Ibokun, Granite gneiss were seen exposed at Ibokun Grammar School junction, Ibokun. It contains inter bedded layers of gneissic rock (dark and light layers), it was migmatitic in nature. There was presence of pegmatitic intrusion, quartzo-feldspathic vein of about (3mm), micro strike slip fault. The rock was highly deformed. it was medium to fine grained, it was an extensive outcrop accessible via a foot path. Also at an abandoned quarry site at Ibokun, Granite gneiss was exposed, the location was accessible via a foot path opposite the Chief Magistrate Court, Ibokun. Quartzo-feldspathic intrusion, micro-fold and micro fault were observed in the outcrop, it was leucocratic, and highly deformed.

Alond Iloko-Iwaraja Road, an extensive high rising outcrop of granite gneiss accessible via a foot path along Iloko - Iwaraja Road was observed, showing weak lineation. It was partly

covered by vegetation (schrubs and trees), with some occurring as boulders. The grain size was fine to medium, and it was leucocratic in colour.

Another high rise granite gneiss outcrop was located along Ilesa - Akure Road, about 30m from the road was of medium grained, showing lineation of minerals, partly covered with vegetation. Erin-Ijesa Granite gneiss occurs as low lying gneissic outcrop close to the quartzite ridge by the water fall (about 1km away). It was fine grained, rich in biotite. There were quartzo-feldspathic and pegmatitic veins. It was covered with vegetation, exposed along a minor foot path. This out crop was not extensive in size.

Also found along Erin-Ijesa Road, was a road cut, with gneiss exposure. It has quartzo-feldspathic vein of about 12cm width. It was fairly elevated and covers about 300m. It was fine grained, covered by vegetation. The out crop was composed mainly of quartz, biotite with little reddish crystals suspected to garnet. The granite gneiss on Iperindo Road was exposed as a low lying outcrop located along the Road. It was partly covered by vegetation. It was medium grained. At Ise-Ijesa, along a road cut exposure, Granite gneiss was seen as flat lying granite gneiss outcrop. It has numerous quartz and quartzo-feldspathic veins cutting across the outcrop. It was fine grained. Also found along the Ise- Ijesa Road the outcrop has been broken into disjointed blocks, though continuous in some part. It was an extensive outcrop; it occurs along the road. The grain size was fine.

4.6.5 Grey Gneiss and Migmatite Gneiss

The grey gneisses were encountered around Idado, while at Idado-Ijesa, it was a high rise granite gneiss outcrop that extends approximately over 1.5km along as a ridge. A migmatite gneiss - shcist outcrop with multiple quartz vein running through the rock. It was folded and highly deformed. The quartz vein was believed to be the first episode of deformation, but later deformed itself after another episode of deformation. it was a high rise outcrop, showing schist, gneiss and migmatite properties.

4.6.6 Biotite and Staurolite-Garnet-Biotite Schist

At Erin-Ijesa, within the compound of the abandoned mine close to a workshop, schist exposure was observed as a highly weathered, flat lying outcrop. About 50m or less from the quarry towards the workshop, a contact between schist and granitic rocks was presumed to occur. Quartz intrusion was also observed. Along the Erin-Ijesa - Ilesa road, was also a mica schist outcrop, with abundance of biotite. It was fine grained. Alond a road cut exposure, it occurred a a fairly elevated outcropt about 100m long. It was covered by vegetation, further at Irogbo is a low lying, fairly extensive schist outcrop which was highly weathered, it was fine grained with pegmatitic intrusion. While along Irogbo Road low lying biotite schist outcrop located at about 10m off Irogbo Road were observed. The outcrop was covered by vegetation, it was fine grained, with greyish colouration. At Ipole-Ijesa, low lying outcrop located some distance (about 300 -400m) from the Chief's palace. It was a very dark rock, suspected to contain amphibole. It has high specific gravity. It has quartz veins running across the rock. There was presence of quartzo-feldspathic intrusion, joints and veins.

4.6.7 Amphibolite

At Ajindo, the outcrop was located some 30m away from FADAMA III market project, Ajindo, along Okemesi - Ijero Road. It occured in a farm land within a cocoa and banana plantation close to the road, as a very big/large sub-rounded to oval boulders. It contains mafic (very dark) minerals, showing very weak foliation. It was very hard and has high specific gravity. There was presence of thin quartz vein (less than 0.3mm), cutting across the boulders. Mafic rocks also occured as cobbles on top of a ridge covered with cocoa crops. The outcrop was located along Okemesi-Imesi Ile road after Esa-Oke Junction to the left, towards Imesi-Ile axis. It was dark greenish in colour, and also contained mafic minerals. It was fine grained, showing schistosity. Highly weathered, contained probably hornblende giving rise to the greenish colouration. There was a presence of another very dark cobbles probably a vein/dyke cutting across the host rock.

4.7 Structural Setting of Okemesi-Iwaraja Area

The attitudes of structural elements were also mapped, in addition to the lithological aspects of the study area. This involved foliation strike and dip, mutual surface strike, lineation strike and plunge, including fold axes, and fault block relative movement. The basement terrain had more complex structural patterns, especially in the areas of granulites, high-grade gneisses, and schists. Although the primary features of metasediments, volcanic, and igneous rocks were often obliterated in the study area, the superposed fabric due to subsequent deformation was comparatively well preserved in such high-grade terrains. In the vicinity of Iwaraja and Okemesi, the region also revealed some of the best formed major shears and areas of slickenedsided surfaces, as well as maintained foliation, super, and small folds (Fig. 4.26 a & b). Major and minor structures were witnessed in Okemesi-Iwaraja area, the major structures were revealed by Satellite images, Synthetic Aperture RADAR, alongside High Resolution Airborne Magnetic Data coupled with field observations. These structures were predominantly tectonic in nature, some of the major structures observed in the area included folds, foliations, joints, veins, and dykes. Minor structures were observed from field exposures.

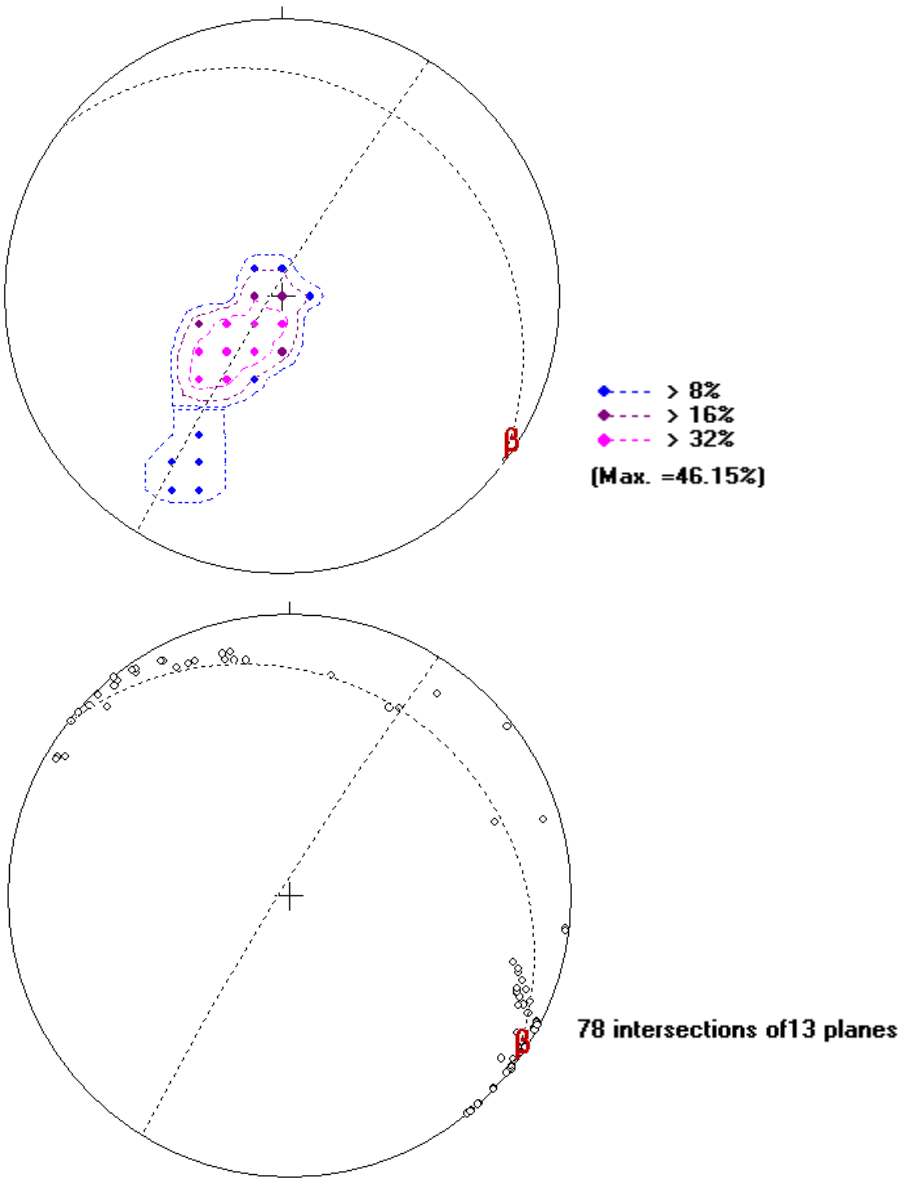

Mean Principal Orientation = 24/038, Mean Resultant dir'n = 25-038, Mean Resultant length = 0.94, (Variance = 0.06), Calculated. girdle: 87/302, Calculated beta axis: 3-122

Fig. 4. 19 (a) and (b): Stereographic projection of planes of foliation and poles to plane on the migmatite gneisses and granite gneisses in a Schmidt net equal area, lower hemisphere.

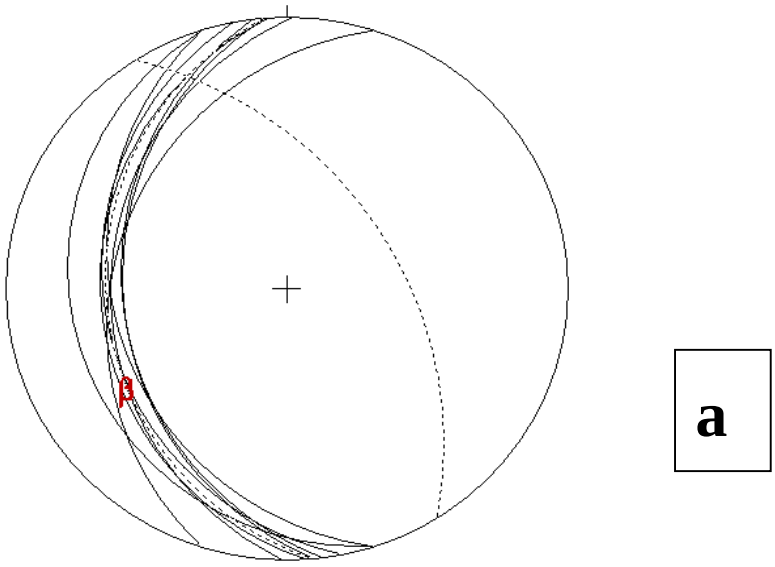

Mean Principal Orientation = 175/36W, Calculated. girdle: 327/58E

Calculated beta axis: 32-237

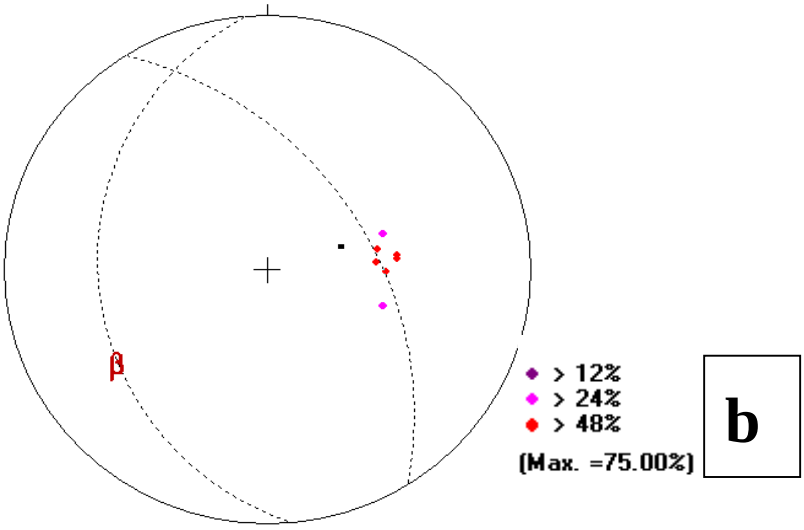

Mean Principal Orientation = 175/36W, Mean Resultant dir'n = 36-265 Calculated. girdle: 327/58E, Calculated beta axis: 32-237

Fig. 4. 20 a and b: Stereographic projection of planes of foliation and poles to plane on the Biotite Schist in a Schmidt net equal area, lower hemisphere.

4.7.1 Foliation

Foliation were formed during the flow stage of recrystallization of magma by the platy minerals due to intense temperature and pressure within the earth crust. This process resulted in parallel orientation of platy minerals or mineral banding in rocks. Generally, the dark bands were composed of mafic minerals and the light bands of felsic minerals. Foliations were found within the Gneisses in the study area, Quartz schist, Biotite schists, Amphibole schists and migmatites. However, in some parts they were not too pronounced because of intensive weathering. The gneisses of the study area showed a major foliation trend of NE – SW and some NNW – SSE, while the quartz schist trended mostly NNW – SSE and NE – SW (Fig. 4.19, 4.20 and 4.21).

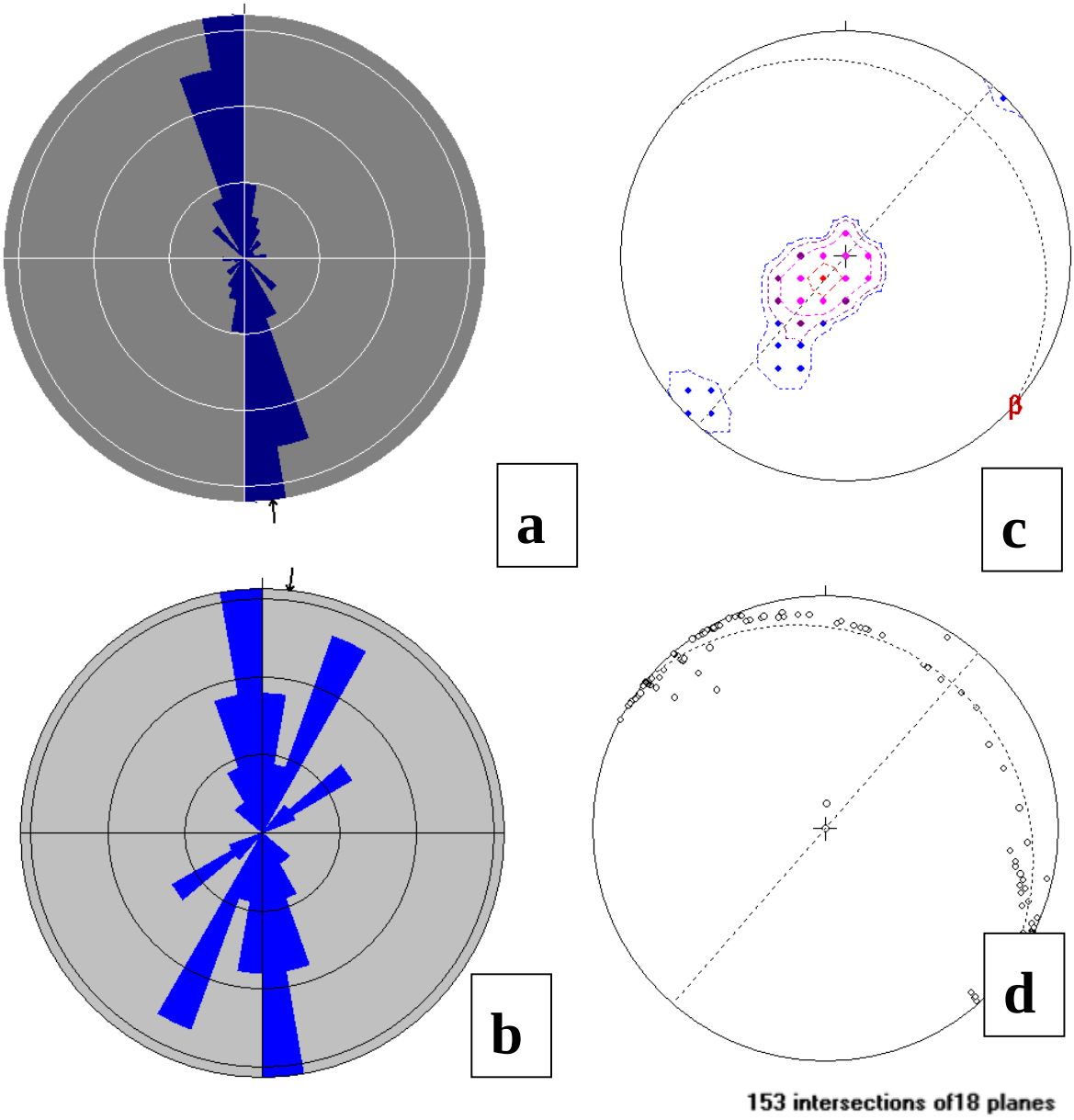

Fig. 4. 21 (a) Rose Diagram for Strike of foliation on Quartz Schist (b) Rose Diagram for Strike of lineation in granite gneiss, (c) and (d) Stereographic projection of poles and beta intersections on great planes for foliation on Quartz Schist in a Schmidt net equal area, lower hemisphere.

4.7.2 Lineation

Lineation occured as linear fabric elements that were repetitive on rock outcrops. The most common type of lineation in the study area were mineral lineation. Mineral lineation was defined by preferred dimensional orientation of in-equant grains or by elongated mineral aggregates. Within the granite gneisses and migmatite gneisses, lineations were seen and marked by linear arrangement of quartz and biotite. This was largely observed on the Gneisses, Quartz Schists, and the migmatite gneisses.

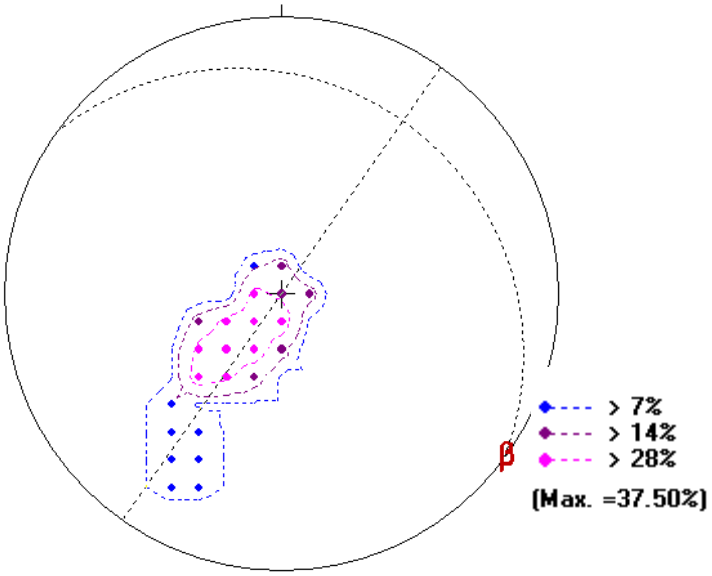

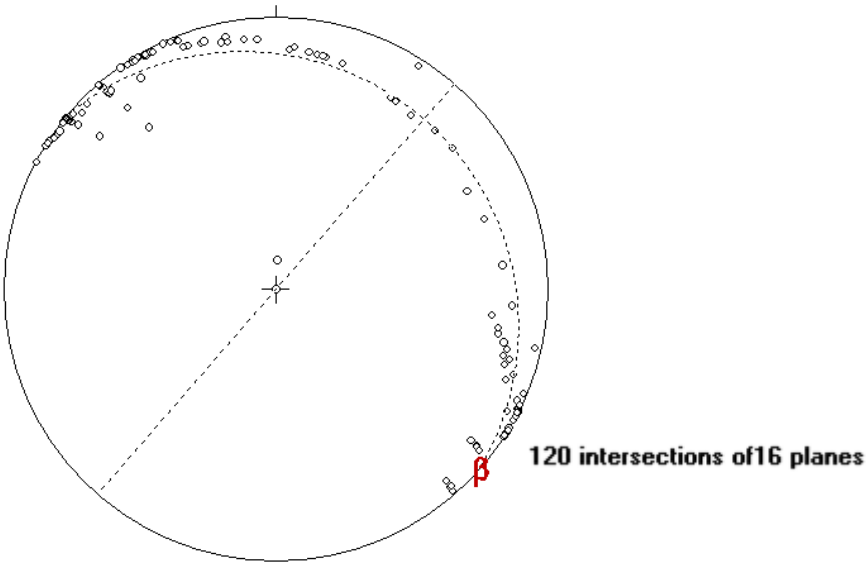

Mean Principal Orientation = 24/036 Mean Resultant dir'n = 25-036, Mean Resultant length = 0.94, (Variance = 0.06) Calculated. girdle: 89/305, Calculated beta axis: 1-125

Fig. 4. 22: Stereographic projection of planes of linneation and poles to plane on Equal angle plot contours and point density for lineation in Granite Gneiss in a Schmidt net equal area, lower hemisphere.

4.7.3 Folds

These are flexures or bends found in rocks and formed due to tectonic stress expressed by bending of reference surface. Large and small scale folds were observed in the study area. The large scale folds were common on the quartzite which was a structurally complex rock unit. A major fold occurred on the quartzite ridge which was again further folded around Okemesi showing large antiforms and synforms, this was seen clearly on the Satellite and RADAR Images of the area. This major quartzite ridge ran from around Ilesha through Okemesi where the main prominent fold was seen and buckled towards Erio and Aramoko-Ekiti then ran further down through Ikogosi and other settlements. The ridge was about 50km in total length about 730m high. It had a general north–south orientation. Folds on the biotite schist occured mostly as mesoscopic folds, some minor recumbent folds were observed in some quartz schist around Okemesi (Fig. 4.25). The strikes and the dips of the foliation (S_2) which was an antiform and a complementary synform. The F_2 structures were identified within biotite schists, the granite gneisses and the migmatite gneisses (Figure 4.26 and 4.27). The strike and dip of foliation (S_2) of rocks within the schists were plotted on stereonet diagrams, the mean strike and dip is $175^0/36^0$ W (Fig. 4.20 A and B). The pole to the plane of foliation showed mostly WSW –ENE (Fig. 4.21 A and B) on the stereogram plot, indicating a general NNW –SSE trend. The strikes and dips of foliation (S_2) of rocks within the granite gneisses, migmatite gneisses, were also plotted on stereo diagrams (Fig. 4.19 A and B) the mean strike and dip direction was $359^0/77^0$E, the poles to the plane of foliations are cylindrical and dominantly indicated most W – E direction (Fig. 4.19). Stereogram plot indicated a principal NNE-SSW trend for the major fold in Okemesi-Iwaraj area. The folds were tight to open and were well developed within the gneiss, migmatites and in some cases the mylonitic gneisses. They showed a simple to complex pattern depending on the stress on the rock. Micro folds and ptygmatic folds were observed, plunging in different directions (Fig. 4.28).

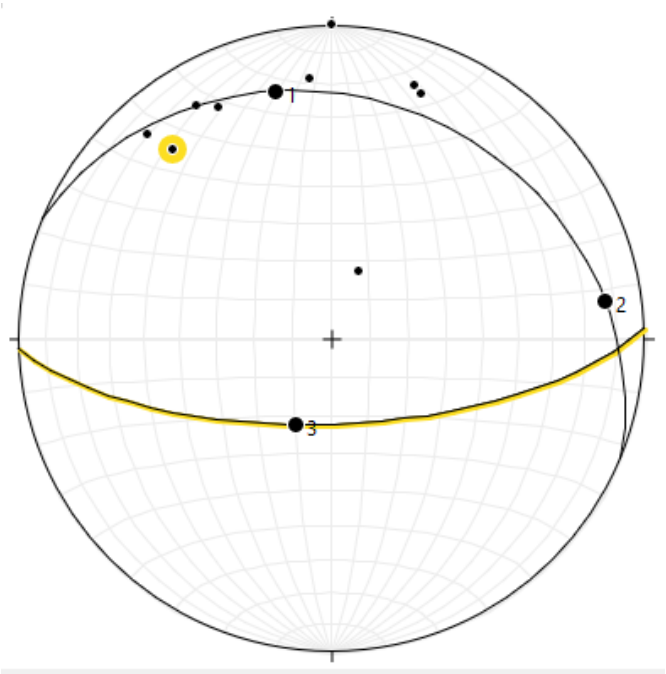

Best fit great circle (strike, dip RHR) = 292.5, 24.3, Trend & plunge of fold axis: 202.5, 65.7, Strike & dip of axial plane: 088.1, 67.7 S, Interlimb angle: 0.0°

Fig. 4. 23 Stereographic projection of planes of foliation and poles to plane on the gneisses in a Schmidt net equal area, lower hemisphere.

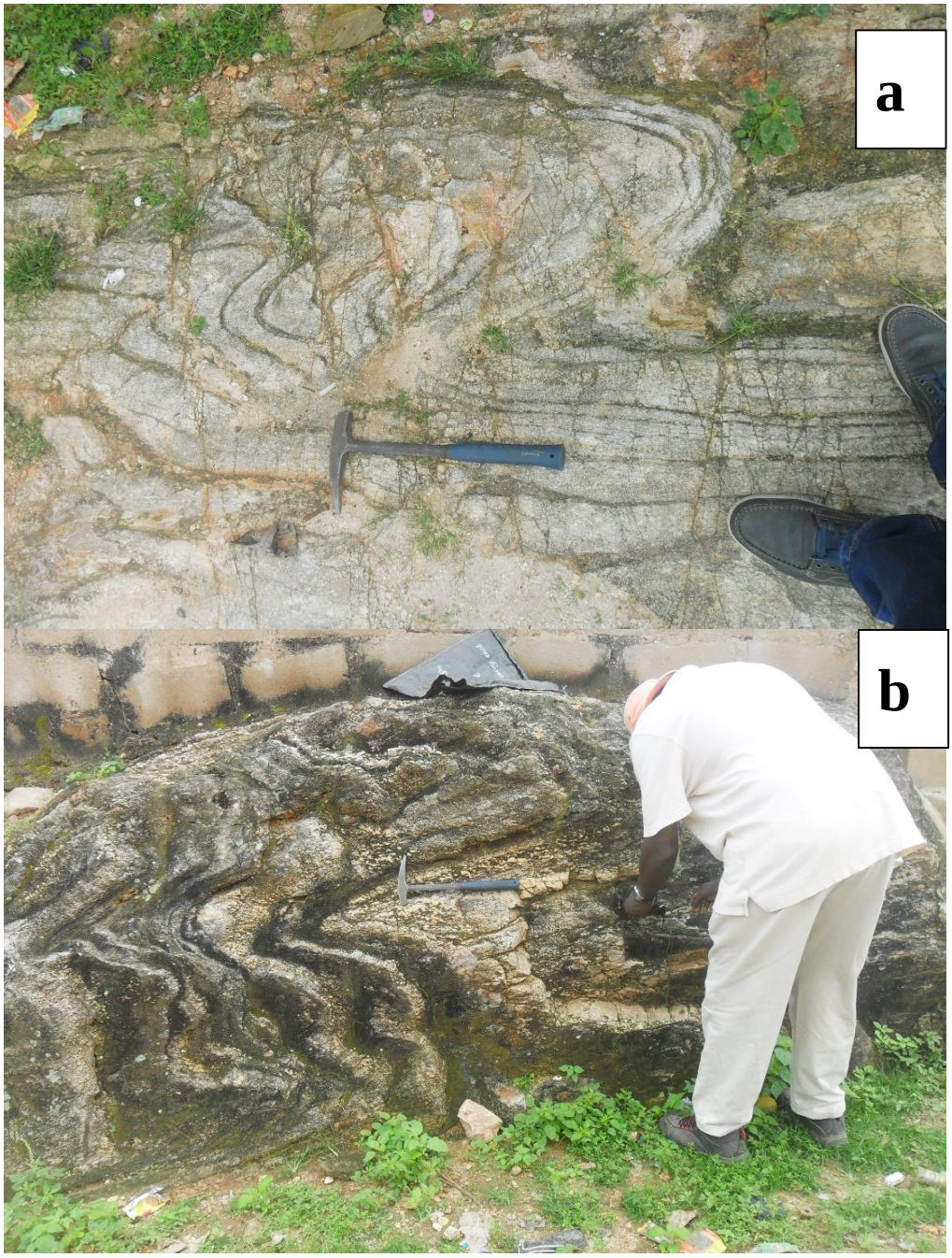

Fig. 4. 24 (a) Overturned folds in quartz schist around the Palace at Ipole (b) Overturned folds in quartz schist around the Palace at Ipole

They may have been veins that were initially intruded as flat sheets and then folded due to parent rock deformation or folding that happened during the injection phase in unusual circumstances. Minor folds were observed on almost all the rocks; the folds differed in styles. Figure 4.37 lillustrated convolute fold in migmatitic grey granite gneisses. Convolute are characteristics of high grade rocks, they have markedly curviplaner axial surfaces and are generally disharmonic. Ptygmatic folds were also observed on granite gneiss (Fig. 4.28). Recumbent fold with diagnostic horizontal axial plan existed on some quartz schist (Fig. 4.24 a and b), while Figure 4.26 and 4.27 illustrated asymmetrical fold traces with tight interlimb angles.

The dorminant orientations of the folds measured, showed that the trend, plunge and axis of the folds concentrated in the NE axis of the stereoplot and approximate axial surface to be NNE-SSW. The folds had moderate to steep plunge as revealed by the stereoplots.

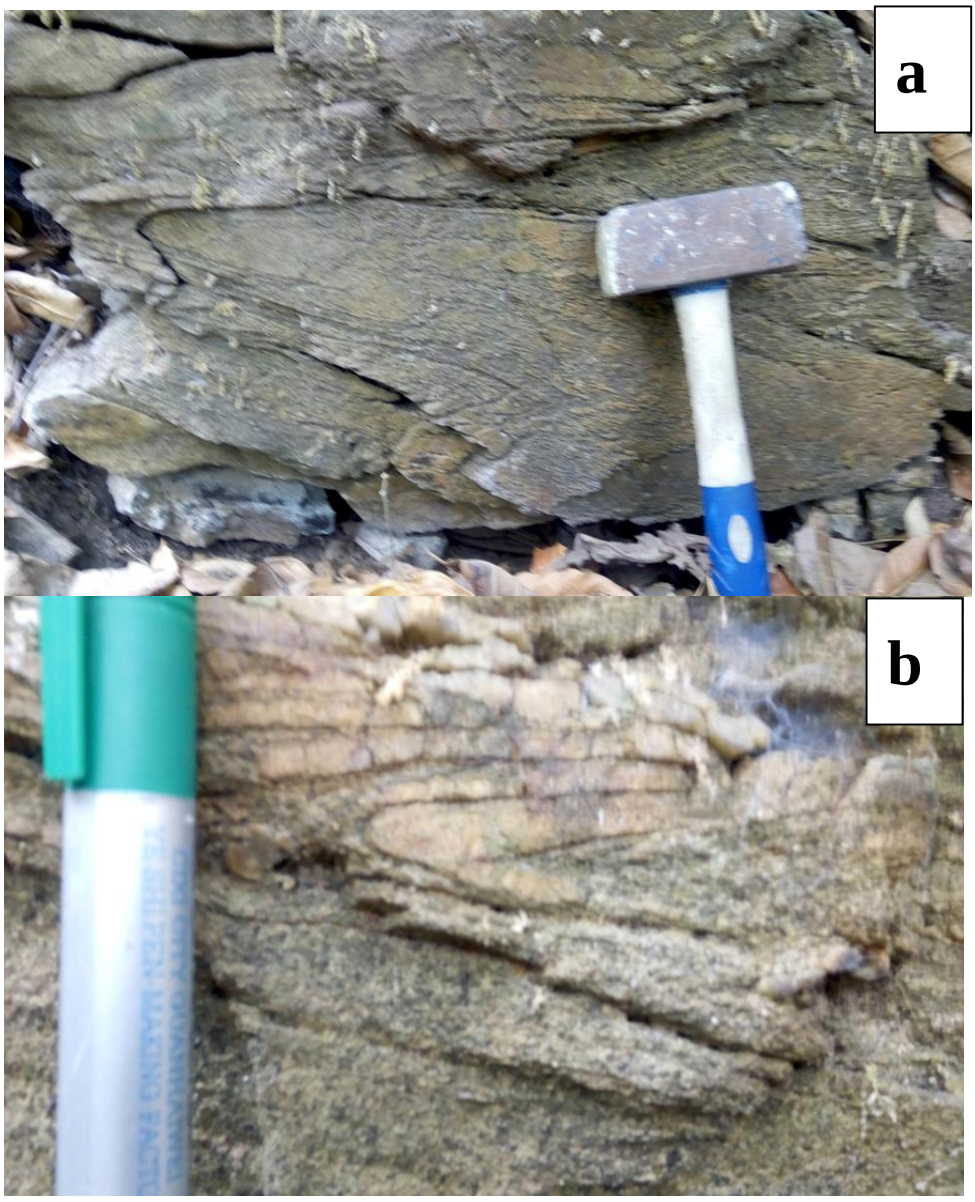

Fig. 4. 25 (a) and (b) Some minor recumbent folds found in the quartz schist around Okemesi

Fig. 4. 26 Open asymmetric folds in Mylonitic Gneisses along the Ilesha – Akure Road around Iwaraja

Fig. 4. 27 Tight Upright fold in Mylonitic Gneiss around Iwaraja

Fig. 4. 28 Ptygmatic folds in Grey gneiss

4.7.4 Schistosity and Crenulation Cleavage

Schistosity is the dominant foliation pattern that occurred on the schists in the study area. This was seen in the Biotite Schist and the Quartz Schists, and defined by the alignment of micaceous minerals (muscovites), giving the rocks a silky shiny lustre (Fig. 4.27)

Crenulation cleavage in the study area was very distinct in that it cut the host rock that possessed a pre-existing continuous cleavage (schistosity) into microfolds, the foliation was typically a zonal crenulation cleavage because the cleavage domains coincided with tight limbs of microfolds in the pre-existing continuous cleavage (schistosity). Crenulation cleavage was recorded about 300 m east of Busso Rock Hotel Atakumosa West LGA, and around the Palace at Ipole (Fig. 4.29 and 4.30 a & b). A total of 21 measurements of strikes, dips and dip directions of foliation surfaces were taken during the field work (Appendix 8). It was observed that schistosity was the most common foliation type in the quartz schist. Foliation planes had NE-SW orientations with medium to high dips ranging from 10° to 82° commonly found in the southeastern portion of the study area (Fig. 4.19A). The overall orientation of the foliation was obtained by plotting poles to planes using the technique derived by Ragan (1973) (Fig 4.19B). These plots revealed that the foliation poles are concentrated in the NW and SE sections of the net (Fig. 4.19B), supporting the prevailing NE-SW patterns in the study area. Rose diagrams were used to determine the precise direction of the foliations. The diagrams showed that the dominant orientation of the foliation is NE-SW (Fig. 4.22 and 4.23).

Fig. 4. 29 Crenulation Cleavage in migmatite gneisses around Busso Rock hotel in Osu, Atakumosa West.

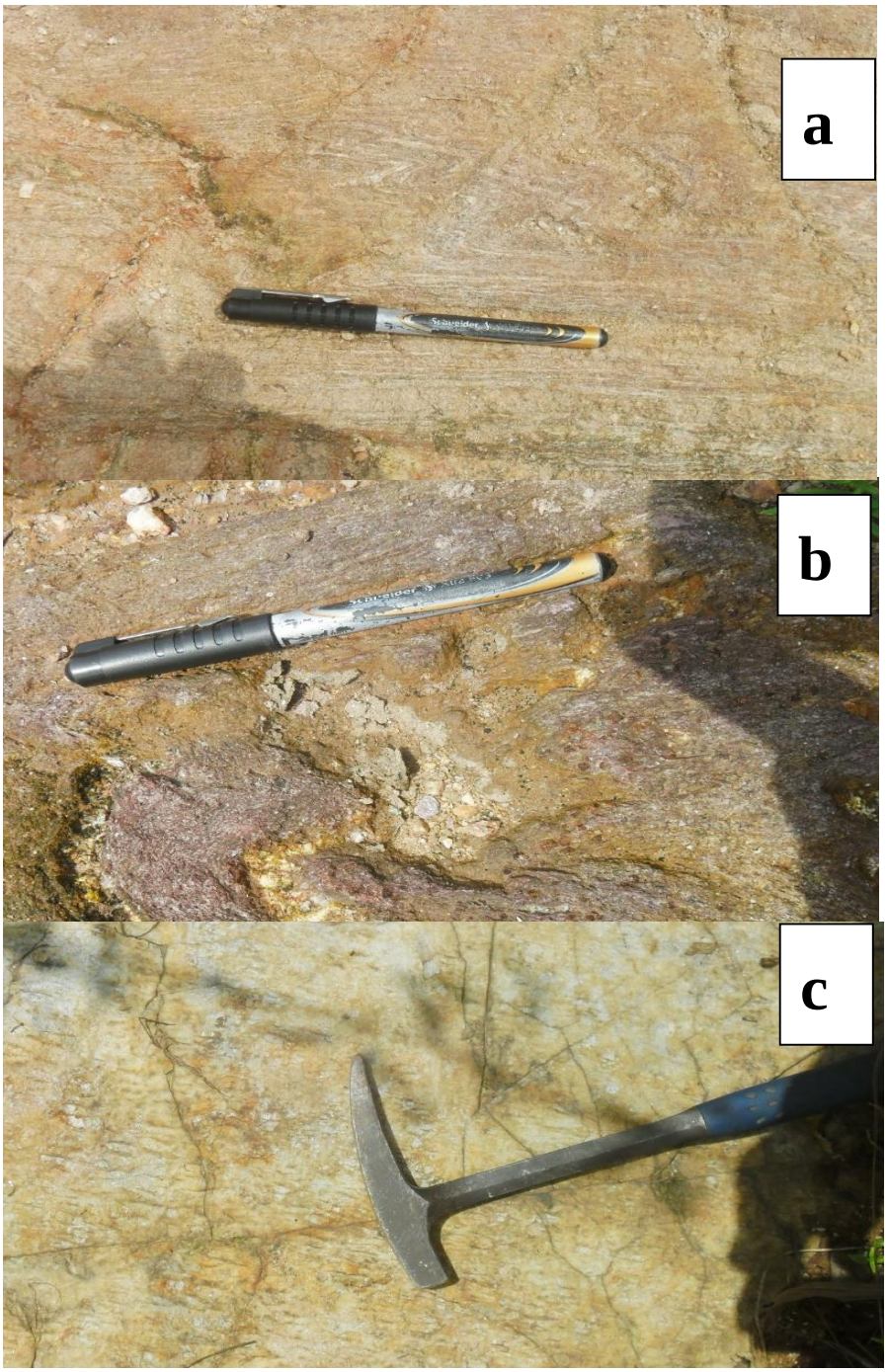

Fig. 4. 30 (a) and (b) Relicts of crenulation foliation in quartz schist near the palace at Ipole (c) Mylonitic quartzite around the C.A.C Ori oke at Itedo-Olorun along Iperindo - Orogbo road.

4.7.5 Joints

All the rocks within the study area were jointed. The joint pattern in the mapped area suggested that the study area suffered deformation. Joint was most common in the quartzite compared to the other rock types, probably due to the high competent nature of the quartzite. Different joint styles were recorded during the field mapping exercise. This included; cross joints and vertical joints (Fig. 4.31and 4.33). The dominant joint style displayed was cross joints, which occurred majorly on the quartzite.

A total of three hundred and eighty-two (382) joints were recorded in the area. Joint analysis was undertaken while all the measured joint planes were plotted on rose diagrams. The joints were trending in the E-W, NW-SE, NE-SW and N-S directions. Rose diagrams were also plotted for all the rocks of the area as well as the individual rocks, the quartzite had NE-SW and NW-SE trends, while the granite had a dominant NNE-SSW trend, Granite gneisses trended WNW – ESE (Fig 4.34 a,b,c).

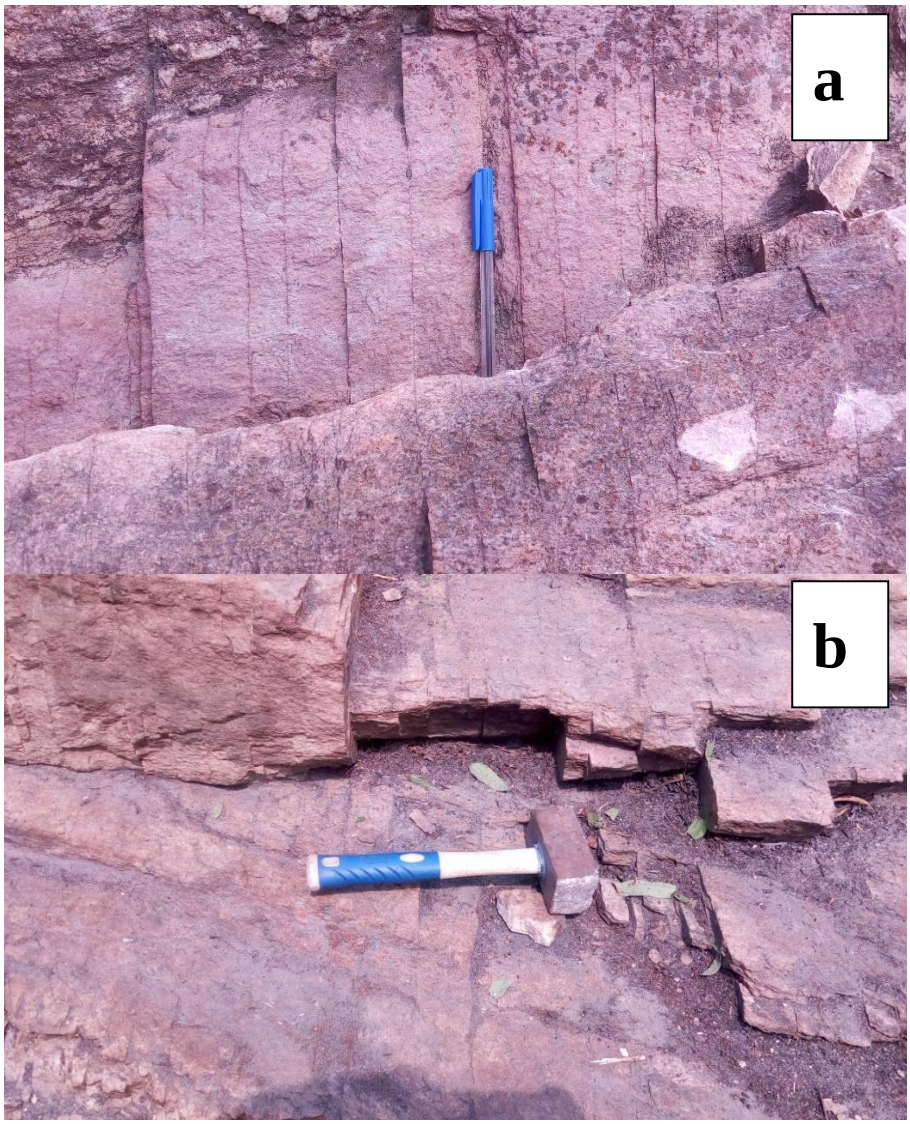

Fig. 4. 31 (a) and (b) Parallel Dilational joints in quartzite

Fig. 4. 32 Open joints in coarse grain granite

The joint set consisted of systematic joints ranging in length from 10 to 78 cm. The typical perpendicular spacing of nonsystematic joints was inconsistent with average perpendicular spacing. The surfaces of joints looked uneven and haphazard in general.

The common intersection geometry of the joints included T-geometries where the individual joint trace meets at right angle and X-intersection geometeries where the individual joint sets meets at acute angles. T- geometries included gradual die out, branch out and y tips.

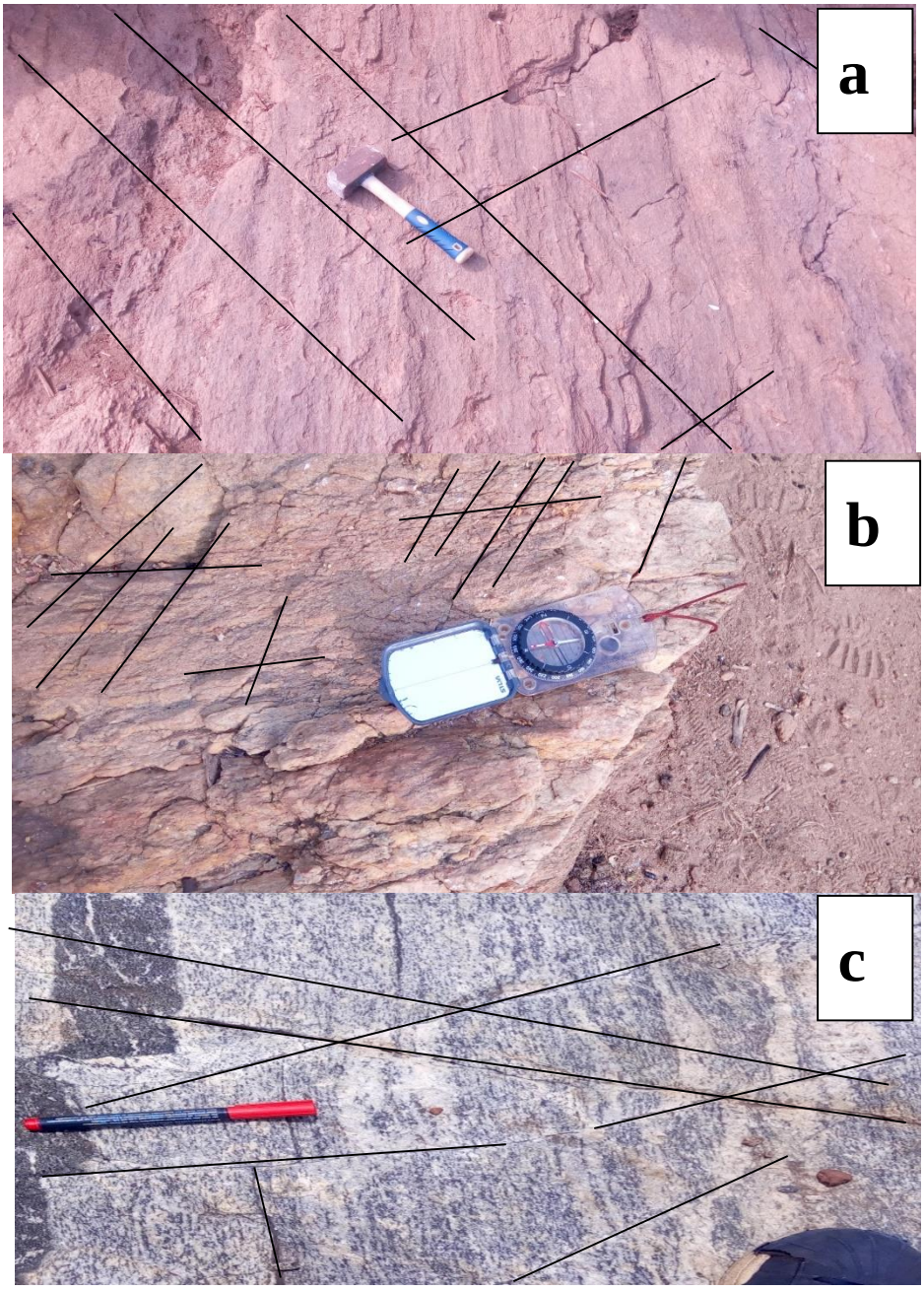

Fig. 4. 33 (a) and (b) Conjugate joints in quartz schist (Shear joints) (c) Conjugate joints (Shear joints) in Granite gneiss at a quarry in Obokun

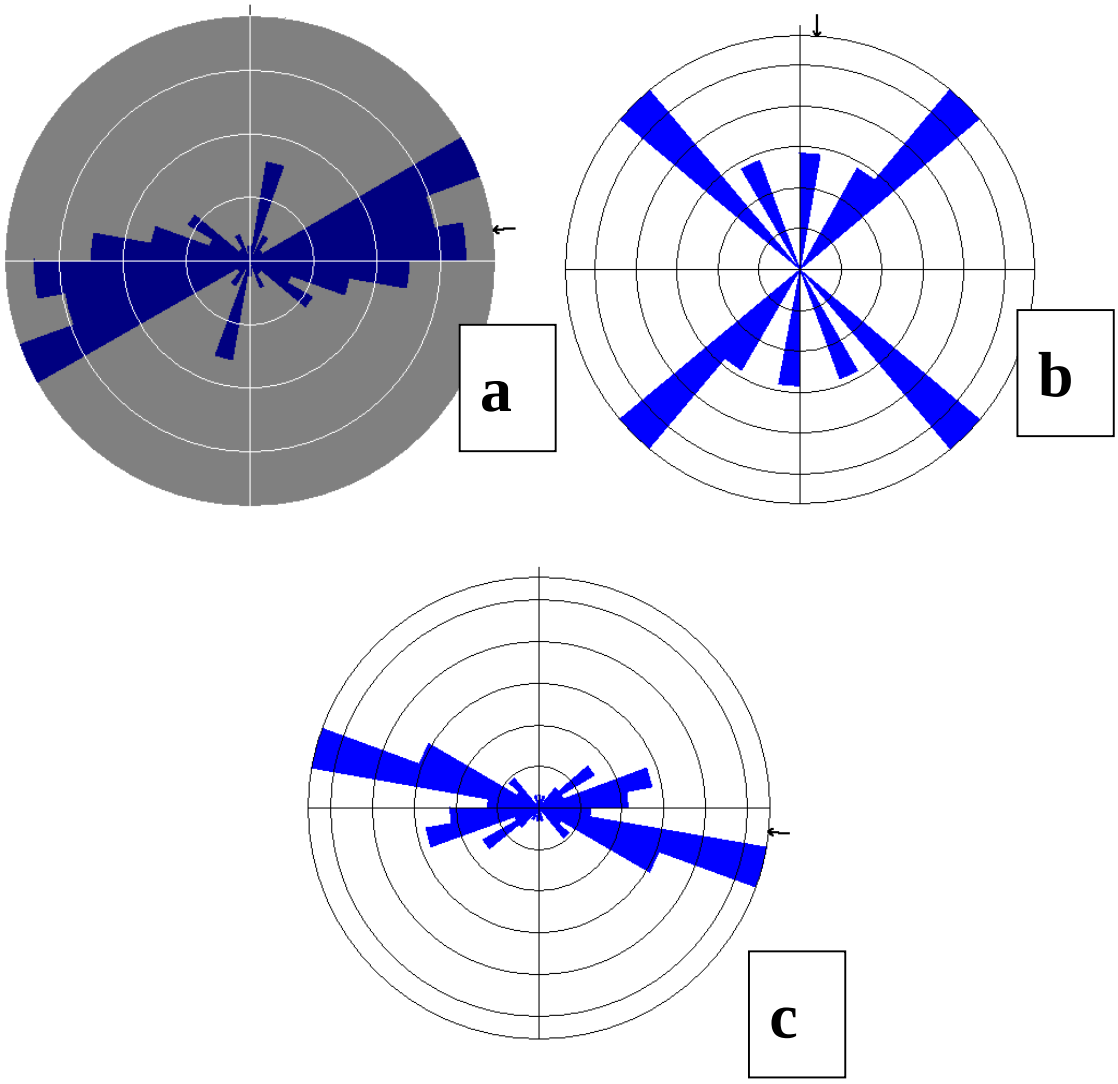

Fig. 4. 34 (a) Rose Diagram for Strike of joints on Quartzite/Quartz Schist (b)Rose Diagram of Strikes for Joints in Porphyritic Granite (c) Rose Diagram of Strikes for Joints in Granite Gneiss

4.7.6 Faults

These are structures in rocks formed by relative displacement occurring between two blocks of rocks, this was caused by deforming stresses. The type of faults observed were strike slip faults which occurred mostly on the gneiss. The strike slip faults were recorded as sinistral and dextral faults in some of the out-crops.

In the study area, minor faults occured on an outcrop scale (mesoscopic) as strike- slip faults with a dextral (right) sense of shear, displacements of about 20 cm and NE-SW trend. Imageries of Okemesi-Iwaraja area also revealed the presence of a major dextral fault which coincided with the Ifewara fault zone that cut through the area with a NNE-SSW direction (Fig. 4.1).

This fault zone was characterized by deep fracture, abundant folded gneisses, quartz veins and strong penetrative cleavage, mylonite and sheared rocks (Fig. 4.27, 4.28). Other fault planes have been recognized mapped and digitized from the satellite image, RADAR and HRAM of the general Okemesi-Iwaraja area (Fig. 4.18).

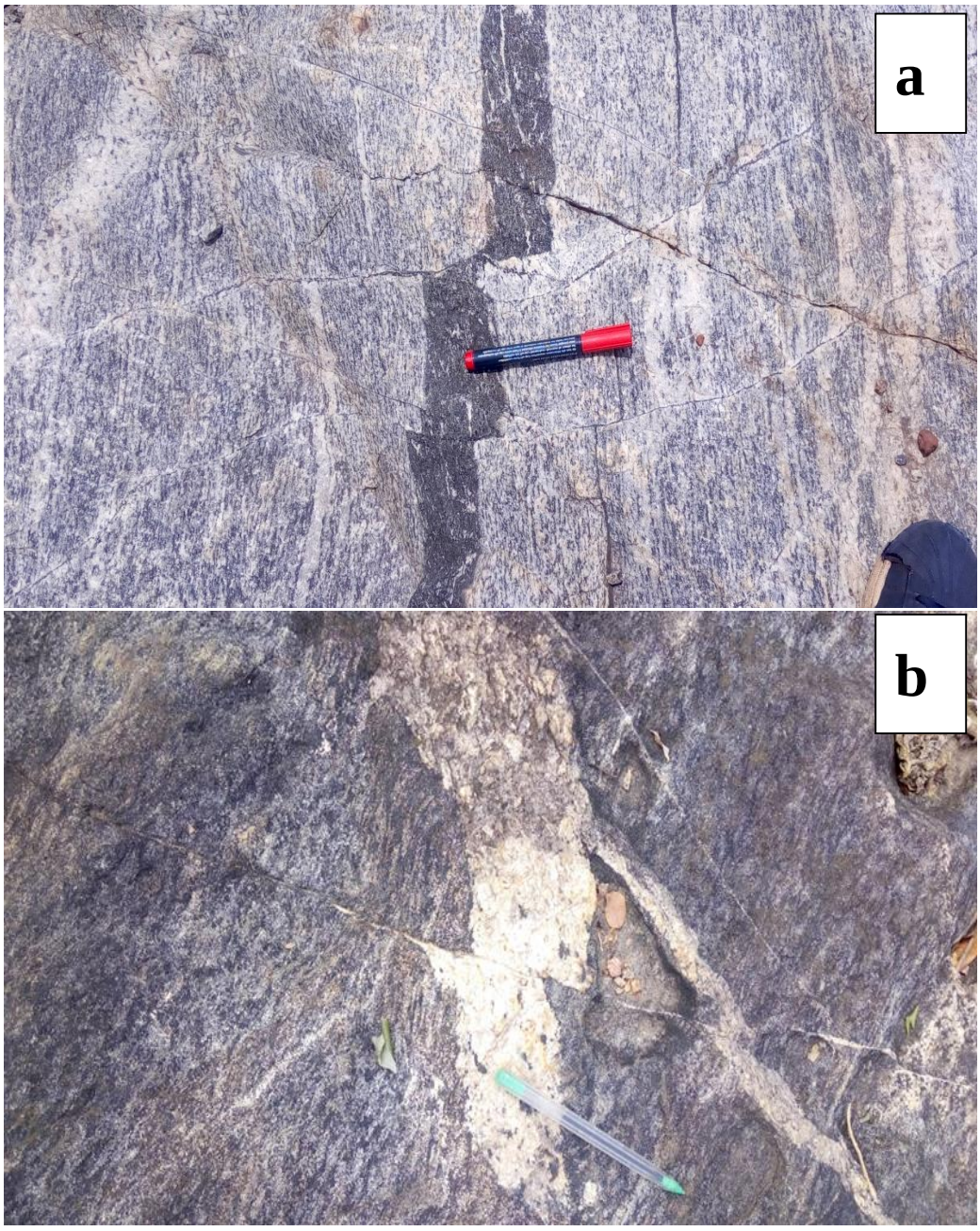

Fig. 4. 35 (a) Faulted Dyke in a granite Gneiss at a quarry near Ibokun (b) Faulted pegmatite intrusion and veins on granite gneiss

4.7.7 Shear Zones

The shear zones occured in regions of localized ductile deformation on the granite gneisses, some of the quartzites and in some cases the migmatite gneiss.

Fig. 4. 36 (a) Slickensides (fault lineation) on the fault plane at a quarry around Iwaraja (b) Shear zone with an evidence right-lateral kinematics (brittle-ductile deformation) exposed at a quarry near Ibokun High court

4.7.8 Quartz Veins

They had been formed by the infilling of pre-existing joints or newly developed joints. In the study area most of the quartz veins were usually thin with chilled margins. They occured in varying sizes and width of about 1cm to 3cm (Fig. 4.37). The sharp contact of the quartz veins with the host rock indicated the presence of pre-existing fractures. The trend for most of the quartz veins was NW-SE and NE – SW (Fig. 4.38 a,b,c)

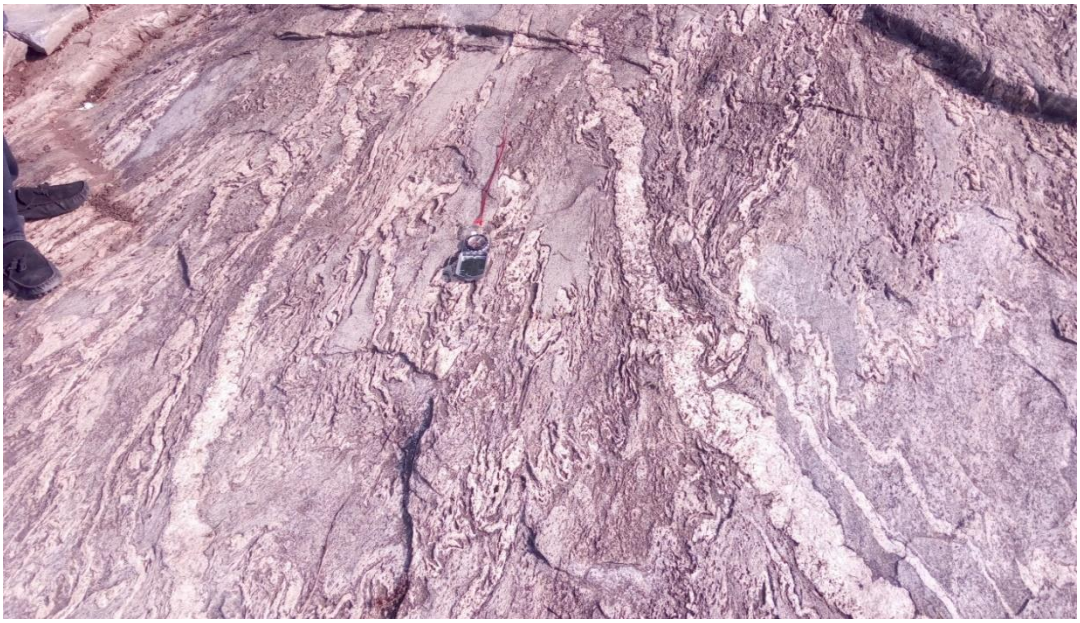

Fig. 4. 37 Deformed and folded quartz stringers in Grey Gneiss

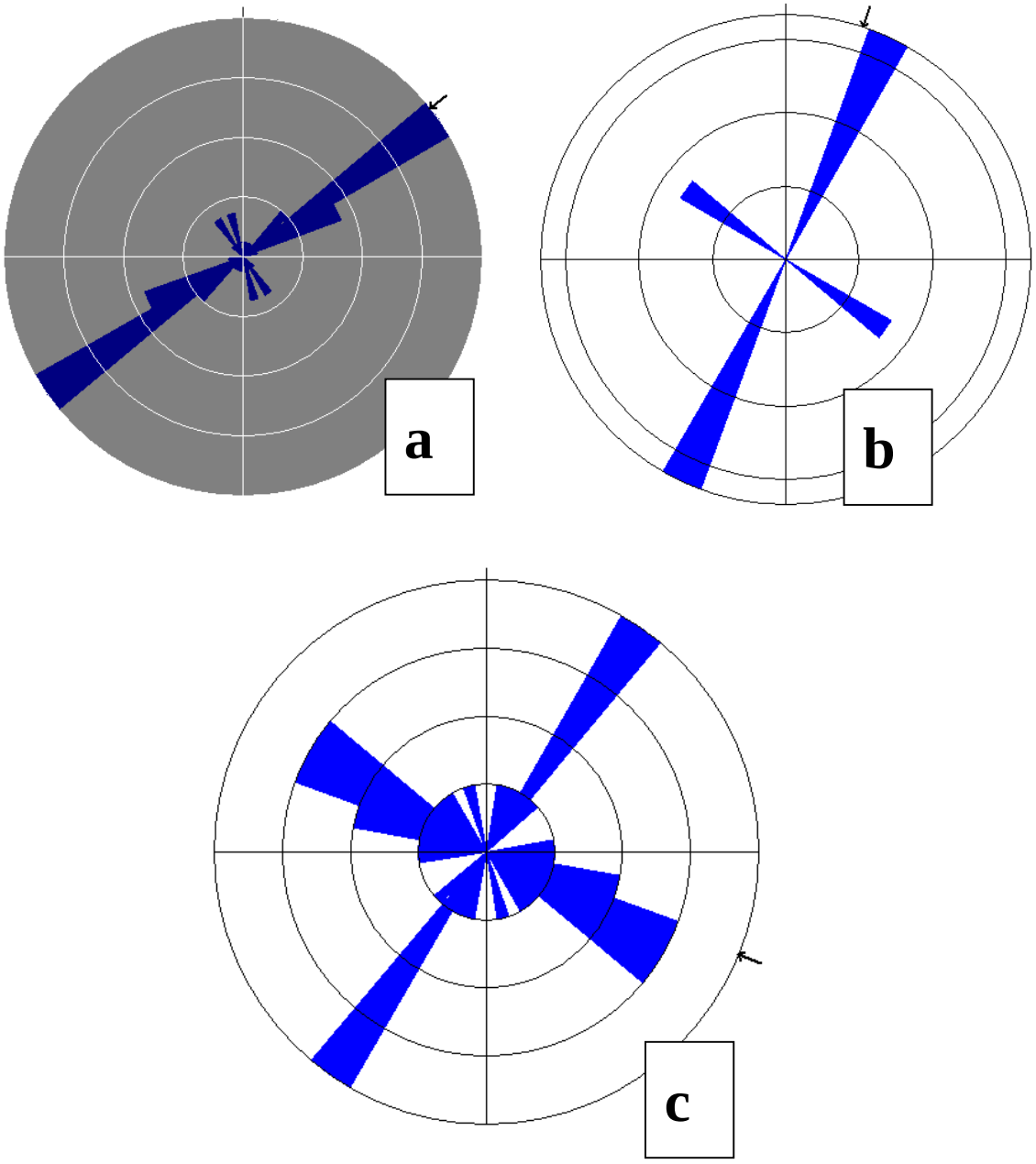

Fig. 4. 38 (a) Orientation Diagram for Strike of veins on Quartzite/Quartzite Schist (b) Orientation Diagram of Strikes for Veins in Porphyritic Granite (c) Orientation Diagram of Strikes for Veins in Granite Gneiss

4.7.9 PEGMATITE

The pegmatite occured as discordant bodies of rocks which intruded the host rock. They were exceptionally coarse grained in texture and characterized by variable thickness ranging from 3cm to about 1m in the field. The pegmatite was randomly spread within the rocks of Okemesi-Iwaraja area. The pegmatite mostly showed sharp contact with the host rocks. (Fig. 4.39 a and b).

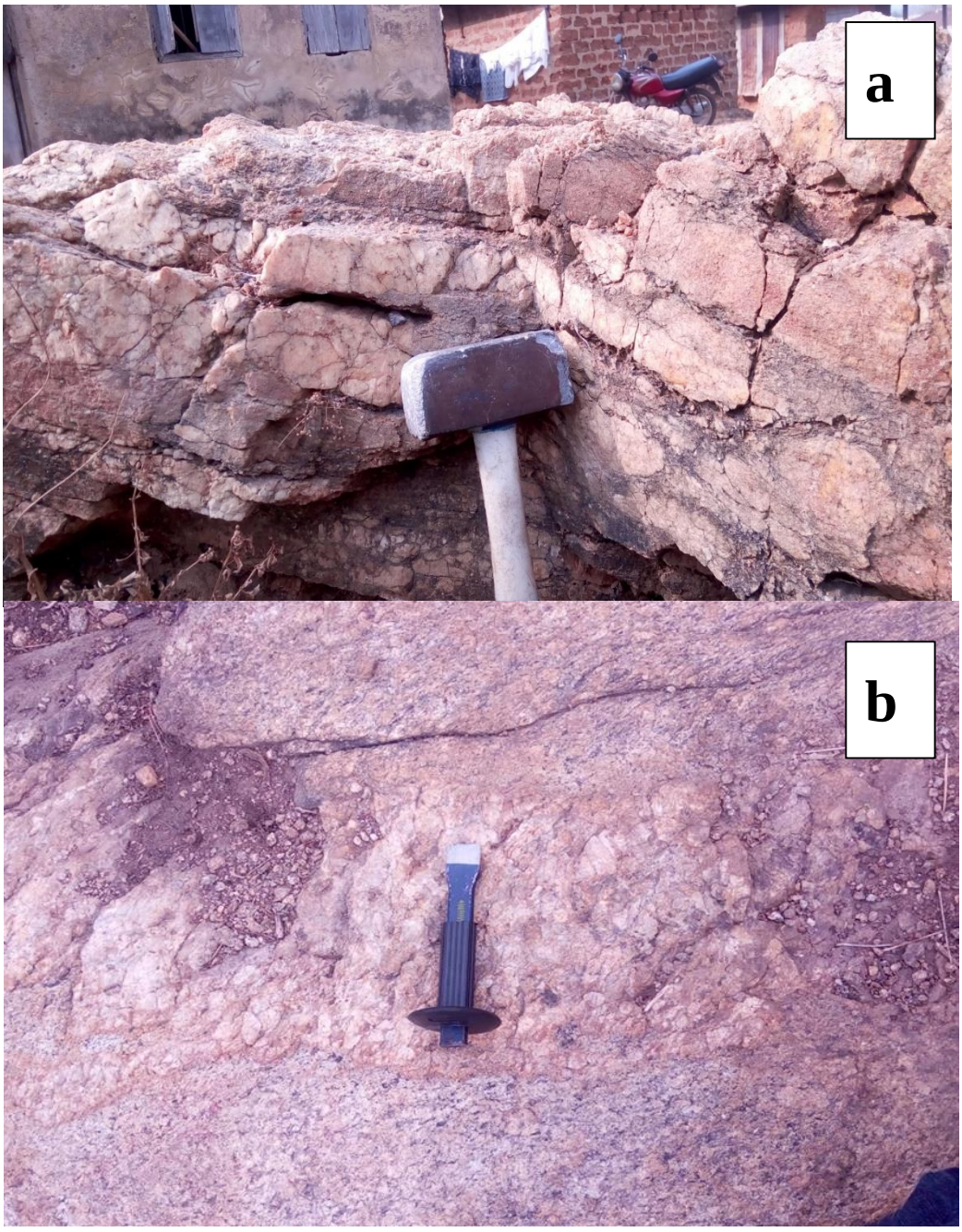

Fig. 4. 39 (a) Pegmatite layers in quartz Schist at Okemesi (b) Pegmatite intrusion in Biotite Granite

4.6.10 Pinch and Swell

According to (Price and Cosgrove, 1990; Pollard and Fletcher, 2005), pinch-and-swell structures (Fig. 4.40 a and b) arise from necking when a stiff layer and its weaker matrix are subjected to layer-parallel extension, or, equivalently, layer-normal shortening. Continuous necking forms pinch-and-swell systems, while isolated boudins (Ramberg, 1955; Pollard and Fletcher, 2005) are formed by either Mode I fracturing or Mode II faulting, often after some continuous necking.

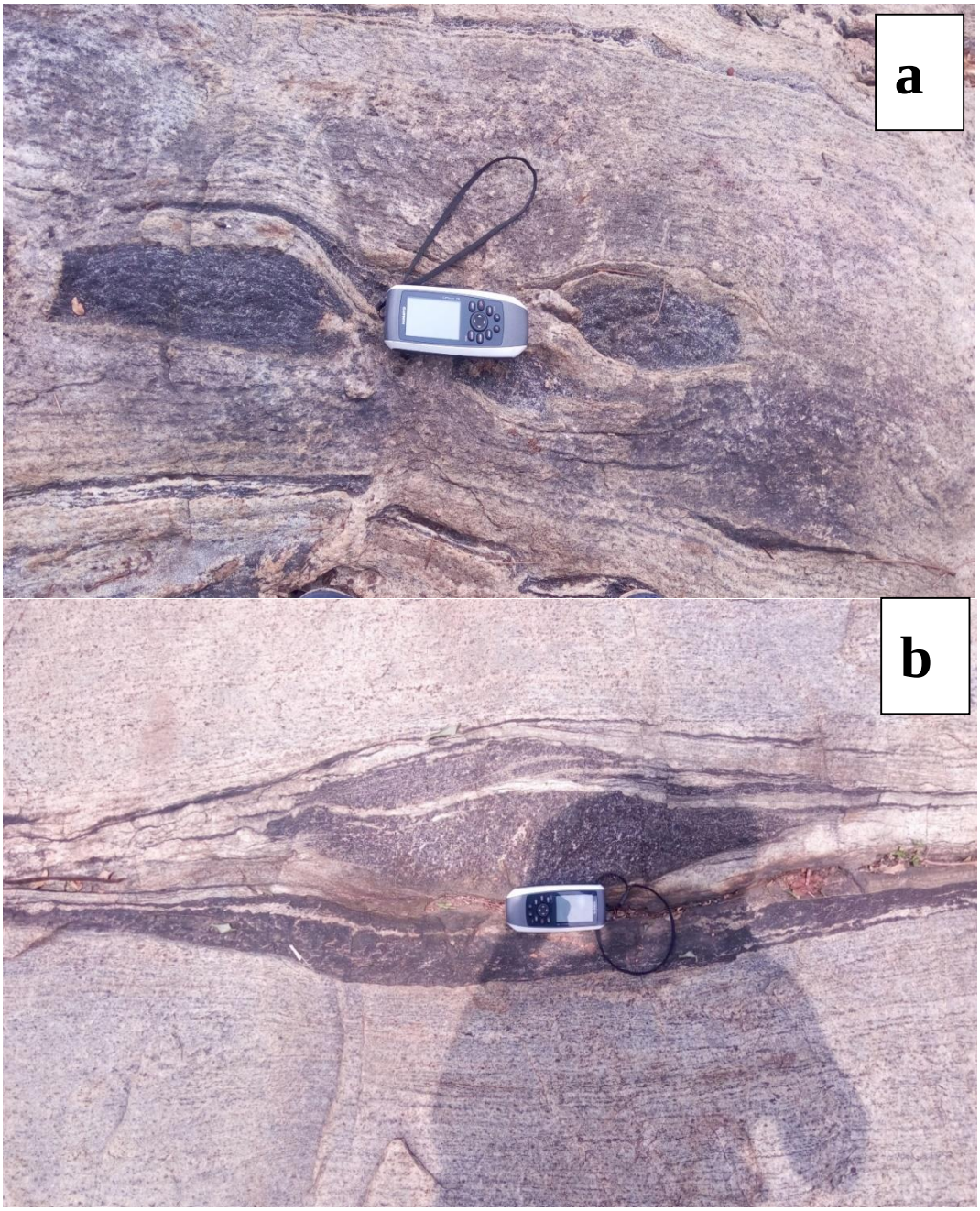

Fig. 4. 40 (a) and (b) Pinch and Swell structures in Migmatitic Gneiss at Ibokun

4.7.11 Xenolith

A xenolith is a rock fragment embedded within another rock type. Most of the time, a xenolith becomes trapped in magma as it cooled. Xenoliths are various types of rock that are found in igneous rock. They are very useful in geology because:

- They are made up of pieces of unexposed rock that are mostly taken from great depths and can be used to Fig. out geology.
- must be older than the rocks in which they are embedded by law
- They can provide evidence of the earth's magmatic, temperature, and chemical conditions.

Xenoliths were found within some rocks in some parts of the study area (Fig. 4.41 a, b, and c).

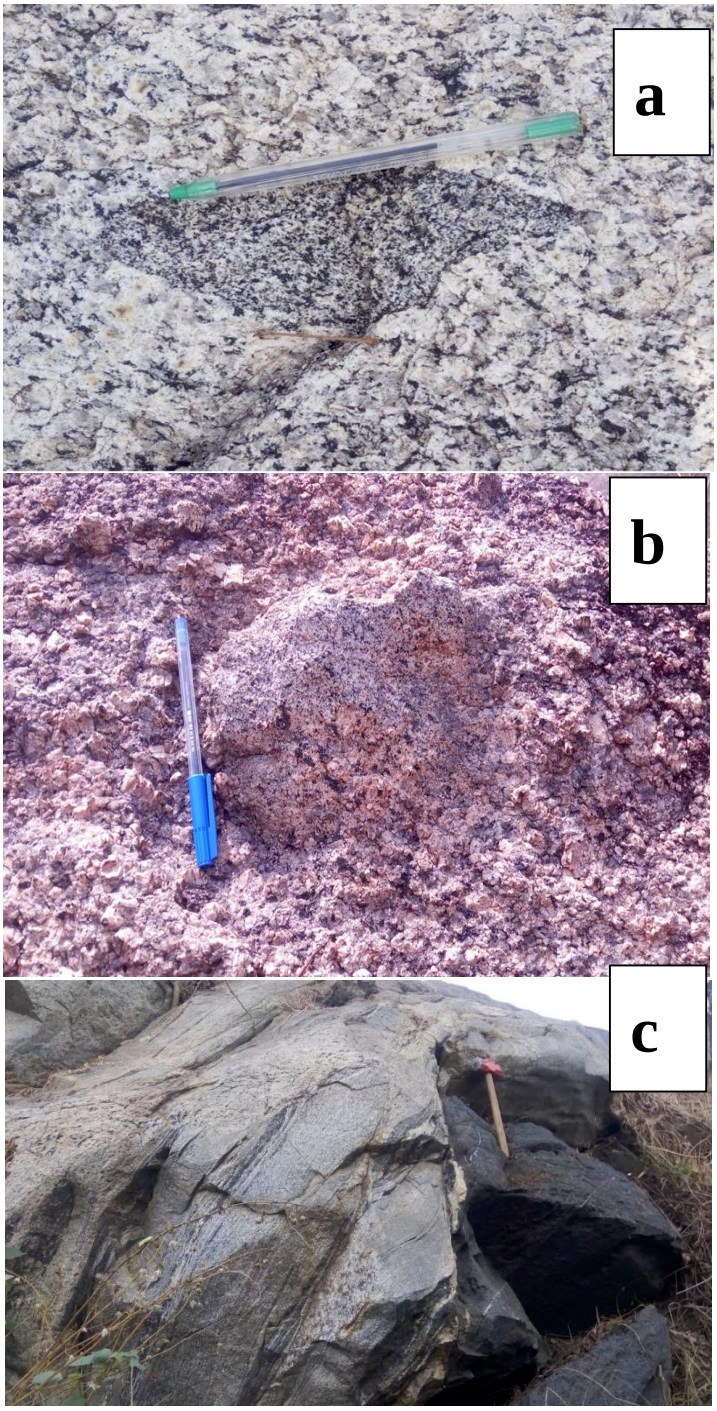

Fig. 4. 41 (a) Xenolith of finer grain biotite granite in a porphyritic granite. (b) Inclusion of a medium grained biotite granite rock within fairly weathered porphyritic granite (c) Inclusion of a fine grained mafic rock within a migmatitic grey gneiss, near a church, outskirts of Ibokun

4.7. Deformation Episodes

4.7.1 First Phase of Deformation (D1)

Only metamorphic rocks showed evidence of the D1 event, which was linked to the formation of S1 schistosity and an F1 folding. The desired orientation of muscovite micas defined the S1 earlier planar arrangement, which was usually parallel to the bedding surface. At microscopic scale, S1 schistosity was recognised by elongated shape of muscovite and biotite flakes. A total of 21 measurements of strikes and dips of S1 surfaces were recorded. Low to high angle dips of (10^0 to 82^0) were seen on the foliation surfaces, mostly to the southeast. The poles to S1 surface lie on the NW-SE axis of the stereographic projection thus confirming F1 folds appeared as flat lying small folds on the muscovite schist, with the axial plane trending ENE-WSW, and were seldom seen. This primary folliation, S1, appeared as axial planar cleavages (Fig. 4.26 and 4.27). This was a common occurrence along the Erimo-Efon Alaye road, where quartz stringers had invaded muscovite schist and this relashionship was also observed at Ipole. There have been no major folds in this generation that have been identified. (Fig. 4.37) F1 folding and S1 schistosity were observed in quartzite veinlets penetrating gray gneisses

4.7.2 Second Phase of Deformation (D2)

In both the muscovite schist and the quartzite, this tectonic stage was well developed. Heterogeneous deformation of the previous D1 fabric was a characteristic of this fabric. The creation of an S2 crenulation cleavage and F2 major folds was associated with D2 deformation.

Fig. 4.42: Weathered quartzites at Ipole around the palace showing So structures

The crenulation cleavage was formed by S2 cleavage cross cutting the S1 cleavage into small regular crinkle folds with an asymmetric structure (Fig. 4.29, 4.30 a,b,c). F2 folds appeared as large scale upright tight to isoclinal folds with an axial plane trend of NNE-SSW (Fig. 4.26 and 4.27). They occurred as open to isoclinal folds in other regions, where they formed a continuous sequence of antiforms and synforms. Brittle tectonics, which seemed to be granitic veins, pegmatite dykes, and joints (cross and longitudinal joints), were attributed to the late stages of deformation. These veins were mostly quartz-filled and trend NE-SW, while the joints had two major orientations: NE-SW and NW-SE, with slight E-W trends.

At Ipole, within Quartzite interbedded with pelitic schist, $D_1(F_1)$ was recorded as Recumbent folds associated with flat lying foliation (lithological and mineralogical banding) (Fig. 4.26, 4.27 & 4.28), while S_0/S_1 relict beds (S_0) (Fig. 4.42) was observerved in weathered quartze schists at Ipole, around the palace.

D_2 Upright folds (F_2) –fold (S_1), style varied from tight to isoclinal folds with wave length s of 20-30cm to a crenulation in mica-rich bands, the F_2 had plung readings of 355/18: 020/18, with a well developed axial plane foliation (S_2) with steeply dipping intersection lineation parallel to the F_2 fold axis. The schist layers were completely weathered, there were no fresh rocks but the structures were preserved; numerous garnet porphyroblasts were also observed in this area.

4.8 Petrographic Description and analysis of the rock samples of the study area.

4.8.1 Texture and mineralogy

For petrographic analysis, thin sections of some rock samples were prepared. The thin sections observed under the petrographic microscope revealed the different mineral constituents of the rock samples. These minerals were identified using their diagnostics optical characteristics under plane polarized light and crossed Nicols. From the observations based their analysis, the rocks were properly named. Based on the observions from the analysis, the rocks were properly named.

4.8.1.1 Migmatitic Grey Gneiss

The grey gneisses were medium –to coarse grained strongly foliated rocks of grey -to dark grey colour. The foliation was recognised by separation into bands of felsic and mafic layers. Plagioclase, quartz, hornblende, and biotite, along with some alkali feldspar, constituting the rock composition were detected in thin sections. Accessory minerals were also present in the form of opaque minerals, zircon and sphene (Fig. 4.43 a & b). The plagioclase was colourless with quartz inclusion in some cases. They were euhedral in outline and characterized by twining. Some also occured as subhedral, and were seen as porphyroblastic to xenoblastic crystals. Quartz was also colourless and clear, some showed conchoidal fracture. Some also showed undulose extinction which is a sign of straining. The quartz shows no pleochroism and alteration. Under plane polarized light (PPL), the alkali feldspar observed was cloudy and colorless, while crossed Nicol showed Carlsbad twinning. Most of the biotite were brown to some point green with high pleochroism and pleochroic haloes. They were often characterized by cleavage and moderate relief. The modal compositions of the grey gneiss presented in Table 4.3. was plotted in a QAP diagram, after Le Maitre et al. 1989 (Fig. 4.44), most of the grey gneisses plotted in the fields of granodiorite and quartze-monzodiorite.

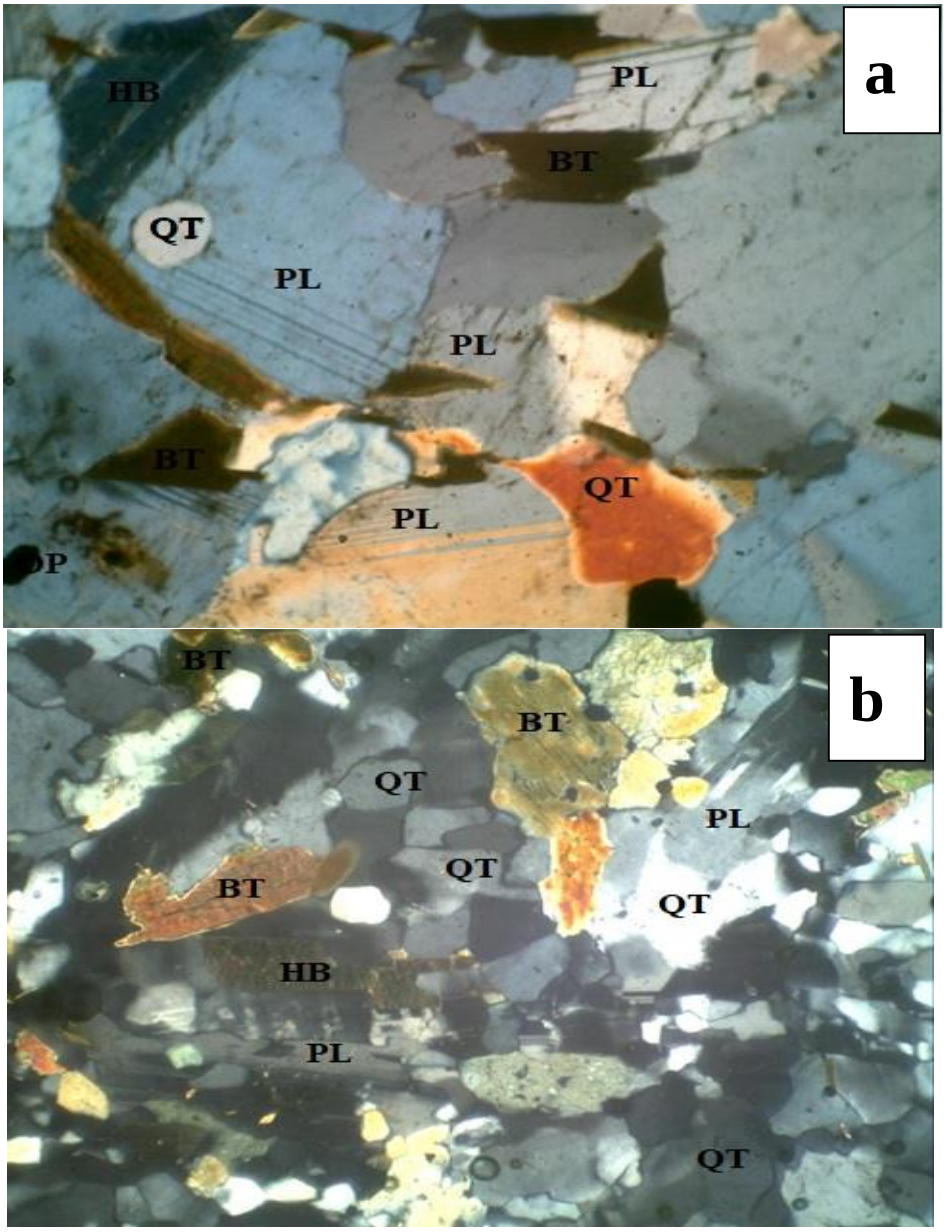

Fig. 4. 43 (a) Photomicrograph of Migmatite grey Gneiss showing in cross Nicol showing granoblastic texture and mineral composition at x10 magnification. (b) photomicrograph of migmatitic grey gneiss showing porphyroblastic texture in cross Nicole at x4 magnification

Texturally, the long axis of the biotite were arranged in aligned positions of same direction. Large prismatic grains of alkali feldspar, plagioclase quartz alongside small fragments of muscovite and biotite made up the matrix of rock. The plagioclase crystals observed is undergoing sericitization, this was mainly in rocks that were undergoing replacement of plagioclase by alkali feldspar, the breaking down of plagioclase to epidot, the sericitization process indicated a hydrothermal occurrence. The hornblendes were greenish in colour and were characterized by cleavage intersection of approximately $56^0/124^0$. They were mostly seen as small xenoblastic grains, strongly pleochroic with some inclusions. This suggested that hornblende was a relatively late mineral.

The Opaque mineral, zircon and apathite constituted the least amount of presence, they were seen as inclusions in the biotites. The opaques ores were black in both Plane Polarised Light and Cross Polarised Light. The biotite in some cases, seemed to be intergrowth within the feldspar, and the quartz crystals were fractured, muscovite appeared to be growing within the fracture.

Table 4. 3 Modal Composition (vol.%) for Migmatitic Grey Gneiss of Iwaraja-Okemesi Area

Sample no.	L37	L37	L83	L56	L38	L39	L37	L38	L36	L38MYLO	L56X	L37X	L83X
Quartz	21.5	26.4	28.3	24.4	22.6	29.4	17.5	23.8	26.6	26.3	21.7	28	29.7
Microcline	18.1	24.1	23.8	22.7	20.4	26.2	14.7	20.3	24.2	25.9	20.4	24.7	21.9
Plagioclase	22.8	31.3	33.2	31.2	27.9	33.3	26.2	30.9	30.2	30.6	25.8	32.3	32.5
Biotite	14.2	10	8.4	10.6	15	7.9	16.9	10.2	9.9	9.2	15.2	7.4	7.9
Hornblende	18.9	4.6	3.1	7	10.3	--	21	9.3	4.5	4	12.1	3.6	3.5
Muscovite	3.6	2.9	2.5	3.3	3	2.5	2.8	4.6	3.8	3.4	4.4	3.2	3.8
Opaque	0.9	0.7	0.7	0.8	0.8	0.7	0.9	0.9	0.8	0.6	0.6	0.8	0.7
Total	100	100	100	100	100	100	100	100	100	100	100.2	100	100

Classification Legend

A. Quartzolite
B. Quartz Rich Granitoids
C. Alkali Feldspar Granite
D. Syenogranite (Granite)
E. Monzogranite (Granite)
F. Granodiorite (Granite)
G. Tonalite
H. Quartz Alkali Feldspar Syenite
I. Quartz Syenite
J. Quartz Monzonite
K. Quartz Monzodiorite (An < 50%)
K. Quartz Monzogabbro (An > 50%)
L. Quartz Diorite (An < 50%)
L. Quartz Gabbro (An > 50%)
L. Quartz Anorthosite (M < 10%)
M. Alkali Feldspar Syenite
N. Syenite
O. Monzonite
P. Monzodiorite (An < 50%)
P. Monzogabbro (An > 50%)
Q. Diorite (An < 50%)
Q. Gabbro (An > 50%)
Q. Anorthosite (M < 10%)

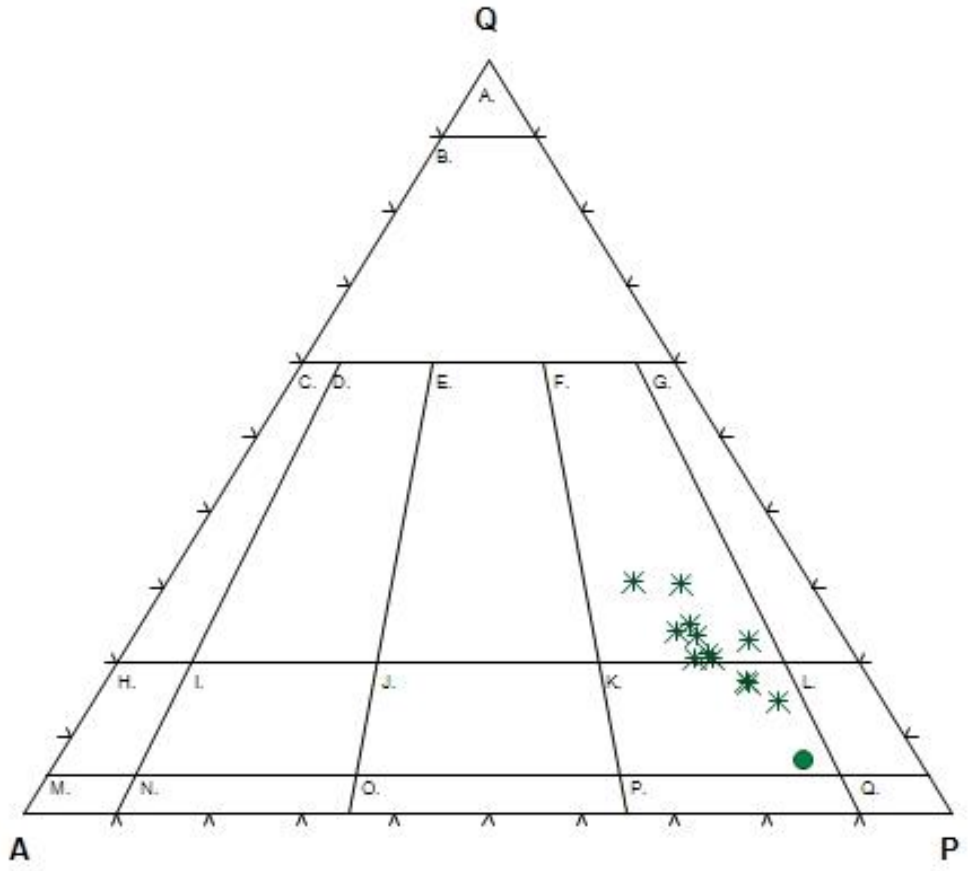

Fig. 4. 44 QAP diagram of grey gneisses of study area (after Le Maitre et al. 1989)

4.8.1.2 Granite Gneiss

The granite gneisses were medium- to coarse-grained light grey to pinkish rocks. They were foliated, with foliations seen as mineralogical banding of light and dark coloured mineral. The light coloured bands were rich in quartz and pink feldspar while the dark coloured bands were rich in biotite and hornblende. The long axis of the mafic minerals were aligned in the direction of the banding.

Thin sections of some samples of granite gneiss from the study area, observed under the microscope showed that within the matrix, there were over at least two grain size ranges. The first range consisted of larger elongated rounded quartz grains whose long dimensions have a preferred orientation (Fig. 4.48). This defined a foliation that was parallel to the preferred orientation of the long axis of the larger microcline grains. The texture was mostly granoblastic, some of the rocks had large microcline crystals surrounded by crystals of quartz with different sizes, giving a porphyritic texture.

Alkali feldspar, quartz, and plagioclase made up the mineralogy of granite gneisses. The accessory minerals present were garnet, apatite, calcite, zircon and sphene, the zircon were rectangular (euhedral), the apatite had reaction rims of epidote around them. Elongated garnet porphyroblasts with quartz inclusions were also observed (Fig.s 4.45, 4.46 and 4.47).

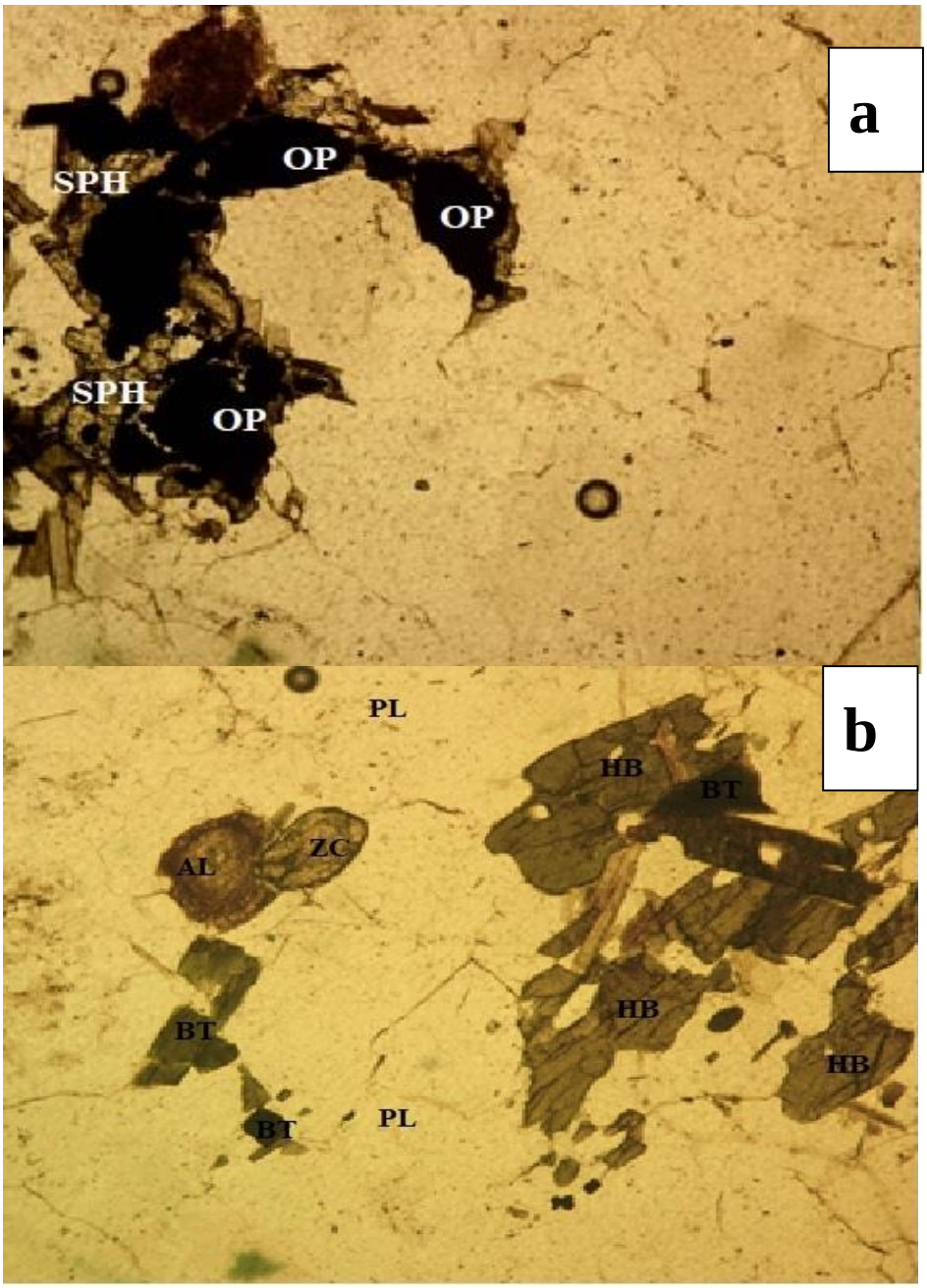

Fig. 4. 45 (a) Photomicrgraph of granite gneiss showing reaction rim of sphene around opaque minerals in plane polarised light x10. (b) Photomicrgraph of granite gneiss showing zircon, alanite, alongside hornblende, biotite and plagioclase in plane polarised light x10.

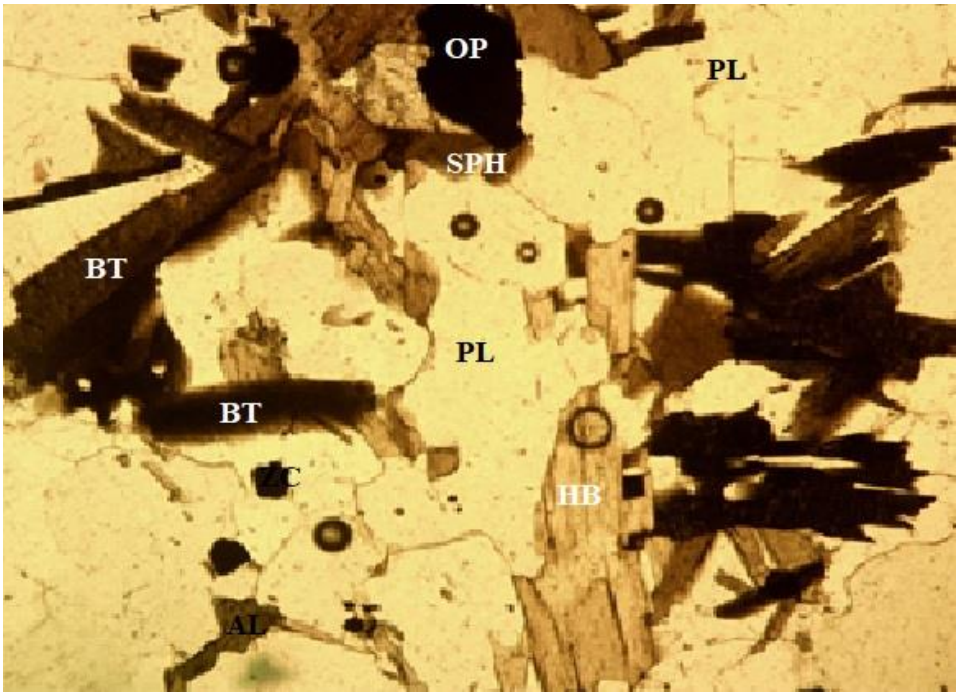

Fig. 4. 46 Photomicrograph of Granite Geiss showing alanite, zircon, hornblende, biotite and plagioclase, with reaction rims of sphene around opaque minerals in plane polarised light at x10 magnification.

Some of the quartz had microcline as inclusion while the main microcline crystal was embedded with accessory minerals as inclusion. The quartz crystals had strong wavy extinction and suture grain boundaries, in some cases the rocks were weakly foliated and had granoblastic texture. In cases, where the gneisses were mylonitic, like samples from Iwaraja and Ibokun, fine grains of quartz formed the main texture with visible flakes of biotite forming visible matrix with the quartz which constituted majority of the minerals in the thin section of the rocks from these areas. The rocks were from weakly foliated to strongly foliated, the strongly foliated gneisses showed mineralogical banding under the microscope; the quartz grains were seen to be elongated, showing preferred orientation of long axis and mineralogical banding with a tendency of bands rich in dark coloured minerals alternating with light coloured bands. The elongated quartz were parallel to the mineralogical banding (Fig. 4.48).

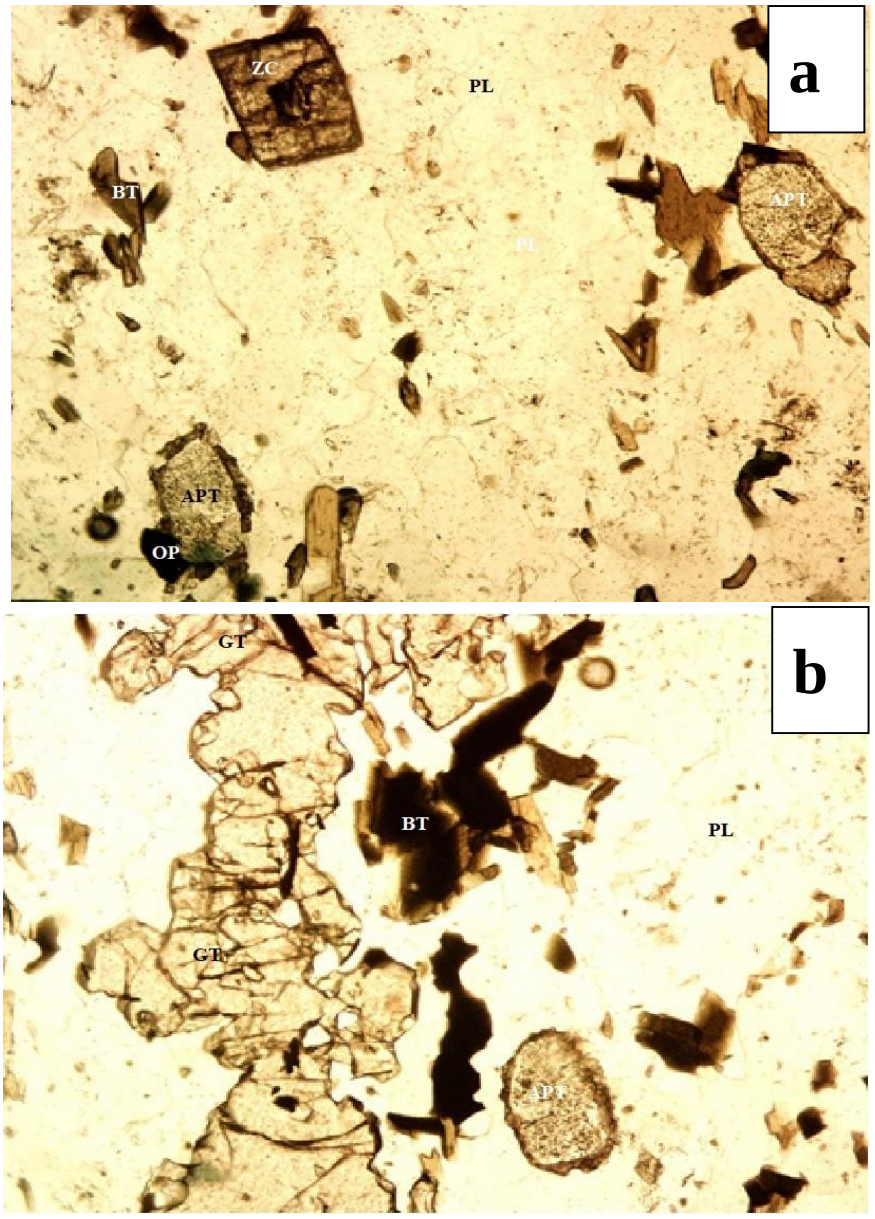

Fig. 4. 42 (a) Photomicrograph of Granite Gneiss showing rectangular (euhedral) zircon, apatite with reaction rim of minerals suspected to be epidote, and some opaque minerals in plane polarised light at x10 magnification (b) Photomicrograph of Granite Gneiss showing elongated garnet porphyroblast with some quartz inclusions andapatite with reaction rim plane polarised light at x10.

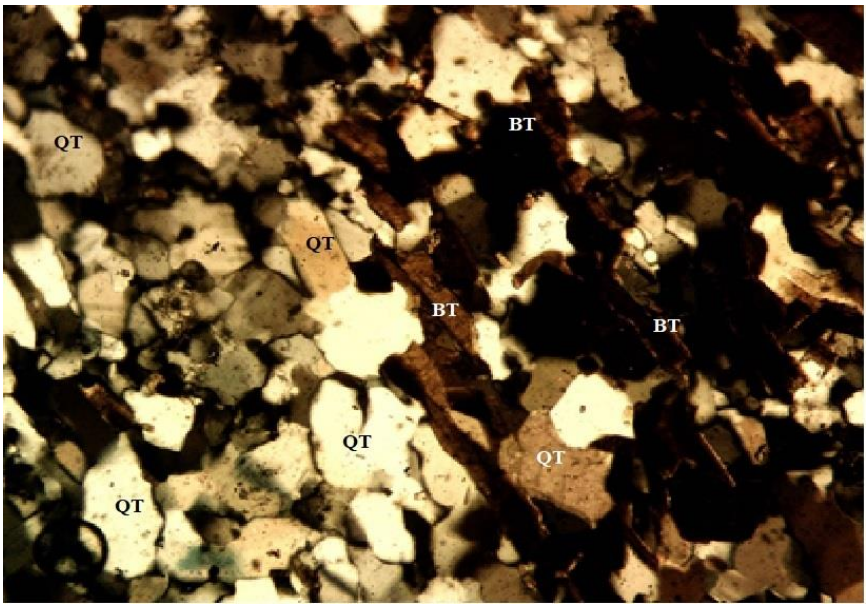

Fig. 4. 48 Photomicrograph of Granite Gneiss showing mineralogical banding and preferred orientation of long axis of elongated quartz and biotite in cross Nicol at x4 magnification.

The biotite were brown in colour and were strongly pleochroic, exhibiting light yellowish brown to dark brown. In some cases, they were being altered to chlorite, they were generally aligned parallel to the foliation plane. The amphibole, probably hornblende were mostly xenoblastic grains with their long axis aligned in preferred alignment to the banding. It was pleochroic, exhibiting light yellowish green to dark green. It occasionally contained inclusions of biotite (Fig. 4.48).

Alkali feldspar was present as microcline and untwined perthetic. Microcline occured either as large porphyroclasts embedded in a finer grained matrix of quartz and feldspar. They showed cross hatch twining typical of microcline. Smaller grains of microcline occured in the matrix. The large porphyroclasts contained numerous inclusions of plagioclase and quartz. Within the matrix, there were untwined alkali feldspars, distinguished by their perthetic intergrowth. Both varieties had strongly developed undulating extinction. This suggested that the rock was exposed to deformation and the minerals had not recovered from the effect of deformation. There ware at least a shear plane running from the matrix into the megacrystals along which there had been some recrystallization (Fig. 4.49).

Plagioclase occured as (anhedral) xenoblastic grains, they showed typical albite twining. In some grains, the twin lamellae were bent, alteration to sericite was common. They also occureed in some cases as inclusion in alkali feldspar, they formed the groundmass of the minerals observed in some of the slides. The modal count of granite gneisses presented in Table 4.4 plotted in a QAP diagram after Streckeisen (1976), modified by Le Maitre et al. 1989, shows that all the granite gneisses fell within the field of granites (Fig. 4.50), see Table 4.4 for the modal count.

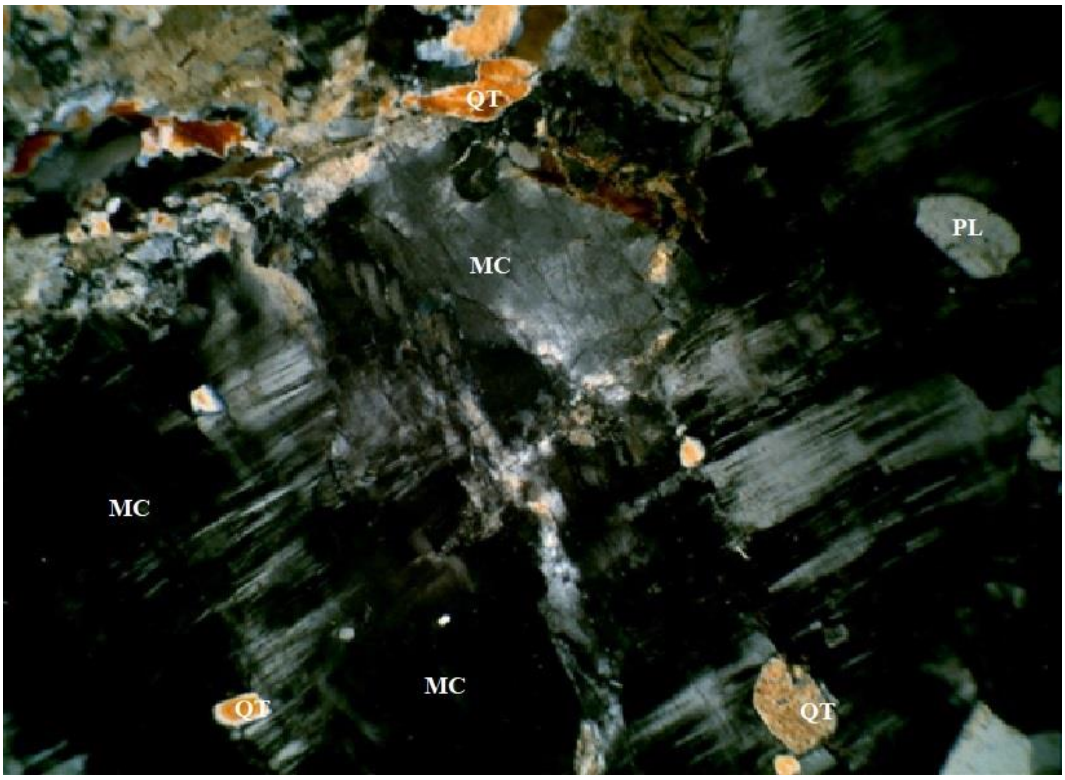

Fig. 4. 49 Photomicrograph of Granite Gneiss showing large prismatic grains of microcline and plagioclase in cross Nicol at x10.

Table 4. 4 Table of Modal Composition (vol.%) for Granite Gneisses from Okemesi-Iwaroja Area

Sample no	L75	L68	L48	L83	L48	L78	L86PINK	L5X	IW1XA	IW1XB	IW1BX	IW1EX	L49
Quartz	24.5	20.6	24.2	28.3	27.2	18.5	25.8	26.4	26.7	19.9	22.4	24.7	27.2
Microcline	32.5	19.3	16.5	23.8	19.7	15.2	30.2	25.2	21.5	15.4	17.2	21.3	24.6
Plagioclase	28.2	24.8	21.2	33.2	30.4	27.1	27.9	40.4	35.2	22.5	27.2	29	33.1
Biotite	8	17.5	19.1	8.4	8	18.5	8.8	3.6	7.9	26.2	18.5	13.2	7.2
Hornblende	3	13.8	12.6	3.1	3.6	16.1	3.4	-	4.3	10.7	9.3	7.9	3.7
Muscovite	3	3.4	5.6	2.5	10.4	3.9	3.1	3.7	3.6	4.6	4.8	3.1	3.4
Opaque	0.8	0.6	0.8	0.7	0.7	0.7	0.8	0.7	0.8	0.7	0.6	0.8	0.8
Total	100	100	100	100	100	100	100	100	100	100	100	100	100

Classification Legend

A. Quartzolite
B. Quartz Rich Granitoids
C. Alkali Feldspar Granite
D. Syenogranite (Granite)
E. Monzogranite (Granite)
F. Granodiorite (Granite)
G. Tonalite
H. Quartz Alkali Feldspar Syenite
I. Quartz Syenite
J. Quartz Monzonite
K. Quartz Monzodiorite (An < 50%)
K. Quartz Monzogabbro (An > 50%)
L. Quartz Diorite (An < 50%)
L. Quartz Gabbro (An > 50%)
L. Quartz Anorthosite (M < 10%)
M. Alkali Feldspar Syenite
N. Syenite
O. Monzonite
P. Monzodiorite (An < 50%)
P. Monzogabbro (An > 50%)
Q. Diorite (An < 50%)
Q. Gabbro (An > 50%)
Q. Anorthosite (M < 10%)

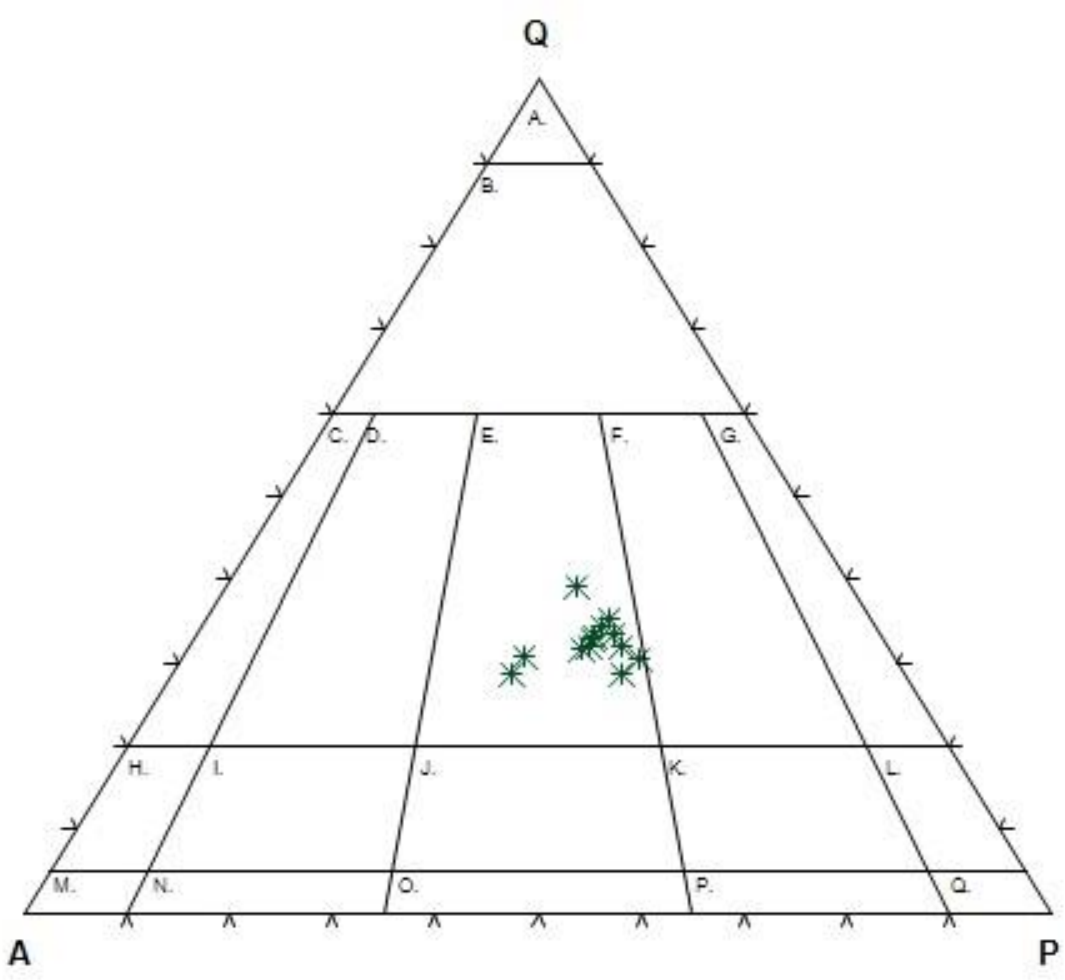

Fig. 4. 50 QAP diagram of granite gneiss of study area (after Le Maitre et al) 1989)

4.8.1.3 Two - Mica Granite

The 2-mica granites are medium-grained light coloured granite. The rock is made up of mainly quartz, plagioclase, biotite, muscovite with some alkali feldspar probably orthoclase. Thin section of rock samples from the Per-aluminous (2-mica) granite observed under the petrographic microscope showed, the rock is granitic, the thin section showed feldspar as very dominant mineral type with biotite and muscovite. The texture was mostly granoblastic with feldspar grain as large crystals while the biotite and muscovite were flaky. In some cases, the biotite is seen to be undergoing chloritization. Larger crystals of microcline which had quartz imbedded in it, alongside muscovite and biotite crystals were also observed. The major minerals were microcline, plagioclase, biotite, muscovite, and quartz (see Figure 4.51 & 4.52). Larger crystals of microcline have quartz, muscovite and biotite imbedded in it, the major minerals are microcline plagioclase, biotite, muscovite, and quartz. Two - Mica Granites potted in Syenogranite and Quartz Syenite fields (Fig. 4.55), see Table 4.6 for the modal count.

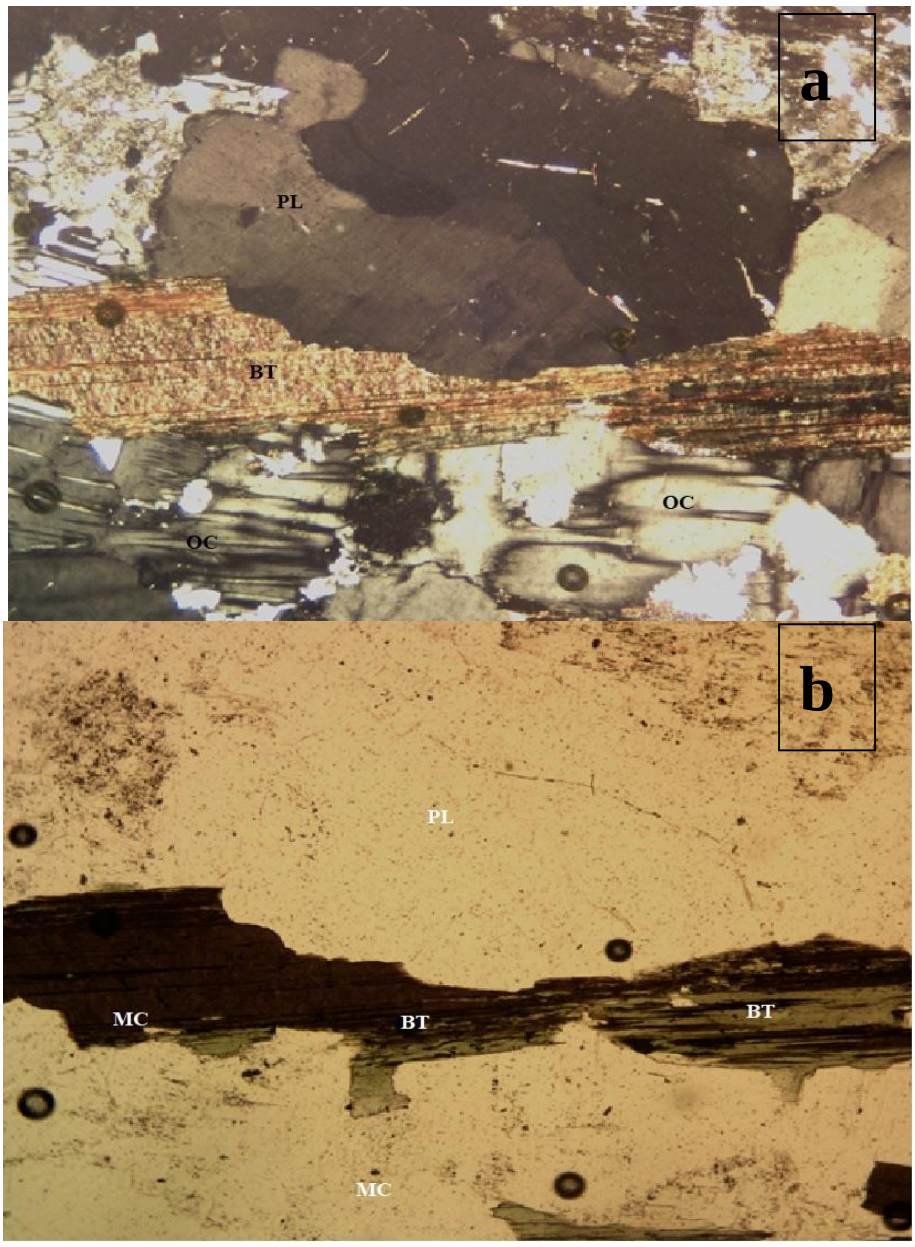

Fig. 4. 51 (a) Photomicrograph of Per-Aluminous Granite in cross Nicol showing a mostly granoblastic texture x10 magnification. (b) Photomicrograph of samples of Per-Aluminous Granite under plain polarised light at x10 magnification showing biotite (BT) undergoing chloritization.

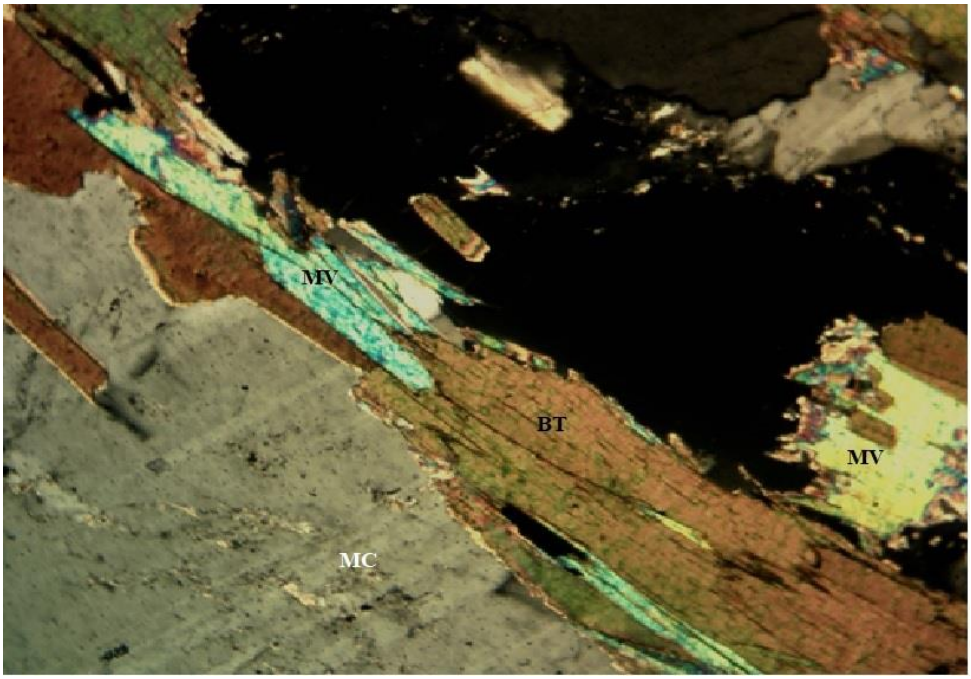

Fig. 4. 52 Photomicrograph of of Per-Aluminus Granite showing feldspar as very dominant mineral type alongside biotite and muscovite with a mostly granoblastic texture in cross Nicole at x10 magnification

4.8.1.4 Porphyritic Granite

Thin sections from samples of Porphyritic granite rock under the petrographic microscope showed large crystals of microcline, the quartz grains in some cases had inclusions of minerals likely to be biotite, biotite were also seen wedging between plagioclase quartz and microcline (Fig. 4.54 a). In some cases, varying crystal sizes of plagioclase with perfect twining were observed alongside microcline, and quartz mostly of large crystals, a few crystals of quartz were seen to be fractured (Fig.4.54 b), quartz of mostly large crystals, quartz and biotite inclusion were found embedded in the large microcline crystal. Some plagioclase were also found in the thin section.

Quartz and biotite inclusion are found embedded in a large plagioclase crystal. Some of the biotite crystals have long axis which were seen to be partially aligned in preferred direction, the texture showed, the rock is porphyritic. Textures such as perthite, myrmeckite were observed, inclusions of various kinds in both quartz and feldspar crystals were also observed in Figures 4.53b & 4.54b respectively.

The minerals included microcline, plagioclase, and quartz biotite with some sphene. The mafic mineral was biotite. Microcline also occured in the sample with quartz of mostly large crystals, a few crystals of the quartz were seen to be fractured. The porphyritic granites plot mostly in Monzogranite (Fig. 4.55) see Table 4.5 the madal count.

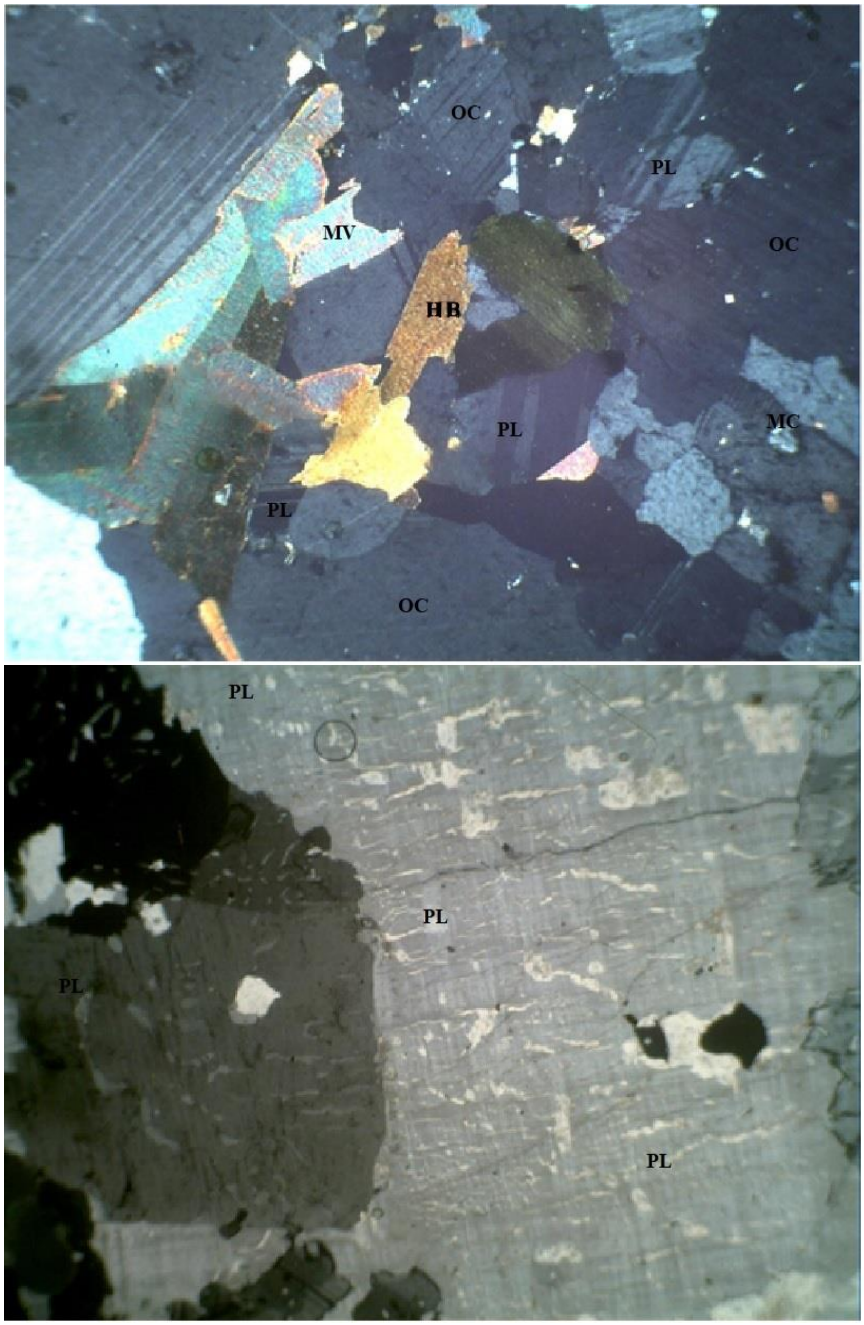

Fig. 4. 53 (a) Photomicrograph of Porphyritic Granite showing varying crystal sizes of plagioclase with perfect twinning in cross Nicole x10 magnification, (b) Photomicrograph of Porphyritic Granite showing varying crystal sizes of plagioclase exhibiting a perthite texture (Exolution) in cross Nicol at x10 magnification

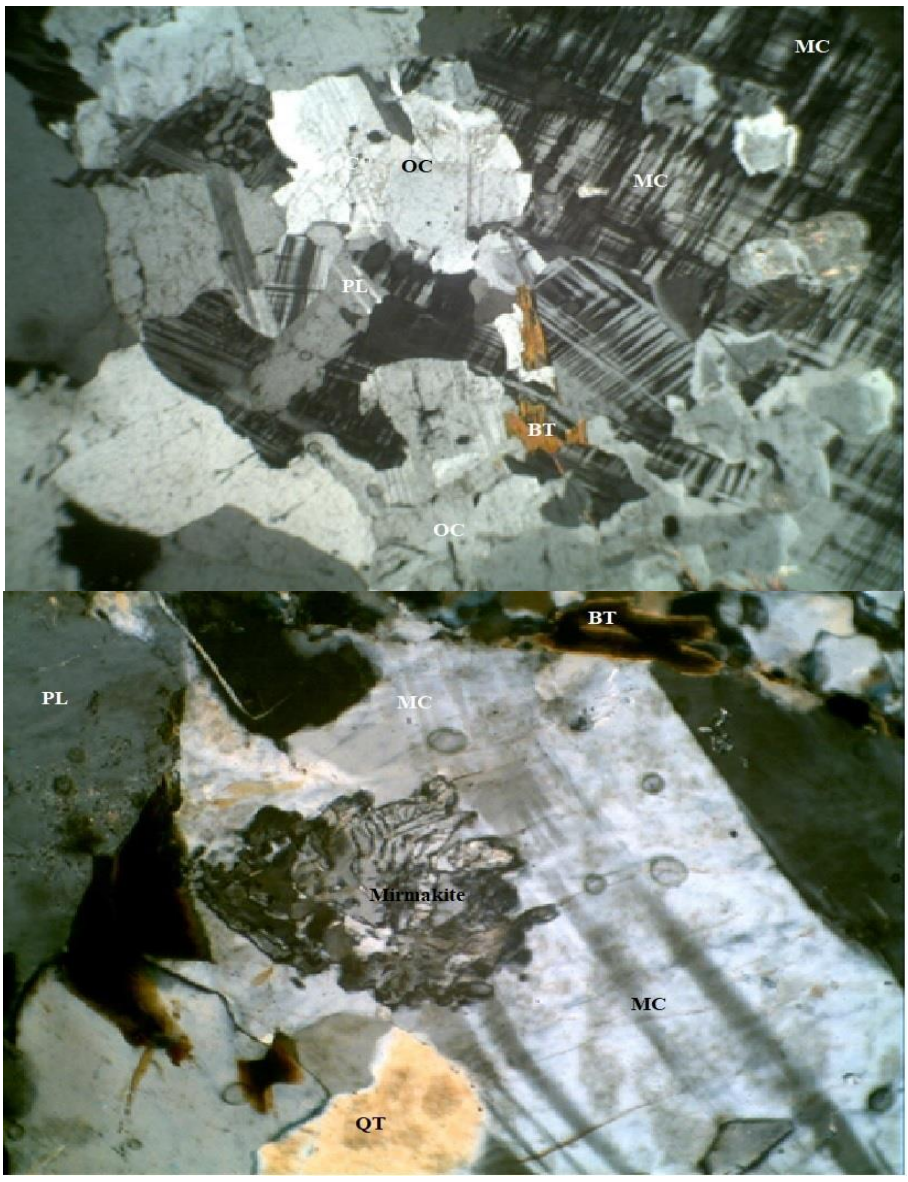

Fig. 4. 54 (a) Photomicrograph of Porphyritic Granite showing large crystal sizes of microcline with perfect cross hatch twining, in cross Nicol at x10 magnification. (b) Photomicrograph of Porphyritic Granite showing a large microcline crystal with poor cross hatch twining and a myrmeckite texture, inclusions of quarts and hornblende in cross Nicol at x10 magnification

4.8.1.5 Medium grained Biotite Granite

Samples of medium grained granite in thin section, observed under petrographic microscope, in plane polarized light, showed quartz was colourless with low relief and had anhedral form. Microcline showed medium reliefs with two dimensional cross-cutting cleavages. Alteration of perthite to sericite is also shown. In cross polarized light, microcline show a tartan twinning pattern and a grey to white interference colour. They plot in the monzogranite field (Fig. 4.55), see Table 4.6 the madal count.

Table 4. 5 Table of Modal Composition (vol.%) for Porphyritic Granite from Okemesi-Iwaroja Area

Sample no.	L39	L34	L33	L42	L41	L42	L43	L33	L39X	L34X	L40X
Quartz	24.6	26.8	23.5	24.3	22.7	11.7	16.8	28.8	26.1	17.6	24.5
Microcline	35.3	29.9	39.7	34.1	41.4	55.4	44.6	37.4	33.7	41	31.8
Plagioclase	24.7	26.3	22.3	26.3	24.9	18.1	21.9	25.3	22.5	23.3	21.8
Biotite	7.5	9.5	8.8	8.9	6.7	8.8	8.5	4.5	8.2	8.6	10.5
Hornblende	2.6	4.1	4.3	3.5	--	2.9	4.8	-	4.9	4.7	7.3
Muscovite	3.8	2.6	0.9	2.3	3.8	2.4	2.9	3.8	3.7	4.9	3.9
Opaque	0.8	0.8	0.8	0.8	0.8	0.8	0.8	0.7	0.7	0.7	0.8
Total	99.3	100	100.3	100.2	100.3	100.1	100.3	100.5	99.8	100.8	100.6

Table 4. 6 Modal Composition (vol.%) for Two Mica Granite and Medium Grained Biotite Granite from Okemesi-Iwaroja Area

Sample no.		L65	L65X		L54*	L45	L46	L45X
Quartz	**Two Mica Granite**	18.1	12.2	**Medium Grained Biotite Granite**	21.3	26.2	23.8	24.7
Microcline		40.3	51.7		33.6	23.9	32.7	39.8
Plagioclase		19.1	16.4		28.5	33.8	26.8	26.5
Biotite		9.1	9.6		12.7	9.3	8.9	3.2
Hornblende		3.2	1.9		--	2.9	3.9	-
Muscovite		8.9	7.4		3.8	3.4	3.4	4.6
Opaque		0.7	0.8		0.6	0.5	0.8	0.6
Total		99.4	100		100.5	100	100.3	99.4

Classification Legend

A. Quartzolite

B. Quartz Rich Granitoids

C. Alkali Feldspar Granite

D. Syenogranite (Granite)

E. Monzogranite (Granite)

F. Granodiorite (Granite)

G. Tonalite

H. Quartz Alkali Feldspar Syenite

I. Quartz Syenite

J. Quartz Monzonite

K. Quartz Monzodiorite (An < 50%)

K. Quartz Monzogabbro (An > 50%)

L. Quartz Diorite (An < 50%)

L. Quartz Gabbro (An > 50%)

L. Quartz Anorthosite (M < 10%)

M. Alkali Feldspar Syenite

N. Syenite

O. Monzonite

P. Monzodiorite (An < 50%)

P. Monzogabbro (An > 50%)

Q. Diorite (An < 50%)

Q. Gabbro (An > 50%)

Q. Anorthosite (M < 10%)

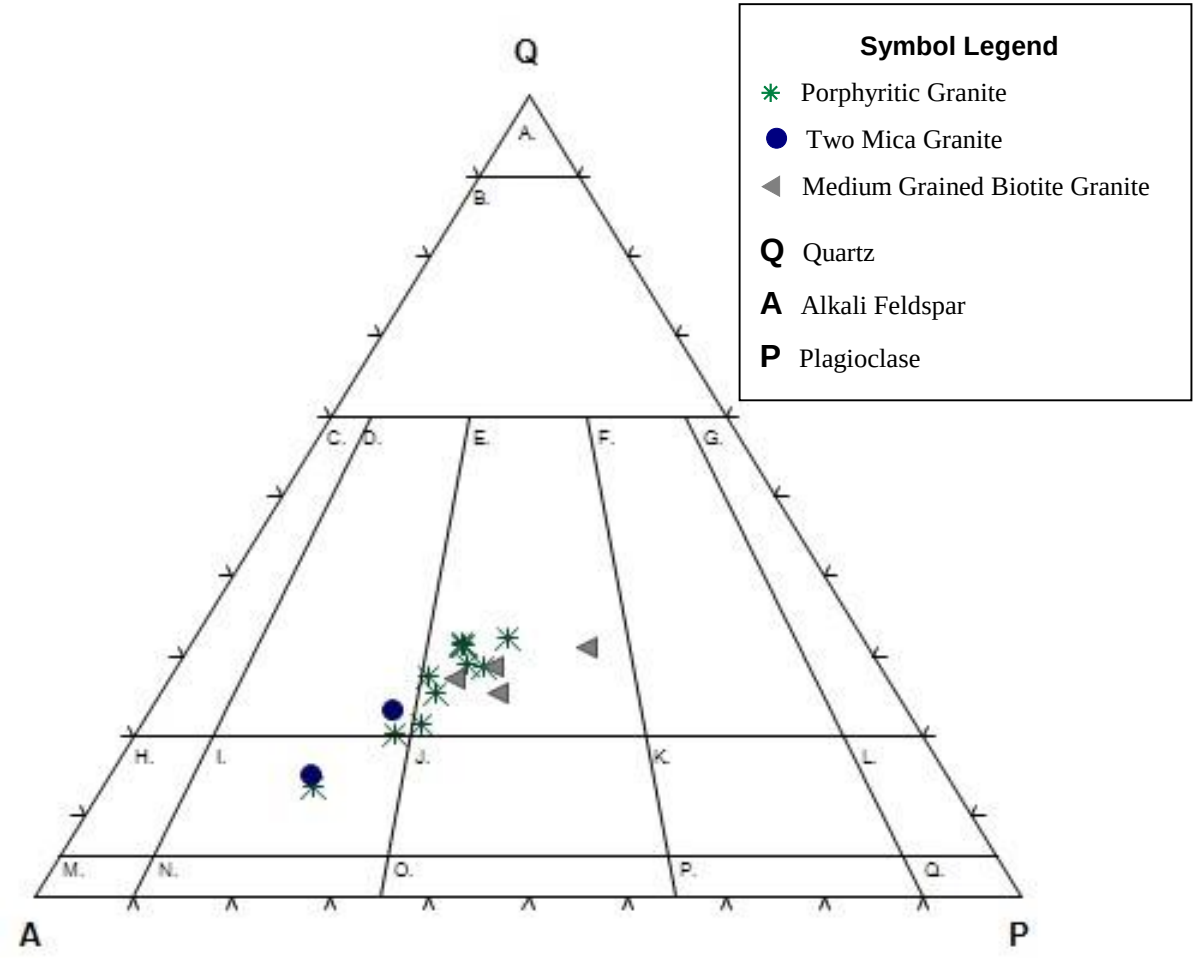

Fig. 4. 55 QAP Diagram of Some Granitic Rocks of Study area (after Le Maitre et al 1989)

4.8.1.6 Quartzite/Quartz Schist

4.8.1.6.1 Quartzite

The quartzites occured largely as high rising ridges traversing the entire length of the study area. They were mostly white to pinkish in colour and were not foliated, with medium grain sizes. The mineralogy was almost all quartz.

Thin sections from samples of Quartzite observed under the microscope, showed quartz as the only mineral found in the thin section, the crystals were large with sutured grain boundaries and wavy extinction. Large prismatic quartz crystals with sutured grain boundaries and fractures with strong undulose extinction, very little muscovite were also observed. A fracture was observed in quartz in one of the thin sections of the quartzite showing recrystallization of finer quartz grains (Fig. 4.56 b), the quartz was seen to exhibit a strong wavy extinction.

Other thin sections showed the rocks were of large quartz grains with fine quartz grains, forming a porphyroblastic texture. In some of the slides, the quartz grains were mainly of unequal sizes, in most cases there were more of the larger grains surrounded by the smaller grain matrix. The porphyroblastic texture was seen to be consistent in these thin sections, sutured grain boundaries were observed as common features, sub-grain boundaries were also prominent with the quartz grains. The smaller grain sizes occured as crushed small grains of quartz, which seemed to have recrystallized after the deformation. While other thin sections from samples of mylonitic quartzite showed Granoblastic texture, fine grained, the quartz grains had wavy extinction, with sub-grain and suture boundaries. The minerals had wavy extinction (strain shadow) the textures were mostly indicative of shearing and brittle deformation. The main minerals were quartz with a few opaque minerals and other accessory minerals (Fig. 4.56 a). see table 4.7 the madal count.

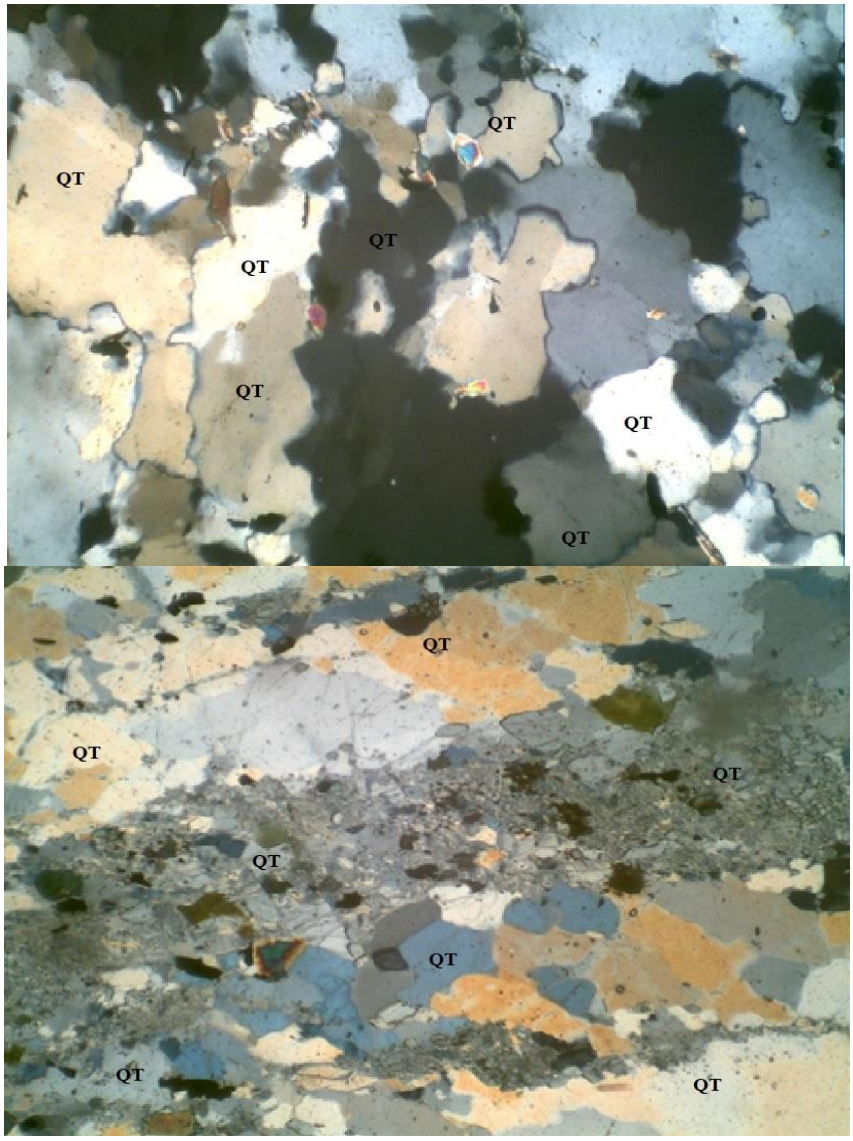

Fig. 4. 56 (a) Photomicrograph of Quartzite showing quartz as the major mineral component with suture grain boundaries and wavy extinction in cross Nicol at x10 magnification (b) Photomicrograph of Quartzite showing unequal grain sizes of quartz, with sutured and sub-grain grain boundaries in cross Nicol at x4 magnification

4.8.1.6.2 Quartz Schist

The quartz schist rocks occured alongside the quartzite in most cases, they exhibited schistosity. The main mineral composition was quartz with some muscovite, tourmaline, silmenite, sphene, zircon and garnet.

The thin section of samples from quartz schist mostly had strong schistosity, the grains were medium to fine with sub-grain boundaries, the texture were mostly granoblastic, and in some cases porphyroblastic. Larger grains of quartz were also observed in the thin section. Some of the thin section from the quartz schist showed finer grains forming the major grandmas while the fewer large grains form the matrix. Most of the quartz from quartz schist samples, under the microscope showed quartz with wavy extinction with muscovite showing mineralogical banding, where the muscovites were arranged in bands. The muscovites awere bent in some cases showing crenulation (crenulation cleavage) this nature of foliation or texture was largely as a result of polyphase deformation of the rocks. (Fig.4.57 a,b,c), see table 4.7 the madal count.

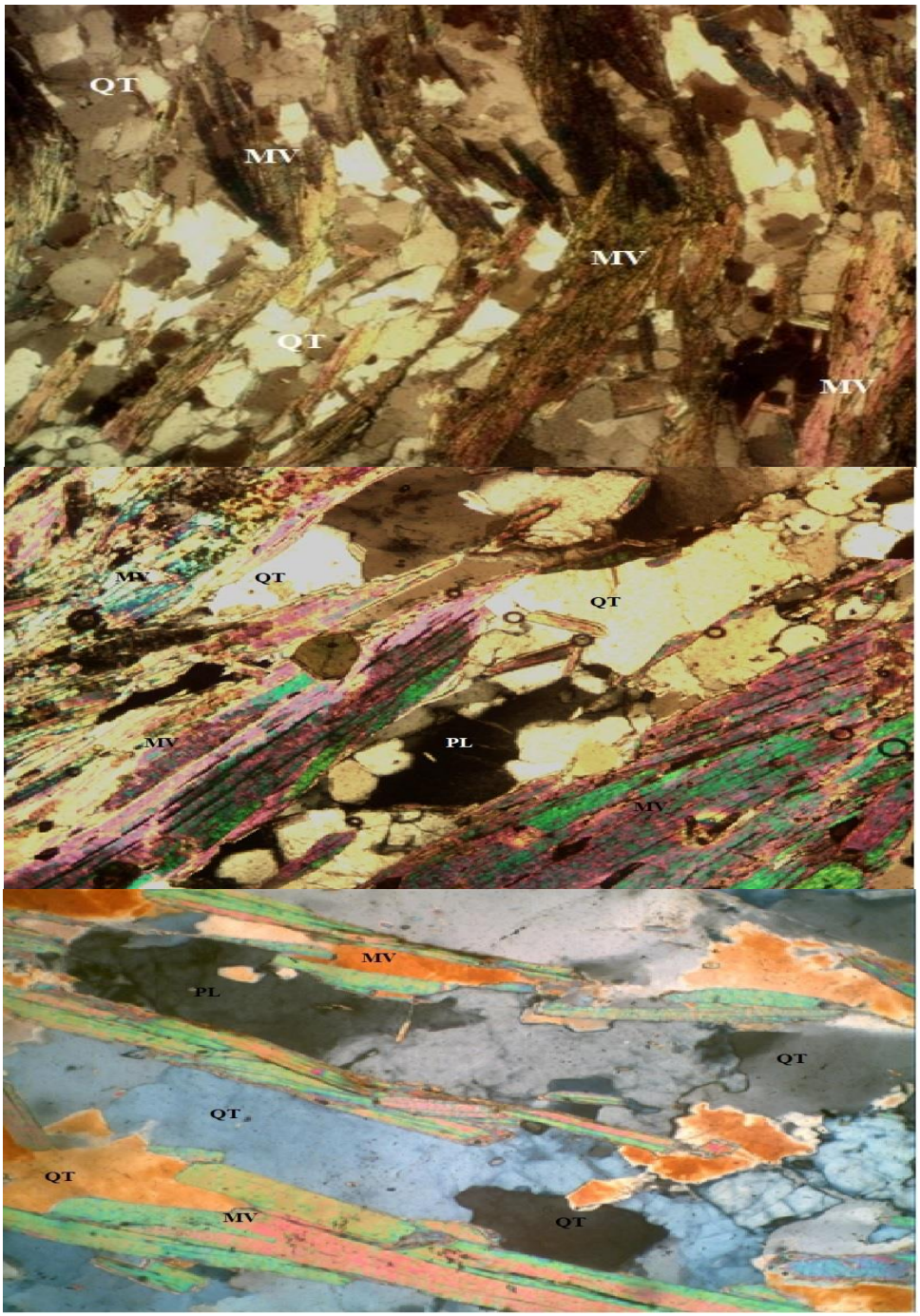

Fig. 4. 57 (a) Photomicrograph of Quartz Schist showing crenulation of muscovite under in cross Nicol light at x4 magnification. (b) Photomicrograph of Quartz Schist showing foliation in cross nicol at x10 (c) Photomicrograph of Quartz Schist showing prfered orientation of minerals in cross Nicol at x10

Some of the thin sections of this area showed mica flakes having roughly rectangular outline under the microscope. Their long axis had preferred orientation giving the rock a strongly foliated texture (Fig.4.57 a,b,c). There was also a tendency for mica to concentrate into distinct bands alternating with bands rich in quartz. The quartz showed strongly developed wavy extinction, suggesting that the rocks were probably sheared after the last episode of deformation, with sutured grain boundaries and development of sub-grain boundaries. In some cases, the quartz grains were elongated and stretched, the rocks showed signs of strong deformation. Small grains of quartz observed in thin sections from the quartz schists, were mostly recrystallized grains, with strong wavy extinction with sub-grain boundaries and a few flakes of muscovite,

Table 4. 7 Modal Composition (vol.%) for Quartzite and Quartz Schist from Okemesi-Iwaroja Area

Sample no.	L3	L53	L59	L15	L72	L4	L2	L2B	L21
Quartz	25.1	92.4	92.6	94.9	92.3	54.7	85.5	92.8	91
Microcline	20.3	-	-	-	--	15.9	--	--	--
Plagioclase	30.1	-	-	-	--	19.1	--	--	--
Biotite	5.3	-	-	-	--	5.9	--	--	--
Hornblende	-	-	-	-	--	--	--	--	--
Muscovite	18.5	7.6	7.4	5.1	7.7	3.8	3.2	--	3.4
Opaque	0.7	--	--	--	--	0.6	--	--	--
Silmenite							11.3	7.2	5.6
Total	100	100	100	100	100	100	88.7	100	100

4.8.1.7 Biotite Schist

The biotite schist, is a schistose rock of medium to fine grain, made up mainly of biotite, muscovite plagioclase with some limited quartz as the main mineral constituent with garnet and staurolite as accessory minerals. The thin section seen under the microscope showed biotite with preferred alignment and mineralogical banding, the biotite were prismatic in shape with the long axis pointing in same direction (Fig 4.58 a). Some of the plagioclase observed, showed bent twin lamellae. In some cases, the biotites were being altered to chlorite (chloritization). While other thin sections from similar rock samples under the microscope showed large crystals of plagioclase feldspar with biotite fragments surrounding them, the feldspar crystals formed the grandmass while the needle shaped biotite grains formed the surrounding matrix, the biotite were also partially aligned in preferred orientation, the rock was foliated with a few accessory minerals. The main minerals were feldspar, biotite, hornblende, quartz, with some muscovite, accessory and opaque minerals.

Large crystals of plagioclase feldspar with biotite fragments surrounded them, the feldspar crystals formed the ground mass while the needle shaped biotite grains formed the surrounding matrix, partially aligned in preferred orientation, the rock was foliated with a few accessory minerals. Bent twin lamellae surrounded by biotite and muscovite (Fig. 4.58 b). see table 4.8 the madal count.

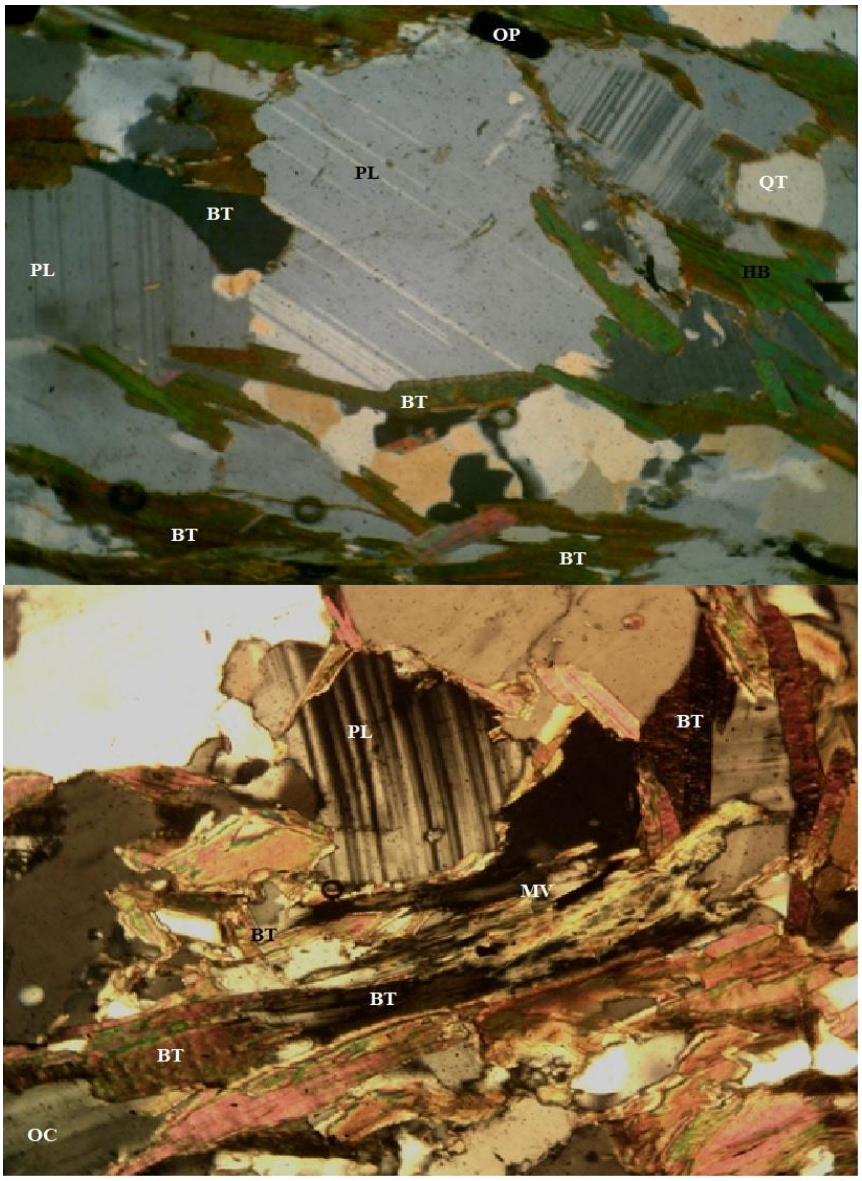

Figure 4. 58 (a) Photomicrograph of Biotite Schist showing biotite and hornblende with preferred alignment and mineralogical banding, the biotites are prismatic in shape with the long axis pointing in same direction under cross Nicol at x10 magnification (b) Photomicrograph of Biotite Schist showing larg ccrystals of plagioclase with bent twin lamellae, surrounded by biotite and muscovite in cross Nicol at x10 magnification

Table 4. 8 Modal Composition (vol.%) for Biotite Schist from Okemesi-Iwaroja Area

Sample no.	L85	L81	L69	L79	L69	L84MYLO	L79	L68X
Quartz	19.7	21.3	27.4	29.5	28.4	27.8	27.3	22
Microcline	17.5	17.1	38.1	25.9	25.8	20	23.7	17.4
Plagioclase	23	20.9	30.2	32.4	30.2	30.4	30.1	23.6
Biotite	19.9	20.3	-	8.7	11.9	12.6	10	19.2
Hornblende	14.5	14.7	-	-	-	4.9	5.6	12.4
Muscovite	4.7	4.9	3.8	2.8	3	3.5	2.4	4.7
Opaque	0.7	0.8	0.5	0.7	0.7	0.8	0.9	0.7

4.8.1.8 Amphibolite and Amphibole Schist

Thin sections from Amphibole schist rock samples under the optical microscope showed the rock was strongly foliated, the minerals with long axis were mostly aligned in preferred orientation. In some cases, Medium grained prismatic quartz grains were observed in an interwoven matrix with fibrous biotite, forming ribbon like structure around the quartz grains. Some of the biotite maintained their grain shapes after the deformation. A few undeformed plagioclase were also observed. Main minerals were largely hornblende with some biotite and quartz and opaque minerals, the rock was observed to be a mylonite with mortar texture, containing some garnet and staurolite as seen to be present on the hand specimen and outcrop (Fig. 4.59 a and b), please see table 4.8 the madal count.

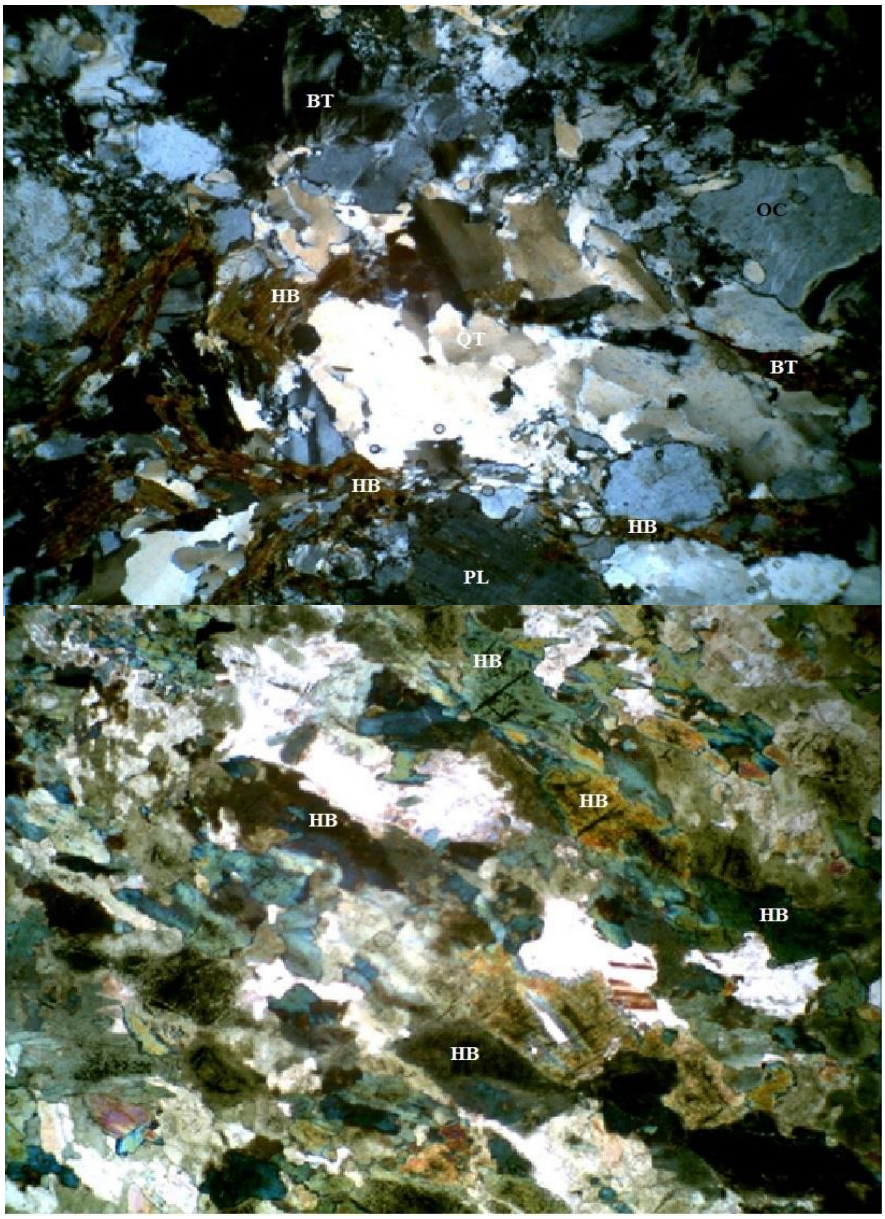

Fig. 4. 59 (a) Photomicrograph of Amphibole Schist showing mortar texture, main minerals are hornblende, plagioclase some biotite, and quartz in cross Nicol at x10 magnification (b) Photomicrograph of Amphibole Schist showing mortar texture with main minerals of hornblend, plagioclase and some accessory and opaue minerals in cross Nicol at x10 magnification

Table 4. 9 Average Modal Count for the all the rocks of Okemesi-Iwaraja Area.

Rock Type	Quartz	Microcline	Plagioclase	Biotite	Hornblende	Muscovite	Opaque	Silmenite	Total
Quartz Schist	67.03	9.63	11.75	2.95	0.73	5.62	0.29	2.01	100.01
Amphibolite - Amphibole schist	25.30	19.97	28.60	10.83	4.85	7.93	0.80		98.28
Biotite schist	25.43	23.19	27.60	14.66	10.42	3.73	0.73		105.76
Migmatitic grey gneiss	25.09	22.11	29.86	10.98	8.49	3.37	0.76		100.66
Granit gneiss	29.21	20.17	27.38	11.78	7.04	4.25	0.68		100.51
Biotite Gneiss	26.63	25.27	30.63	9.47	3.87	3.30	0.83		100
Porphyritic biotite granite	25.50	21.20	30.80	10.50	7.30	3.90	0.80		100
Medium grained biotite granite	26.90	26.93	31.65	8.40	3.40	3.80	0.63		101.71
2 mica granite	25.15	26.5	29	10.55	5.05	3	0.75		100

The samples analyzed demonstrated that Okemesi-Iwaraja area has been exposed to high metamorphism, as shown by changes in mineralogical components (elongated crystals) and textures. This is due to metamorphic agents such as temperature pressure and chemically active fluid altering the zones for a long period, causing pre-existing rocks (mostly granites) to transition to metamorphic rocks. During the metamorphism, new minerals were formed, and some of the newly formed minerals were altered from pyroxene to amphibole, muscovite to chlorite, sericite, and feldspar to kaolinite. Table 4. 9 shows the Average Modal Count for the all the rocks of Okemesi-Iwaraja Area.

4.9 Geochemical Analysis

Twenty Four (24) fresh representative rock samples were obtained from parts of the Okemesi-Iwaraja area (sampling areas A and B) for whole-rock chemical analysis, out of which 7 were samples of Grey gneisses and amphibolites while the remaining 17 samples were of other granitoids **(granite gneiss, porphyritic biotite granite, medium grained biotite granite and 2-mica granite)** respectively. Using a steel jaw crusher, all of the rock samples were crushed into 3-cm fragments. Fresh fragments were chosen, polished, and crushed to 3-mm pieces once more. The secondary crushing products were then separated and a portion of representative samples were pulverized in an agate mill. 20 grams was measured for each of the samples, and carefully sealed for further shipment to MS Analytical Laboratory, Unit 1, 20120 102nd Avenue, Langley, BC V1M 4B4 Canada, for analysis.

The samples were prepared by mixing pulverized sample (<200 mesh) with calcined $LiBO_2$ (lithium metaborate) at a ratio that varied from 1:10 to 1:4 until optimized recoveries were determined. Prior to fusion, samples are mixed by stirring with a platinum rod in a platinum crucible. Two types of platinum crucibles, 99.95% Pt and 95% Pt/5% Au were employed to determine which material produced the best recovery of REE. The open crucibles were heated to 1,100°C for five minutes in a Phoenix microwave muffle furnace (CEM). After fusion, the melt was removed out of the oven and later allowed to cool to a homogeneous glass. The glass was digested in 5% HNO_3 on low heat with continuous stirring. The platinum crucibles were rinsed in triplicate with 5% HNO_3 to ensure that the sample glass was completely digested and the sample was diluted to a final volume of 100 ml. These samples were further diluted between 10-100x in 2% HNO_3 before analysis to determine the optimal balance between internal standard recovery and limit of detection. For each set of fusions prepared for this study, blank samples containing only the lithium metaborate were prepared and processed identically to the samples. All data presented in this study are blank subtracted. The concentrations of major, trace (Co, Cu, Zn, Sr, Y, Ga, and Nb), and rare earth elements (REE) in whole-rock samples were measured using a standardized ICP-MS method.

4.9.1 Geochemistry of the Grey Gneisses and Amphibolites

Five samples of grey gneisses and two samples of amphibolites from the study area were analysed for their major, trace and rare earth element compositions. The major, trace and rare earth element compositions for the Grey Gneisses and Amphibolites are presented in Table 4.10 – 4.12.

4.9.1.1 Major Element Geochemistry of the Grey Gneisses and Amphibolites

Samples of the grey gneisses from the study area had SiO_2 contents varying from 51.22 to 80.74 wt.% and low Al_2O_3 contents (Al_2O_3=9.7–14.67wt.%) (Low aluminum < wt 15%). They had moderately low MgO (0.4–1.26 wt.%), and Cr_2O_3 contents with values generally <0.04. They were sodium-rich (Na_2O=1.24–4.23wt.%) and had low K_2O contents resulting in an average Na_2O/K_2O greater than 1.9 alongside low amounts of P_2O_5. Four of grey gneiss samples were metaluminous (A/CNK=1.83–2.35) while one sample was peraluminous (A/CNK =2.75) Table 4.10 and Apendix i, (Huang et al. 2013). Samples from the amphibolite had SiO_2 content ranging between 45.92 – 55.21wt%, and also a low aluminum content, Al_2O_3=2.5-14.37wt%. the magnesium contents were relatively higher as compared to those of the grey gneisses, MgO = 7.85-20.02wt%, the sodium content was also lower Na_2O=0.2-1.53 wt%, with an A/CNK=0.18-1.09, the amphibolites were also metaluminouse (Fig. 4.69).

Table 4. 10 Major elements for grey gneisses and amphibolites from Okemesi-Iwaraja area.

Sample ID Petrology	L36 Grey Gneiss	L37 Grey Gneiss	L55 Grey Gneiss	L56 Grey Gneiss	IDA1 Grey Gneiss	L24 Amphibolite	L30 Amphibolite
			Major Elements (w%)				
Al_2O_3	11.46	13.08	9.76	11.23	14.62	14.37	2.5
BaO	0.11	0.02	0.15	<0.01	0.09	<0.01	<0.01
CaO	1.57	9.6	1.09	3.56	2.91	12.86	13.37
Cr_2O_3	<0.01	<0.01	<0.01	<0.01	<0.01	0.03	0.22
Fe_2O_3	3.55	12.44	1.94	3.36	3.33	12.92	5.4
K_2O	4.6	1.29	4.22	0.48	3.34	0.15	0.07
MgO	0.4	6.01	0.78	0.9	1.24	7.85	20.02
MnO	0.06	0.2	0.03	0.05	0.05	0.21	0.08
Na_2O	2.25	3.01	1.24	2.81	4.23	1.53	0.2
P_2O_5	0.06	0.12	0.06	0.12	0.14	0.11	0.08
SiO_2	75.29	51.22	80.74	77.54	68.37	45.92	55.21
SrO	0.02	0.02	0.02	0.02	0.07	0.02	<0.01
TiO_2	0.37	1.51	0.3	0.5	0.4	1.55	0.05
LOI	0.85	0.65	0.61	0.49	0.73	0.79	1.12
Total	100.58	99.15	100.93	101.06	99.52	98.33	98.32
CIA	57.645	48.48	59.84	62.11	58.24	49.705	15.489
A/N+K	1.67	3.04	1.79	3.41	1.93	8.55	9.26
A/CNK	1.84	1.18	1.83	2.75	2.32	1.09	0.18
Na2O/K2O	0.49	2.33	0.29	5.85	1.27	10.20	2.86
Fe_2O_3/MgO	3.74	6.29	2.57	4.08	6.57	6.53	17.94

4.9.1.2Trace Element Geochemistry of the Grey Gneisses and Amphibolites

The trace element geochemistry of the grey gneisses presented in Table 4.11, showed that the grey gneiss samples were categorised by high amounts of Sr, Zr, Ba, W and Rb but low amounts of Cr, V, U and absent in Ni, this reflected the high amount of feldspar and zircon in their modes (Frost et al 2006). The amphibolites had much higher Cr with lower Th and U than the grey gneisses.

Table 4. 11 Trace elements for grey gneisses and amphibolites from Okemesi-Iwaraja area

Sample ID	L36	L37	L55	L56	IDA1	L24	L30
Petrology	Grey Gneiss	Grey Gneiss	Grey Gneiss	Grey Gneiss	Grey Gneiss	Amphibolite	Amphibolite
				Trace Elements (ppm)			
V	20	290	20	41	49	316	62
Cr	14	62	24	36	30	218	1640
Ga	19.9	19.7	11.4	16.2	19.2	17.9	5.6
Rb	159.4	35.1	119.1	24	120.8	2.9	2.4
Sr	141.1	131.9	132.7	150.3	546.3	148.5	15.5
Y	44.1	35	12	22.1	15	30.1	4.2
Zr	378	145	199	180	182	65	28
Nb	26.5	6.1	6.2	8.7	11.2	4.6	0.5
Sn	<5	<5	<5	<5	<5	<5	<5
Ba	1002.9	146.3	1347.5	88.8	823.7	26.3	10.4
Cs	0.83	0.15	1.72	0.44	1.4	0.11	0.05
Hf	9.8	3.6	5.8	5.2	5.1	2.2	0.8
Ta	1.4	0.8	1	1.1	1.1	0.8	0.6
W	251	105	239	320	197	42	28
Th	14.78	2.82	5.89	8.81	15.03	<0.05	<0.05
U	0.86	1.25	1.21	0.81	1.75	<0.05	0.13
Y/Nb	1.66	5.74	1.94	2.54	1.34	6.54	8.4

4.9.1.3 Rare Earth Element Geochemistry of the Grey Gneisses and Amphibolites

These rocks (grey gneisses) had strongly fractionated REE patterns (La/ Yb)n=2.98–22.49) and displayed negative Eu anomalies (Eu/Eu*=0.44–0.91) and negative to positive Ce anomalies (Ce/Ce*=0.86–1.01) (Fig. 4.60). In chondrite normalized plot, the grey gneisses exhibited higher values for Light Rare earth LREE and lower Heavy Rare Earth HREE values, with negative Eu anomaly, suggesting a strongly fractionated melt. While the amphibolite samples had relatively low values for both LREE and HREE, showing a relatively flat plot with no Eu anomaly in one sample, and another sample showing a negative Eu anomaly with low LREE and HREE. The amphibolite samples had relatively flat HREE patterns compared to the other samples, that had moderately, more depleted HREE ((Gd/Yb)N 1.35-2.31, while the amphibolites were relatively depleted in LREE ((La/Sm)N = 0.69–1.31) and slightly more enriched in HREE ((Gd/Yb)N = 1.01–1.09) and also lack an Eu-anomaly (Table 4.12).

The following characteristics where observed for both grey gneisses and amphibolites: (1) positive Zr anomalies (Zr/Zr*=2.63–7.05); (2) negative to positive Sr anomalies (Sr/Sr*=0.54–6.76) (Appendix 4).

Table 4. 12 Rare earth elements for grey gneisses and amphibolites from Okemesi-Iwaraja area.

Sample ID	L36	L37	L55	L56	IDA1	L24	L30
Petrology	Grey Gneiss	Grey Gneiss	Grey Gneiss	Grey Gneiss	Grey Gneiss	Amphibolite	Amphibolite
				REE (ppm)			
La	132.7	12.6	34.5	47.5	39	4	1.1
Ce	236.6	24.9	67.1	91.1	76.9	12	2.4
Pr	24.14	3.58	7.52	10.51	8.9	2.08	0.41
Nd	80.9	16.1	27.2	37.9	32.3	11.2	2
Sm	12.26	4.18	4.64	6.17	5.47	3.65	0.53
Eu	1.61	1.34	0.98	1.13	1.14	1.27	0.09
Gd	9.97	4.81	3.42	4.96	4.05	4.12	0.59
Tb	1.35	0.83	0.45	0.68	0.5	0.76	0.11
Dy	7.98	5.38	2.42	3.92	2.58	5.15	0.72
Er	5.12	3.34	1.26	2.33	1.61	3.22	0.5
Ho	1.55	1.08	0.43	0.72	0.49	1.06	0.15
Tm	0.75	0.46	0.17	0.34	0.23	0.46	0.08
Yb	4.98	2.88	1.04	2.22	1.42	3.05	0.47
Lu	0.75	0.41	0.15	0.31	0.2	0.45	0.06
Eu/Eu*	0.44	0.91	0.75	0.62	0.74	1	0.47
(La/Yb)N	18.09	2.98	22.49	14.53	18.63	0.89	1.6
(La/Sm)N	6.76	1.89	4.65	4.8	4.46	0.69	1.31
(Ce/Yb)N	12.47	2.27	16.92	10.77	14.2	1.04	1.35
(Gd/Yb)N	1.62	1.35	2.66	1.81	2.31	1.09	1.01

4.9.2 Comparison of Okemesi-Iwaraja grey gneisses with other Archean granite gneisses, tonalite granite and Tonalite-Trondhjemite Granodiorite (TTGs).

Frost et al. (2006) highlighted some geochemical features that are key attributes of Archean TTG suites. These features include high SiO_2 that are commonly about 70 wt.% or in some cases greater, high Na_2O (>3.0 wt.%), alongside high Na_2O/K_2O (>2) (Table 4.10). The grey gneiss samples from Okemesi-Iwaraja area, showed patterns ((La/Yb)N ranging from 2.98 – 22.49, and a low-Al group (Al2O3 < 15 wt.%) with lower Sr and moderately fractionated REE. This suggested a phase in which plagioclase was present rather than garnet.

In comparison with average compositions for rocks of variable ages (Table 4.13 a-e), from the late Archean plutonic rocks of the central Wyoming Province, (Frost etal 2006) (B), Ancient Gneiss Complex of Swaziland (Kronner etal 1998) (C), Tonalitic Granitoid Rocks from the Superior Province of Canada, (Whalen etal, 2002) (D) and tonalite–trondhjemite–granodiorite (TTG) suites and granites in the Fiskenæsset region, southern West Greenland (Huang etal. 2013)(E); the gneisses of this study area were similarly calcic to marginally calc-alkalic (Table 4.13) and (Fig. 4.65 & 4.66). Average TTG have alumina saturation indices near 1 (Frost et al. 2006), which compared closely with Okemesi-Iwaraja grey gneisses that were somewhat more metaluminouse, while one sample in particular was paraluminouse.

The average of major element composition of the Okemesi-Iwaraja grey gneisses (column A) had very similar values to that of column B C D and E in table 4.13. When compared with column B and D in table 4.13, the Okemesi-Iwaraja grey gneisses were richer in SiO_2 and K_2O, but poorer in Al_2O_3 and Na_2O, while they had more TiO_2 than values of samples in column B, C, D and E in table 4.13

A subset of samples from grey gneiss samples from the area shared the diagnostic Na_2O contents and Na_2O/K_2O ratios of Archean TTG. They were characterized by low K_2O and by Na_2O between 1.24 and 4.23 wt.%, which in turn produced Na_2O/K_2O of 0.49–5.85 (table 4.10). These “sodic” samples also had low Al_2O_3 (<15w%) that typifies the low-Al

group of Archean TTG, but are not limited to a single intrusion or specific geographic area within that environment. (Frost et al. 2006).

The average trace element composition of Okemesi-Iwaraja area when compared to those from the late Archean plutonic rocks of the central Wyoming Province, (Frost etal 2006) (B), Ancient Gneiss Complex of Swaziland (Kronner et al 1998) (C), Tonalitic Granitoid Rocks from the Superior Province of Canada, (Whalen et al, 2002) (D) and tonalite–trondhjemite–granodiorite (TTG) suites and granites in the Fiskenæsset region, southern West Greenland (Huang et al. 2013) (E), showed that the Okemesi-Iwaraja grey gneisses were Lower in Sr, absent in Co and Ni, more in Rb except samples represented in column (C) which had slightly higher values for Cr, Y and V, and W, than the other samples. See Table 4.11. On an AFM diagram (Fig. 4.65), the grey gneisses of Okemei-Iwaraja area plotted in the calc- alkaline field and the amphibolites (mafic) samples were medium –K and plotted in the tholeiitic field (Whalen et al. 2002).

Table 4. 13 Average chemical analysis of Okemesi-Iwaraja grey gneisses (major elements, (w%); trace elements, ppm; REE ppm) and compositionally similar rocks

A		B	C	D	E	Camp1	Camp2
Major Elements (w%)							
SiO_2	70.632	58.49	70.62	68.50		71.28	70.33
TiO_2	0.616	0.46	0.42	0.41		0.38	0.29
Al_2O_3	12.03	15.71	14.22	15.98		15.17	15.64
FeO	_	3.07	1.89	2.39		_	_
Fe_2O_3	4.924	_	1.00	1.03		2.85	2.36
MnO	0.078	0.04	0.06	0.54		0.04	0.03
MgO	1.866	1.19	0.75	1.33		0.78	0.78
CaO	3.746	3.61	2.62	3.81		3.22	3.35
Na_2O	2.708	4.40	3.98	3.88		4.38	4.62
K_2O	2.786	1.71	3.39	1.17		1.49	1.41
P_2O_5	0.1	0.12	0.16	0.13		0.10	0.11
BaO	0.074	-	-	0		-	-
Cr_2O_3	<0.01	-	-	0		-	-
SrO	0.03	-	-	0		-	-
LOI	0.666	0.34	0.81	0.27		0.25	0.17
Total	100.248	98.66	99.92	83.27		99.81	99.05
A/CNK	1.37	1.01	1.42	1.80		1.03	1.03
N/K	2.05	2.57	1.17	3.31		3.18	3.35

Table 4.13 Continued

	A	B	C	D	E Camp1	Camp2
			Trace Elements (ppm)			
Rb	91.68	57.86	97.90	67.00	44.00	29.00
Sr	220.46	329.43	317.00	464.67	523.50	435.50
Zr	216.8	173.86	238.00	138.17	193.83	132.25
Nb	11.74	7.71	16.87	5.63	4.10	2.62
Y	25.64	18.43	11.80	7.00	6.14	2.05
Ba	681.84	728.29	-	433.67	486.17	398.75
V	84	-	18.01	43.83	26.50	23.88
Co	_	_	7.23	0	5.50	5.88
Cr	33.2	_	18.67	17.15	16.17	18.00
Sn	<5	-	-	0.55	-	-
Ni	-	_	_	3.75	17.00	13.25
Sc	_	_	_	6.33	3.17	3.13
Pb	-	-	-	8.00	10.78	10.18
Cs	0.908	_	_	1.42	_	_
Ga	17.28	_	_	20.00	_	_
Hf	5.9	-	-	3.82	-	-
Ta	1.08	_	_	0	0.18	0.06
W	222.4	-	-	0	-	
Th	9.466			5.34	16.19	2.36
U	1.176			0.34	0.95	0.68

Table 4.13 (a-e): Average chemical analysis of Okemesi-Iwaraja grey gneisses (major elements, (w%); trace elements, ppm; REE ppm) and compositionally similar rocks. Continued

	A		B	C	D	E	Camp1	Camp2
				REE (ppm)				
La	53.26	16.86	23.29	27.00	63.47	16.87		
Ce	99.32	32.09	39.86	49.73	120.14	33.46		
Pr	10.93	_	0.57	5.46	12.56	3.43		
Nd	38.88	12.97	9.30	18.32	40.25	11.86		
Sm	6.544	2.41	1.04	2.81	4.87	1.74		
Eu	1.24	0.82	0.32	0.78	0.99	0.60		
Gd	5.442	1.16	0.89	2.01	2.58	1.06		
Tb	0.762	0.30	-	0.29	0.30	0.12		
Dy	4.456	0.71	0.74	1.42	1.35	0.51		
Ho	0.854	0.13	0.15	0.27	0.22	0.08		
Er	2.732	0.31	0.41	0.71	0.66	0.23		
Tm	0.39	0.03	_	0.11	0.07	0.03		
Yb	2.508	0.84	0.33	0.69	0.38	0.16		
Lu	0.364	0.12	0.07	0.11	0.06	0.03		

A Average of grey gneisses from Okemesi-Iwaraja area, Ogbole (2021)

B Average of the tonalite–trondhjemite–granodiorite (TTG) to granodiorite–granite (GG) transition in the late Archean plutonic rocks of the central Wyoming Province. Frost, etal. (2006)

C Average of Ancient Gneiss Complex of Swaziland, Kroner etal. (1998)

D Average of Tonalitic Granitoid Rocks from The Superior Province, Of Canada. Whalen etal. (2002).

E Average of Archean tonalite–trondhjemite–granodiorite (TTG) suites and granites from the Fiskenæsset region, southern West Greenland. Huang etal. (2013)

4.10 Geochemistry of the other granitoids (granite gneiss, porphyritic biotite granite, medium grained biotite granite and 2-mica granite) from Okemesi-Iwaraja area

Out of the 24 representative samples collected from the study area for whole-rock geochemical analysis, 17 were of other granitoid rocks excluding the grey gneisses ((pink) granite gneisses, porphyritic biotite granites, medium-grained biotite granite and 2-mica granite). The samples were prepared through the same standard process as described above and analysed for their major, trace and rare earth element compositions. The major, trace and rare earth element compositions are presented in Table 4.14 – 4.16. The REE patterns are shown in Figure 4.61.

Table 4. 14 Major elements for granitoids (granite gneiss, porphyritic biotite granite, medium grained biotite granite and 2-mica granite) study area

Sample ID	IW1D	L78	L50	L58	L75	L33	L34	L42	L43	L44	L46	L54	L63	L76	L77	L79	L65
Petrology	**Granite Gneiss**	**Granite Gneiss**	**Granite Gneiss**	**Granite Gneiss**	**Granite Gneiss**	**Porphyritic Biotite**	**Porphyritic Biotite Granite**	**Porphyritic Biotite**	**Porphyritic Biotite Granite**	**Medium - grained Biotite**	**Medium - grained Biotite**	**Medium - grained**	**Medium-grained Biotite**	**Medium-grained Biotite Granite**	**Medium-grained Biotite Granite**	**Medium-grained Biotite Granite**	**Two Mica Granite**
Major Elements (w%)																	
Al2O3	13.14	14.33	12.44	9.08	12.8	11.86	13.18	13.21	10.98	12.33	13.52	13.57	14.54	13.85	14.86	12.58	13.62
BaO	0.05	0.13	0.05	<0.01	0.05	0.01	0.03	0.1	0.05	0.01	0.11	0.06	0.19	0.16	0.12	0.04	0.09
CaO	1.08	2.04	1.22	0.1	1.02	0.58	0.81	1.01	1.08	0.86	1.59	1.4	2.16	0.87	3.71	0.79	1.35
Cr2O3	<0.01	<0.01	<0.01	<0.01	<0.01	<0.01	<0.01	<0.01	<0.01	<0.01	<0.01	<0.01	<0.01	<0.01	<0.01	<0.01	<0.01
Fe2O3	1.93	4.54	1.73	2.19	0.85	1.83	2.58	2.74	2.36	1.73	2.7	2.08	3	1.57	5.03	1.56	2.37
K2O	4.56	4.72	4.42	0.05	5.52	4.5	5.17	6.23	4.33	4.42	4.24	4.82	4.71	4.92	3.7	4.6	5.52
MgO	0.44	1.34	0.22	0.25	0.12	0.11	0.14	0.22	0.17	0.09	0.45	0.43	1.37	0.19	1.49	0.26	0.63
MnO	0.05	0.06	0.03	<0.01	0.01	0.03	0.05	0.03	0.03	0.03	0.04	0.04	0.03	0.03	0.08	0.04	0.03
Na2O	3.37	2.36	2.94	0.11	2.65	2.84	2.97	2.5	2.45	3.31	3.3	2.98	3.55	3.3	3.15	3.13	2.34
P2O5	0.03	0.13	0.04	0.02	0.04	0.04	0.04	0.08	0.05	0.02	0.1	0.06	0.21	0.03	0.17	0.03	0.14
SiO2	73.68	67.6	77.56	86.6	75.7	76.1	75.03	72.08	78.76	77.8	74.12	73.18	70.19	72.24	64.83	74.67	73.77
SrO	0.01	0.04	0.01	<0.01	0.02	<0.01	<0.01	0.01	0.01	<0.01	0.02	0.02	0.12	0.02	0.05	0.02	0.03
TiO2	0.19	0.53	0.16	0.51	0.09	0.13	0.18	0.28	0.25	0.12	0.32	0.25	0.49	0.21	0.62	0.17	0.4
LOI	0.64	1.87	0.48	1.72	0.53	0.46	0.41	0.45	0.45	0.73	0.55	0.41	0.56	0.67	0.95	0.56	0.61
Total	99.17	99.7	101.3	101	99.5	98.49	100.59	98.95	100.96	101.45	101.06	99.31	101.13	98.06	98.76	98.44	100.88
CIA	59.32	61.10	59.18	97.20	58.30	59.96	59.56	57.56	58.28	58.94	59.69	59.60	58.25	60.37	58.45	59.62	59.65
A/NK	2.85	3	2.79	151	2.45	2.62	2.52	2.11	2.52	2.77	3.16	2.79	3.28	2.8	3.93	2.52	2.45
A/CNK	2.31	2.1	2.19	56.8	1.97	2.32	2.19	1.82	2.01	2.32	2.3	2.17	2.11	2.38	1.98	2.32	1.97
Fe_2O_3/MgO	1.81	3.25	4.62	3.07	3.39	29	18.74	5.2	6.57	3.43	2.718	3.96	1.56	2.89	3.59	6.12	0.95

Table 4.15: Trace elements for the other granitoids from the study area excluding the grey gneisses

Sample ID	IW1D	L78	L50	L58	L75	L33	L34	L42	L43	L44	L46	L54	L63	L76	L77	L79	L65
Petrology	Granite Gneiss	Granite Gneiss	Granite Gneiss	Granite Gneiss	Granite Gneiss	Porphyritic Biotite Granite	Porphyritic Biotite Granite	Porphyritic Biotite Granite	Porphyritic Biotite Granite	Medium Graind Biotite Granite	Medium Graind Biotite Granite	Medium Graind Biotite Granite	Medium Graind Biotite Granite	Medium Graind Biotite Granite	Medium Graind Biotite Granite	Medium Graind Biotite Granite	Two Mica Granite
Trace Elements (ppm)																	
V	14	57	11	16	<10	<10	<10	13	<10	<10	18	19	44	<10	60	<10	28
Cr	<10	25	<10	15	<10	26	<10	<10	<10	<10	<10	10	46	<10	32	<10	14
Ga	17.9	18.3	16.6	10.6	19.4	22.9	26.3	23.1	21.4	21.6	22.9	20.9	20.4	17.3	19.6	17.2	19.7
Rb	279.8	186.3	251.1	2	296	319.2	325.6	239.1	185.4	188.9	208.3	285.6	131.1	158.6	161.5	227.4	215.2
Sr	111.8	344.5	118.9	38.5	152	28.1	43.6	110.3	86.7	43.1	195.1	158.8	1029.1	193.5	396.9	150.1	237.8
Y	31.8	27	27.6	25.6	18.5	86	96.6	39.9	37.5	16.4	34.3	29.5	11	26.8	40.6	28.7	6.5
Zr	148	238	144	648	80	170	162	270	262	210	239	212	257	250	314	132	301
Nb	13.5	11.8	13.2	11.9	9.7	38.7	53.6	22.5	20.7	15.5	23.3	21.3	8	13.2	17.7	16.8	11
Sn	6	<5	5	<5	<5	8	7	<5	<5	<5	7	6	<5	<5	<5	<5	5
Ba	474.6	1256.3	426.9	13.4	515	109.3	236.4	911.2	480.6	140	995.8	589.4	1693.2	1559.6	1092.1	326.6	881.4
Cs	2.22	1.21	1.74	0.06	1.41	8.54	4.13	2.18	2.23	5.46	8.66	2.12	0.93	1.03	1.78	1.2	1.91
Hf	5	6.7	5.2	16.4	2.3	6.4	5.8	8.4	8	6.7	6.8	6.8	6.5	7	8.6	4.8	8.8
Ta	1.4	1	1.4	1.3	1.1	1.9	1.8	1.2	1.2	1.2	2	1.6	1.1	1.3	1.2	1	0.9
W	406	190	313	247	357	201	231	209	350	290	328	360	260	346	195	173	282
Th	35.04	23.42	26.7	8.63	15.3	19.14	25.07	16.7	19.8	13.95	12.05	42.33	9.06	12	27.34	28.87	24.45
U	5.79	1.28	4.61	3.32	2.43	3.81	5.87	1.9	2.14	2.62	2.47	7.82	1.44	2.15	3.29	5	1.08
Y/Nb	2.36	2.29	2.09	2.15	1.91	2.22	1.8	1.77	1.81	1.06	1.47	1.38	1.38	2.03	2.29	1.71	0.59

Table 4. 3 Rare earth elements for the other granitoids from the study area, excluding the grey gneisses

Sample ID	IW1D	L78	L50	L58	L75	L33	L34	L42	L43	L44	L46	L54	L63	L76	L77	L79	L65
Petrology	Granite Gneiss	Granite Gneiss	Granite Gneiss	Granite Gneiss	Granite Gneiss	Porphyritic Biotite Granite	Porphyritic Biotite Granite	Porphyritic Biotite Granite	Porphyritic Biotite Granite	Medium Graind Biotite Granite	Medium Graind Biotite Granite	Medium Graind Biotite Granite	Medium Graind Biotite Granite	Medium Graind Biotite Granite	Medium Graind Biotite Granite	Medium Graind Biotite Granite	Two Mica
REE (ppm)																	
La	52.6	54.7	29	29.8	30.6	61.7	82.4	96.6	101.1	46.9	46.7	82.1	55.2	43.1	78.6	55	67.9
Ce	101.4	80	62.4	54.8	59.8	140.8	183.9	201.3	212.7	97.5	91.4	157.8	101.4	81.7	146.7	104.1	136
Pr	11.2	10.86	6.56	7.02	6.51	17.09	21.98	23.82	25.15	11.35	10.53	16.71	11.26	8.92	15.92	11.79	15.12
Nd	38.8	39.2	23	27.1	22.3	61.8	79.9	86	91.6	41.4	39.2	55.6	40.6	31.4	55.9	40.5	53.1
Sm	6.96	6.97	4.62	5.09	4.04	15.28	18.37	15.66	16.22	7.02	7.94	9.05	6.71	5.41	9.66	6.96	7.99
Eu	0.74	1.44	0.64	1.1	0.65	0.36	0.54	1.51	1.25	0.6	1.29	0.92	1.57	1.1	1.84	0.57	1.28
Gd	5.77	5.61	4.05	4.48	3.11	13.29	15.67	11.69	11.69	4.93	6.62	7.04	4.39	4.19	8.01	5.52	5.03
Tb	0.81	0.81	0.66	0.64	0.49	2.46	2.8	1.63	1.5	0.63	1.03	0.96	0.46	0.62	1.14	0.79	0.43
Dy	5.13	4.66	4.15	4.04	2.91	15.5	16.77	8.37	7.92	3.24	6.22	5.24	2.29	3.89	6.63	4.55	1.65
Er	3.25	2.82	2.78	2.7	1.92	9.26	9.79	4.32	3.78	1.69	3.49	3.02	1.05	2.78	3.95	3.14	0.71
Ho	1.02	0.9	0.83	0.81	0.57	2.95	3.21	1.49	1.34	0.56	1.15	0.98	0.38	0.79	1.22	0.88	0.24
Tm	0.5	0.4	0.45	0.44	0.28	1.32	1.39	0.52	0.5	0.29	0.51	0.42	0.15	0.41	0.54	0.49	0.09
Yb	3.35	2.67	3.01	2.71	1.96	7.94	8.79	3.32	2.93	1.66	3.13	2.67	0.85	2.81	3.55	3.42	0.58
Lu	0.48	0.38	0.43	0.43	0.28	1.03	1.21	0.44	0.4	0.24	0.43	0.39	0.12	0.4	0.5	0.52	0.09
Eu/Eu*	0.36	0.7	0.45	0.7	0.56	0.08	0.1	0.34	0.28	0.31	0.54	0.35	0.88	0.7	0.64	0.28	0.62
(La/Yb)N	10.69	13.9	6.54	7.48	10.6	5.28	6.37	19.76	23.44	19.14	10.16	20.84	44.39	10.4	15.03	10.93	79.43
(La/Sm)N	4.72	4.9	3.91	3.65	4.74	2.52	2.8	3.85	3.89	4.17	3.68	5.66	5.14	4.97	5.08	4.93	5.3
(Ce/Yb)N	7.96	7.86	5.44	5.32	8.01	4.66	5.49	15.93	19.06	15.39	7.67	15.5	31.51	7.62	10.85	8.01	61.52
(Gd/Yb)N	1.39	1.7	1.09	1.34	1.28	1.35	1.44	2.85	3.23	2.4	1.71	2.13	4.21	1.2	1.82	1.31	7

4.10.1 Major Element Geochemistry of other granitoids from Okemesi-Iwaraja area

The major element contents of the samples of the other granitoids rocks (granite gneiss, porphyritic biotite granite, medium grained biotite granite, two-mica granite) from the study area, showed slight variations within the same sample suite, with SiO_2 contents ranging from 64.83 to 78.76 wt.% and low Al_2O_3 contents (Al_2O_3=10.98–14.86wt.%) (Low aluminum < wt 15%). They had relatively low MgO (0.09–1.4 wt.%), and Cr_2O_3 contents with values generally <0.04. They are sodium rich (Na_2O=2.34–3.55wt.%) and have low K_2O (4.24-6.23wt.%) contents resulting in an average Na_2O/K_2O less than 1 alongside low amounts of P_2O_5 (0.02-0.21wt.%) (Table 4.14).

4.10.2 Trace Element Geochemistry of other the granitoids

The trace element geochemistry of the other granitoids rocks (granite gneiss, porphyritic biotite granite, medium grained biotite granite, two-mica granite) from Okemesi-Iwaraja area presented in Table 4.15 shows that their samples are characterized by high amounts of Sr, Zr, Ba, W and Rb but low amounts of Cr, V, U, Sn, Ta, Cs, Hf and absent in Ni, this also reflects the high amount of feldspar and zircon in their modes similar to that of the grey gneisses within the study area.

4.10.3 Rare Earth Element Geochemistry of other granitoids from Okemesi-Iwaraja area

These rocks have strongly fractionated REE patterns (La/Yb)n=4.28–79.43) and displayed negative Eu anomalies (Eu/Eu*=0.05–0.44) with a negative to positive Ce anomalies (Ce/Ce*=0.72–1.05) (Table 4.16 and Appendix iii). The chondrite normalized plot shows that the other granitoids rocks showed higher values for Light Rare earth LREE values and lower Heavy Rare Earth HREE values, exhibiting negative Eu anomaly, suggesting a highly fractionated melt, and has low amounts of LREE and HREE. The following characteristics where also observed for other granitoids rocks: (1) positive Zr anomalies (Zr/Zr*=1.10–14.35); (2) negative to positive Sr anomalies (Sr/Sr*=0.16–8.49) (appendix 3).

Figure 4.63 shows chondrite-normalized REE distribution trends for both granitoids and associated rocks. The parallel, conformable, and highly fractionated patterns in each suite

are identical ((La/Yb)N = 5.28–79.43). The granitoid rocks are abundant in light rare earth elements (LREE) ((La/Sm)N = 2.52–5.66) but deficient in heavy rare earth elements (HREE) ((Gd/Yb)N = 1.09–7.0), with mild to moderate negative Eu-anomalies (Eu/Eu* = 0.08–0.88). The LREE distribution patterns for the Biotite granite rocks and the gneisses are parallel (see Table 4.16 and Figure 4.61).

4.11 Explanation for Geochemical Analysis

4.11.1 Geochemical composition

One obvious difference between the grey gneisses and the other granitoids of Okemesi-Iwaraja area is that most of the grey gneisses were associated with mafic to -intermediate plutonic rocks. The grey gneisses are largely granodioritic to tonalitic in composition, they have Na_2O/K_2O ratios < 0.6 (Table 4.10), they show Na-enrichment and one sample in particular, plotted in the trondhjemitic field (Fig. 4.64). The amphibolite samples plotted in the tonalite field in a feldspar ternary plot (Fig. 4.64). On the other hand, the granite gneisses and the other granitoids are typically granodioritic to granitic in composition with an average K_2O/Na_20 ratio of 0.72 (Table 4.14). In the K_20 vs SiO_2 plot, they plot in a classical calc-alkaline field, which is characterized by K-enrichment during differentiation (Fig. 4.65). There is a close similarity in MgO composition between most of the rocks except amphibolites which had relatively higher FeO+MgO, Although Fe_2O_3*+MgO is higher in the granite gneisses and the other granitoids than in the grey gneisses. The composition with respect to major and trace elements also showed remarkable differences as presented Table 4.10. In comparison with the grey gneisses, the granite gneisses and the other granitoids are enriched in all incompatible elements (Rb, Ba, Th, U, K). For instance, the grey gneisses are Rb-poor and Sr-rich, Both the grey gneisses and granite gneisses alongside other granitoids display similar Nb, Ta, anomalies (Table 4.11, 4.12, 4.15 4.16), whereas Eu exhibits significant negative anomalies in the granite gneisses and the other granitoid rocks (Eu/Eu* = 0.08–0.91) Table 4.16. Another significant difference is the strong depletion in HREE observed in the grey gneisses (Archean TTG) (Table 4.12 and Appendix iv).

Figures 4.60-4.61 indicate that the samples in each suite have identical properties of parallel, conformable, and highly fractionated patterns ((La/Yb)N = 5–19) of chondrite-normalised REE distribution patterns for both the granitoids and related rocks. The granitoid rocks are rich in light rare earth elements (LREE) ((La/Sm)N = 0.69–6.76) and low in heavy rare earth elements (HREE) ((Gd/Yb)N = 1.01–7.0), with strong negative Eu-anomalies (Eu/Eu* = 0.08–0.91). In comparison to the other granitoid samples which have somewhat more depleted HREE ((Gd/Yb)N = 1.68–3.24), the grey gneisses , have comparatively flat HREE patterns ((Gd/Yb)N = 1.14–1.71). The amphibolites are comparatively deficient in LREE ((La/Sm)N = 2.08–3.14) and marginally more enriched in HREE ((Gd/Yb)N = 0.96–1.91), with no Eu-anomaly. While the LREE distribution patterns for the Biotite granite rocks and the gneisses are somewhat parallel.

The Rb, Sr and Ba variations are useful in estimating the extent of fractionation of feldspar, amphibole and biotite minerals and whether magmatic evolution was controlled dominantly by fractional crystallization; partial melting or more complex processes are used in evaluating mineralization potentials of granites (Imeokparia 2015). The granites in the area exhibite intermediate to high abundance of Sr, Ba, Rb, Nb and Y and high concentration of light rare-earth elements e.g. La Ce and Nd. When all the samples are also plotted on Rb-Ba-Sr ternary diagram, 60% of the samples fell within anomalous and normal granite fields and 40% showing strongly differentiated nature (Fig. 4.62). This suggests that the granitoids are partly fractionated, differentiated and fertile in nature.

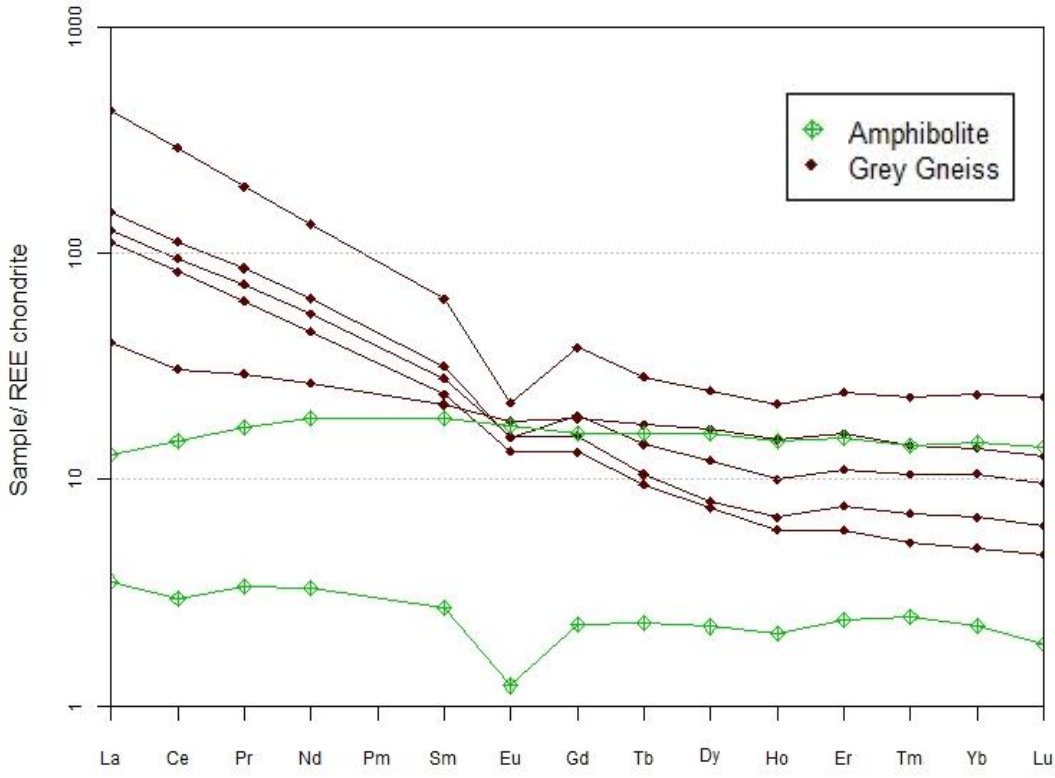

Fig. 4. 60 Chondrite-normalised REE distribution patterns for grey gneisses and amphibolites of study area, after Boyton 1984

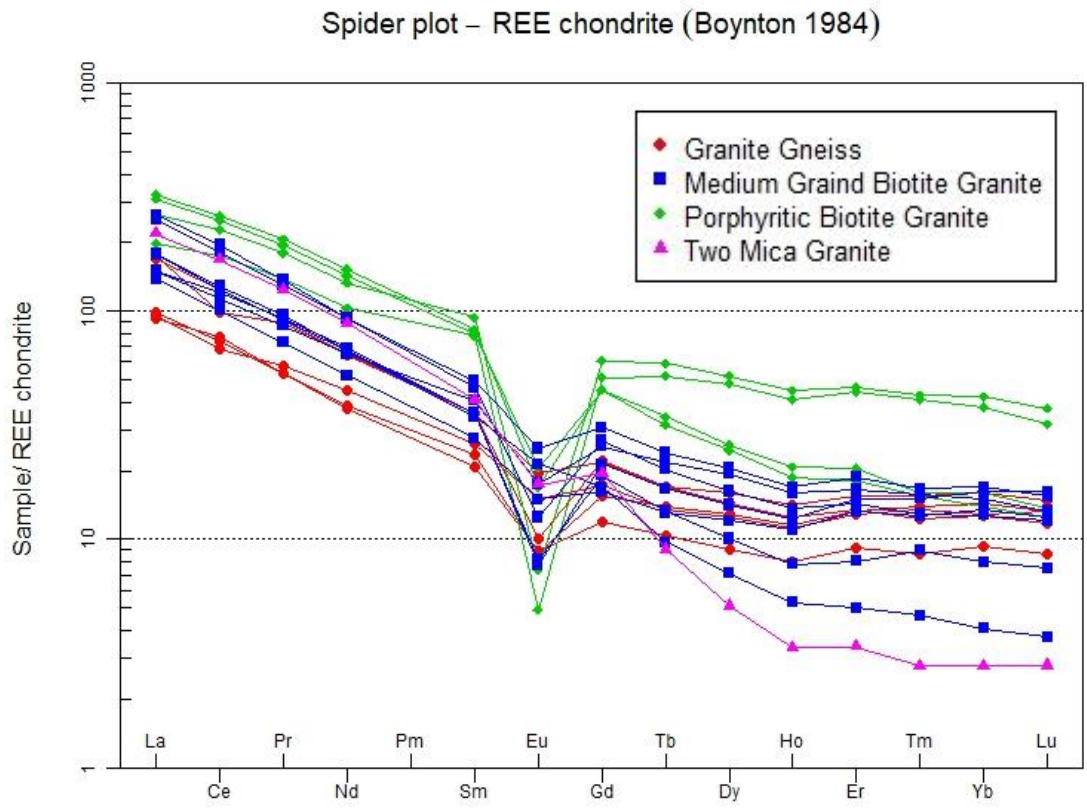

Fig. 4. 61 Chondrite-normalised REE distribution patterns for all the granitoids and associated rocks after Boyton 1984,

(Barriere and Cotton, 1979; Moazamy, 2006) have all used the Fe_2O_3, MgO, Al_2O_3 compositional diagram to explain the nature of granitic magma. Discrimination diagrams based on major - elements (FeO, MgO, Al_2O_3) in igneous rocks shows that they crystallized from A, P, and C magma types, this was proposed by Abdel-Rahman (1994). According to his classification, Fe_2O_3, MgO, and Al_2O_3 composition in anorogenic alkaline suites (field A) are mainly iron-rich, siliceous (near annite), and have an average FeO*/MgO ratio of 7.04; those in peraluminous (including S-type) suites (field P) are siderophyllitic in composition and have an average FeO*/MgO ratio of 3.48; In calc-alkaline orogenic suites (field C), the composition of Fe_2O_3, MgO, and Al_2O_3 is mildly rich in Mg, and an average FeO*/MgO ratio of 6.02. It is important to have in mind that the typical FeO*/MgO ratio doubles from calc-alkaline through peraluminous to alkaline suites (Fig. 4.63)

The rocks under investigation were found in fields C to P. It implies that the rocks are mainly formed from calc-alkaline to peraluminous magma, based on chemistry. This finding is consistent with the whole-rock analysis, which revealed the rocks' peraluminous and calc alkaline composition. The early dissociation of H_2O and release of H in such magmas at an early stage, would enrich the system in oxygen (Fig. 4.63).

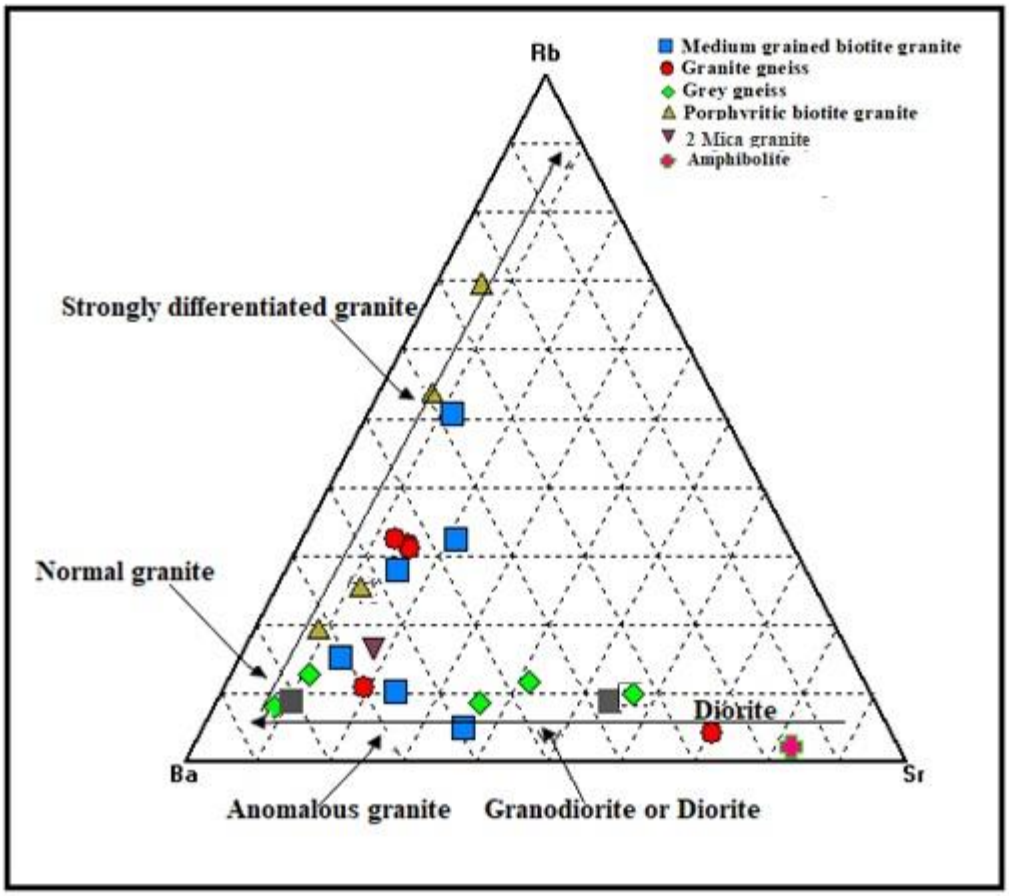

Fig. 4. 62 Plot of Rb-Ba-Sr for all the rock samples of study area, (after El Bouseily and El Sokkary, 1975)

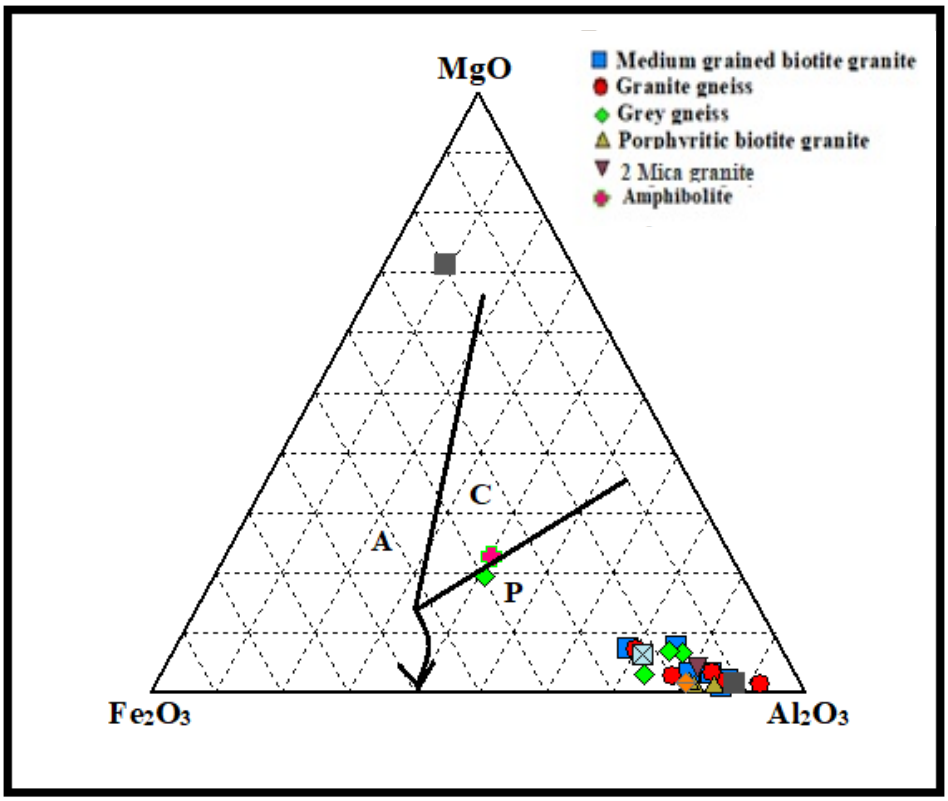

Fig. 4. 63 Fe2O3, MgO, Al2O3 compositional diagram for all the rock samples from the study area showing the classification of magmas after Abdel-Rahaman, (1994) (C = calk-alkali, P = Peraluminous, A = Alkali)

4.11.2 Geochemical Charaterisation

Granitoids are generally the most common rock types in the continental crust therefore making it difficult to adopt a single classification scheme. This may be as a result of the different modes by which they are derived. Granitic melts, for example, may be formed entirely from crustal materials, evolved mantle derived melts, or a combination of crustal and mantle derived melts, and partial melting of a variety of rock types (Frost et al. 2001,2008). Because of this complication, petrologists focused on chemical classification to classify the various granitoid classes, and over the last 30 years, about 20 new classification schemes have emerged. The origin of these schemes is either genetic or tectonic (Frost et al. 2001,2008).

The rocks of Okemesi-Iwaraja area were classified based on three broad classification approach, Ferron Magnesia, MALI, ASI and Rock type.

The ternary feldspar plot of Anorthite (An), Albite (Ab) and Orthoclase (Or) for the rock samples from the study area atfter O'Connor 1965, showed that the grey gneiss samples plot mostly in the Tonalite and Granodiorite/Quartz monzonite fields respectively, while the mafic samples plotted in Tonalite. The granite gneisses mostly plotted in granite field with a few of the samples falling in the quartz monzonite and tonalite fields. While the other granitoids generally plotted in the granite fields except one medium –grained biotite granite sample, which fell in granodiorite field (Fig. 4.64). Furthermore, as observed from the AFM ternary plot, a calc-alkaline differentiation trend from thoelitic field was indicated by the amphobolite samples as seen in (Fig. 4.65), (Fig. 4.66 and 4.67) after Peccerillo and Taylor (1976) and Irvine and Baragar, (1971), all aother samples including the grey gneisses, granite gneisses and the other granitoids plotted in the calc-alkaline series.

The granitic rocks of the region plotted in the magnesian and ferroan (Fe-enriched) fields in the FeOtotal/(FeOtotal+MgO) against SiO2 plot (Appendix 2). Away from the subduction zone, the granitoids became increasingly potassic and alkalic. Peraluminous leucogranite may also be magnesian or ferroan, with MALI ranging from calcic to alkaline (Frost etal 2001). This is similar to the granitic rocks found in the Idofin-Osi-Eruku district, which are

mostly peraluminous, magnesian to ferroan granites with MALI ranging from calcic to alkalic.

The plot of SiO_2 against K_2O showed that the grey gneisses were mostly High-K calc – alkaline and Calc –alkaline series. While the mafic samples of the study area are of tholeiitic series (Fig. 4.66), this agrees with the results of the AFM plot in Figure 4.65. On the Zr/TiO2–Nb/Y diagram (Fig. 4.71), most granitoids and felsic metavolcanic rocks plotted in fields ranging from rhyolite to rhyodacite (similar to granitic compositions for plutonic rocks), whereas amphibolites and metabasite plotted in the sub-alkaline basalt area. The felsic metavolcanic rocks and metabasite shown in two chemically different compositional fields with no intermediate (andesite) composition, consistent with the bimodal nature of these rocks predicted from general lithological features. On the SiO_2–K_2O diagram (Fig. 4.66), The Porphyritic Biotite Granite, Medium Grained Biotite Granite, and Two-mica Granites plotted in the High-K calcalkaline to Calcalkaline series region, despite being less metamorphosed than the other sample suites. Except for one Porphyritic Biotite Granite sample, which plotted in the shoshonitic series field, and one Migmatitic grey gneiss and one granite gneiss, which plotted in the theolitic field, the rest of the samples plotted in the same field, with the exception of one Porphyritic Biotite Granite sample, which plotted in the shoshonitic series field, but due to the apparent disturbance of K contents in most of these samples, no significance was placeed on this discrimination.

MALI

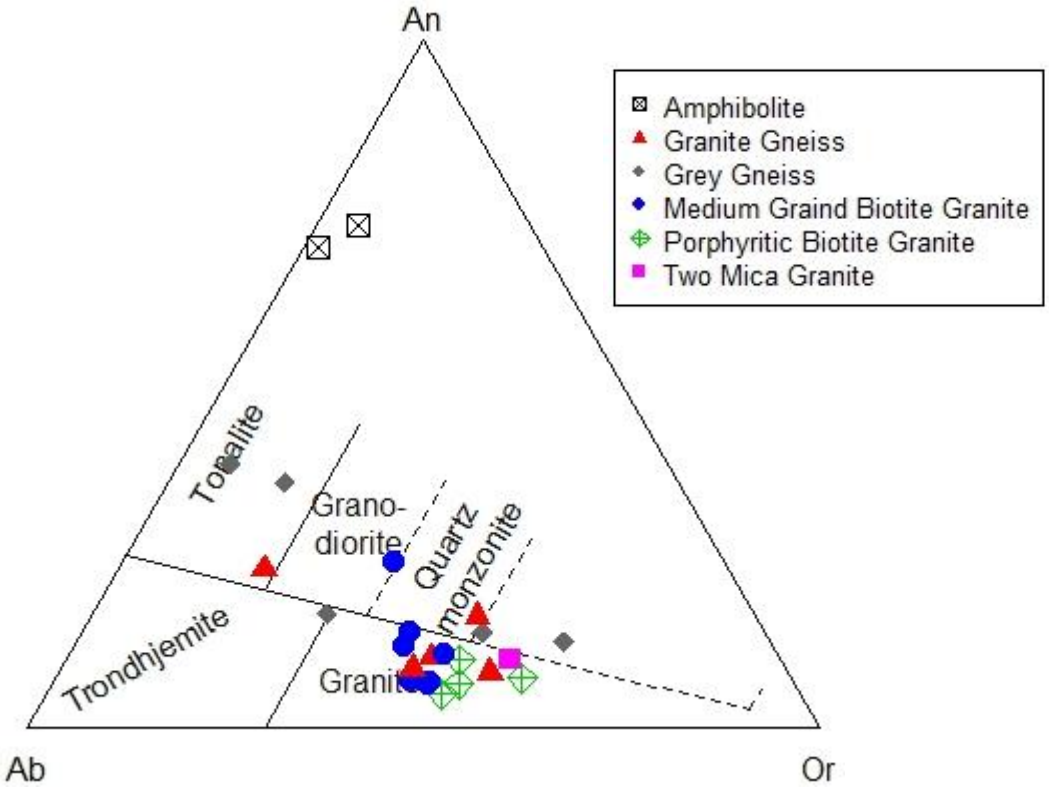

Fig. 4. 64 Feldspar ternary plot for all the samples from Okemesi-Iwaraja area (after O'Connor 1965)

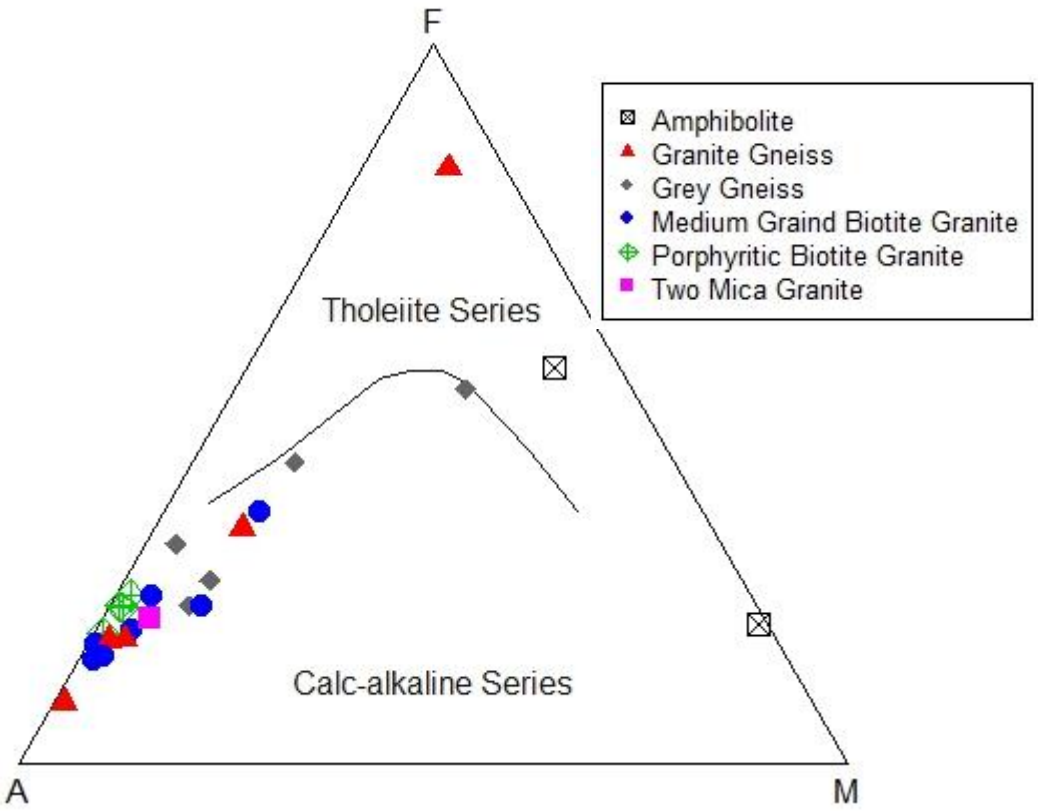

Fig. 4. 65 AFM Plot for all samples from the study area, after (Irvine and Baragar 1971)

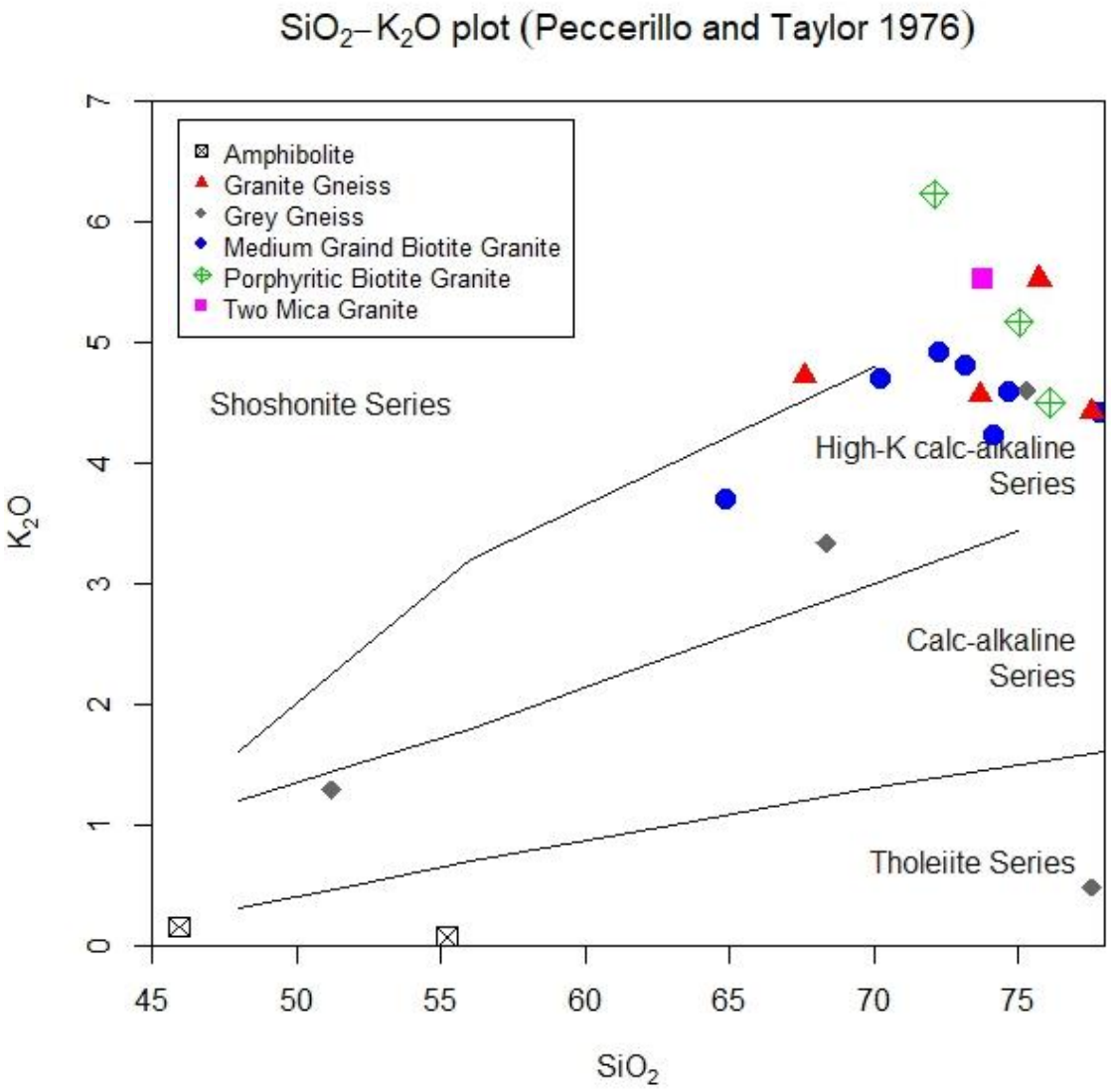

Fig. 4. 66 SiO_2-K_2O Plot for all samples from the study area after Peccerillo and Taylor 1976

Cox et al.,1979 and Middlemost 1994 classified most granitoids as granites (Fig. 4.67 &4.68), with aluminium saturation index varying from metaluminous to slightly peraluminous (Fig. 4.69). A/NK v A/CNK diagram for the all samples showed ranges between 0.18 and 1, suggesting strong metaluminous granite characters, (Figure 4.70 and Appendix i).

Previously, granitoids were classified into types: I - S-, and A-type, (Chappell and White, 1974); meanwhile, these classifications have changed significantly since their inception. S-type granites were believed to be produced by partial melting of metasedimentary source rocks, I-type granites from igneous source rocks not exposed to surface weathering, and A-type or anorogenic granites from rocks formed far from an orogenic belt. The I-S- and A-types can now be formed in a variety of settings and ways (Barbarin, 1999).

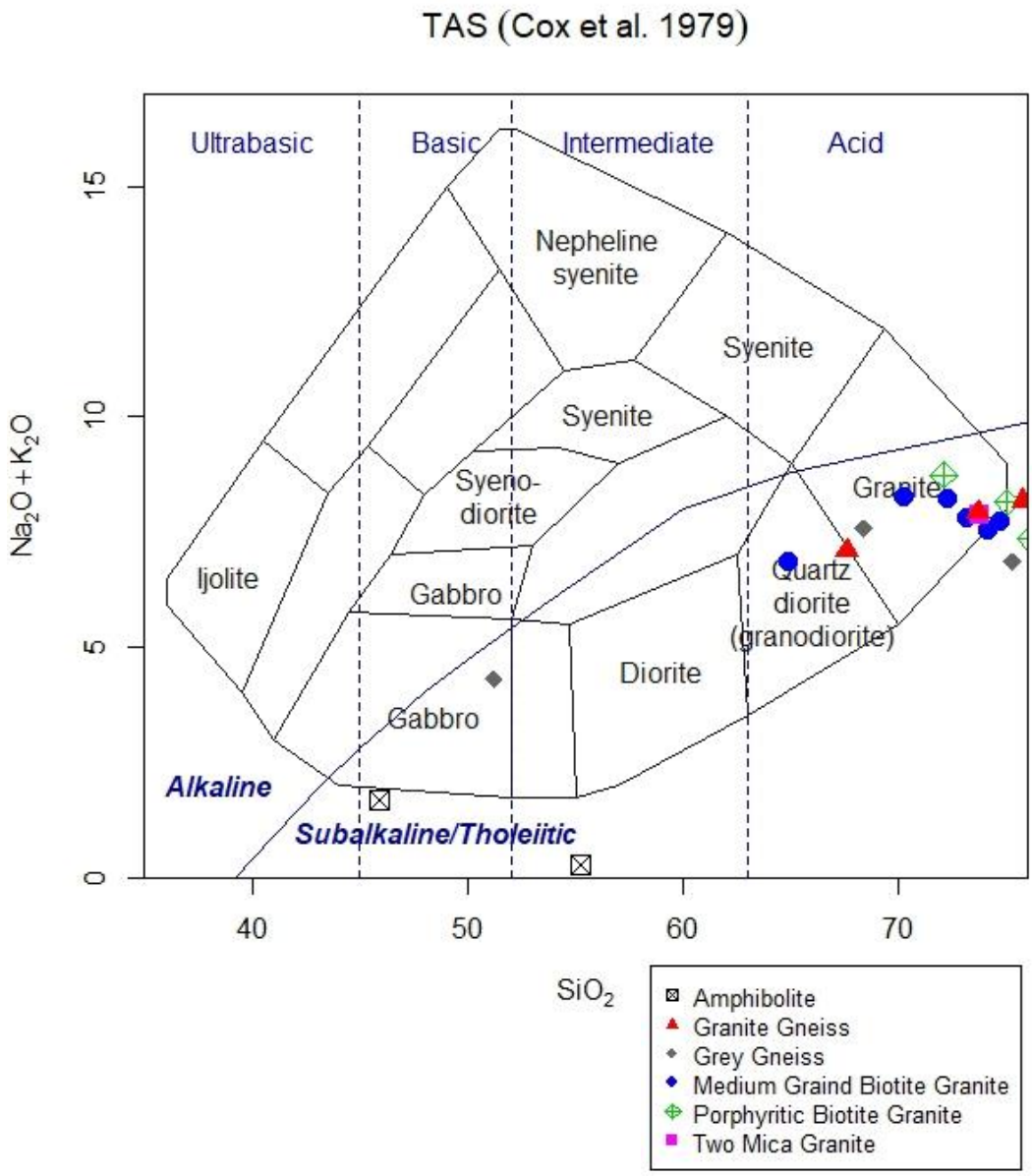

Fig. 4. 67 Chemical classification and nomenclature of plutonic rocks for all samples, using the total alkalis (Na2O+K2O) vs SiO2 (TAS) diagram of Cox et al., (1979)

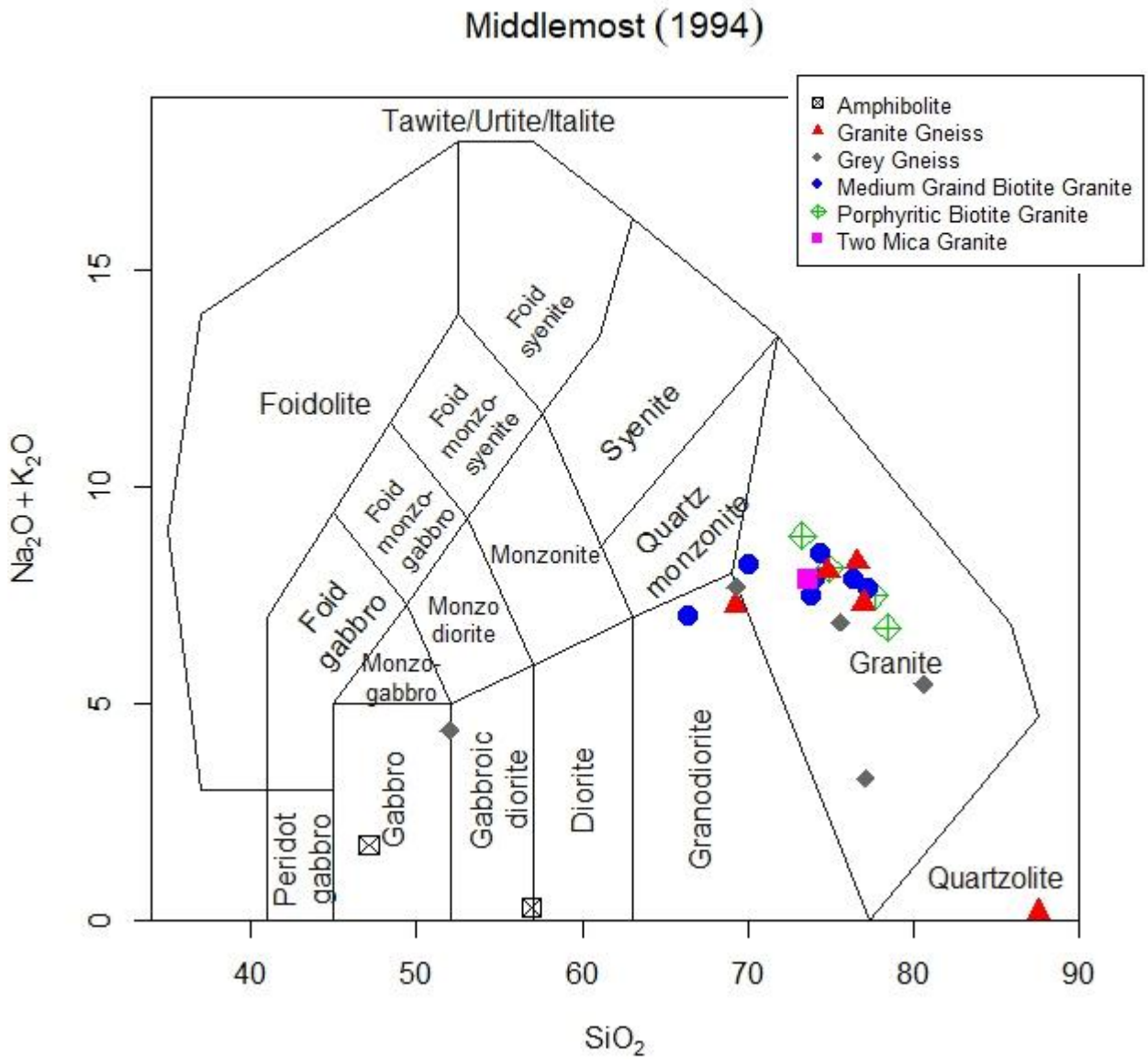

Fig. 4. 68 Plot of Na2O + K2O/SiO2 for all samples from the study area, (TAS) Classification diagram of Middlemost (1994)

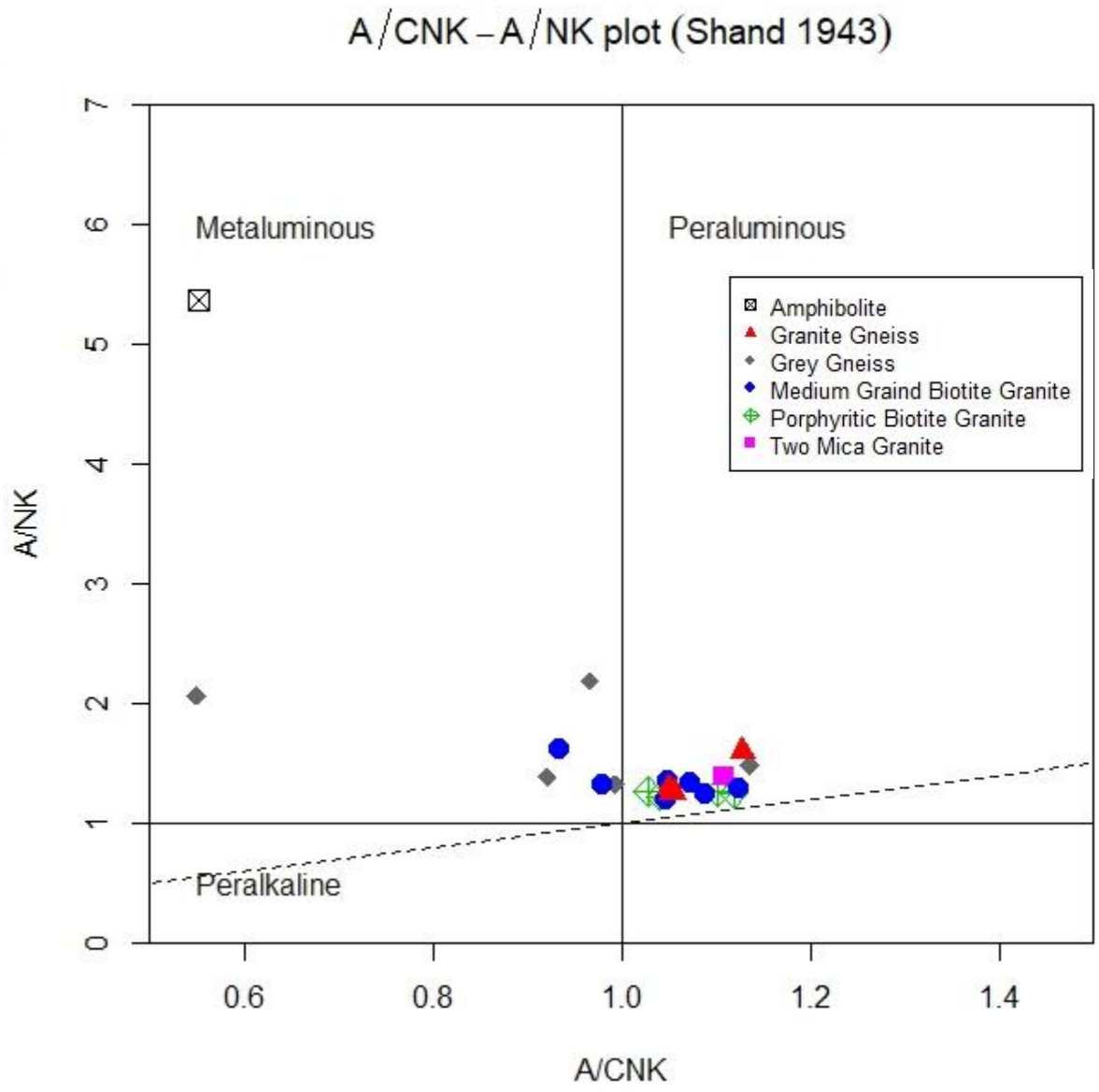

Fig. 4. 69 A/NK-A/CNK Plot for all the rock samples after (Shand 1943)

To differentiate between S and I-type granites, the aluminum saturation index (ASI: molar Al2O3/(CaO + Na2O+K2O)) is employed (Chappell, 1999). Despite faults and evident CaO, Na2O, and K2O interference in several of the samples, the ASI categorization method was utilised. All of the samples fell into the S-type granite area on the $Al_2O_3/Na_2O+K_2O/Al_2O_2$/CaO+Na2O+K2O diagram. On the A/NK–A/CNK diagram (Fig. 4.69), 80 percent of the samples including at least one Grey Gneiss sample plotted in the peraluminous field (A/CNK > 1), while the others plotted in the metaluminous field (A/CNK<1).

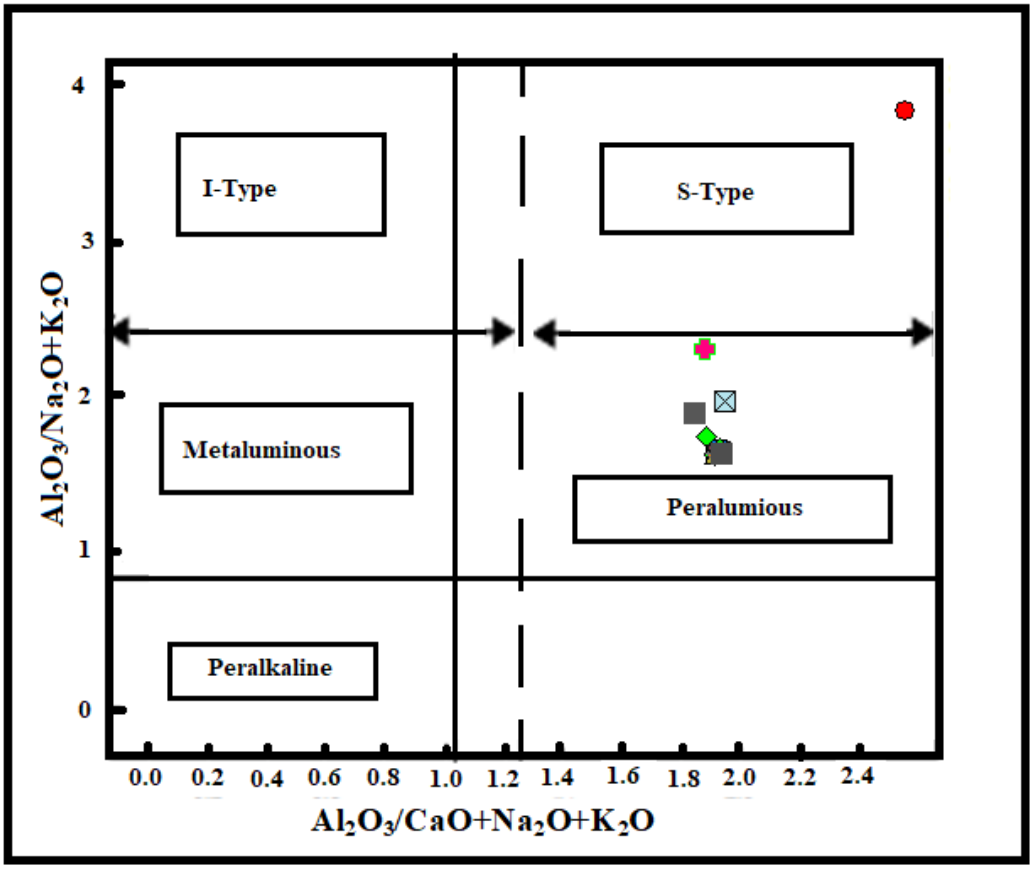

Fig. 4. 70 Plot of Al2O3/Na2O+K2O/Al2O2/CaO+Na2O+K2O, A/NK vs A/CNK diagram for all the samples, showing the peraluminous character of the Granite in the area (Fields after Shand, 1943 and Ngnotue et al., 2012).

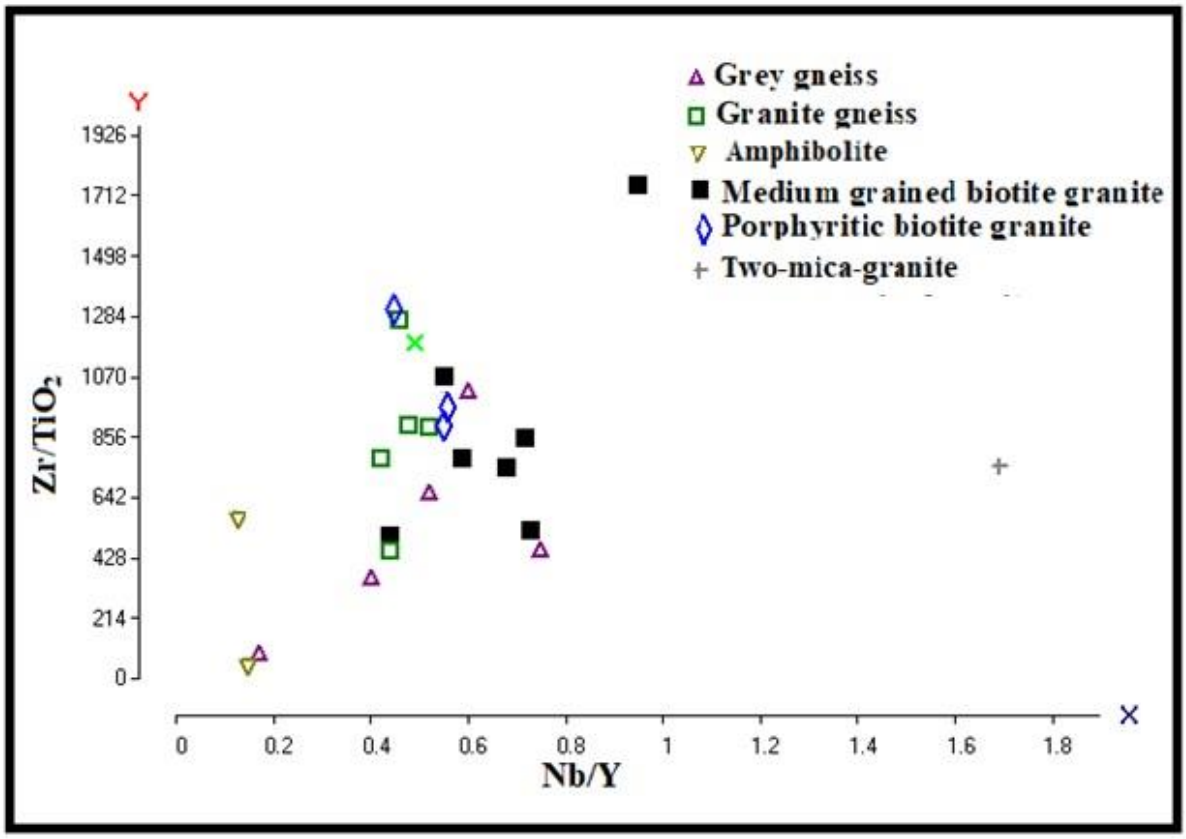

Fig. 4. 71 Plot of Zr/TiO2 - Nb/Y of study area (after Pearce etal 1996)

The samples on the $Na_2O + K_2O – Fe_2O_3– MgO$ (AFM) ternary plot (Fig. 4.65 and 4.66) after Irvine and Baragar (1971) and Peccerillo and Taylor (1976) showed a clear calc-alkaline differentiation trend from thoelitic field, and this characteristic was also seen in the Biotite mineral discrimination diagram of Abdel-Rahman (1994), (Fig. 4.63). Molar A/CNK ranged between 0.18 and 56.75 suggesting strong peraluminous and S-type granite characters, see appendix 1. These granitoids, according to Chappell and White (1974), are comparatively potassic and restricted to rocks with a higher silica content of 86.62 SiO_2, which could be obtained from the melting of metasedimentary rocks, but similar granitic composition could also be formed by partial melting of a number of sources (Miller, 1985).

The K_2O vs SiO_2 diagram after Peccerillo and Taylor, (1976) (Fig. 4.66), indicated a medium to high- k affinity for the granitoids. (silica content)

4.11.3 Geochemical alteration

Large ion lithophile elements (LILE: e.g., Rb, Sr, Ba, Th) and Mobile elements such as alkalies (K_2O, Na_2O), CaO, of the samples analyzed in this study, which had undergone varying degrees of metamorphism, have been mobilized, therefore do not reflect original premetamorphic concentrations. Secondary alteration and metamorphism were indicated by the contents of CaO, K_2O, and Na_2O, meanwhile, the $K_2O–SiO_2$ and ASI discrimination diagrams (Fig. 4.68) are only theoretically useful for weakly metamorphosed samples such as quartzite. The chemical indices of alteration (CIA Appendix i) of 49–62, were relatively similar to those of unaltered Biotite granite rocks (50 and 42, respectively; Nesbitt and Young, 1982) CIA values of 15 was recorded for some of the porphyritic Biotite Granite, those rocks were found to be fresh and un altered whereas other rock samples among the quartzite gave CIA values the indicated that some of them were extremely altered rocks. However, a look at the ACNK and ANK table in Appendix 1 shows that some samples have Na/K ratios that are characteristic of common felsic igneous rocks, implying substantial alkali mobilisation. Some quartzites and quartz schist, have a very high CIA value of 94, suggesting that the parent rock has been severely altered (Smith, 1963; Mallick, 1966). But for samples L 30, L58, and L78, which had higher values of 1.2, 1.7, and 1.87 wt %, all of the other samples had low levels of loss on ignition (LOI 1 wt %). The majority of rock

samples from the study area revealed that the rocks have experienced very little alteration, and their elemental compositions matched the initial magmatic concentrations to a large degree. Rare earth elements (REE) and high field strength elements (HFSE: e.g., Nb, Ta, Zr, Hf, Ti, P, Y) that are usually known for their comparatively immobility during metamorphism were used to characterize and differentiate the granitoids and related rocks in this analysis (Rollinson, 1993). Mobile main element material geochemical characterisation schemes were used with caution, particularly for the most metamorphosed samples.

4.11.4 Origin and Evolution

The $CaO/(MgO+Fe_2O_3)$ vs. $Al_2O_3/(MgO+ Fe_2O_3)$ plot of composition of major elements from results of whole rock analysis (Altherr et al., 2000) in Figure 4.72, below indicated that the basin type granite was derived from partial melting of metagreywackes, which was responsible for most of the grey gneisses, with contribution from metabalsaltic to metatonalitic source, source which was largely responsible for the amphibolites. According to experimental and geochemical studies, peraluminous and S-type granitods may be formed by partial melting of detrital metasediments, particularly shales and greywackes (Condie et al., 1999; Frost et al., 2001). When biotite-bearing metaluminous felsic rocks are melted, they can also develop (Miller and Thomas, 1985). Different source rocks provided the composition field of partial melts (Wolf and Willie, 1994).

Geochemical characteristics, especially Nb–Ta (HFSE) depletions relative to LILE, indicated that these granitoids were emplaced in a convergent-margin setting or derived from a source previously affected by subduction. The granites were deposited in a convergent-margin environment at the time of the Pan-African orogeny, according to the regional setting and chemistry.

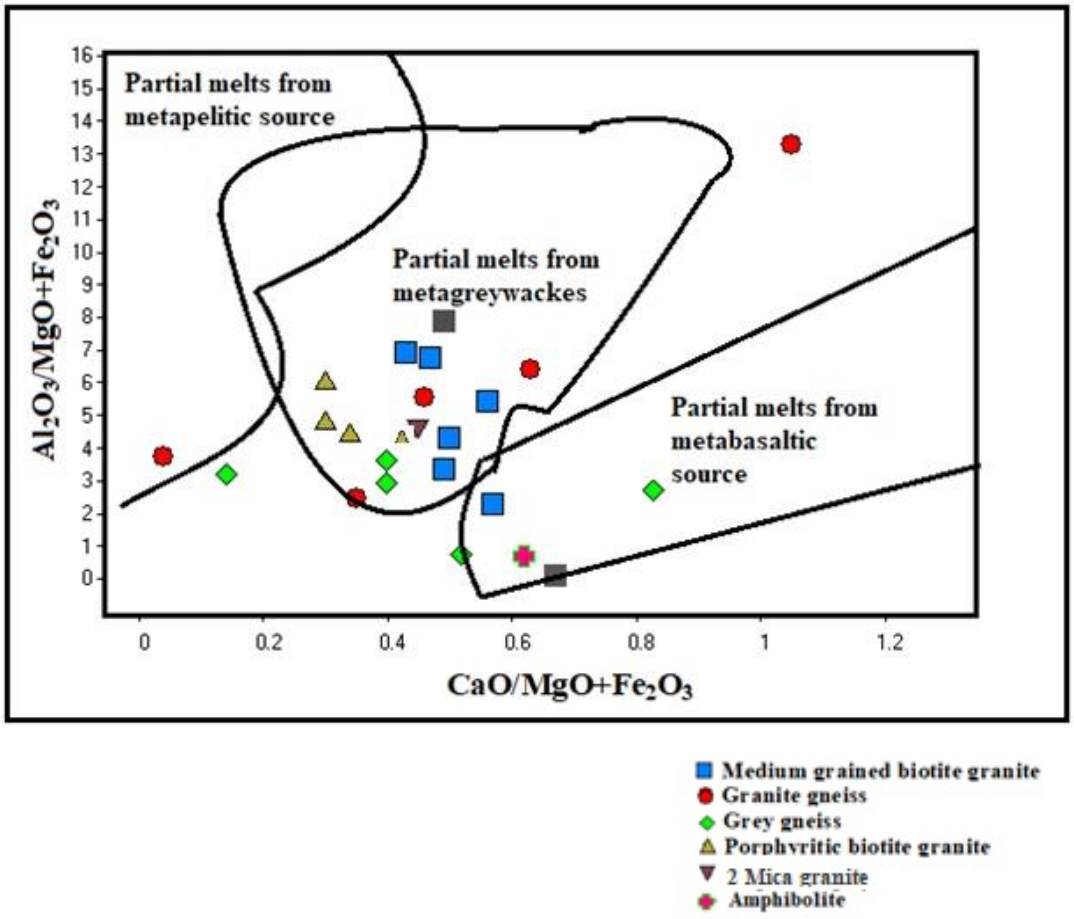

Fig. 4. 72 Chemical composition of the Al2O3/ (MgO + Fe2O3) vs CaO/(MgO +Fe2O3) (after Altherr et al 2000).

Harker diagram of the composition of major element showed an evolutionary trend as seen in the Figures 4.73 a-h, showing a negative correlation of most oxides with SiO_2 except Na_2O and P_2O_5 which showed roughly scattered patterns indicative of major element mobility during metamorphism while K_2O showed a partially positive correlation. With increasing SiO2 content, all of the main element compositions seemed to decrease and displayed a mild to high-K affinity. The general decrease in Fe_2O3 and MgO suggests that mafic minerals like biotite were highly fractionated.

Figures 4.73 a-h demonstrated an evolutionary trend in major element composition, with a negative association with SiO_2 except for Na_2O and K_2O, which displayed approximately dispersed trends suggestive of major element mobility during metamorphism. With the SiO_2 content, all of the major element compositions seemed to decrease and indicated medium to high-K affinity. The overall decrease in Fe_2O_3 and MgO suggested that mafic minerals like biotite were highly fractionated. The Harker diagrams (Fig. 4.73 a–h) showed the variations of SiO_2 with other major elements.

Generally, Fe_2O_3, TiO_2, and P_2O_5 all had a consistent negative correlation with SiO_2. SiO_2 also had a negative correlation with CaO and, to a lesser degree, MgO. In contrast, K_2O and Na_2O exhibited a lot of scatter, which indicated main elements mobility during metamorphism. Large ion lithophile elements (LILE) like Rb, Th, and to a lesser degree Ba showed a weak correlation with SiO_2, suggesting that metamorphism had altered their original contents (Fig. 4.74 a–h). Zr represents high field strength elements (HFSE), which displayed linear coherent patterns.

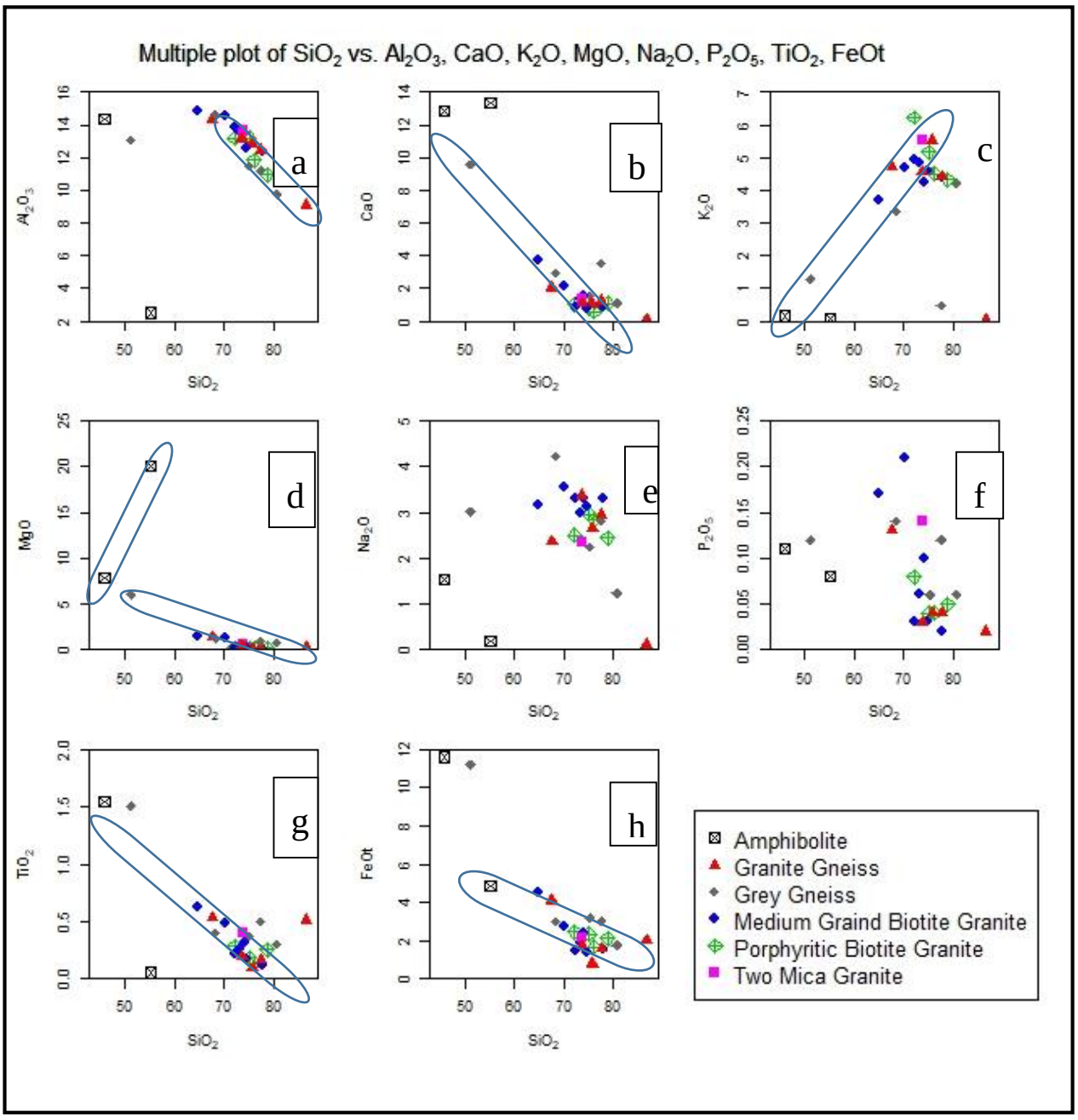

Fig. 4. 73 a - h: Harker Variation diagrams showing variations of major element oxides with silica for all the rock samples.

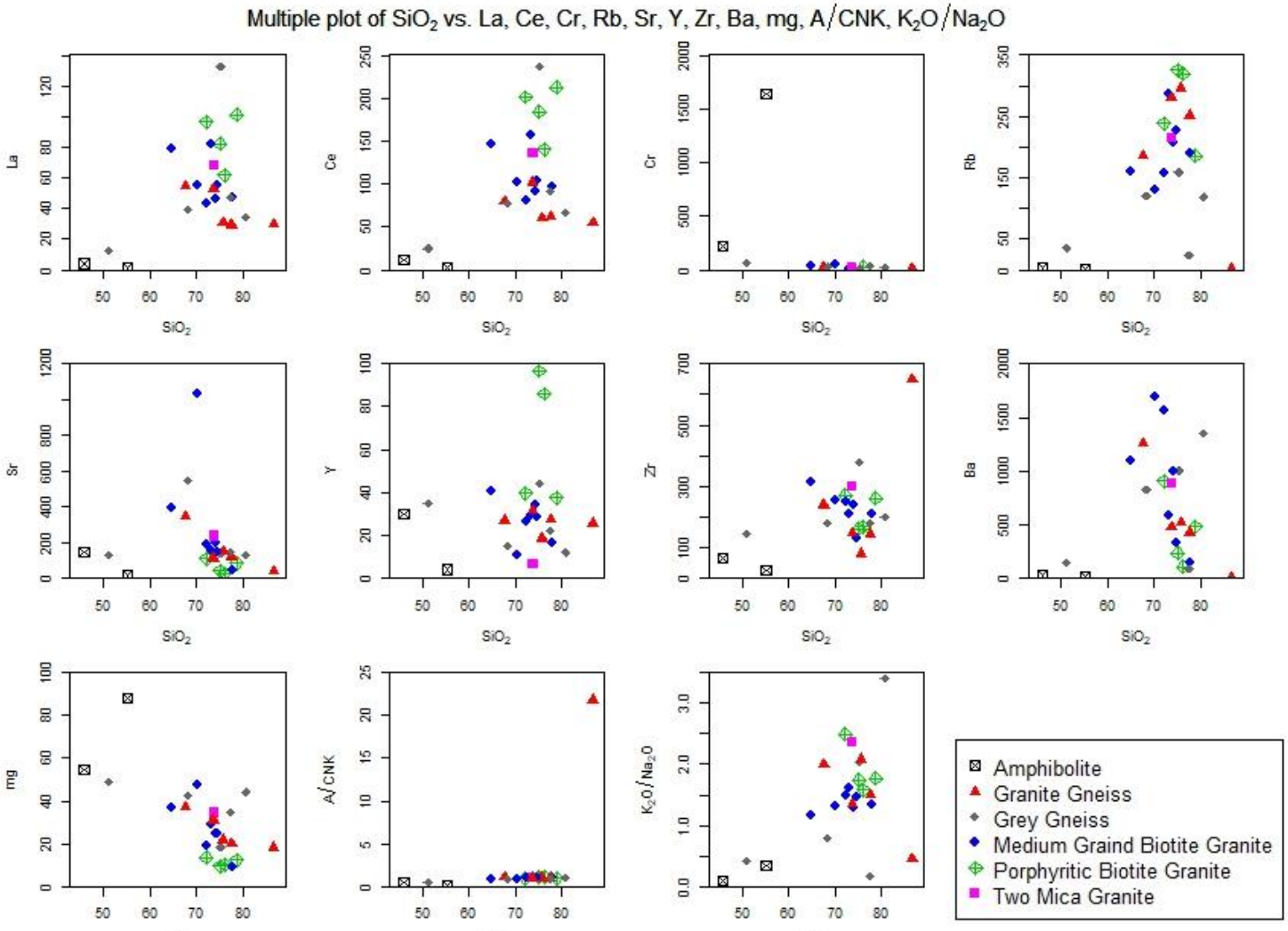

Fig. 4. 74 a - h: Harker Variation diagrams showing variations of trace element oxides with silica for all the rock samples.

All of the samples are S-type compositions and of high-K calcalkaline, except the grey gneisses that are metaluminous. The granites were derived from a mixture of crustal sources that were previously deposited in a continental convergent plate environment, based on these basic compositional properties (Barbarin, 1999). Felsic continental crust is characterized by fractionated REE and incompatible multi element patterns observed in granitoids and felsic metavolcanic rocks. The Eu-anomalies in the chondrite-normalised REE diagrams indicated to a crustal origin or plagioclase-depleted fractionation during magmatic seperation. There seemed to be no Eu-anomaly in the chondrite-normalised REE patterns of amphibolites, though HREE is somewhat more enriched than LREE. The trend is identical to MORB that was been enriched or that was contaminated with continental crust (Katongo et al 2004).

4.11.5 Geotectonic Setting

Tectonic activity is directly or indirectly associated with the generation of granitic liquid, these relationships can be due to extensional or compressional movement of the earth, this has a close relationship between the granite type and their tectonic setting. Streckeisen, (1970); Pearce et al. (1984) and other scholars have over the years, addressed the strong association between granite varieties and tectonic settings. Fyfe (1988) went on to elucidate the apparent clear relation between tectonic setting and granite generation, which he believes occurs by collision mechanisms or crustal thickening, which he believes provides an appropriate mechanism in crustal melting for massive granite bodies with continental crust chemistry and isotope systems.

According to intrusive settings, Pears et al. (1984) classified varying groups of granite into Four main classes as follows: ocean ridge granites (ORG), volcanic arc granites (VAG), within-plate granites (WPG) and collision granites (COLG). Within each group, these granites can be further subdivided based on their specific settings and petrological characteristics.

The ocean ridge granite group generally includes only granitic rocks that are either part of the oceanic crust or part of layered ophiolite sequences. Based on the chemistry of their

associated basalts, the ORG rocks can be subgrouped further into subduction-related and subduction unrelated on tectonic requirements and further into normal, anomalous and supra-subduction zone (SSZ). Tholeiitic through calcalkaline to shoshonite affinities are common in Volcanic arc granites, which have a subduction-related origin. Those of the tholeiitic series anr among these rocks, although the calc-alkaline rocks are more common. The VAG rocks can be divided into intra-oceanic and intra-continental groups based on tectonic parameters. Depending on the kind of crust into which they were intruded, within-plate granites can be categorized as intra-oceanic, intra-continental, or attenuated continental lithosphere. The kind of collision (continent-continent, continent-arc, arc-arc) and the time gap between the primary deformation event and the collision are used to classify collision granites tectonically (syn-collision, post-collision). Harris et al. (1986) defined four distinct types of intrusions, each of which corresponds to a distinct stage in the tectonic evolution of a collision zone.

i. i. Pre-collision calc-alkaline (volcanic-arc) intrusions, which are marked by preferential enrichments in LIL elements and are often formed from mantle altered by a subduction component.
ii. ii. Syn-collision peraluminous intrusions (leucogranites), which are characterized by strong Rb/Zr, Ta/Nb, and low K/Rb ratios and may be derived from the hydrated bases of continental thrust sheets.
iii. Late or post-collision calc-alkaline intrusions that may have come from the mantle but have been heavily contaminated by the crust and can only be differentiated from volcanic-arc intrusions by their higher Ta/Hf and Ta/Zr ratios.
iv. Post-collision alkaline intrusions originating from mantle lithosphere under collision zones and containing elevated concentrations of both LIL and HFS elements. (Harris e tal 1986).

To understand the tectonic setting of the study area, the four key diagrams viz. Yb+Ta-Rb, Yb-Ta, Nb- Y and Rb-Nb+Y were plotted after Pearce et al (1984), for the grey and granite gneisses alongside other granitoids Fig. 4.75, while plots of Rr-Nb-Y and FeO-MgO-Al_2O_3

in a discrimination diagram were for amphibolites Fig. 4.78 and 4.79. The granite gneisses generally plotted in the VAG field in the Rb-Y+Nb, Ta-Yb diagrams Fig. 4.75 a, d, and plot in VAG + Syn-COLG field in the Nb-Y plotted Fig. 4.75 b, while in the Yb+Ta vs Rb plot Figure 4.108 c, they fell in Syn-COLG. This might have suggesed a generally pre-collision environment to the early phase of syn-collision stage of the plates. When found in calc-alkaline arcs, VAG-setting granites tend to fall into the quartz diorite, quartz monzonite, tonalite, and granodiorite fields of the Streckeisen diagram. These granites are distinguished by the presence of hornblende and biotite as their distinctive ferromagnesian minerals (Pearce et al., 1984). This is similar to the grey gneisses from the study area as observed from the petrographic study and their geochemical classification.

The medium –grained biotite granite samples also plotted generally in the VAG field in all plots except in the Rb/Ta + Yb plot where 45% of the samples plotted in the VAG and the other 55% plot in syn-COLG, also suggesting same tectonic environment as the granite gneisses (Fig. 4.77 c). While the porphyritic -biotite granite plotted in the within -plate environment for all four plots which might have suggested a late to post tectonic setting and the two-mica granite plotted in the syn-COLG field. The grey gneisses plotted generally in the VAG field in all the plots, with one sample falling in WPG in all the plots, this is also consistent with the setting of other granitoids (Fig. 4.75 a-d). According to Pearce et al. (1984), syn-tectonic granites, usually plot within the granite area on the Streckeisen diagram, and are muscovite-bearing yet peraluminous, and have much of the characteristics of S-type granites. This was also a similar characteristic exhibited by the granite samples from the study area as described in their chemical classification and petrography as presented in Figures 4.55 and 4.68. Although post-tectonic granites primarily contain biotite ± and hornblende as ferromagnesian minerals, they are calc-alkalic, metaluminous to mildly peraluminous, and exhibit much of the characteristics of I-type granites, they also plot in the same portion as VAG on the Strechesen diagram according to Pearce et al (1984).

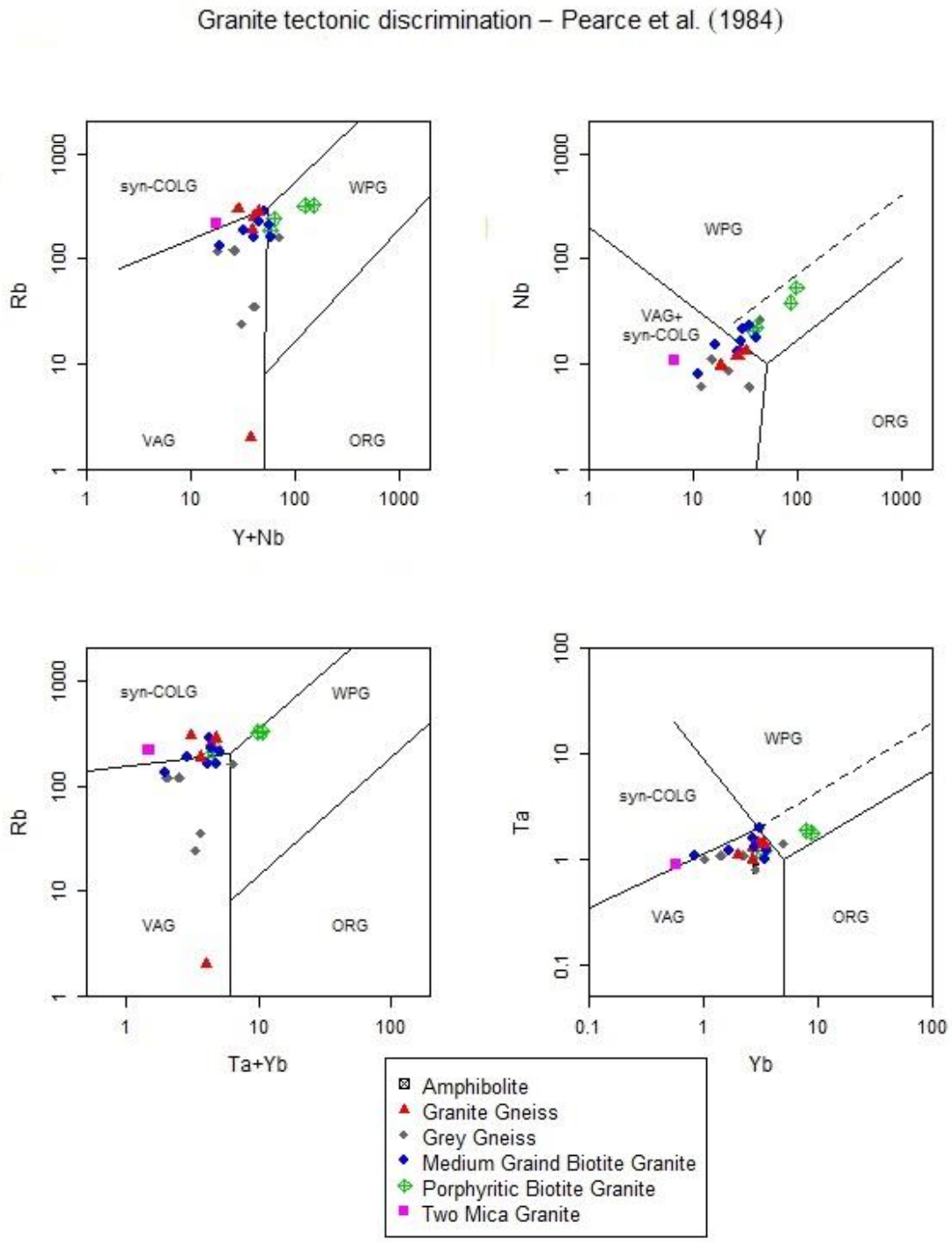

Fig. 4. 43 Plot of tectonic setting for grey gneisses, granite gneisses and the other granitoids of the study area after Pearce etal (1984)

On the other hand, the Zr-Nb-Y discrimination diagram for the amphibolites after (Meschede, 1986, Bolarinwa 2017) revealed the tectonic setting of the amphibolites as N-type MORB, Within-plate theoleiites and volcanic-arc basalts (Fig. 4.76). The discrimination diagrame of FeO – MgO - Al_2O_3 after Pearce et al., (1977) and Bolarinwa (2017) indicated that most of the samples fell within the Ocean Island basalt and Ocean ridge and floor which is equivalent to Mid oceanic ridge basalt (MORB) (Fig. 4.77).

Figure 4.75 shows Syn-COLG= syn-collision granite, post-COLG=post-collision granite, WPG= within-plate granites, VAG= volcanic-arc granites and ORG= ocean ridge granite (after Pearce et al., 1984).

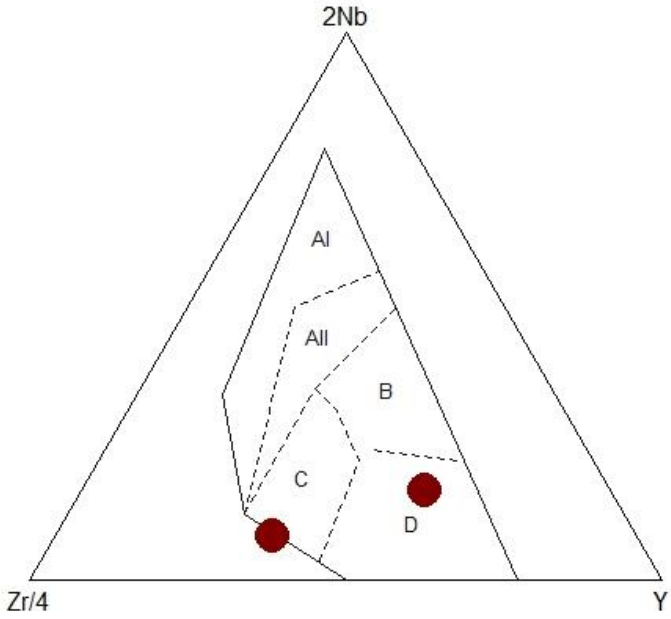

A1: Within-plate alkali basalts, A2: Within-plate alkali basalts and within-plate tholeiites, B: E-type MORB, C: Within-plate tholeiites and volcanic-arc basalts, D: N-type MORB and volcanic-arc basalts.

Fig. 4. 76: Zr-Nb-Y discrimination diagram for basalt (after Meschede 1996),

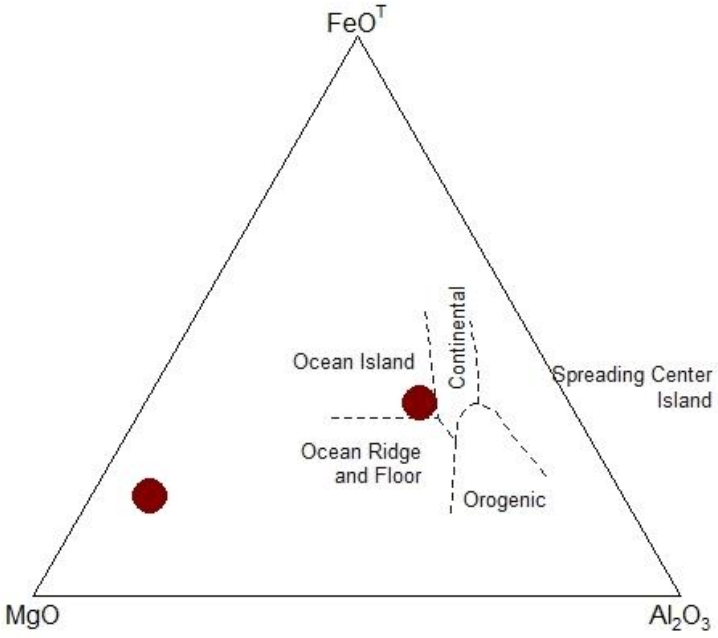

Spreading Center Island=Continental Basalts, Orogenic=Island arc theoleitic, Ocean ridge and floor=MORB- Mid-oceanic ridge basalts, Ocean Island=Ocean Island basalt, Continental =Within plate basalts

Fig. 4.77: Discrimination diagram of FeO-MgO-Al_2O_3 of amphibolite samples, (Pearce et al 1977).

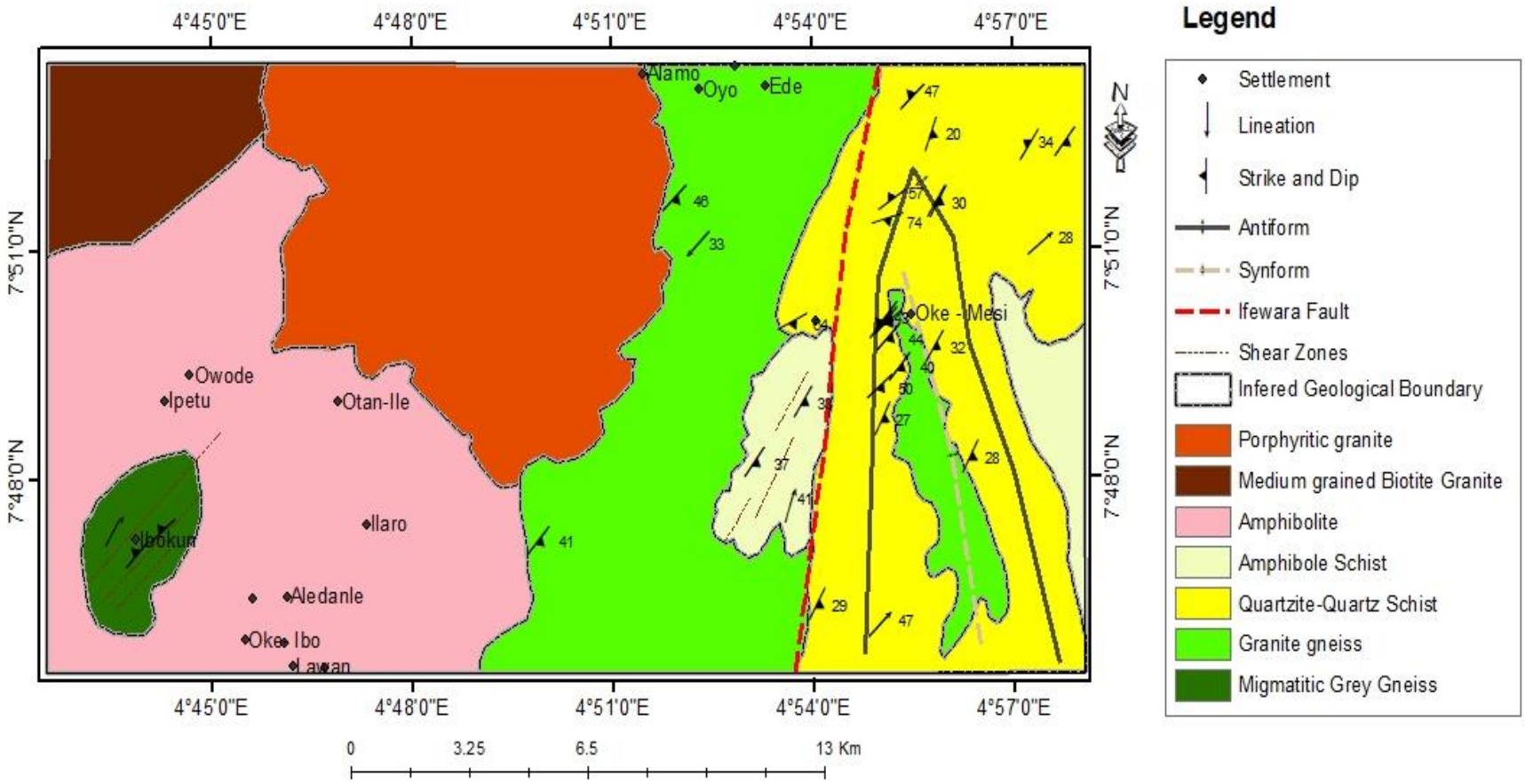

Fig. 4. 78 Detailed Structural Geological Map of Sampling Area A

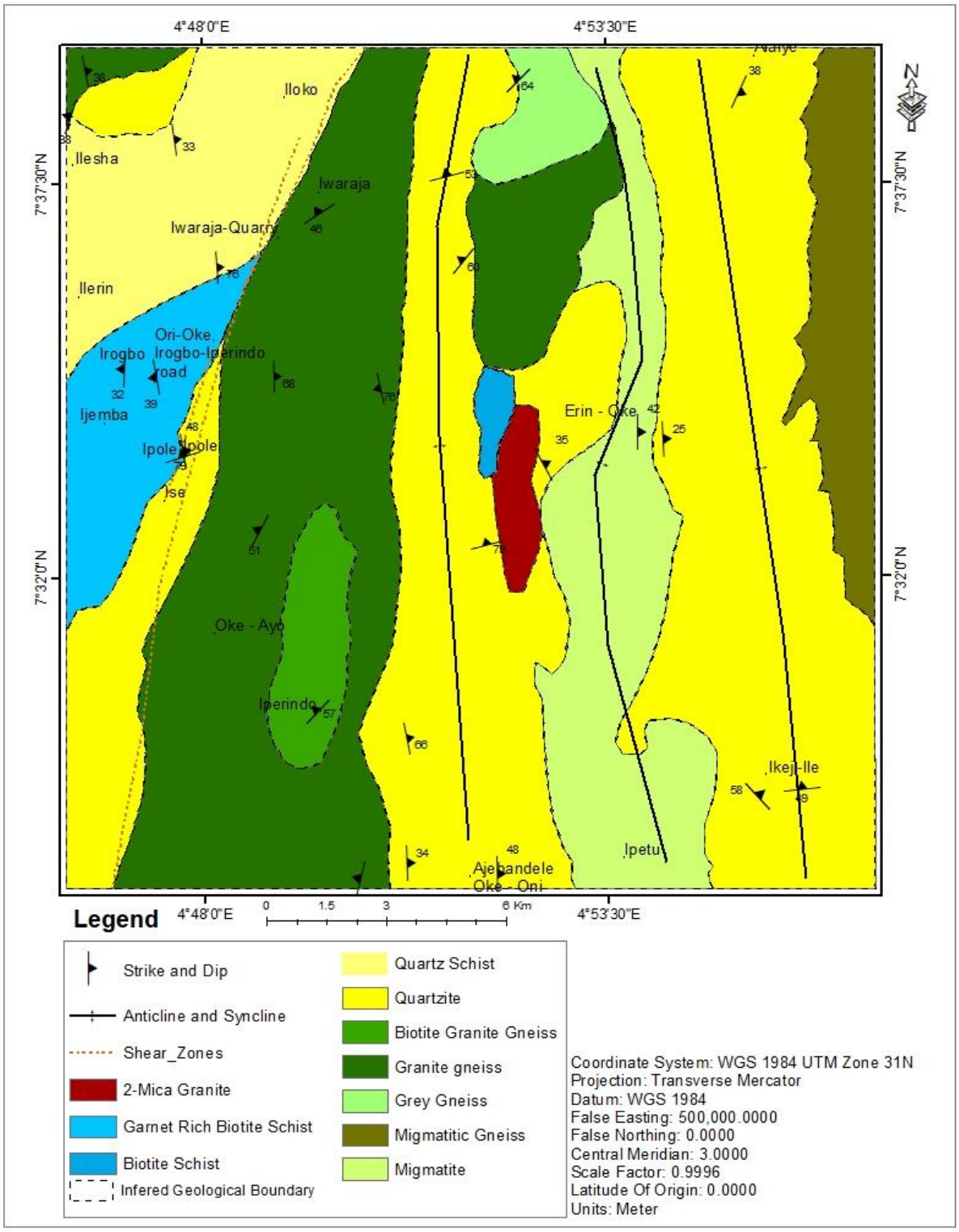

Fig. 4. 79 Detailed Structural Geological map of Sampling Area B

CHAPTER FIVE

SUMMARY AND CONCLUSION

Okemesi-Iwaraja area is underlain by Quartzite, Quartz schist, Migmatitic Grey Gneiss, Grey Gneiss, Granite Gneiss, Two Mica granite, Biotite schist, Medium grained biotite granite, Porphyritic Biotite granite and Amphibolites. The Quartzites outcroped as hilly bodies and were underlain by the granite gneisses. The medium grained biotite granite occupied the north eastern part of Okemesi – Iwaraja area. While the porphyritic biotite granite was found in the north central portion of sampling area A, and around north central portion, along Okemesi – Imesi-ile road and Okemesi town. Observations suggest the quartzites have undergone high temperature and brittle deformations. lineation in muscovite suggested the readjustment of minerals during metamorphism. The area has undergone high grade metamorphism and weathering on the rocks. The mineralogical assemblages of these rocks were quartz, micas (muscovite and biotite), chlorite, sillimanite, garnet for the quartzites; quartz, muscovites, biotite, chlorite for the biotite schist and quartz, biotite, microcline, perthite, sericite for the granites.

The lineaments showed that the dominant orientation is NE-SW with (56.87%) lineaments; other orientations were NNE-SSW with 36 (17.06%) lineaments, NW-SE with 47 (22.27%) and E-W with 8 (3.791%) and N – S. Dominance of the NE-SW lineaments suggested widespread effect of the Pan- African Orogeny within the study area. According to Ike (1988), the NE-SW lineaments developed along pure shear axis perpendicular to the maximum principal stress.

The E-W collision of the West African Craton with the Congo Craton's westward advancing plate resulted in N-S to NE-SW trending structures parallel to the West African Craton's tip (Black et al., 1979, Egesi and Ukaegbu, 2010). The regional influence of these motions is mirrored in the Nigerian Basement Complex as a deeply deformed sequence of

multidirectional orientations observed in folds, lineaments, faults, and joints (McCurry, 1976, Toteu et al., 1990). Joints served as palaeostress identifiers, recording the direction of tension at the time of propagation (Dyer, 1983; Pollard and Segall, 1980).

The study area was subjected to two episodes of deformation (D1 and D2). The D1 phase was associated with the development of an S1 schistosity and an F1 minor asymmetrical fold, the nature of its asymmetry suggested a non-coaxial deformation. The D2 tectonic phase is associated with an S2 crenulation cleavage and an F2 tight to isoclinal fold. The intensity of folding increased with time as D2 was more intense and occurred majorly on the quartzite rock units, while D1 was moderately intense with asymmetrical minor folds geometry and mostly occurred on the Biotite schist. The major folding associated with the second phase of deformation is similar in style and orientation to the major folding events recognized as F2 in other parts of Nigerian Basement Complex rocks (McCurry, 1973; Grant, 1978; Danbatta, 1991; 2002; 2003) while the trend and plunge of the fold axis were dominantly NE, suggesting an E-W compression, which is expressed in the surface lineaments and the subsurface structures.

The findings of geochemical (major, trace elements, and REE) research on rock samples from the study area (sampling Areas A & B) revealed that all of these crystalline rocks were genetically related (comagmatic) and formed by progressive differentiation of a parent basaltic magma to give rise to amphibolite protoliths. Chemical analysis showed that the magma of these rocks' protoliths came from a metasomatized mantle. Mineral alteration of perthite to sericite in the granitoids and the calculated Chemical Index of Alteration (49.71 – 62.11) for granites, indicated onset of weathering. The granitoids were relatively potassic K_2O (3.34 – 6.23), and classified as high-K calc-alkaline, with high SiO_2 composition of 64.83–86.63wt% and molar A/CNK (1.18-2.75) suggesting strong peraluminous, S-type granite. The grey gneisses were however metaluminous and mostly Granodioritic to Quartz Monzodiorite, the granite gneisses are mostly Monzogranitic, and the other granitoids are mostly Monzogranite except the two-mica granite that is Syenogranitic to Quartz Syenite. While The light REE enrichment and depleted heavy REE with negative Eu anomaly in the granitoids, as revealed by spider plots, confirmed a felsic crustal origin. Plots of Rb/Y+N

and Rb/Ta+Yb revealed, the tectonic environments were mainly post collision and within plate granite settings.

The tectonics, petrology, geology, as well as geochemistry studies and interpretations carried out in the Okemesi-Iwaraja area pointed to a back arc tectonic setting as the emplacement environment for these rocks. In this kind of tectonic environment, an ocean slab collided with a continental shelf and was subducted into the mantle. This magma extruded and intruded previously deposited sediments in southwestern Nigeria, separating and giving rise to the protoliths of these crystalline rocks.

RECOMMENDATIONS

Further detailed studies to better understand the geotectonic evolution of the entire Ilesha Schist Belt should be undertaken to correlate its structural geometry, age and mineralogical composition with other schist belts within the Nigerian Basement Complex.

Other strain analytical techniques should be employed to further improve our understanding of the deformation patterns of the Ilesha Schist Belt.

CONTRIBUTION TO KNOWLEDGE

The following are the contributions of this study to knowledge

i. The lineament maps of the area were produced

ii. The structural and metamorphic history of Okemesi-Iwaraja area was documented

iii. The relationship between the grey gneisses of Okemesi-Iwaraja area and tonalic grey gneisses and TTG from other parts of the world was etablished

iv Relationship between subsurface and surface structures was also established

v. Depths to magnetic structures within Okemesi- Iwaraja areas were determined

vi. The geotectonic setting, the origin of the rocks and their chemical classifications were determined.

vii. Shear zones were identified from petrographic studies.

REFERENCES

Abdel-Rahman, A. M., (1994). Nature of biotites from alkaline, calcalkaline and peraluminous magmas. Journal of Petrology, 35, 525–541.

Abdus-Salam M. O., Bolarinwa, A. T., Olatunji, A. S., and Omotunde, V., (2020). Geochemical Characteristics of Amphibolites in Parts of Iseyin-Oyan Schist Belt, Southwestern Nigeria. European Journal of Environment and Earth Sciences Vol 1 | Issue 5 | October 2020 www.ej-geo.org.

Abiye TA, Tigistu H (2008). Geophysical exploration of the Boku geothermal area, Central Ethiopian Rift. Geothermics, 37(6):586-596.

Abrams, M., (2000). "The Advanced Spaceborne Thermal Emission and Reflection Radiometer (ASTER): Data Products for the High Spatial Resolution Imager on NASA's Terra Platform." *International Journal of Remote Sensing* 21 (5): 847–859. doi:10.1080/014311600210326.

Adeoti, B., (2015). Structural evolution of the basement complex rocks in Iwaraja area, southwestern Nigeria. unpublished master of technology thesis, Federal University of Technology, Akure,

Adeoti, B., and Okonkwo, C. T. (2017). Structural evolution of Iwaraja shear zone, southwestern Nigeria, *Journal of African Earth Sciences*, 131, 117-127. doi: 10.1016/j.jafrearsci.2017.04.008.

Adetunji, A., Olarewaju, V.O., Ocan, O.O., Macheva, L., Ganev, V.Y., (2018). Geochemistry and U-Pb zircon geochronology of Iwo quartz potassic syenite, southwestern Nigeria: Constraints on petrogenesis, timing of deformation and terrane amalgamation. Precambrian Research (2018), doi: https://doi.org/10.1016/ j. precamres. 2018.01.015.

Adepitan, J. O., Falayi, E. O. and Ogunsanwo, F.O., (2017). Confirmation of Climate Change in Southwestern Nigeria through Analysis of Rainfall and

Temperature Variations over the Region, Covenant Journal of Physical & Life Sciences (CJPL) Vol. 5 No. 1, June 2017.

Ajayi, T. R., (1980). On the geochemistry and origin of the amphibolites in Ife-Ilesha area, SW Nigeria. *Journal of Mining and Geology*, *17*(2), 179-196.

Ajayi, T. R., (1981). Statistical analysis of stream sediment data from the Ife-Ilesha area of southwest Nigeria Journal of Geochemical Exploration 15 (1-3), 539-548

Ajibade, A.C., (1980). Geotectonic evolution of the Zungeru region, Nigeria. Unpublihed Ph.D. Thesis, University Wales, Aberystwyth, 320p.

Ajibade, A.C., (1982). The Origin of Older Granite of Nigeria: some evidence from the Zungeru region, Nigeria. *Journal of mining and Geology*, 19(1), 223-230.

Ajibade, A.C., Woakes, M., and Rahaman, M.A., (1987). Proterozoic crustal development in the Pan-African regime of Nigeria. In: A. Krooner (Editor), Proterozoic Crustal Evolution. Geodyn. Ser., Am. Geophysics Union, 17: pp259-271.

Ajibade, A.C., Rahman, M.A., Ogezi, A.E.O., (1988). The Precambrian of Nigeria: a geochronological summary. In: Oluyide P.O., et *al.* (Eds.), Precambrian Geology of Nigeria.

Ajibade, A.C., and Wright, J.B., (1989). The Togo-Benin-Nigeria shield: evidence of crustal aggregation in the Pan-African belt. Tectonophys 165, pp. 125-12.

Ako, B.D., Ajayi T.R., and Alabi., A.O., (1978). A geo-electrical study of ife-wara area. Journal of Mining Geology 15, 84-89.

Altherr, R., Holl, A., Hegner, E., Langer, C., & Kreuzer, H. (2000). High-potassium, calc-alkaline I-type plutonism in the European Variscides: Northern Vosges (France) and northern Schwarzwald (Germany) Lithos,50,51–73.

AlSaud, M.M., (2008). Structural mapping from high resolution aeromagnetic data in west central Arabian Shield, Saudi Arabia using normalized derivatives. *Arab J Geosci* **1,** 129–136 (2008). https://doi.org/10.1007/s12517-008-0012-2.

Anifowose, A.Y.B., (2004). Remote sensing analysis of Ifewara-Zungeru Megalinear in Nigeria. PhD thesis, Federal University of Technology, Akure, Nigeria, 169p

Anifowose, A. Y. B., Borode A. M., (2007). Photogeological study of the fold structure in Okemesi area, southwestern Nigeria. *Journal of Mining and Geology*, 43 (2), 125-130

Anifowose, A.Y.B., Odeyemi, I.B. and Borode, A.M., (2006). The tectonic significance of the Ifewara-Zungeru Megalinear in Nigeria. Proceedings of the 1st international workshop on Geodesy and Geodynamics, centre for Geodesy and Geodynamics, Toro, Bauchi State, Nigeria.

Annor A. E., (1995). U-Pb Zircon age for Kabba-Okene granodiorite gneiss: Implication for Nigeria's Basement Chronology. Africa Rev 2: 101-105.

Annor, A.E. & Freeth, S.J., (1985). Thermo-tectonic evolution of the basement complex around Okene, Nigeria, with special reference to deformation mechanism. Precambrian Research 28, 269-281.

Arthaud, M. H., Caby, R., Fuck, R. A., Dantas, E. L., and Parente, C. V., (2008). Geology of Northern Borborema Province, NE Brazil and its correlation with Nigeria, NW Africa. Geological Society; London, Special Publications. V.294; p. 49-67.

Ball. E., (1980). An example of very consistent brittle deformation over a wide intracontinental area: the late Pan-African Fracture Systems of the Tuareq and Shield. Tectonophysics 61(4). pp363-379.

Balogun, O. B., (2019). Tectonic and structural analysis of the Migmatite–Gneiss–Quartzite complex of Ilorin area from aeromagnetic data. NRIAG Journal of Astronomy and Geophysics Volume 8, 2019 - Issue 1

Barbarin, B., (1999). A review of the relationships between granitoid types, their origins and their geodynamic environments. Lithos, 46, 605-626. http://dx.doi.org/10.1016/S0024-4937(98)00085-1

Barriere, M., and Cotton, J., (1979). Biotites and associated minerals as markers of magmatic fractionationand deuteric equilibration in granites. Contr. Miner. Petrol 70 183-92

Benomar, T. B., Fuling, B., (2005). Improved geological mapping using landsat-5 TM data in Weixi area, Yunnan province China. Geo-spatial Information Science, June 2005, Volume 8, Issue 2, pp 110–114

Black, R., Ball, E., Bertrand, J. M., Boullier, A.M., Caby, R., Davison, I., Fabre, J., Leblanc, M., and Wright, L.I., (1979). Outline of the Pan-African Geology of Adrar des Iforas (Republic of Mali), Band 68, Heft 2, seite pp543-564. xi .

Black, R., Latouche, L., Liegeois, J.-P., Caby, R., Bertrand, J.M., (1994). Pan African displaced terranes in the Tuareg shield (central Sahara). Geology 22, 641-644.

Boesse, J. M., and Ocan, O.O., (1988): Geology and evolution of the Ife-Ilesa schist belt, southwestern Nigeria. International meeting on proterozoic geology and tectonics of high grade terrains. Obafemi Awolowo University. Pp26.

Boesse, J.M., Ocan, O.O., Rahaman, M.A., (1989). Lithology and the structure of the Ife-Ilesha area (abstract), 25th Annual Conf. Nig. Mining and Geosc. Soc. (1989) 6-7.

Bolarinwa, A. T., & Adepoju, A. A., (2017). Geochemical Characteristics and Tectonic Setting of Amphibolites in Ifewara Area, Ife-Ilesha Schist Belt, Southwestern Nigeria. Published by Canadian Center of Science and Education, Earth Science Research; Vol. 6, No. 1; 2017 ISSN 1927-0542 E-ISSN 1927-0550.

Boynton, W.V. (1984) Geochemistry of Rare Earth Elements: Meteorite Studies. In: Henderson, P., Ed., Rare Earth Element Geochemistry, Elsevier, New York, 63-114. http://dx.doi.org/10.1016/B978-0-444-42148-7.50008-3

Caby, R., (1989). Precambrian terranes of Benin-Nigeria and northeast Brazil and the Late Proterozoic south Atlantic fit- Geol. Soc. Am. Spec. pap. 230: pp145 – 158.

Caby, R., and Boesse, J.M., (2001). Pan-African nappe system in southwest Nigeria: the Ife Ilesha schist belt. *Journal African Earth Sciences* 33, pp211-225.

Campbell, G., Lubkowski, Z., Villani, M., Polidoro, B., (2018) A Seismic source model for West Africa. 16th European conference on earthquake engineering, Thessaloniki, 16–18 June 2018

Chappell, B. W., (1999). Aluminium saturation in I- and S-type granites and the characterization of fractionated haplogranites. Lithos 46, 535-551.

Chappell, B.W., White, A.J.R., (1974). Two contrasting granite types. Pacific Geology 8: 173-174.

Casas, A.M., Cortes, A.L., Maestro, A., Soriano, M.A., Riaguas, A., and Bernal, J. (2000), "A program for lineament length and density analysis", Computers and Geosciences, Vol. 26, No. 9/10, 1011-1022.

Chinedu, U. I., Smart, C. O., (2019). Geochemical characterization of Granitoids in Katchuan Irruan area: further evidence for peraluminous and shoshonitic compositions and post-collisional setting of granitic rocks in the Precambrian Basement Complex of Nigeria. Science Press and Institute of Geochemistry, CAS and Springer-Verlag GmbH Germany, part of Springer Nature 2019

Chukwu, A. and Obiora, S. C., (2021). Petrogenetic characterization of pegmatites and their host rocks in southern Akwanga, North-Central Basement Complex, Nigeria. J. Earth Syst. Sci. (2021) 130:18

Condie, K. C., and Des Marais, D. J., (1999), Black shales and paleoweathering: Response to mantle plume events and the supercontinent cycle, *Geol. Soc. Am. Abstr. Programs*, 31(7), A-325.

Cordell, I., Grauch, V.J.S., (1985). Mapping basement magnetisation zones from aeromagnetic data in the San Juan basin, New Mexico. In: Hinze, W.J. (Ed.),

The Utility of Regional Gravity and Magnetic Anomaly Maps: Soc. Expl. Geophys, pp. 181e197.

Cox, K. G., Bell, J. D., & Pankhurst, R. J. (1979). *The interpretation of igneous rocks.* George Allen and Unwin, London.

Dada, S.S., (1998). Crust-forming ages and Proterozoic crustal evolution in Nigeria: a reappraisal of current Interpretations. Precambrian Research 87, 65-74.

Dada, S.S. (2006) Proterozoic Evolution of Nigeria. In: Oshi, O., Ed., The Basement Complex of Nigeria and Its Mineral Resources (A Tribute to Prof. M. A. O. Rahaman), Akin Jinad & Co., Ibadan, 29-44.

Dada, S.S., Birck, J.L., Lancelot, J.R., and Rahaman M.A., (1993). Archaean migmatite-gneiss complex of Northcentral Nigeria: its geochemistry, petrogenesis and evolution. *International Colloquim on African Geology, Mbabane, Swaziland* (1), pp 97-102.

Dada, S.S., Lancelot, J.R.. Briqueu, I., (1989). Age and origin of the annular charnockitic complex at Toro, Northern Nigeria: U-Pb and Rb-Sr evidence. Journal African Earth Sciences 9, 227-234.

Dada, S.S., Respaut. J.P., (1989). La monzonite 8 fayalite de Bauchi (bauchltel: nouveau ternoh d'un magmatisme syntectonique pan-africain au nord du Nigeria. Comptes Rendus Academic Sciences Paris 309, 887-892.

Danbatta, U.A., (1991). Geologic investigations of the SW portion of the Zuru schist belt, NW Nigeria. Unpublished M.Sc. Thesis, A.B.U. Zaria, 150p.

Danbatta, U.A., (2002). Rb-Sr Isochron Dating of Granitoids from the Kazaure Schist Belt, NW Nigeria. Global *Journal of Pure and Applied Sciences* 8(3), pp319-322.

Danbatta, U.A., (2003). The tectonic significance of the NNE continuation of the Kalangai fault zone into the Kazaure schist belt of northwest Nigeria: Scientia Africana. Vol.2 (1&2): pp. 17-25. xii

De Swardt, A.M.J., (1947). The Ife-Ilesa gold field. (Interim report no. 2). Geological Survey of Nigeria Annu. Rep. pp. 14-19.

De Swardt, A. M. J., (1953). The geology of the country around Ilesha. **(**Lagos) : Government Printer, Bulletin (Geological Survey of Nigeria), no. 23

Dyer, J.R., (1983). Jointing in sandstones, Arches National Park, Utah. Unpublished PhD. Dissertation, Stanford University.

Egbuniwe, I.G., (1982). Geotectonic Evolution of the Maru Belt NW Nigeria, Unpublished PhD Thesis, University of Wales, Aberrystwyth, 411p.

Egesi, N., and Ukaegbu, V. U., (2010). "Petrologic and Structural Characteristics of the Basement Units of Bansara Area, South-eastern Nigeria". Pacific *Journal of Science and Technology*. 11(1): pp510-525.

Elueze, A.A., (1977). Geology and geochemical studies in the Ilesha gold belt. Thesis, University of Ibadan (unpubl.).

Elueze, A.A., (1981). Petrography and geochemistry of metasedimentary rocks of the schist belt of Ilesha area, Southwestern Nigeria, *Journal of Nigeria Mining and Geosciences Society*, Vol(18): pp5-7.

Elueze, A.A., (1985). Petrochemical and petrogenetic characteristics of Precambrian amphibolites of the Alawa District, NW Nigeria. Chem. Geol. 48, pp. 29-41.

Elueze, A.A., (1986). Geology of the precambrian Nigeria. Geological Surv. Nig. 22(4): 77-82.

Elueze, A.A., (1992). Rift system for Proterozoic schist belts in Nigeria. Tectonophysics, 209: pp167 – 169.

El Bouseily, A.M., and El Sokkary, A.A., (1975) The relation between Rb, Ba and Sr in granitic rocks [J]. *Chem. Geol.* **16**, 207–219

Fagbohun, B. J., Adeoti, B., Aladejana, O. O., (2017). Litho-structural analysis of eastern part of Ilesha schist belt, Southwestern Nigeria. Journal of African Earth Sciences, Volume 133, p. 123-137.

Falconer, J.D., (1911). The geology and geography of northern Nigeria. Macmillian, London.

Ferre, E. C., Caby, R., Moni&, P., Peucat, J.J., (1998). Pan-African, post-collisjonal, A2 type alkaline granite and monronite plutons of Eastern Nigeria. Lithos 45, 225-279.

Ferré, E. C, Gleizes, G., Caby, R. (2002). Obliquely convergent tectonics and granite emplacement in the Trans-Saharan belt of Eastern Nigeria: a synthesis. *Precambrian Research*, 144, 199–219

Fitches, W. R., Ajibade, A.C., Egbuniwe, L.G., Holt, R.W., and Wright, J.B., (1985). Late Proterozoic schist belts and plutonism in NW Nigeria. *Journal of Geological Society. London,* 142: pp319-337.

Frost, B. R., Barnes, C. G., Collins, W. J., Arculus, R. J., Ellis, D. J., and Frost, C. D., (2001). "A Geochemical Classification for Granitic Rocks," *Journal of Petrology*, Vol. 42, No. 11, pp. 2033-2048. 3doi:10.1093/petrology/42.11.2033.

Frost B. R., and Frost, C.D., (2008). A Geochemical Classification for Feldspathic Igneous Rocks. Journal of Petrology Volume 49 Number 11 Pages 1955-1969, 2008.

Gad, S., & Kusky, T., (2007). ASTER spectral ratioing for lithological mapping in the Arabian-Nubian shield, the Neoproterozoic Wadi Kid area, Sinai, Egypt. Gondwana Research, 11: 326-335.

Gillepsie, A., Kahle, A., & Walker, E. R., (1987). Color enhancement of highly correlated images. II. Channel ratio and chromaticity transformation techniques. Remote sensing of Enviromnt, 22, 343-365.

Grant N.K., (1978). Structural distinction between metasedimentary cover and an underlying basement in the 600m.y. old Pan-African domain of Northwestern Nigeria, West Africa. *Geological society America Bulletin* 89, pp50-58.

Gunn, P.J., and Dentith, M.C., (1997). Magnectic response associated with mineral deposits. Article in AGSO journal of Australian geology & geophysics · January 1997.

Gupta, R. P., (1991). Remote Sensing Geology. Berlin, Heidelberg: xvi + 356 pp. Springer-Verlag.

Harris, N. B. W., Pearce, J. A., Tindle, A. G. (1986). Geochemical characteristics of collision-zone magmatism. Geological Society, London, Special Publications 1986; v. 19; p. 67-81.

Haruna, I.V., (2017). Review of the Basement Geology and Mineral Belts of Nigeria. IOSR Journal of Applied Geology and Geophysics (IOSR-JAGG) e-ISSN: 2321–0990, p-ISSN: 2321–0982.Volume 5, Issue 1 Ver. I (Jan. - Feb. 2017), PP 37-45

Huang, H., Polat, A., Fryerab, B. J., (2013). Origin of Archean tonalite–trondhjemite–granodiorite (TTG) suites and granites in the Fiskenæsset region, southern West Greenland: Implications for continental growth. Gondwana Research Volume 23, Issue 2, March 2013, Pages 452-470

Hubbard, F.H., (1975). Precambrian crustal development in western Nigeria: indications from the Iwo region. *Bulletin of the Geological Society of America*, 86, 548-554.

Ibeneme S., I., Oha, I. A., Abdulsalam, N. N., Onuoha, M. K., (2018). Improved Mapping of the Structural Disposition of Some Younger Granite Ring Complexes of Nigeria Using High Resolution Aeromagnetic Data. J Geol Geophys 7: 443. an open access journal, doi: 10.4172/23818719.1000443

Ike, E.C., (1988). Late stage geological phenomena in the Zaria basement granites. In Precambrian geology of Nigeria. Geological Survey of Nigeria publications.

Irvine T.N., Baragar W.R.A., (1971). A guide to the chemical classification of the common volcanic rocks. Canadian Journal of Earth Sciences, 8(5):523-548.

Jacobson, R., and Webb, J.S., (1946). The pegmatites of Central Nigeria. – Geological Survey of Nigeria, Bulletin No. 17: 1-61.

Jensen, J. R., (2000). Remote Sensing of the Environment: An Earth Resource Perspective, 2000, Prentice Hall, New Jersey. (Excellent on RS but no image processing).

Jensen, J. R., (2005). Introductory Digital Image Processing. Pearson Prentice Hall, Upper Saddle River.

Katongo, C., Ko¨ller, F., Koeberl, C., & Tembo, F., (2004). Geochemistry and petrography of granitoid rocks in the Neoproterozoic Lufilian–Zambezi Belt, Zambia: implications for tectonic setting. Abstracts, Geoscience Africa 2004, Johannesburg, 327-328.

Karim, A. & Hamoudi, M. (2008). Regional-scale aeromagnetic survey of the south-west of Algeria: A tool for area selection for diamond exploration. Journal of African Earth Sciences 50(2):67-78

Kayode, J.S., Nyabaze, P., Adelusi, A.O., (2010). Ground magnetic study of Ilesha east, southwestern Nigeria. African Journal of environmental science and technology. 4(3): 122-131.

Kinnaird, J. A., (1984). Contrasting styles Sn-NbZn-Ta Mineralization in Nigeria. J. Afr. Earth Sci. 2, 81-90.

Klemm, D. D., Schneider, W., Wagner, B., (1984). The Precambrian metavolcano-sedimentary sequence east of Ife and Ilesha/SW Nigeria. A Nigerian "greenstone belt"? *Journal of African Earth Sciences*, 2 (2), 161–176. doi:10.1016/S0731-7247(84)80011-7

Kogbe C. A., (1975). Geology of Nigeria. [Lagos, Nigeria: Elizabethan Pub. Co., 1975] (OCoLC)754663525.

Kroner, A., Ekwueme, B.N., Pidgeon, R.T., (2001). The oldest rocks in west Africa: SHRIMP zircon age for Early Archasan migmatitic orthognelss at Kaduna, Nonhern Nigeria. Journal Geology 109, 399-406.

Küster, D., (1990). Rare-metal pegmatites of Wamba, central Nigeria — their formation in relationship to late Pan-African granites. Miner Depos 25: 25–33.

Latouche, L., Boughrara, M., Liégeois, J.P., Navez, J., Guiraud, M., (2000). Pan-African thrust sheets and eclogites in the central Hoggar terranes, Algeria. In: Wallbrecher, E., Loizenbauer, J., Fritz, H., Unzog, W., Mogessie, A. (Eds.), 18th Colloquium of African Geology, Graz. Special Abstract Issue, Journal African Earth Sciences 30 (4A), 52.

Le Maitre, R.W., (1989). A Classification of Igneous Rocks and Glossary of Terms. Blackwell Scientific Publications, Oxford, 193 pp.

Liegeois, J.-P., Black, R., Navez, J., Latouche, L., (1994). Early and late Pan-African orogenies in the Air assembly of terranes (Tuareg shield, Niger). Precambrian Research 67. 59-88.

Liegeois, J.-P., Latouche, L., Navez, J., Black, Ft., (2000). Pan-African collision, collapse and escape tectonics in the Tuareg Shield: relations with the East Saharan Ghost Craton and the West African Craton. In: Wallbrecher, E., Loizenbauer, J., Fritz, H., Unzog, W., Mogessie, A. (Eds.1, 18’” Colloquium of African Geology, Graz. Special Abstract Issue, Journal African Earth Sciences 30 (4A), 53.

Masoud, A., and Koike, K., (2006). Tectonic Architecture through Landsat-7 ETM+/SRTM DEM-Derived Lineaments and Relationship to the Hydrogeologic Setting in Siwa Region, NW Egypt. Journal of African Earth Sciences, 45, 467477.

Matheis, G., and Caen-Vachette, M., (1983). Rb-Sr isotopic study of rare metal bearing and barren pegmatites in the Pan African reactivation zone of Nigeria. Journal of African Earth Sciences 1, 35-40.

Matheis, G., (1987). Nigerian rare metal pegmatites and their lithological framework. Journ, Geol. 22, 271-291.

McCurry, P., (1973). The geology of degree sheet 21, Zaria, Nigeria. Overseas Geology and Mineral Reserves, No. 45.

Mc Curry, P., (1976). The Geology of the Precambrian to Lower Paleozoic rocks of Northern Nigerian, a Review in C. A. Kogbe (Ed.), *Geology of Nigeria (*pp. 15-39). Lagos, Elizabethan Publishing Co.

Mc Curry, P., (1989). Geology of the Precambrian to Lower Paleozoic rocks of northwestern Nigeria, a review. In: C.A. Kogbe (ed) Geology of Nigeria. Elizabethan publ. Lagos Nigeria pp15-39.

Mc leod, W.N., Turner, D.C., (1971). The Younger Granite 2a Geology of 30sPlateau, Geol. Survey of Nigeria, 32 (1) 48-90.

Middlemost, E.A.K., (1994). Naming Materials in the Magma/Igneous Rock System. Earth-Science Reviews, 37, 215-244.

Miller, C. F., (1985) Are strongly peraluminous magmas derived from pelitic sedimentary sources. J Geol 93: 673-689.

Miller, K. G., and Thomas, E., (1985). Late Eocene to Oligocene benthic foraminiferal isotopic record, Site 574, equatorial Pacific. Initial Reports Deep Sea Drilling Project, 85: 771-777

Moazamy, F., (2006). "Application of Biotite Composition in Determination of Tectonic Setting of Granitoids of BorujerdHamedan," M.S.C. Thesis, Tarbiat Moalem University of Iran, Tehran.

Nesbitt, H. W., & Young, G. M., (1982). Early Proterozoic Climates and Plate Motions Inferred from Major Element Chemistry of Lutites. *Nature 199*; pp. 715–717.

Ngnotue, T., Ganno Sylvestre, Nzenti Jean Paul, Schulz Bernhard, Tchaptchet Tchato Depesquidoux, Suh Cheo Emmanuel, (2012). Geochemistry and Geochronology of Peraluminous High-K Granitic Leucosomes of Yaoundé

Series (Cameroon): evidence for a Unique Pan-African Magmatism and Melting Event in North Equatorial Fold Belt. *International Journal of Geosciences*, 2012, 3, 525-548.

Obini, N., Omietimi, E. J., (2020). Geological Mapping, Petrographic and Structural Attributes of Basement Rocks at Eiyenkorin Area, Southwestern Nigeria. International Journal of Scientific and Research Publications, Volume 10, Issue 5, May 2020.

Odeyemi I. B. (1992) The Ifewara fault in Southwestern Nigeria. Its relationships to fracture zones and seismicity along the Nigerian coast. Kluwer Acad. Publ., Dordrecht, Netherlands.

Odeyemi I. B., (1993). A comparative study of remote sensing images of structure of the Okemesi fold 659 belt, Nigeria. *ITC Netherlands Journal*, 1, 77-81.

Odeyemi, I.B., Anifowose, A.Y.B., and Asiwaju-Bello, Y.A., (1999). Multi-technique graphical analysis of fractures from remotely-sensed images of basement region of Nigeria. Journal of Mining and Geology, 35 (1) pp. 9-21.

O`Connor, J.T. (1965) A classification of quartz rich igneous rock based on feldspar ratios.

US Geological Survey, 525B, B79-B84.

Ogezi, O. A. E., (1988). Origin and Evolution of Basement complex of Northwestern Nigeria in the light of new geochemical data. In Oluyide, P. O. etal., (eds) Precambrian Geology of Nigeria Publication, Kaduna 231 – 239.

Olade, M.A., Elueze, A.A., (1979). Petrochemistry of the llesha amphibolites and Precambrian crustal evolution in the Pan-African domain of SW Nigeria. Precambrian Research 8, 303-318.

O'Leary, D. W., Friedman, J. D., Pohn, H. A., (1976). Lineament, linear, lineation: Some proposed new standards for old terms. *Geological Society America Bulletin*, Vol.87, 1463-1469.

Oluwatoyin, O. A., and Romanus, A. O., (2020). Migmatite and Gneisses in the Basement Complex of Southwestern Nigeria: a re-appraisal of their structural, mineralogical, and geochemical diversity. IJRDO - Journal of Applied Science, Volume-6 | Issue-8 | August, 2020.

Oluyide, P.O., (1988). "Structural Trends in the Nigerian Basement Complex". In: P.O. Oluyide. Precambrian Geology of Nigeria. Geological. Survey. Nigeria: Lagos, Nigeria. pp. 93-98.

Ominigbo, E. O., Ukwang1, E. E., Omo-Irabor, O. O., Emudianughe, J. E., and Okumoko, D. P., (2021). Petrology, Geochemistry and Structural Attributes of the Irruan Basement Rocks, Southern Obudu Plateau, Southeastern Nigeria. Asian Journal of Geological Research 4(1): 1-18, 2021; Article no. AJOGER.63784.

Omitogun, A.O., Caby, R., Debat, P., Mercier, A., (1991). Le metamorphisme pan-africain de la partie centrale de la zone mobile du Nigeria. Comptes Rendus Academic Sciences Paris 313, 1417-1423.

Onougu, S. A., and Ferrante, M. L., (1986). A Geochemical oriented survey for nickel and gold in the Ife-Ilesha area, Oyo State, Nigeria. Records Geol Surv Nigeria, 9: 22-50.

Onyeagocha A.C., Ekwueme B. N., (1982). "The Pre-Pan-African Structural Features of North central Nigeria". *Nigerian Journal of Mining Geology*. 19(2) pp74-77.

Onyeagocha, A.C., Ekwueme, B.N., (1990). Temperaturepressure distribution patterns in metamorphosed rocks of the Nigerian Basement Complex a preliminary analysis. Journal African Earth Sciences 11, 83-93.

Oruç, B., Selim, H.H., (2011). Interpretation of magnetic data in the Sinop area of Mid Black Sea, Turkey, using tilt derivative, Euler deconvolution, and discrete wavelet transform. J. Appl. Geophys. 74, 194–204.

Osinowo, O. O., Fashola, O. E., Ayolabi, E. A., & Olayinka, A. I., (2021). Structural mapping and gold mineralisation potential evaluation from airborne time – domain electromagnetic (TDEM) data of Ilesha Schist Belt, southwestern Nigeria. Journal of Exploration geophysics 2019.

Owusu, E.A., Woldai, T., Barritt, S.D., Carranza, E.J.M., and Hale, M., (2006). Spatial association of gold deposits with remotely - sensed faults, south ashanti belt, Ghana. In: AARSE 2006: Proceeding of the 6th AARSE international conference on earth observation and geoinformation sciences in support of Africa's development, 2006, Cairo, Egypt. Cairo: The National Authority for Remote Sensing and Space Science (NARSS), 2006. ISBN 1-920-01710-0. 8 p.

Oyawoye, M.O., (1964). The petrology of a potassic syenite at shaki, Western Nigeria. Contributions Mineralogy Petrology. 16, pp123-129.

Oyawoye, M.O., (1970). The basement complex of Nigeria. In: Dessuvagie TFJ, whiteman AJ (ed.) African Geology. University of Ibadan.

Oyawoye, M.O., (1972). The basement complex of Nigeria. In: Africa Geology (edited by Dessauvagie, T.F.I. and hiteman, A.J), Ibadan, Nigeria, pp67-99.

Oyinloye, A.O., (1992). Genesis of the Iperindo gold deposit, Ilesha schist belt, Southwestern Nigeria. Unpublished thesis of the University of Wales, Cardiff, U.K. pp. 1-267.

Oyinloye, A.O., (2002b). Geochemical characteristics of some granite gneisses in Ilesha area southwestern Nigeria: Implication on evolution of Ilesha schist belt, southwestern Nigeria. Trends in Geochemistry India vol.2, 59-71.

Oyinloye, A.O., (2011). setting of the Basement Complex rocks in Southwestern Nigeria: Implications on provenance and evolution. Earth and Environmental sciences.;21(2):97-118.

Oyinloye, A.O., and Steed, G.M., (1996). Geology and Geochemistry of the Iperindo Primary gold deposits Ilesha schist belt Southwestern Nigeria. Inferences from stable carbon isotope studies. Africa J. Sc. Tech. 8 (1) pp 16-19.

Pearce, J.A., Harris, N.B.W., Tindle, A.G., (1984) Trace Element Discrimination Diagrams for the Tectonic Interpretation of Granitic Rocks. J Petrology 25: 956-983.

Pearce, J.A., (1996). Sources and settings of granitic rocks. Episodes 19, 120–125. Pearce, J.A., Harris, N.B.W., Tindle, A.G., 1984. Trace element discrimination diagrams for the tectonic interpretation of granitic rocks. J. Petrol. 25, 956–983.

Peccerillo, R., Taylor, S.R., (1976). Geochemistry of Eocene calcalkaline volcanic rocks from the Kastamonu area, northern Turkey. Contrib. Mineral. Petrol. 58, 63–81.

Phillips, J.D., (2000). Locating Magnetic Contacts: a Comparison of the Horizontal Gradient, Analytic Signal, and Local Wavenumber Methods. SEG 2000 Expanded Abstracts.

Pollard, D.D., and Segall P., (1980). Mechanisms of discontinuous faults. *Journal of Geophysical Research.* 85: pp4337-4350.

Price, N.J., and Cosgrove, J.W., (1990). Analysis of Geological Structures. Cambridge University Press, Cambridge, 502 p.

Pollard, D. D., & Fletcher, R. C., *(*2005). Fundamentals of Structural *Geology*. xii + 500 pp. Cambridge, New York, Melbourne: Cambridge University Press.

Rahaman, M.A., (1976). Review of the basement geology of southwestern Nigeria. In: Kogbe, C.A., (eds) geology of Nigeria, 2nd Ed. Elizabethan publication. Lagos, pp 41-58.

Rahaman, M.A., (1988). Recent advances in the study of the basement complex of Nigeria. In Precambrian geology of Nigeria. Geological Survey of Nigeria.pp. 11-14

Rahaman, M.A., (1989). Review of the basement geology of southwestern Nigerian. In C.A. Kogbe 2nd Ed. of Geology of Nigeria, Rock View, Jos, Nigeria. 39-56 pp.

Rahaman, M.A., Ajayi, T.R., Oshin, I.O., and Asubioji, F.O., (1988). Trace element geochemistry and geotectonic setting of Ife-Ilesha schist belt. In Precambrian Geology of Nigeria Publish by Geological Survey of Nigeria. pp 241-256.

Rahaman, M.A., and Ocan, O., (1978). On relationships in the Precambrian Migmatite-gneisses of Nigeria.*Niger Journal of Mining Geology* 15:pp 23–32.

Rahaman, M.A., Tubosun, I.A., Lancelot, J.R., (1991). UPb geochronology of potassic syenites from SW Nigeria and the timing of deformation events during the Pan-African Orogeny. Journal African Earth Sciences 13, 387-395.

Rahiman, T. I. H., and Pettinga, J. R., (2008). Analysis of lineaments and their relationship to Neogene fracturing, SE Viti Levu, Fiji; Geol. Soc. Am. Bull. 120(11–12) 1544–1555.

Ramberg, H., (1955). Natural and experimental boudinage and pinch-and-swell structures, *J. Geol.*, 63, 512– 526.

Rollinson, H. R., (1993). Using geochemical data: evaluation, presentation, interpretation. Harlow, Essex, England: Longman Scientific & Technical; New York: Copublished in the U.S. with J. Wiley & Sons, 1993.

Russ, W., (1957). The geology of parts of Niger, Zaria and Sokoto provinces with reference to the occurrence of gold. Geological Survey Nig; Bulletin 29.

Salem, A., Williams, S., Fairhead, J. D., Ravat, D., Smith, R., (2007). Tilt-depth method: A simple depth estimation method using first-order magnetic derivatives. Article in The Leading Edge · December 2007.

Shand, S. J., (1943). *The Eruptive Rocks*, 2nd edn. New York: John Wiley, 444 pp.

Singh, B., and Dowerah, J., (2010). ASTER DEM Based Studies for Geological Investigation around Singhbhum Shear Zone (SSZ) in Jharkhand,

India," *Journal of Geographic Information System*, Vol. 2 No. 1, 2010, pp. 11-14. doi: 10.4236/jgis.2010.21003.

Soulakellis, N. A., Novak, I. D., Zouros, N., Lowman, P., and Yates, J., (2006). Fusing Landsat-5/TM Imagery and Shaded Relief Maps in Tectonic and Geomorphic Mapping: Lesvos Island, Greece. Photogrammetric Engineering and Remote Sensing, 72(6):693-700 ·

Streckeisen, A., (1974). Classification and nomenclature of plutonic rocks: recommendations of the IUGS subcommission on the systematics of igneous rocks. Geologische Rundschau,63, 773–786.

Streckeisen, A. L., (1976). Earth Sci. Rev. 12, 1-33

Tietz, G. F., (1983). Chemical and mineralogical alterations in the lateritic cover in Nigeria. West africa in A. J. Melfi and A. Carvalhol (Eds.) Lateritization processes, 500p.

Toteu, S.F., Macaudiere, J., Bertrand J .M, and Dautel, D., (1990). "Metamorphic Zircons from North Cameroon: Implications for the Pan-African Evolution of Central Africa". Geological. Rundsch. 79:pp777-788.

Truswell, J.F., and Cope, R.N., (1963). The geology of parts of Niger and Zaria provinces, northern Nigeria. Bulleting of Geological Survey. Nigeria, 29.

Tubosun, I.A., Lancelot, J.R., Rahaman, M.A., Ocan, O.O., (1984). U-Pb Pan-African ages of two charnockite-granite associations from SW Nigeria. Contributions Mineralogy Petrology 88, 188-l 95.

Turner, D.C., (1983). Upper Proterozoic schist belts in the Nigerian sector of the Pan-African Province of West Africa. *Prec.Res*.21, pp.5-79.

Viegas L.G.F., Archanjo C.J., Hollanda M.H.B.M., Vauchez A. 2014. Microfabrics and zircon U–Pb (SHRIMP) chronology of mylonites from the Patos shear zone (Borborema Province, NE Brazil). Precambrian Research, 243, 1-17. https://doi.org/10.1016/j.precamres.2013.12.020.

Wolf, M. B., and Willie, P. J., (1994). Dehydration-melting of amphibolite at 10 kbar; the effect of temperature and time. Contribution to mineralogy and petrology. 115, 366-383.

Wright, J.B., Hastings, D.A., Jones, W.B., and Williams, H.R., (1985). Geology and mineral resources of West Africa. George Allen and Unwin, London, 187p.

Yesou, H., Besnus, Y., Rolet, J., (1993). Extraction of spectral information from Landsat TM data and merger with SPOT panchromatic imagery — a contribution to the study of geological structures. ISPRS Journal of Photogrammetry and Remote Sensing 48(5):23-36 · October 1993.

Appendix i: Table of ratios of A/NK and A/CNK for all samples from study area

Sample ID	Al2O3/Na2O+K2O	Al2O3/CaO+Na2O+K2O
L44	2.77	2.32
L46	3.16	2.3
L54	2.79	2.17
L63	3.28	2.11
L77	3.93	1.98
L79	2.52	2.32
L50	2.79	2.19
L58	151.33	56.75
L75	2.45	1.97
L78	3	2.1
IW1D	2.85	2.31
L36	2.46	1.84
L37	8.78	1.18
L55	2.3	1.83
IDA1	4.31	2.32
L33	2.62	2.32
L34	2.52	2.19
L42	2.11	1.82
L24	39.92	1.09
L30	16.99	0.18
L43	2.52	2.01
L56	21.19	2.75
L65	2.45	1.97
L76	2.8	2.38

Appendix ii: FeO/(FeO+MgO) V SiO_2 plot for all rock samples of Okemesi-Iwaraja area (after Frost etal 2001)

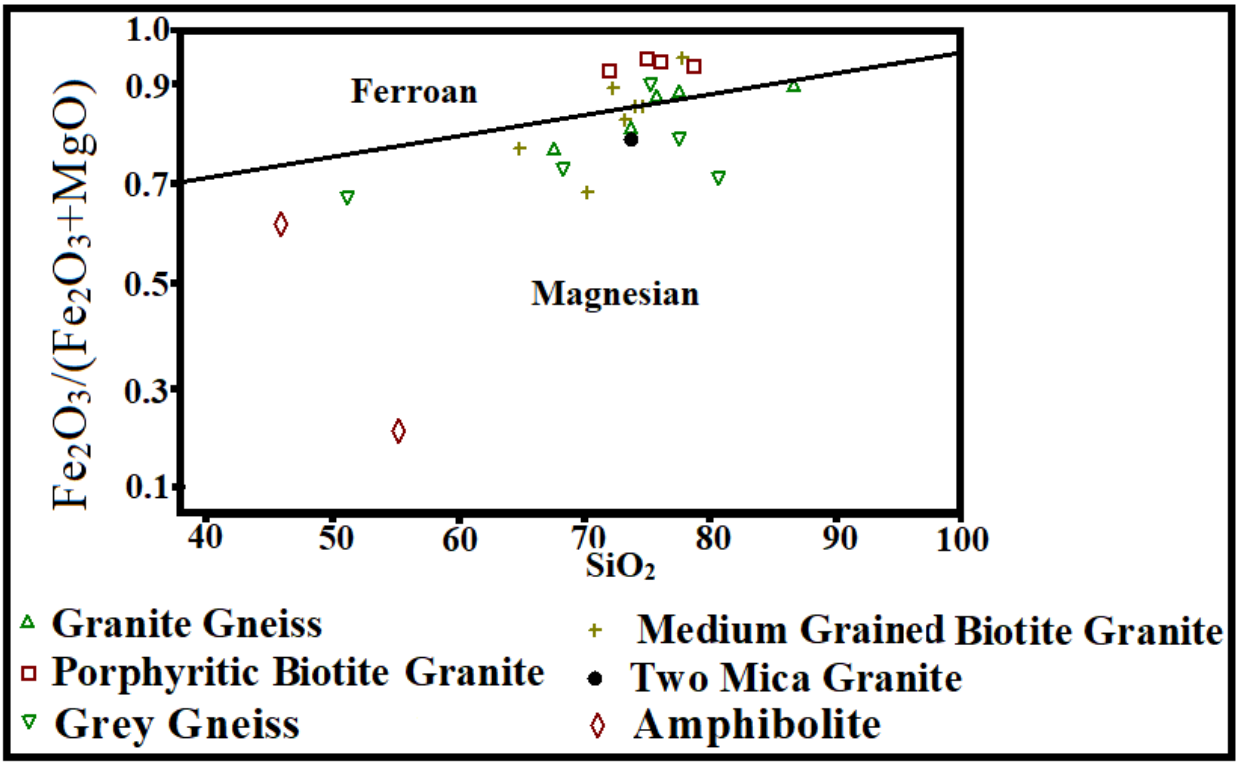

Appendix iii: Table of ratios of trace elements of the other granitoids

Sample ID	L33	L34	L42	L43	L46	L50	L54	L58	L63	L65	L75	L76	L77	L78	L79	IW1D
Petrology	Porphyritic Biotite Granite	Porphyritic Biotite Granite	Porphyritic Biotite Granite	Porphyritic Biotite Granite	Medium Graind Biotite Granite	Granite Gneiss	Medium Graind Biotite Granite	Granite Gneiss	Medium Graind Biotite Granite	2 Mica Granite	Granite Gneiss	Medium Graind Biotite Granite	Medium Graind Biotite Granite	Granite Gneiss	Medium Graind Biotite Granite	Granite Gneiss
(La/Yb)N	5.28	6.37	19.76	23.44	10.16	6.54	20.84	7.48	44.39	79.43	10.61	10.40	15.03	13.90	10.93	10.69
(Ce/Yb)N	4.66	5.49	15.93	19.06	7.67	5.44	15.50	5.32	31.51	61.52	8.01	7.62	10.85	7.86	8.01	7.96
(Gd/Yb)n	1.35	1.44	2.85	3.23	1.71	1.09	2.13	1.34	4.21	7.00	1.28	1.20	1.82	1.70	1.31	1.39
(La/Sm)n	2.52	2.80	3.85	3.89	3.68	3.91	5.66	3.65	5.14	5.30	4.74	4.97	5.08	4.90	4.93	4.72
Sr/Sr*	0.16	0.19	0.44	0.33	1.73	1.66	0.90	0.53	8.49	1.48	2.20	2.02	2.32	3.25	1.22	0.94
Zr/Zr*	1.44	1.10	1.91	1.77	3.52	3.63	2.46	14.35	4.05	3.80	2.19	4.98	3.52	3.74	2.05	2.34
Ce/Ce*	1.05	1.03	0.98	0.99	0.93	1.03	0.95	0.86	0.89	0.97	0.95	0.92	0.91	0.72	0.92	0.94
Eu/Eu*	0.05	0.06	0.19	0.15	0.34	0.29	0.19	0.43	0.44	0.29	0.32	0.39	0.37	0.40	0.16	0.21

Appendix iv: Table of ratios of trace elements of the grey gneisses and amphibolites

Sample ID	L24	L30	L36	L37	L55	L56	IDA1
Petrology	Amphibolite	Amphibolite	Grey Gneisses	Grey Gneisses	Grey Gneisses	Grey Gneisses	Grey Gneisses
(La/Yb)N	0.89	1.60	18.09	2.98	22.49	14.53	18.63
(Ce/Yb)N	1.04	1.35	12.47	2.27	16.92	10.77	14.20
(Gd/Yb)n	1.09	1.01	1.62	1.35	2.66	1.81	2.31
(La/Sm)n	0.69	1.31	6.76	1.89	4.65	4.80	4.46
Sr/Sr*	6.76	3.72	0.54	3.48	1.64	1.35	5.80
Zr/Zr*	2.64	7.05	3.12	4.59	4.61	3.06	3.56
Ce/Ce*	1.01	0.86	0.89	0.86	0.94	0.92	0.94
Eu/Eu*	0.92	0.38	0.24	0.75	0.40	0.34	0.40

Appendix v: Felspar triangle (An-Or-Ab) plot for granitic rocks

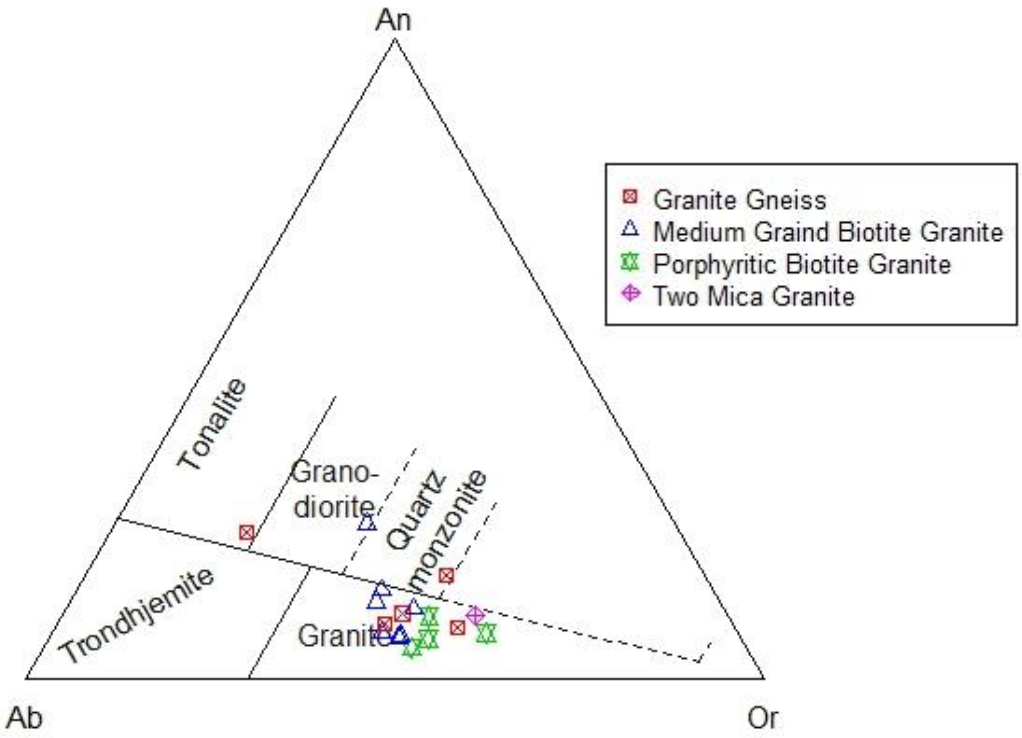

Appendix vi: Plot of Hf-Rb/30-3Ta (Harris Et al. 1986) for other granitoids

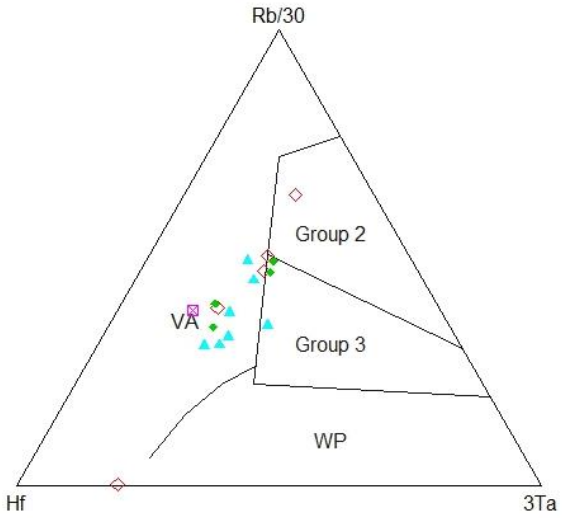

Appendix vii: Plot of Hf-Rb/30-3Ta (Harris Et al. 1986) for the grey gneisses (B)

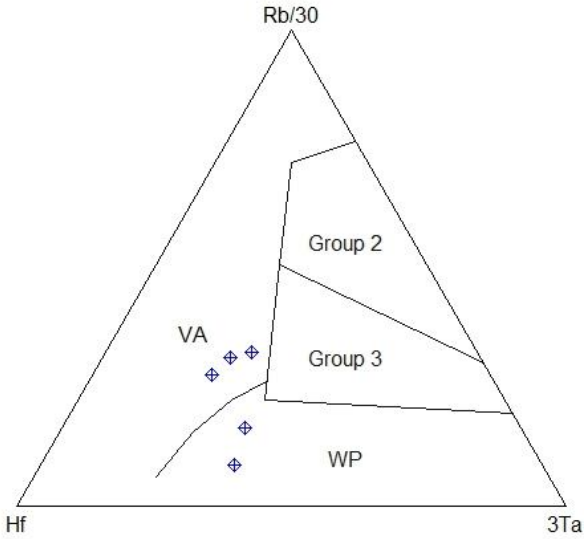

Appedix 8: Table of some Sampling locations and rock discriptions

Location	Latitude	Longitude	Elevation (M)	Town	Rock type	Strike	Dip	Joint	Vein
L2	N 07 51' 19.0"	E004 55' 07.4"	515	Okemesi	Quartz schist	17	81E	73	
L3	N 07 51' 34.6"	E004 55' 53.7"	532	Okemesi	Quartz schist	354	32E	102	330
L4	E004 55' 51.0"	N 07 52' 29.1"	580	Okemesi area	Quartz schist	330	20E	79	
L7	E 004 55' 52.0"	N 07 49' 40.5"	511	Okemesi area	Quartzite	19	32E		
L8	E 004 55' 21.3"	N 07 49' 25.7"	395	Okemesi	Quartz schist	358	40E	96	74
L9	E 004 55'00.9"	N 07 49' 08.3"	517		Schist	343	52E		
L10	E 004 56' 3.6"	N 07 48' 43.9"	468		Quartz schist	48	27E		
L11	E 004 56'23.6"	N 07 48' 13.8"	508		Quartz schist	282	28E		355
L12	E 004 57'01.4"	N 07 45' 59.8"	476		Quartz schist				
L13	E 004 55'06.7"	N 07 49' 59.7"	420	Okemesi	Quartz schist	354	42E	243	
L15	E 004 54'23.5"	N 07 48' 40.8"	444		Quartzite				
L16	E 004 54'05.4"	N 07 46' 18.6"	461		Quartzite	354	29E	64,47,63,85,88,97,	
L17	E 004 55'10.0"	N 07 51' 41.8"	471		Quartz schist	22	64W	99,94,99,101,87,109	
L18	E 004 55'25.4"	N 07 53' 02.6"	382		Quartz schist	347	47W	152	
L19	E 004 56' 5.8"	N 07 53' 4.9'	385		Quartz schist				
L20	E 004 55'11.3"	N 07 49' 59.1"	413		Quartz schist	348	54E	283	
L21	N 07º 50' 05.6"	004º 55' 10.0"	397		?Gneiss	331	41E	243	
L22	N 07º 52' 21.8"	E 00º 57' 10.8"	438		Quartz schist	3	31		
L23	N 07º 52' 23.0"	E 004º 57' 32.0"	429		Quartz schist				
L24	N 07º 52' 23.9"	E 004º 58' 02.5"	442	Ajido	Aphibolite???				
L25	N 07º 52' 16.4"	E 004º 57' 52.6"	436	Ajido	Quartzite				
L26	N 07º 52' 21.9"	E 004º 57' 49.5"	434	Along Okemesi-Ijero Road	Schist	6	53		
	N 07º 50' 03.4"	E 004º 54' 58.3"	397	Okemesi	Schist	309	45W		
L28	N 07º 49' 51.1"	E 004º 54' 59.1"	407		Quartz schist				
L29	N 07º 49' 47.6"	E 004º 55' 10.3"	428		Schist	346	44E	255	284
L30	N 07º 49' 41.5"	E 004º 53' 47.7"	425						

Appedix 8: Table of some Sampling locations and rock discriptions contd

Location	Latitude	Longitude	Elevation (M)	Town	Rock type	Strike	Dip	Joint	Vein
L31	N 07º 49' 48.2"	E 004º 53' 47.6"	409	Kajola	Quartz schist	17			
L32	N 07º 49' 59.3"	E 004º 53' 43.0"	386	Along Esa Oke Road	Quartz schist	290	64E		
L33	N 07º 50' 40.4"	E 004º 51' 37.9"	423		Porphyritic granite				
L34	N 07º 49' 36.0"	E 004º 51' 16.3"	409		Porphyritic granite			317	
L35	N 07º 49' 21.6"	E 004º 48' 17.4"	446	Imesi-Ile - Osogbo road	Porphyritic granite			32	
L36	N 07º 47' 17.1"	E 004º 44' 09.3"	389		Granite gneiss				289
L37	N 07 º 47' 05.1"	E 004º 43' 50.4"	360	Ibokun	Granite gneiss	356	43 W	286,	296
L38	N 07º 47' 23.0"	E 004º 44' 12.5"	365	Ibokun	Granite gneiss	327	61 W	94	280
L39	N 07º 51' 20.7"	E 004º 43' 32.0"	374	Ibokun	Granite				
L40	N 07º 52' 01.9"	E 004º 43' 15.4"	412	Ada	Granite			130	
L41	N 07º 52' 13.0"	E 004º 43' 07.0	415	Ada	Granite			230	128
L42	N 07º 53' 40.1"	E 004º 44' 09.2"	402	Ada	Weakly P. granite				
L43	N 07º 53' 49.0"	E 004º 44' 10.4"	416	Ada	Porphyritic Granite				
L44	N 07º53' 40.3"	E 004º 43' 03.9"	420	Ada - Igbajo Road	Medium G. Granite				
L45	N 07º 54' 00.6"	E 004º 42' 40.5"	451	Iree Road (Church)	Porphyritic granite				
L46	N 07º 53' 32.1"	E 004º 42' 17.8"	440	Aagba Methodist High School, Ada	Medium G. granite			251	

Appedix 8: Table of some sampling locations and rock discriptions contd

Location	Latitude	Longitude	Elevation (M)	Town	Rock type	Strike	Dip	Joint	Vein
L48	N 07º 38' 38.1"	E 004º 46' 17.9"	477		Granite gneiss	59	28W		
L49	N 07º 37' 38.5"	E 004º 49' 36.6"	476	Iloko Road	Granite gneiss	359		105	341
L50	N 07º 37' 07.6"	E 004º 49' 32.9"	434	Ilesa -Akure 'Way	Granite gneiss	28	46W		
L51	N 07º 36' 08.0"	E 004º 50' 59.2"	425	Ore Egba	Quartzite ridge			316	
L52	N 07º 37' 39.3"	E 004º 51' 19.6"	487	Erinmo Ijesha	Quartz schist	349		268	
L53	N 07º 38' 24.4"	E 004º 51' 59.9"	410	Erinmo -Ekiti Road	Quartzite - quartz schist				
L57	N 07º 38' 44.3"	E 004º 55' 20.4"	565	Oke Adun Comm.	Quartz schist	24	38E	107	
L59	N 07º 37' 55.3"	E 004º 55' 57.5"	497	?Iwaji Ekiti	Quartzite			50	
L60	N 07º 35' 47.9"	E 004º 56' 01.7"	469	Iloro Ekiti	Quartzite				
L61	N 07º 29' 04.3"	E 004º 56' 07.7"	412	Ikeji-Ile	Quartzite	83	39W	102	2
L62	N 07º 28' 58.1"	E 004º 55' 33.8"	417	Ikeji-Ile	Quartz schist	318	58E		58
L63	N 07º 28' 50.6"	E 004º 54' 24.9"	311	Ikeji-Ile/ Ipetu axis	Granite				315
L64	N 07º 29' 26.6"	E 004º 53' 49.5"	285	Ipetu Ijesa	Granite				61
L65	E 004º 52' 37.6"	313	Erin Ijesa	Granite					58
L66	N 07º 33' 36.1"	E 004º 52' 39.9"	315	Erin Ijesa	Schist	332	35E		62
L67	N 07º 36' 41.8"	E 004º 50' 54.9"	425	Erin Ijesa	Quartzite			84	57
L68	N 07º 35' 19.1"	E 004º 52' 01.1"	382	Erin Ijesa Road	Gneiss	2	13E		56
L69	N 07º 34' 39.3"	E 004º 52' 06.2"	352	Erin Ijesa Road	Mica schist	356			60

Location	Latitude	Longitude	Elevation (M)	Town	Rock type	Strike	Dip	Joint	Vein
L73	N 07º 27' 51.4"	E 004º 52' 01.4"	275	Ipetu - Ajegunle Rd	Quartz schist	359	48E		
L74	N 07º 28' 01.7"	E 004º 50' 47.3"	327	Ayeni Temidire	Quartz schist	358	34E	84	331
L75	N 07º 27' 47.7	E 004º 50' 02.9"	339	Iperindo Road	Granite gneiss ?PG	13	13W	296	
L76	N 07º 29' 58.3"	E 004º 49' 15.3"	303	Iperindo	Granite				
L77	N 07º 31' 53.1"	E 004º 49' 14.6"	341	Iperindo - Odo Rd.	Granite				
L78	N 07º 32' 42.7"	E 004º 48' 41.5"	430	Ise-Ijesa	Granite gneiss	24	40W	280	
L79	N 07º 33' 41.6"	E 004º 48' 18.2"	426	Ise- Ijesa Road	Granite gneiss			103	44
L80	N 07º 34' 55.8"	E 004º 46' 50.5"	367	Irogbo	Schist	2	32W	286	
L81	N 07º 34' 44.5"	E 004º 47' 03.8"	359	Irogbo Road	Schist				
L82	N 07º 34' 47.2"	004º 47' 17.7"	341		Quartz schist - Quartzite	350	39W	58	37
L83	N 07º 34' 16.1"	E 004º 48' 20.1"	394	Idado Ijesa	Granite gneiss				
L84	N 07º 33' 46.9"	E 004º 47' 46.1"	403	Ipole Ijesa	Quartz schist	343	48E		
L85	N 07º 33' 45.9"	E 004º 47' 40.9"	387	Ipole Ijesa	Amphibolite schist	72	79W	101	